ANL/NE-16/19

Argonne NATIONAL LABORATORY

The SAS4A/SASSYS-1 Safety Analysis Code System

Nuclear Engineering Division

About Argonne National Laboratory

Argonne is a U.S. Department of Energy laboratory managed by UChicago Argonne, LLC under contract DE-AC02-06CH11357. The Laboratory's main facility is outside Chicago, at 9700 South Cass Avenue, Argonne, Illinois 60439. For information about Argonne and its pioneering science and technology programs, see www.anl.gov.

Document Availability

Online Access: U.S. Department of Energy (DOE) reports produced after 1991 and a growing number of pre-1991 documents are available free via DOE's SciTech Connect (http://www.osti.gov/scitech/)

Reports not in digital format may be purchased by the public from the National Technical Information Service (NTIS):

U.S. Department of Commerce
National Technical Information Service
5301 Shawnee Rd
Alexandria, VA 22312
www.ntis.gov
Phone: (800) 553-NTIS (6847) or (703) 605-6000
Fax: (703) 605-6900
Email: **orders@ntis.gov**

Reports not in digital format are available to DOE and DOE contractors from the Office of Scientific and Technical Information (OSTI):

U.S. Department of Energy
Office of Scientific and Technical Information
P.O. Box 62
Oak Ridge, TN 37831-0062
www.osti.gov
Phone: (865) 576-8401
Fax: (865) 576-5728
Email: **reports@osti.gov**

Disclaimer

ANL/NE-16/19

The SAS4A/SASSYS-1 Safety Analysis Code System

Chapter 16:
LEVITATE: Voided Channel Fuel Motion Analysis

A. M. Tentner
Nuclear Engineering Division
Argonne National Laboratory

March 31, 2017

TABLE OF CONTENTS

LIST OF FIGURES

LIST OF TABLES

NOMENCLATURE

Symbol	Description	Units
$A_{k,i}$	Cross sectional area of component k, in the coolant channel in the axial cell i	m^2
$A_{k,ca,i}$	Cross sectional area of component k, in the fuel-pin cavity, in axial cell i.	m^2
$A_{j,k,i}$	Contact lateral area between component j and component k in the axial cell i	m^2
AXMX	Reference cross-sectional area which determines the volume $AXMX \cdot \Delta z_i$, over which all component densities are smeared to yield the generalized smeared densities	m^2
AFRV	Input, sodium vapor friction coefficient	
BFRV	Input, exponent of vapor friction coefficient	
C_{AREA}	Coefficient used to define the contact area between two components. Has values between 0 and 1	
$C'_{D,Mi,fu,i}$	Generalized drag coefficient between the gas mixture and the molten fuel in the axial cell i	Kg/m^4
$C'_{in,Mi,fu,i}$	Generalized inertial force coefficient, used in the definition of the inertial force exerted between the gas mixture and the molten fuel in the axial cell i	Kg/m^3
$C_{ff,cl,i}$	Coefficient defining the fraction of the cladding perimeter covered by the solid fuel crust in the axial cell i	
$C_{ff,sr,i}$	Coefficient defining the fraction of the hexcan wall perimeter covered by the solid fuel crust in the axial cell i	
$C_{fu,cl,i}$	Coefficient defining the fraction of the cladding perimeter covered by the molten and frozen fuel in the axial cell i	
$C_{fu,sr,i}$	Coefficient defining the fraction of the hexcan wall covered by the molten and frozen fuel in the axial cell i	
$C_{fu,ff,cl,i}$	Coefficient defining the fraction of the frozen fuel crust on the cladding covered by molten fuel	
$C_{fu,ff,sr,i}$	Coefficient defining the fraction of the frozen fuel crust on the hexcan wall covered by molten fuel	
$C_{mfu,cl,i}$	Coefficient defining the fraction of the cladding perimeter covered by molten fuel only, in cell i	
$C_{mfu,sr,i}$	Coefficient defining the fraction of the hexcan wall covered by molten fuel only, in cell i	
$C_{p,fu}$	Specific heat for the fuel	$J/(kg \cdot K)$

Symbol	Description	Units
$C_{se,ff,cl,i}$	Coefficient defining the fraction of the frozen fuel crust on the cladding covered by molten steel	
$C_{se,ff,sr,I}$	Coefficient defining the fraction of the frozen fuel crust on the canwall covered by molten steel	
CMNL	Input, liquid sodium compressibility	Pa^{-1}
CMFU	Input, liquid fuel compressibility	Pa^{-1}
$D_{H,Mi,i}$	Hydraulic diameter for the gas mixture in the coolant channel in cell *i*	m
$f_{Mi,i}$	Friction coefficient used to characterize the friction between the gas mixture and the channel walls in cell *i*	
$F_{area,bd,lu,i}$	Fraction of lateral chunk area in contact with the channel boundaries in cell *i*	
$h_{k,i}$	Enthalpy of component k in the axial cell *i*	J/kg
$H_{j,k,i}$	Heat-transfer coefficient between components *j* and *k* in cell *i*.	$J/(m^2 \cdot s \cdot K)$
$H'_{j,k,i}$	Generalized heat transfer coefficient, similar otherwise to $H_{j,k,i}$ $H'_{j,k,i} = H_{j,k,i} \cdot \frac{A_{j,k,i}}{AXMX \cdot \Delta zi}$	$J/(m^3 \cdot s \cdot K)$
$h_{Na,liq,i}$	Enthalpy of liquid sodium at saturation in cell *i*	J/kg
$h_{Na,vap,i}$	Enthalpy of sodium vapor at saturation in cell *i*	J/kg
$h_{Na,lg,i}$	Heat of vaporization for sodium in cell *i*	J/kg
$h_{fv,lg,i}$	Heat of vaporization for fuel	J/kg
$k_{Mi,I}$	Conductivity of the sodium and fission-gas mixture in the axial cell *i*	J/(M·s·K)
$L_{cl,I}$	Perimeter of all pins in a subassembly in the axial cell *i*	m
$L_{sr,i}$	Same as above, for the canwall	m
$L_{ff,cl,I}$	Perimeter of the cladding fuel crust in a subassembly in the axial cell *i*	m
$L_{ff,sr,i}$	Same as above, for the canwall fuel crust	m
$l_{ff,cl,i}$	Thickness of the fuel crust on cladding in the axial cell *i*	m
$l_{ff,sr,i}$	Same as above for the canwall fuel crust	m
$M_{k,i,ic}$	Mass of component k is the axial cell *i* of one subassembly of channel *ic*	kg
$M^{0}_{k,i,ic}$	Same as above, but referring to the initial conditions	kg
N_{pins}	Number of fuel pins in the subassembly	

Symbol	Description	Units
$P_{ch,i}$	Total pressure in the coolant channel in the axial cell i	Pa
$P_{k,i}$	Partial pressure of component k in cell i	Pa
$P_{k,sat,i}$	Saturation pressure for component k in the cell i, e.g., $P_{Na,sat,i} = P_{sat}(T_{Na,i})$	Pa
$Q_{k,i}$	Energy source in the component k in cell i	J/(s·kg)
$Q_{cl,i}$	Energy source in the cladding in the axial cell i of one subassembly	J/s
R	Universal gas constant	
R_k	Gas constant specific for the component k, $R_k = R/M_k$ where M_k is the molar mass of the component k.	
$R_{ca,k}$	Radius of cavity in the axial cell k	m
$R_{cl,os,i}$	Outer radius of the cladding in the axial cell i	m
$R_{lu,i}$	Radius of the fuel/steel chunks in cell i	m
Re	Reynolds number	
$T_{k,i}$	Temperature of component k in cell i	K
$u_{k,i}$	Velocity of component k in the coolant channel at the boundary $i - 1/2$	m/s
$v_{Na,i}$	Specific volume of sodium in cell i	m^3/kg
$v_{Na,liq,i}$	Specific volume of the liquid sodium at saturation in cell i	m^3/kg
$v_{Na,vap,i}$	Specific volume of the sodium vapor at saturation in cell i	m^3/kg
$V_{k,i}$	Volume occupied by component k in cell i	m^3
$X_{Na,i}$	Quality of the two-phase sodium in cell i	
z	Axial coordinate	m
Δz_i	Length of axial cell i	m
$\Delta T_{j,k,i}$	Temperature difference between components j and k in the axial cell i	K
Δt	Time increment	s
$\Delta R_{cl,i}$	Current thickness of the cladding in the axial cell i	m
ΔR_{cl}^0	Thickness of the original cladding in cell i	m
$\rho_{k,i}$	Physical density of component k in the cell i.	kg/m^3
$\rho'_{k,i}$	Generalized density of component k in cell i, $\rho'_{k,j} = \rho_{k,i} \cdot \frac{A_{k,i}}{AXMX}$	Kg/m^3
σ_{fu}	Liquid fuel surface tension	J/m^2
σ_{se}	Liquid steel surface tension	J/m^2

Symbol	Description	Units
$\theta_{k,i}$	Volume fraction of component k in the axial cell *i* $\theta_{k,i} = \frac{Q_{K,i}}{AXMX}$	
Subscripts		
bd	Refers to a quantity defined at the cell boundary	
ca	Cavity	
ch	Coolant channel	
cl	Cladding	
ch,op	Open channel. The open channel at any axial location can become smaller than the original coolant channel due to fuel and steel freezing. It can also increase due to the ablation of the cladding and hexcan wall and to the disruption of the fuel pins	
ff	Frozen fuel	
ffc	Frozen fuel on cladding	
ffs	Frozen fuel on structure	
fi	Fission gas	
fu	Molten fuel	
fv	Fuel vapor	
fl	Fuel chunks	
i	Cell number, on the channel grid	
is	Inner cell of cladding or structure	
IN	Inertial	
J	Other components in the coolant channel, exchanging mass, momentum or energy with component *k*	
k	Component subscript, referring to the component being described. Also used as cell number on the fuel-pin grid	
liq	Indicates a physical property for the saturated liquid, e.g., $h_{Na,liq,i}$	
lq	Indicates a physical property at liquidus	
lu	Solid fuel/steel chunks	
lv	Indicates a physical property that characterizes the transition from liquid to gas, e.g. h_{lv}	
Mi	Mixture of sodium vapor, fission gas, fuel vapor, steel vapor, and liquid sodium	

Symbol	Description	Units
Mo	Momentum	
Na	Sodium	
Nl	Liquid sodium	
Nv	Sodium vapor	
Os	Outer cell of cladding or structure. The "outer" surface is always the surface facing the coolant channel	
pin	Fuel pin	
sat	Indicates a physical property at saturation, e.g., T_{sat} ($P_{k,i}$)	
se	Molten steel	
sl	Steel chunks	
so	Indicates a physical property at solidus	
sr	Structure, i.e., hexcan wall or wall of the experimental loop	
st	Refers to a stationary component, such as the solid fuel in the pin	
sv	Steel vapor	
vap	Indicates a physical property for the saturated dry vapor, e.g., $h_{Na,vap,i}$	
vg	Vapor/gas mixture	
Superscripts		
cond	Condensation	
L	Used to indicate a lateral area, as opposed to a cross-sectional area	
N	The value of any quantity at the beginning of the current time step	
$n+1$	The value of any quantity at the end of the current time step. If no superscript is present, the default is n	
N	Used in relation to the cylindrical chunks, to indicate the area of the lower and upper base	
vap	Vaporization	

LEVITATE: VOIDED CHANNEL FUEL MOTION ANALYSIS

16.1 Overview

16.1.1 Historical Background and Physical Description of the LEVITATE Model

In an unprotected loss-of-flow (LOF) accident in an LMFBR, the boiling and voiding of the coolant sodium in the high-power subassemblies will lead to an overpower situation if the sodium void worth of the reactor considered is moderately positive. A high-power level causes the subsequent events in the voided channels such as cladding motion, fuel-pin breakup, and fuel motion to occur nearly simultaneously. A positive reactivity contribution from these effects could lead to a potentially energetic LOF-driven-TOP accident, whereas a negative contribution would most likely lead the accident into a transition phase much like that predicted as the likely outcome of a LOF accident in a low-void-worth LMFBR.

The LEVITATE model [16-1] has been designed to treat both the high-power and the near-nominal power conditions in voided assemblies. This means that cladding and fuel motion can be treated in a combined or sequential fashion. The earlier CLAZAS [16-2] and SLUMPY [16-3] models in SAS3A [16-4] were designed only to treat these phenomena in a sequential fashion. The new LEVITATE model also treats several relevant phenomena not considered in the earlier models. The most important of these are several pin-disruption modes, continuous fuel-steel flow regimes and fuel-steel crust and plug formation, and a tight coupling with the sodium dynamics. LEVITATE has also been designed to incorporate a fuel-chunk model, describing the motion of the solid fuel chunks present in the coolant channel. This model has become operational in the developmental version of LEVITATE and was not available in the initial release version of SAS4A. Since two-phase sodium which is generated by the chugging of the lower sodium slug may penetrate the disrupted region, fuel may be pushed upwards or "levitated," prompting the name of this model.

The LEVITATE development used the PLUTO2 code [16-5] as a starting point and still shares some features with that code. PLUTO2 and LEVITATE are complementary models with some degree of overlap. PLUTO2 can treat overpower situations in sodium-filled channels, i.e., fuel-coolant interactions and fuel sweepout, but not the later cladding motion, fuel-steel mixing, and pin disintegration.

16.1.2 Physical Description of the LEVITATE Model

LEVITATE models the fuel subassembly in a one-dimensional geometry, assuming that all pins in the subassembly behave coherently. Three basic thermal-hydraulic models are used for each subassembly:

1. The hydrodynamic model describing the cavities inside the fuel pins, which initially contain liquid fuel and fission gas.

2. The hydrodynamic model describing the coolant channel, bounded by the outside cladding surface and the hexcan wall. This channel contains initially liquid sodium and sodium vapor.
3. The heat-transfer and melting/freezing model, describing the solid fuel-pin stubs, which separate the outer channel from the inner cavity.

A typical LEVITATE configuration illustrating some of the recently introduced models is presented in Fig. 16.1-1. Other features presented in this figure are introduced below.

16.1.2.1 Fuel-pin Disruption and In-pin Fuel Motion

As the loss-of-flow accident proceeds, the inside of the fuel pin begins to melt, leading to the formation of an internal cavity. This cavity is filled with a mixture of molten fuel and fission gas, and expands continuously, both radially and axially, due to fuel melting. The fuel-gas mixture in the cavity is pressurized due to the presence of fission gas and fuel vapor. As the cavity walls continue to melt and the cladding temperature approaches the melting point, this continued pressurization of the cavity leads to fuel-pin failure, as illustrated in Fig. 16.1-2. Based on the mechanism of fuel-pin failure, two disruption modes are currently modeled in LEVITATE.

1. Total disruption of the fuel pin at a certain axial location. When a large fraction of the pin has become molten at a certain axial location and the cladding is no longer effective in restricting radial motion, the fuel pin is totally disrupted. In this case, the area previously occupied by pins becomes part of the coolant channel and only the two fuel-pin stubs remain, as shown in Fig. 16.1-1. The flow of molten fuel and fission gas inside the stubs continues to be described by a hydrodynamic model. As exemplified in Fig. 16.1-1, this mode of disruption leads to significant area changes in the coolant channel. This situation has made necessary an accurate treatment of abrupt area changes in the hydrodynamic modeling.
2. Mechanical cladding failures at a certain axial location. If a large fraction of the fuel is still in a solid state, the initial geometry of the fuel pin remains intact. However, due to low cladding resistance and a higher pressure inside the pin than in the coolant channel, molten fuel and fission gas from the pin cavity are ejected into the coolant channel through a cladding rupture.

Due to the fuel-pin failure, the inner cavity is connected to the coolant channel which is at a significantly lower pressure, and the molten fuel inside the pin is accelerated rapidly toward the pin failure location. This motion is modeled by the in-pin hydrodynamic model. An ejection model transfers molten fuel and fission gas from the pin cavity to the coolant channel, thus connecting the two main hydrodynamic models.

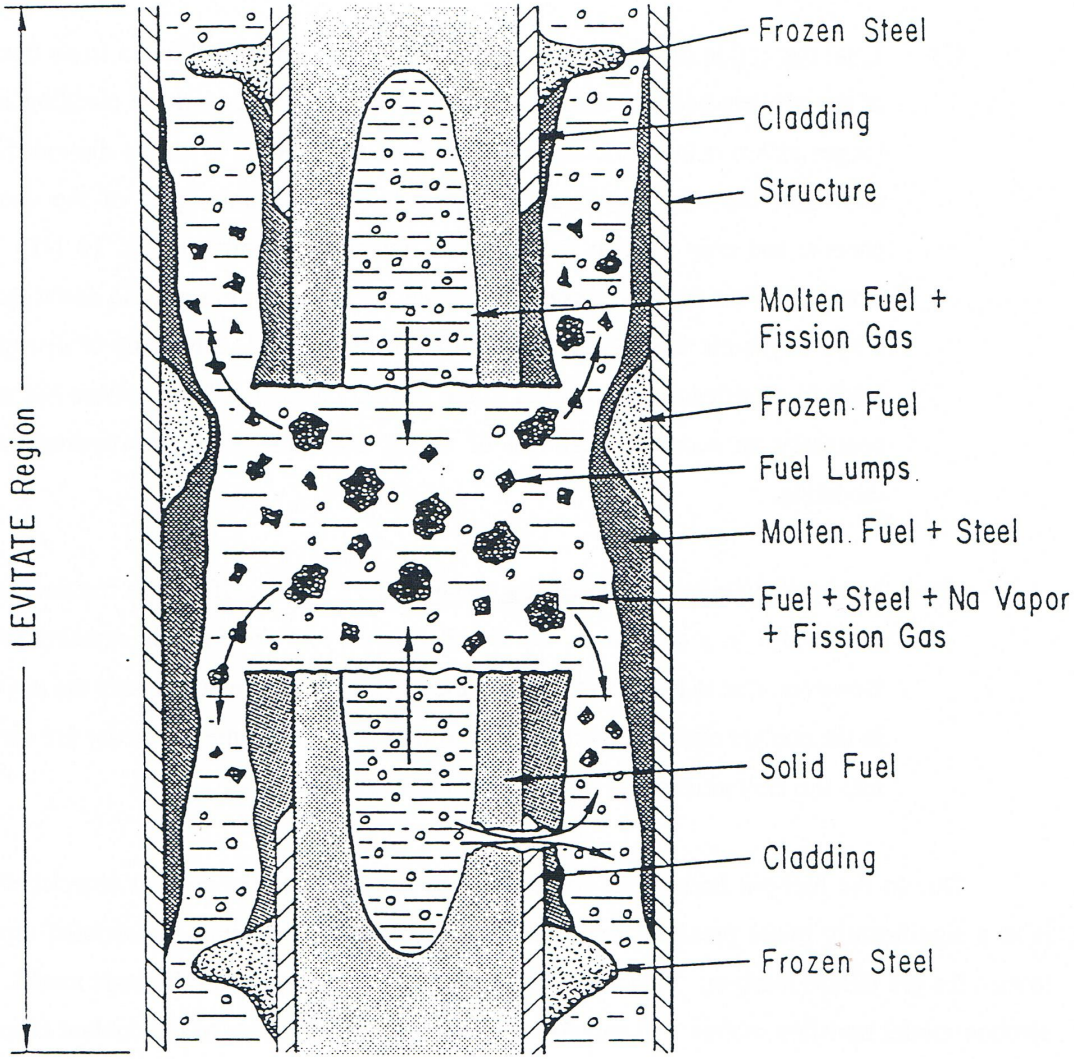

Fig. 16.1-1: Typical LEVITATE Configurations Fuel-pin Cavity Formation

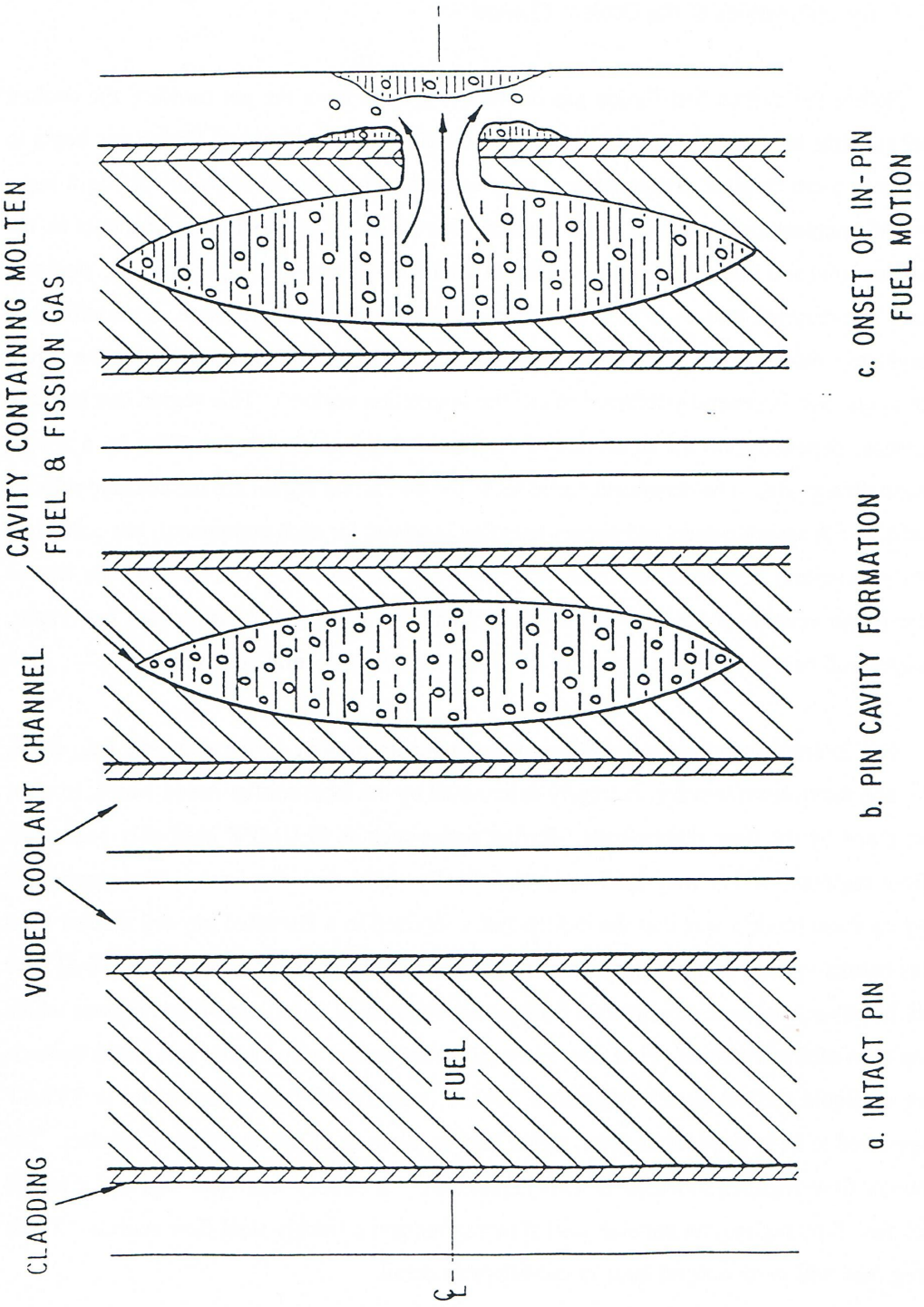

Fig. 16.1-2: Fuel Pin Cavity Formation

16.1.2.2 Hydrodynamics of the Coolant Channel

Before the molten fuel-fission gas mixture is ejected from the pin cavities, the coolant channel contains only sodium and perhaps molten steel; but as the fuel and fission gas begin to interact with these original components, a very complex situation develops, involving a large number of components that have to be tracked separately. The moving components in the channel are solid and liquid fuel, solid and liquid steel, fission gas, and vapors of fuel, steel and sodium. The material motion is described by a multi-component, multi-phase, nonequilibrium hydrodynamic model. The region described by this model is bounded axially by the liquid sodium slugs, and is generally referred to as "the interaction region". This region can increase or decrease, depending on the dynamics of the liquid slugs which are described by a simple incompressible model. The dependent variables in the interaction region are the density, velocity and enthalpy. A separate mass and energy equation is solved for each component, but only three coupled momentum equations for three velocity fields are solved. The components treated together in the velocity fields are: (a) liquid fuel and liquid steel, (b) fission gas, fuel vapor, steel vapor and two-phase sodium and (c) solid fuel chunks and solid steel chunks.

The interaction between the different components present in the channel, i.e., mass, energy, and momentum transfer, is largely determined by the local configuration which, in turn, is determined by the flow regime used. Earlier codes such as SLUMPY used only particulate fuel flow regimes, which may lead to unrealistically rapid fuel dispersal. The assumption underlying these models was that the molten fuel contained in a disrupted pin cell ejected from the pins breaks up into droplets upon entering the coolant channels. Tentner et al. [16-6] have argued, however, that such a particulate flow cannot be justified in sodium-voided regions which develop soon after pin failure. First, there is no apparent reason why molten fuel which contacts little or no liquid sodium should fragment. Second, most of the frozen fuel found in TREAT tests appeared to be in continuous form, rather than in the form of rounded frozen droplets. The continuous flow regimes modeled in LEVITATE are: a bubbly fuel flow regime, a partial annular fuel flow regime, an annular steel flow regime and a bubbly steel flow regime. These flow regimes will be described later in considerable detail.

16.1.2.3 The Freezing/Melting Models Describing the Solid Fuel-pin Stubs

At the axial locations where solid fuel pins are still present, the coolant channel is separated from the pin cavity by the cladding and the remaining solid fuel. The temperature field in the cladding and fuel is calculated by a transient heat-transfer model, using the temperatures in the channel and cavity as boundary conditions. Continuous melting occurs at the fuel pin cavity boundary, leading to an increase in cavity diameter and addition of molten fuel and fission gas to the moving components in the cavity. The situation is more complicated at the channel boundary. It has been previously argued that, in the sodium-voided regions which develop during a loss-of-flow situation, continuous fuel flow regimes are likely to exist. Under these conditions, the molten-fuel/cladding interface temperature usually falls between the freezing temperatures of these substances, resulting in solidification of the initially molten ceramic fuel and melting of the initially solid steel. The assumption which was

generally made in the modeling of the simultaneous fuel freezing steel melting phenomena was that the frozen fuel crust is mechanically stable and does not break up under the influence of fluid frictional shear or buoyancy forces [16-7]. However, experiments conducted by Spencer et al. [16-8] indicate that this is not the case for the flow of molten fuel in pin bundles. In these experiments, significant steel ablation and fuel-steel mixing were observed that could not have occurred in the presence of a stable crust [16-9].

The fuel-freezing model used in LEVITATE allows for the formation of a partial fuel crust when the temperature of the fuel in the channel drops below an input freezing temperature. This input temperature is always between the liquidus and solidus temperatures.

When the dominant component in the channel is molten steel, steel freezing can occur, leading to the formation of steel plugs.

The temperature of the fuel crust, at any given location, is calculated by the heat-transfer model. Depending on its temperature and other local conditions, which will be described in detail later, the fuel crust can continue to grow, can start to remelt or can break up when the underlying cladding begins to melt.

16.1.2.4 Geometry Description and Interaction among LEVITATE Models

The geometry modeled in LEVITATE is illustrated schematically in Fig. 16.1-3, which will also be used to describe the interaction of the physical models described previously.

LEVITATE calculates all the thermal hydraulic events that occur in a pin subassembly. The subassembly is bounded axially by the lower and upper plena. Although only one pin is shown in Fig. 16.1-3, LEVITATE will account for the appropriate number of pins per subassembly, as specified in the input description. The hydrodynamic in-pin calculations are performed on a mesh grid using the subscript K, having the origin at the bottom of the lower blanket. The top node of the upper blanket is indicated by the variable MZ. The active fuel core extends from KCORE1 to KCORE2. The fuel pin cavity, which increases gradually both radially and axially, cannot extend beyond the active core boundaries. The disrupted pin region extends from KDISBT to KDISTP. The hydrodynamic coolant channel calculations as well as the freezing and melting calculations are performed on a mesh-grid using the subscript I, with the origin at the bottom of the fuel pins. The integer IDIFF indicates the offset between the I and K grids, i.e.,

$$I = K + IDIFF \tag{16.1-1}$$

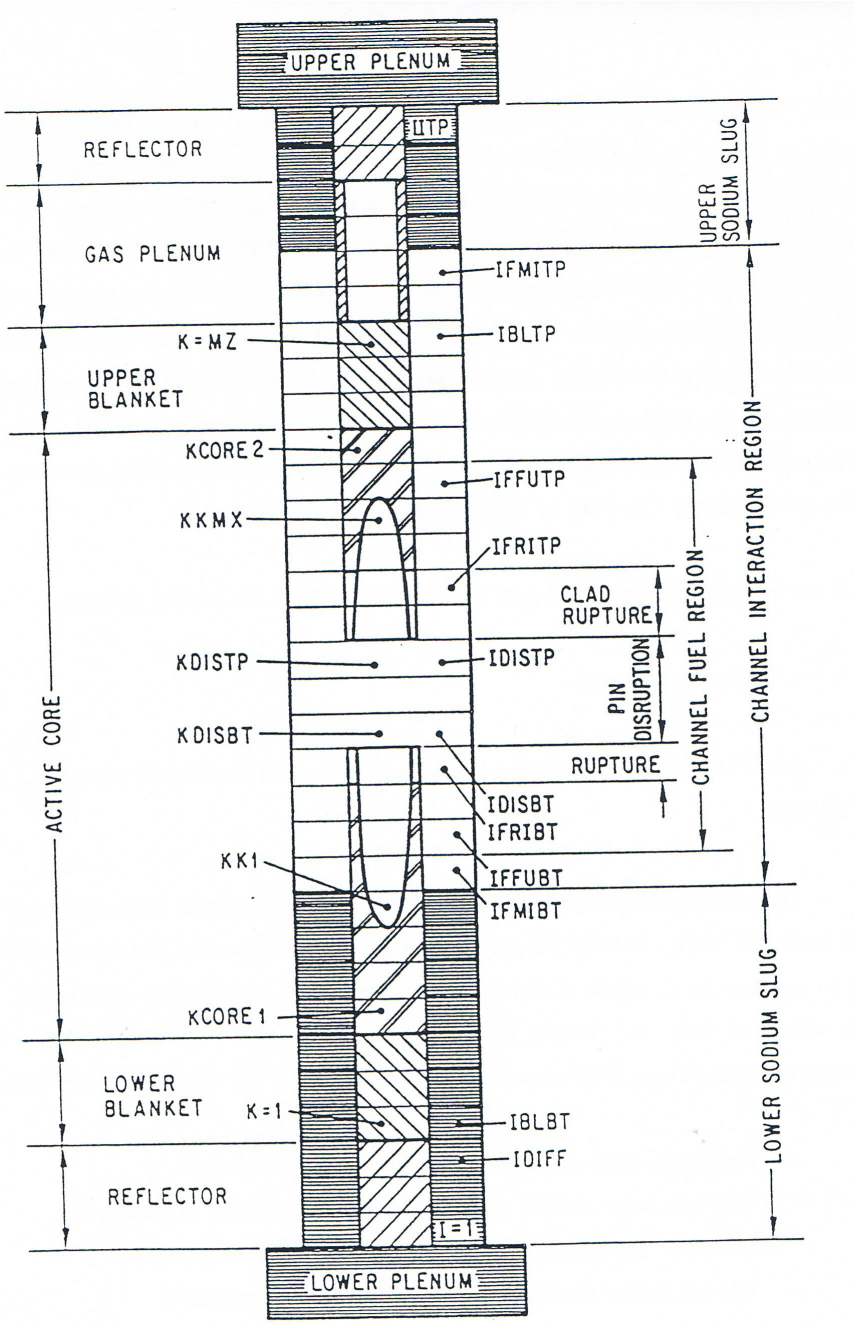

Fig. 16.1-3: Geometry Modeled by LEVITATE

The top node in the subassembly and in the LEVITATE domain is indicated by the variable IITP. The hydrodynamic and melting/freezing models, however, operate only in the interaction region, which extends from IFMIBT to IFMITP. This region is bounded axially by the lower and upper sodium slugs and can expand or contract depending on the dynamics of the slugs. The slug motion is determined by the pressure difference acting on them, e.g., the lower slug motion is determined by the pressure difference between the cell IFMIBT and the lower plenum. The slug motion is calculated by an incompressible model to be described later. Each material component is restricted to its own region, with moving boundaries which are tracked continuously. The procedure reduces significantly the undesirable numerical diffusion effects. Figure 16.1-3 illustrates only the liquid fuel region, which extends from the cell IFFUBT to IFFUTP. The pin disrupted region extends from the cell IDISBT to IDISTP, corresponding to the integers KDISBT and KDISTP on the K grid. The cladding rupture extends from IFRIBT to IDISBT-1 and from IDISTP+1 to IFRITP. If no pin disruption is present, the cladding rupture extends from IFRIBT to IFRITP. It is noted that IFRIBT and IFRITP are the lowermost and uppermost cells with a cladding rupture but that it is not necessary that all the intermediate cells exhibit a cladding rupture, although this is generally the case. The in-pin hydrodynamic model is connected to the coolant channel hydrodynamic model via the ejection process. Fuel and fission gas can be ejected from the cavity into the channel either via the cladding rupture or, when the pins have been disrupted, via the open ends of the remaining pin stubs. These ejection processes are described by appropriate physical models.

16.1.3 Interaction of LEVITATE with Other Models within the SAS4A System

16.1.3.1 LEVITATE Initiation

LEVITATE can be initiated by only two routines of the SAS4A code, i.e., FUINIT and PLUTO2.

The initiation of fuel motion is decided, for any given channel, in the routine FAILUR, called from TSTHRM. If FAILUR predicts the onset of fuel motion, the module FUINIT is called to prepare the transition to the fuel motion modules, LEVITATE or PLUTO2, and to decide which of these two models should be used (Fig. 14.7-1 in Chapter 14). Several conditions characteristic of LOF situations have to be met for the initiation of LEVITATE:

- Pin failure must occur after sodium boiling has occurred.
- Only one large sodium vapor bubble must be present in the coolant channel. The bubble must extend over at least four axial cells.
- The pin failure should be located within the vapor bubble.

The objective of these constraints is to insure that the pin failure occurs in a largely voided region, where the LEVITATE models are valid. If, however, the pin failure occurs in a region containing significant amounts of liquid sodium, PLUTO2 should be initiated. In such a case, the molten fuel is likely to fragment into droplets upon contact with the sodium, leading to the more rapid fuel sweepout characteristic of TOP situations. This type of event is modeled in PLUTO2, but not in LEVITATE. If any of the above

conditions are not met, the PLUTO2 fuel motion model will be initiated by FUINIT. One particular case must be noted. If two or more bubbles are present, a check is made for the presence of a dominant voided region. If such a region is found (length of voided region/length of boiling region >0.7), a flag is set (ILEPLI = 1), which will then be used in PLUTO2, as described below. Control is still transferred to PLUT02, whether or not a dominant bubble has been found.

When LEVITATE is initiated in FUINIT, an interface routine, LESAIN, is called to prepare all variables characteristic for LEVITATE. If the steel motion module, CLAP, was operational prior to LEVITATE initiation, an additional interface routine, LECLIN, is called from FUINIT. LECLIN is used to translate the CLAP steel-related variables to LEVITATE variables. Then two initialization routines, common for LEVITATE and PLUTO2, are called: PLINPT and PLSET. At the same time the flag ICALC used in TSTHRM is set to 2 [ICALC(ICH)=2] the value reserved for LEVITATE. Control is then returned to TSTHRM, which checks on ICALC(ICH) to decide which model has to be used in channel ICH.

The other path for LEVITATE initiation is via PLUTO2. Although some accident sequences can begin as TOP situations in any given channel, eventually the presence of the molten fuel in the coolant channel leads to a disrupted geometry, requiring the use of LEVITATE. The PLUTO2 module checks at the end of each primary time step whether or not control should be transferred to LEVITATE. Control should be transferred to LEVITATE whenever the original bundle geometry has to be changed due to steel ablation or possible pin disruption. Control is also transferred to LEVITATE whenever the fuel vapor pressure in the channel becomes significant. PLUTO2 does not model geometry changes due to ablation or pin disruption, and the fuel vapor is not currently included in the PLUTO2 channel hydrodynamic model.

The criteria for the transfer are as follows:

- Three or more axial cladding cells (see the input variable NCPLEV) are completely molten, indicating that steel ablation and fuel-steel mixing should occur, or
- The temperature of the molten fuel is above 4000 K, indicating the presence of a significant fuel vapor pressure, or
- The flag ILEPLI is found to have the value 1, indicating the presence of an initial large voided region.

When any of these criteria is satisfied, the flag ICALC(ICH) is set to 2, and a number of LEVITATE variables not used in PLUTO2 are set by executing LEPLIN. Control is then returned from PLUTO2 to TSTHRM, which will transfer control to LEVITATE. The relationship between LEVITATE and other SAS4A modules is illustrated schematically in Fig. 16.1-4.

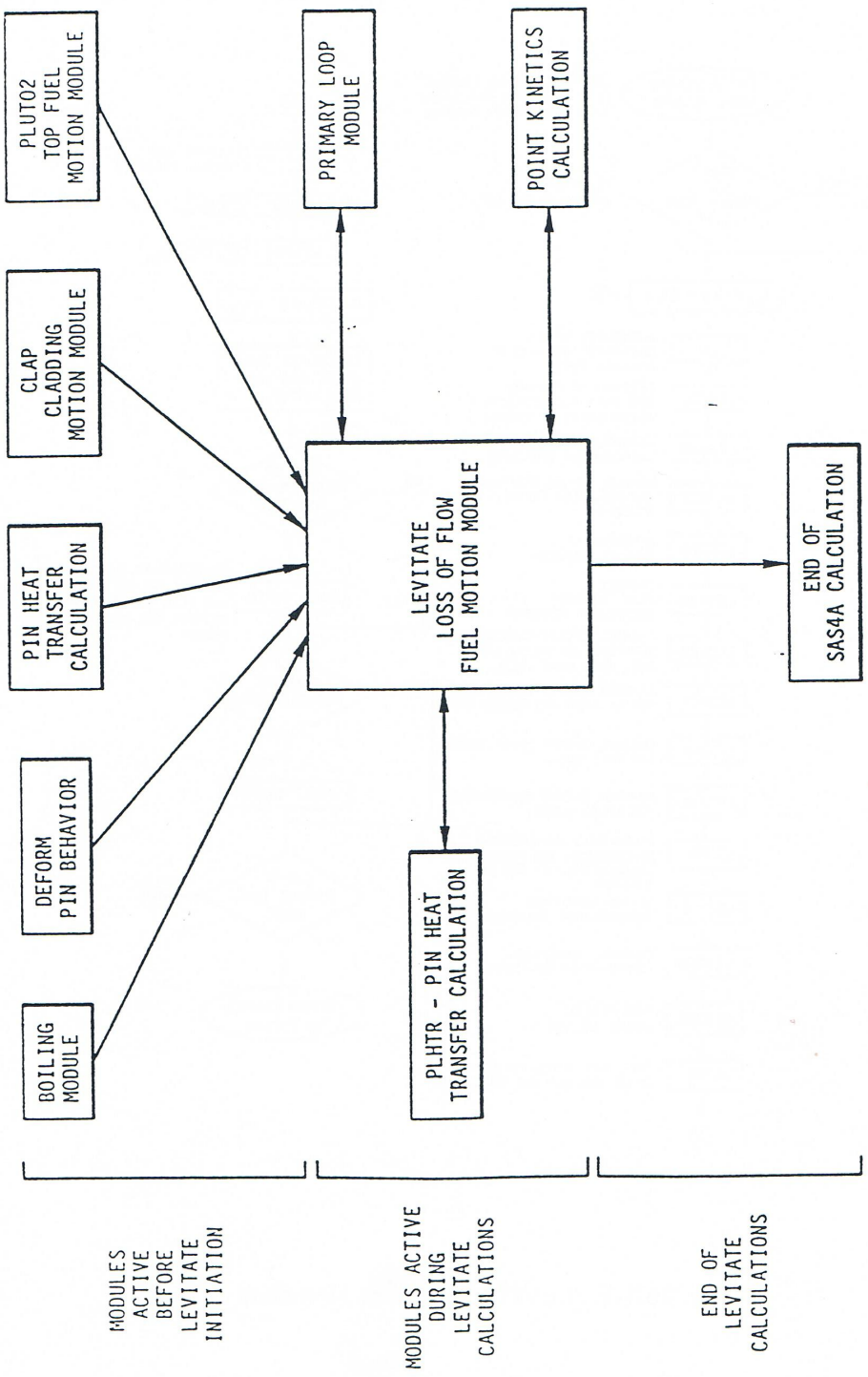

Fig. 16.1-4: Relationship between LEVITATE and Other SAS4A Modules

16.1.3.2 LEVITATE Calculations

Once the LEVITATE initialization routines have been executed and the flag ICALC (ICH) has been set to 2, the SAS4A transient driver TSTHRM will transfer control to the LEVITATE driver routine LEVDRV. LEVDRV will retain control and advance the solution in the channel ICH until the end of the primary loop time step is reached. It should be noted that once LEVITATE is initiated, the coolant time step is set equal to the primary-loop time step and these two steps can be used interchangeably. The flow chart in Fig. 16.1-5 shows the logic of the LEVITATE driver.

First LEVDRV will execute LESET2. This subroutine initializes all temporary integers and arrays. These are values that can be calculated using the permanent quantities. They are kept only as long as LEVDRV retains control in the channel ICH. The solution is then advanced in the channel ICH by calling a sequence of subroutines from LEIF through LEDISR. The solution for the hydrodynamic in-pin model and the ejection of material from the pin cavities into the coolant channel are obtained in the routines LElPIN and LE2PIN. All the other routines in the sequence mentioned above are used to model the thermal and hydrodynamic processes which occur in the coolant channel.

Next, the LEVITATE driver routine determines the maximum time step acceptable for the coolant channel calculation in the next cycle. This value is compared with the maximum time step calculated for the in-pin model in LE2PIN, and the smaller of the two will be the LEVITATE time step for the next calculational cycle. It is noted that the LEVITATE time step is not allowed to exceed the time remaining until the end of the heat-transfer time step. If this happens, the LEVITATE time step will be cut back, so that the end of the next LEVITATE time step will coincide with the end of the heat-transfer time step. The next task of LEVDRV is to calculate the data for the fuel, steel and sodium reactivities. These calculations are described in more detail in the next section on LEVITATE interaction with the FEEDBK routine.

If the end of the LEVITATE time step coincides with the end of a heat-transfer time step the PLHTR routine is called. This routine calculates the new temperatures in the solid fuel pin and in the cladding outside the interaction region at the end of the current heat transfer time step. Then a new heat transfer time step is calculated.

If it is time to produce output, LEVDRV will print the output described in Section 16.9. Then if the end of the LEVITATE time step does not coincide with the end of the primary loop time step, a new computational cycle begins. Otherwise LEVDRV returns control to TSTHRM.

16.1.3.3 LEVITATE Interfaces

During the time period when LEVITATE performs calculations in a given channel, it interacts with the PRIMAR hydrodynamic model, the PLHTR heat transfer model, and the FEEDBK reactivity model (Fig. 16.1-4).

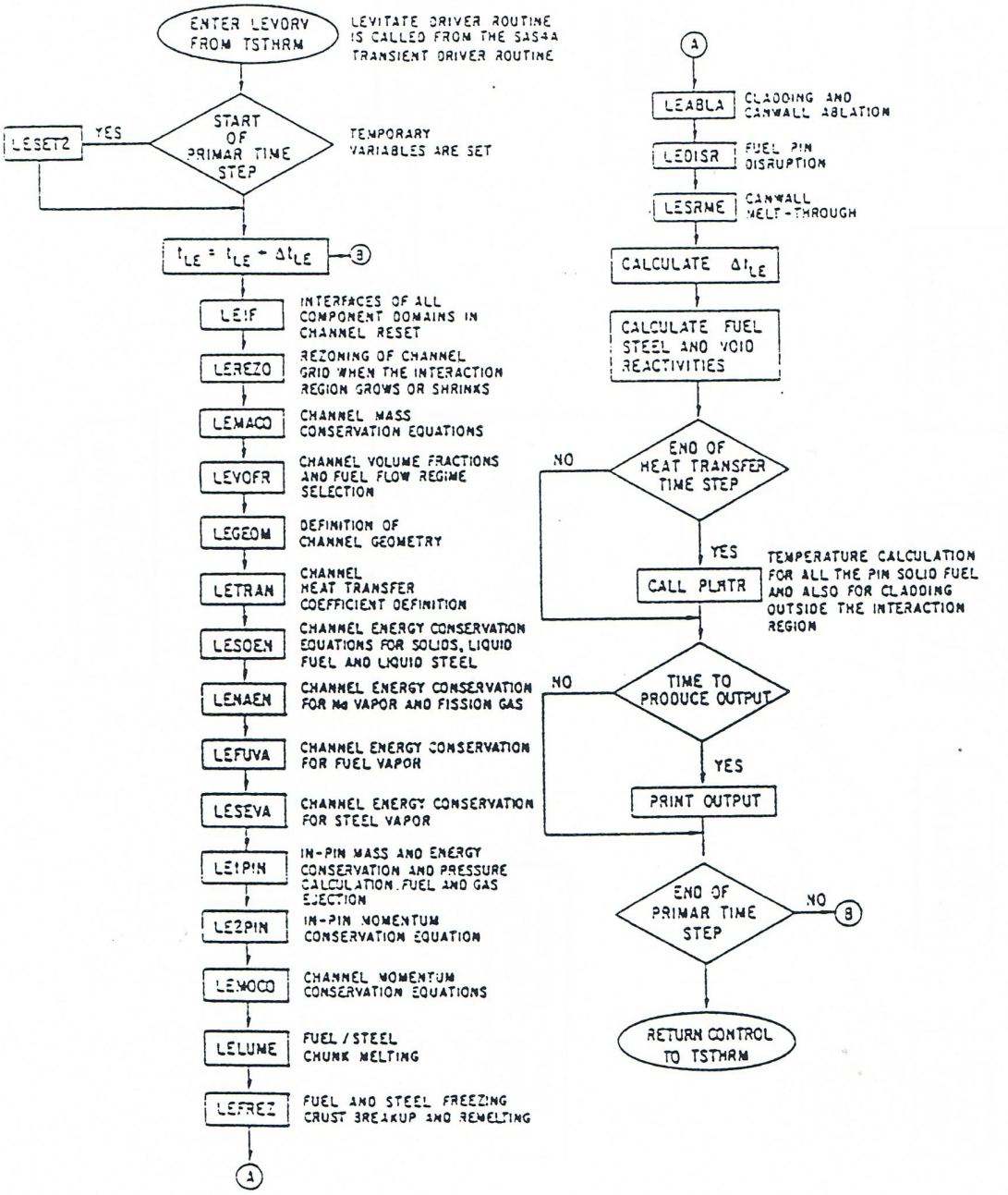

Fig. 16.1-5: LEVITATE Driver Flowchart

16.1.3.3.1 LEVITATE Interface with the PRIMAR Hydrodynamic Model

PRIMAR calculates the hydrodynamic behavior of the sodium loop outside the reactor vessel. Two options are now available, PRIMAR-1 and PRIMAR-4. PRIMAR-1, which can be selected by setting the input IPRION equal to 0, calculates the inlet and outlet sodium pressures, using the pump flow decay curve, without accounting for the pressure events occurring in the LEVITATE region. Thus, no feedback is returned from LEVITATE to PRIMAR-1. LEVITATE uses the pressures calculated by PRIMAR-1, together with the pressures in the voided region to model the motion of the liquid sodium slugs which bound the voided region. The quantities PREX and PRIN, which in LEVITATE designate the upper and lower plenum pressures, respectively, are set in LEVDRV, using the pressures PX and PIN received from PRIMAR-1. PRIMAR-4 is a more sophisticated model, which accounts for the events calculated by LEVITATE. LEVITATE receives the inlet and outlet pressures from PRIMAR-4, as well as the time derivatives of these pressures. This information is used to determine the behavior of the sodium slugs. It also integrates the mass flow rates for the two slugs over the PRIMAR-4 time step and returns this information to PRIMAR-4. These calculations are performed in the LEVITATE routine LEMOCO, after solving the momentum conservation equations. The PRIMAR-4 model can be selected by setting the input variable IPRION equal to 4.

16.1.3.3.2 LEVITATE Interface with the PLHTR Heat-Transfer Module

PLHTR calculates the temperature transients in the fuel pin. As such, it interfaces with LEVITATE at the pin cavity surface and at the outer fuel-pin surface.

A heat flux, based on the temperature difference between the temperature of the pin inner node and the cavity temperature and an appropriate heat-transfer coefficient is calculated in the routine LElPIN. This flux is then used in LEVITATE as a boundary condition to calculate the fuel temperature in the pin cavity. The same flux is integrated over the heat-transfer time step and the resulting energy HFCAWA is then made available to the PLHTR module, for use as the boundary condition on the cavity side in the transient pin temperature calculation.

A similar heat flux, based on the temperature difference between the fuel-pin outer node and the inner node of the cladding is calculated in the LEMISC routine. The heat-transfer coefficient used is generally based on the gap conductance. A more complex situation exists when the cladding has been completely ablated at a certain axial location. In this case, the fuel is in direct contact with the materials in the channel, and the heat-transfer coefficient and temperature difference used are dependent on the local configuration. The heat flux calculated is then used as a boundary condition in LEVITATE for the calculation of the transient cladding temperature, or, when the cladding has been ablated, for the calculation of the temperatures in the channel. This heat flux is also integrated over the heat-transfer time step, and the resulting energy, HFPICL is then returned to the PLHTR module, where it is used as the outer-pin boundary condition in the transient pin temperature calculation.

16.1.3.3.3 LEVITATE Interface with the FEEDBK Reactivity Model

FEEDBK calculates the net reactivity changes for the whole reactor during a time step and transfers this information to the neutronic model which calculates the changes

in the reactor power. LEVITATE calculates the sodium, fuel and steel axial mass distributions for the SAS4A channel under its control at the end of each time step. In other channels, these masses can be updated by other modules, e.g., PLUTO2, which have control at the given time. The transient axial mass distributions are used in subroutine FEEDBK to calculate the coolant void, cladding motion, and fuel motion reactivity feedbacks. When all channels have been calculated, the material relocation reactivities are used in FEEDBK, together with the Doppler reactivity, to determine the total reactivity of the core. Using this information, the neutronic model determines the new power level which is used by LEVITATE in the following time step. The power level at the end of each LEVITATE time step is determined in LEVDRV, using an exponential fit of the power-time history supplied by the neutronic model. This fit is based on the power level at the beginning of the previous main time step, the power level at the beginning of the current main time step and the precalculated power level at the end of the current main time step. By using this calculated power level and the axial input power distribution, the specific power for each axial cell is calculated.

16.1.3.4 LEVITATE Termination

At the present time, LEVITATE is the last phenomenological module called by SAS4A. Thus the decision to terminate a SAS4A run will generally be made in LEVITATE. This decision is made in the routine LEABLA, where the number of completely molten hexcan wall cells are counted. If this number $N_{sr,melt}$ is greater or equal to an input specified number, NSLEEX, LEVITATE will print an explanatory message and will terminate the calculations. The reason behind this is that once the hexcan walls have been totally molten at a certain axial location it is likely that inter-channel lateral material exchanges will be initiated, i.e., a transition-phase domain is being entered that is not modeled in SAS4A.

Other possibilities to terminate the SAS4A calculations, which are not necessarily specific to LEVITATE are: (a) exceeding the maximum number of main time steps in the transient calculation MAXSTP; (b) exceeding the maximum problem time TIMAX; and (c) decreasing the fuel motion reactivity below the input value NFUELD.

16.1.4 Improvements and New Models Relevant to the LEVITATE Module in SAS4A Version 1.1

This section describes the differences between the LEVITATE module present in the SAS4A Release 1.1 version and that used in the SAS4A Release 1.0.

The most important enhancement to the LEVITATE Release 1.1 is the availability of the chunk model, which describes the formation and relocation of solid fuel and/or steel chunks. Although the chunk model was described in the documentation to Release 1.0, the actual code did not incorporate this capability which was still being tested at the time of release. The chunk modeling capability has been fully integrated in the Release 1.1 LEVITATE module. However, the user should be aware that this model has not yet been validated by experiment analysis and its results should be used cautiously at this time.

The chunk model can be switched on by setting the input variable ICHUNK=1 (Blkl/Loc 47). If ICHUNK is set to zero, the chunk model is completely disabled and the code will work in the same manner as in Release 1.0, i.e., will homogenize the moving solid fuel with the liquid fuel in the channel. The new input variables relevant for the chunk model are ICHUNK (Blk 1/47), ILUBLK (Blk 1/48), ASRALU (Blk 13/1280), RALUDI (BLk 13/1284) and RALUFZ (Blk 13/1285). These variables are described in Table 16.8-1.

Another feature added to the current LEVITATE version is the presence of a partial annular steel flow regime. This flow regime is described in Section 16.4.1.4. The partial annual steel flow regime is used only when the chunk model is used, i.e., ICHUNK=1. If ICHUNK=0 the full annular flow regime is still used. It should be noted here that the annular steel flow regime becomes more important when the chunk model is used, because the frozen fuel can separate from the molten fuel-steel field, leading to the presence of more cells characterized by the steel annular flow regime.

A mechanistic model describing the ejection of the molten fuel from the pin cavity into the coolant channel has also been added to the LEVITATE module. This model is optional and can be used by setting the input variable INRAEJ=1. The velocity of the ejected fuel is calculated using a radial momentum conservation equation. The radial momentum can also be convected axially, in axial cells where the cladding failure has occurred.

A complete calculation of the sodium and structure temperatures in the sodium slug region has also been added and the corresponding temperature map is now part of the LEVITATE regular output.

16.2 In-pin Hydrodynamic Model

16.2.1 Physical Models

The in-pin hydrodynamic model describes the motion of the molten fuel and fission gas mixture in the cavity formed inside the fuel pins during a loss of flow accident. As the accident proceeds, the size of the cavity increases, both radially and axially (Fig. 16.1-2). Newly molten fuel and fission gas are added to the moving components in the cavity. Some of the fission gas is dissolved in the molten fuel, in the form of small bubbles constrained by surface tension. The effect of this fission gas is controlled by the input variable PRSFTN. If PRSFTN is less than 10^7, the volume of the dissolved gas is assumed to be negligible, and thus it does not contribute immediately to the cavity pressure. If PRSFTN > 10^7, the volume occupied by the dissolved gas is taken into account in the cavity pressure calculation, as described in Section 14.2.6. The remainder of the fission gas is in the form of free gas, residing in bubbles that are too large to be constrained by surface tension. This gas contributes immediately to the pressurization of the cavity. Because of the continuous coalescence of the small bubbles, leading to the formation of new larger bubbles, the originally dissolved gas is continuously released from the molten fuel and is added to the free fission gas. The continuous heating of the molten fuel and fission gas leads to the pressurization of the cavity and eventually to the cladding failure. The fuel and fission gas in the vicinity of

the failure location are ejected into the coolant channel leading to a local depressurization of the cavity. This depressurization causes the fuel motion inside the pin toward the failure location.

The in-pin fuel motion is treated as a one-dimensional, compressible flow with a variable flow cross section. The fuel and fission gas are assumed to form a homogeneous mixture in thermal equilibrium. However, if the local fuel volume fraction is less than an input value FNFUAN, the pressure gradient is assumed to act only on the fuel cross section. This is an attempt to roughly account for the annular fuel flow regime which may exist for large void fractions. Fuel vapor pressures are also included in the in-pin hydrodynamic model. The fuel vapor pressure is based on the average fuel temperature in any axial cell, with the assumption that no significant radial temperature profiles can be maintained after the onset of fuel motion.

As the cladding heats up and the in-pin pressures increase, the cladding rip can propagate from the original location, allowing the ejection of fuel and fission gas from the cavity into the channel at new axial locations. The fuel pin can also be totally disrupted at certain axial locations where the cladding becomes very weak and the solid pin is largely molten. The pin disruption leads to the formation of upper and lower pin stubs with cavities that can eject fuel axially into the disrupted region.

16.2.2 Method of Solution and General Numerical Considerations

16.2.2.1 Variables and Mesh Grid Used in Calculations

The independent variables used in the in-pin model are the axial coordinate z and the time t. Only one spatial coordinate is necessary, as LEVITATE models the pin cavity in a one-dimensional geometry. The dependent variables calculated by the in-pin hydrodynamic model for each component are the generalized density ρ′, the enthalpy h (or temperature T), and the velocity u. The generalized densities have been introduced in Chapter 14.0 and, for the component j in the cavity, are defined as follows:

$$\rho'_{j,ca,k} = \rho_{j,ca,k} \cdot \frac{A_{j,ca,k}}{AXMX} = \rho_{j,ca,k} \cdot \theta_{j,ca,k} \qquad (16.2\text{-}1)$$

where

$\rho_{j,ca,k}$ is the physical density of component j at the axial location k in the pin cavity

$A_{j,ca,k}$ is the cross sectional area occupied by component j at location k in the pin cavity. This area refers to all the pins in the subassembly.

AXMX is the reference input area

$\theta_{j,ca,k}$ is the generalized volume (or area) fraction of component j at location k in the pin cavity

The mass, energy and momentum partial differential equations are solved using the Eulerian finite difference semi-explicit formulation, as explained in Section 16.2.2.2. A staggered mesh grid is used to obtain the numerical formulation, with the densities and enthalpies defined at the center of each cell while the velocities are defined at the boundaries. Variable flow areas are treated in the in-pin model. However, the cavity geometry is not as irregular as the coolant channel geometry, and the conventional single velocities were used at the boundaries, as opposed to the dual velocities used in the coolant channel model (see Section 16.4.2.1). The components treated in the cavity model are the molten fuel, the dissolved fission gas and the free fission gas. They are assumed to form a homogeneous mixture and move with the same velocity at all axial locations. A full donor cell formulation was used in the finite difference formulation in order to improve the stability characteristics of the solution.

16.2.2.2 Description of the Method of Solution and Logic Flow

The in-pin hydrodynamic model is solved in the routines LE1PIN and LE2PIN. First, the cavity enlargement is calculated in LE1PIN, using the solid fuel temperatures provided by PLHTR. If melting occurs, the quantities of molten fuel and fission gas to be added to the moving components are determined. Then the mass conservation equation is solved for all axial cells, accounting for the changes in fuel and free fission-gas mass due to convection and melt-in. LE1PIN then solves the energy conservation equations for the fuel and fission-gas mixture. It is assumed that the fuel and fission gas remain at the same temperature in all the axial cells. Using the new masses and temperatures, the new pressures are then calculated. It is noteworthy that at this point the pressures have also been updated in the channel (see Section 16.4.2.2) so that we can use a consistent set of pressures for the ejection calculation, which is the next step in the LE1PIN routine. The ejection calculation leads to changes in the mass and pressure in all nodes that are ejecting fuel and fission gas into the coolant channel. The ejection can take place radially, via the cladding rip or axially, via the open ends of the fuel-pin stubs when the fuel-pin disruption has already occurred. Both modes of ejection can be present simultaneously. The LE1PIN routine also examines the possibility of pin disruption. If an axial cell is found which has to be disrupted, a flag is set (IDISR(I)=9), but no other changes are preformed. The actual pin disruption is performed in the routine LEDISR, as described in Section 16.5.

The routine LE2PIN then solves the momentum conservation equation for all cells, obtaining the new velocities at the end of the time step. These velocities are obtained by using the new pressures calculated in LE1PIN, and in this sense, the method of solution is mixed, explicit-implicit, rather than purely explicit. The routine LE2PIN also solves the mass conservation equations for the dissolved gas and calculates the maximum time step acceptable for the in-pin hydrodynamic model in the next computational cycle.

16.2.3 Finite Difference Forms and Solution Technique, Special Situations

The equations describing the in-pin hydrodynamic and thermal process are solved in the LE1PIN and LE2PIN routines. The partial differential equations, as well as the finite difference formulation, are generally the same in LEVITATE and PLUTO2. The

reader is referred to the PLUTO2 chapter (Section 14.2) for a detailed description of the equations. Only the features of the in-pin model that are specific to LEVITATE will be discussed here.

The main feature of LEVITATE is the fuel-pin disruption mode. The decision for disruption of a certain axial pin cell is made in the routine LE1PIN. An undisrupted cell will be disrupted if the molten fuel cavity covers a large fraction of the original pin cross section.

$$\frac{R_{ca,k}}{R_{pin,os,k}} > FNDISR \tag{16.2-2}$$

and the cladding is molten or close to melting, i.e.,

$$T_{cl,os,i} > T_{se,so} \tag{16.2-3}$$

and:

$$T_{cl,in,i} > T_{se,so} - 50 \quad \text{if } \Delta R_{cl,k} > 0.5 \cdot \Delta R_{cl}^{0} \tag{16.2-4}$$

or:

$$T_{cl,in,i} > T_{se,so} - 150 \quad \text{if } 0 < \Delta R_{cl,k} < 0.5\ \Delta R_{cl}^{0} \tag{16.2-5}$$

The disruption of one or more axial pin nodes leads to the formation of a disrupted region, extending from the cell IDISBT to IDISTP. Note that the axial position of the in-pin cells is denoted in Eq. 16.2.1 by the subscript k, while the subscript used in the channel is i. The correspondence between i and k is given below:

$$i = k + IDIFF \tag{16.2-6}$$

that is, the in-pin cell k will have the same axial location as the channel cell k + IDIFF.

The motion of the material present in this region is calculated by the coolant channel hydrodynamic model. In the disrupted region, the coolant channel covers the entire cross sectional area of the subassembly. Only one disrupted region is allowed in LEVITATE. Thus, if two or more disjoint disrupted regions appear at any given time (e.g., cells 8 and 10 are disrupted, but not 9), the undisrupted nodes between the regions will also be forced to disrupt. In this case, a message is printed indicating that one or more nodes have been disrupted due to the disruption of neighboring nodes and the formation of large fuel/steel chunks is likely to occur. Only the decision about disruption is made LE1PIN. The nodes to be disrupted are flagged (IDISR(I)=9), but the disruption process will only be modeled later in the cycle, in the routine LEDISR. This process is described in Section 16.3.

After the occurrence of the fuel-pin disruption, the model describing the hydrodynamics of the molten fuel/fission gas in the pin cavity continues to operate. However, instead of modeling a continuous channel, it now describes the hydrodynamic behavior of two disjoint channels, i.e., the cavities remaining in the upper and lower undisrupted pin stubs. These cavities communicate directly with the channel via the open ends of the pin stubs. The channel pressure in front of these open ends is used as the boundary condition for the in-pin hydrodynamic model.

16.3 Fuel Ejection from the Pins and Fuel-pin Disruption

The hydrodynamic in-pin model is connected to the channel model via the mechanisms of molten fuel ejection into the channel and fuel-pin disruption. The models describing these processes are described below.

16.3.1 Fuel Ejection via a Cladding Rupture

The molten fuel/fission-gas mixture can be ejected from the pin cavity into the channel in any axial cell where a cladding rupture has already occurred. The original cladding failure location is determined in the routines FAILUR and FUINIT, just before LEVITATE is initiated. Once control passes to LEVITATE, additional nodes can fail, leading to the increase of the original failure and, occasionally, the initiation of new failures. Thus, two or more disjoint failures can be present in a channel under certain circumstances. The fuel-pin rip enlargement is performed in the routine LEIF.

The stress in the cladding in the axial cell is calculated as follows:

$$\sigma_{cl,i} = \frac{P_{ca,k} \cdot R_{ca,k} - P_{cl,i} \cdot R_{cl,os,i}}{\Delta R_{cl,i}} \tag{16.3-1}$$

The ultimate tensile strength for the cladding is calculated using the function $\sigma^U(T)$ for each radial cladding node in the axial cell i:

$$\sigma^U_{cl,i} = \frac{\sigma^U\left(T_{cl,os,i}\right) \cdot \left(R_{cl,os,i} - R_{cl,in,i}\right) + \sigma^U\left(T_{cl,in,i}\right) \cdot \left(R_{cl,in,i} - R_{cl,is,i}\right)}{\left(R_{cl,os,i} - R_{cl,is,i}\right)} \tag{16.3-2}$$

The rupture will be extended to cell i if:

$$\sigma_{cl,i} > \sigma^U_{cl,i} \tag{16.3-3}$$

during any time step. All the nodes in the LEVITATE region are scanned every cycle. Once the rupture has occurred in one axial node, that node will continuously be checked for fuel ejection in each cycle.

The ejection of the molten fuel from the pin cavity into the channel is performed in the LE1PIN routine. Only the nodes where the cladding has been ruptured can eject fuel. Ejection will occur in these nodes if:

$$P_{ca,K} > P_{ch,i} \tag{16.3-4}$$

and

$$\alpha_{fu,ca,k} = \frac{\theta_{fu,ca,k}}{\theta_{ca,k}} > 0.1 \tag{16.3-5}$$

An additional constraint, designed to avoid numerical problems related to a fully incompressible channel configuration, is:

$$\frac{\left(\theta_{ch,i} - \theta_{ch,op,i}\right) + \theta_{fu,i} + \theta_{se,i} + \theta_{fu,i}}{\theta_{ch,i}} \leq 0.95 \tag{16.3-6}$$

i.e., the volume fraction of the incompressible components (crust, fuel, steel, and chunks) should not be more than 95% of the original channel volume. If all the conditions 16.3-4 through 16.3-6 are satisfied, the injection calculation begins by calculating the in-pin pressure after injection. An estimate of the amounts of fuel that can be ejected during a typical LEVITATE time step indicated that at the time of failure, the limiting factor in the ejection process is the inertia for the molten fuel. For the time steps usually used in LEVITATE (approximately $2 \cdot 10^{-5}$ s) and the typical conditions for a loss-of-flow situation, where the coolant channel is voided, it was found that the pressure in the pin cavity will decrease initially by about 0.5% of the pressure difference between the cavity and the channel. However, the fuel in the cavity can be accelerated laterally quite rapidly, and the inertial constraint becomes insignificant within a few milliseconds of the failure time. Afterwards, the ejection process is rapid enough to equilibrate the pressures in the cavity and channel within one or two typical LEVITATE time steps.

$$P_{ca,k}^{n+1} = P_{ca,k}^{n} - \left(P_{ca,k} - P_{ch,i}\right) \cdot CIPINJ \cdot DTPLU \tag{16.3-7}$$

The input constant CIPINJ has the recommended value $2.5 \cdot 10^4$. For this value of CIPINJ, the product CIPINJ · DTPLU has the value 0.5 and the pressure difference between the cavity and the coolant channel will be equilibrated very rapidly. This model does not account for the inertial effects mentioned above, which are present for a short time after the failure has occurred. A more mechanistic model accounting for these effects is currently being developed. With the assumption that the fuel, fission gas and fuel vapor in the axial cell k are homogeneously mixed, we can now calculate the amount of fuel which has to be ejected from the cavity in order to establish the pressure $P_{ca,k}^{n+1}$:

$$\begin{aligned}\Delta\rho'_{fu,k} = &\left\{\left[\theta_{fi,ca,k} - \theta_{fu,ca,k} \cdot CMFU \cdot \left(P_{ca,k} - P_{fv,ca,k}\right)\right] \cdot P_{ca,k}\right. \\ &\left. + \left(R_{fi} \cdot \rho'_{fi,ca} + R_{fv} \cdot \rho'_{fv,ca,k}\right) \cdot T_{fu,ca,k}\right\} \cdot \rho_{fu,ca,k} \\ &\div \left(P_{ca,k} + f_{fi,fu,k} \cdot R_{fi} \cdot T_{fu,ca,k} \cdot \rho_{fu,ca,k}\right. \\ &\left. + f_{fv,fu,k} \cdot R_{fv} \cdot T_{fu,ca,k} \cdot \rho_{fu,ca,k}\right)\end{aligned} \tag{16.3-8}$$

where the input variable CMFU represents the compressibility of the molten fuel and

$$f_{fi,fu,k} = \frac{\rho'_{fi,ca,k}}{\rho'_{fu,ca,k}} \tag{16.3-9}$$

$$f_{fi,fu,k} = \frac{\rho'_{fv,ca,k}}{\rho'_{fu,ca,k}} \tag{16.3-10}$$

In the derivation of Eq. 16.3-8, we used the assumption that, for injection purposes, the fuel vapor behaves as a gas. Further fuel vaporization can take place in the next cycle. It should also be noted that $\Delta\rho'_{fu,k}$ represents the change in the generalized density of the in-pin fuel. This change refers to the fuel in all the pins in the subassembly, as explained in the corresponding PLUTO2 section.

The amount of fission gas and fuel vapor ejected is then calculated as

$$\Delta\rho'_{fi,k} = f_{fi,fu,k} \cdot \Delta\rho'_{fu,ca,k} \tag{16.3-11a}$$

$$\Delta\rho'_{fv,k} = f_{fv,fu,k} \cdot \Delta\rho'_{fu,ca,k} \tag{16.3-11b}$$

The fuel vapor mass ejected is then added to the mass of the liquid fuel ejected. It is noteworthy that the fuel vapor pressure is used only for the momentum calculation in the pin and for the fuel ejection. No fuel vapor conservation equations are solved in the pin cavity.

The new channel partial pressures are then recalculated:

$$P_{fv,i} = \frac{R_{fv} \cdot \rho'_{fv,i} \cdot T_{fv,i}}{\theta^{n+1}_{vg,i}} \tag{16.3-12}$$

$$P_{sv,i} = \frac{R_{sv} \cdot \rho'_{sv,i} \cdot T_{sv,i}}{\theta^{n+1}_{vg,i}} \tag{16.3-13}$$

If $\theta_{\mathrm{Na},lq,i}/\theta_{ch,op,i} \leq 0.3$

$$P_{fi,i} = \frac{R_{fi} \cdot \left(\rho'_{fi,i} + \Delta\rho'_{fi,k}\right) \cdot T_{fi,i}}{\theta^{n+1}_{vg,i}} \tag{16.3-14a}$$

If $\theta_{\mathrm{Na},lq,i}/\theta_{ch,op,i} > 0.3$ then

$$P_{fi,i} = \frac{-\theta^{n+1}_{vg,i} + \sqrt{\left(\theta^{n+1}_{vg,i}\right)^2 + 4\ \theta_{Na,\ell q,i} \cdot CMNL \cdot \left(\rho'_{fi,i} + \Delta\rho'_{fi,ca,k}\right) \cdot R_{fi} \cdot T_{fi,i}}}{2\,\theta_{Na,\ell q,i} \cdot CMNL} \tag{16.3-14b}$$

If $\theta_{Na,\ell q} = 0$, i.e., if the sodium present is in the form of single-phase vapor:

$$P_{Na,i} = \frac{R_{Na} \cdot \rho'_{Na,i} \cdot T_{Na,i}}{\theta^{n+1}_{vg,i}} \tag{16.3-15a}$$

If $0 < \theta_{Na,lq,}$ i.e., two-phase sodium is present:

$$P_{Na,i} = P_{Na}\left(T_{Na,i}\right) \tag{16.3-15b}$$

where CMNL is the compressibility coefficient of the liquid sodium and $\theta^{n+1}_{vg,i}$ is:

$$\theta^{n+1}_{vg,i} = \theta_{vg,i} - \frac{\Delta\rho'_{fu,ca,k}}{\rho_{fu,k}} \tag{16.3-16}$$

The new tentative channel pressure is:

$$P^{n+1}_{ch,i} = P_{Na,i} + P_{fi,i} + P_{sv,i} + P_{fv,i} \tag{16.3-17}$$

If this pressure is below the pressure in the cavity after injection, i.e.,

$$P^{n+1}_{ch,i} < P^{n+1}_{ca,k} \tag{16.3-18}$$

then no further iterations are necessary and $P^{n+1}_{ch,i}$ remains the new pressure in the channel. If Eq. 16.3-18 is not satisfied, too much material was ejected from the cavity into the channel. A new pressure in the pin cavity is selected:

$$P_{ca,k}^{n+1} = \left(P_{ca,k}^{n} + P_{ca,k}^{n+1}\right) \cdot 0.5 \tag{16.3-19}$$

and the procedure outlined in Eqs. 16.3-7 through 16.3-17 is repeated until the condition in 16.3-18 is satisfied.

It should be noted that in Eq. 16.3-14, the fission-gas pressure is calculated by assuming that the fission gas injected has the same temperature as the fission gas in the channel. This is necessary because the fission gas and sodium have to be at the same temperature, which has already been calculated in the routine LENAEN. The additional energy carried by the injected fission gas, which in fact has the temperature $T_{fu,ca,k}$ will be added to the fission gas/sodium mixture in the next cycle, when solving the energy equation for these components. Finally, the fuel and fission-gas densities in the pin and channel are updated.

$$\rho'_{fu,ca,k} = \rho'_{fu,ca,k} - \Delta\rho'_{fu,ca,k} \tag{16.3-20}$$

$$\rho'_{fi,ca,k} = \rho'_{fi,ca,k} - \Delta\rho'_{fi,ca,k} \tag{16.3-21}$$

$$\rho'_{fu,i} = \rho'_{fu,i} + \Delta\rho'_{fu,ca,k} \tag{16.3-22}$$

$$\rho'_{fu,i} = \rho'_{fi,i} + \Delta\rho'_{fi,ca,k} \tag{16.3-23}$$

In the Release 1.1 version of LEVITATE a mechanistic calculation of the in-pin fuel ejection has been added. This model can be used by setting the input variable INRAEJ=1 in Block 1 location 44. If INRAEJ=0 the ejection of the fuel into the channel is calculated as described above.

The mechanistic ejection model calculates the radial velocity of the in-pin molten fuel/gas mixture, $u_{ca\text{-}ch,k}$, at each axial location where the cladding has been ruptured. This velocity is recalculated each time step. The amounts of fuel and fission gas ejected each time step are calculated as follows:

$$\Delta\rho'_{fu,k} = \rho'_{fu,k} \cdot \frac{V_{fuel\ ejected}}{V_{vuel\ cavity}} = \rho'_{fu,k} \cdot \frac{u_{fu,ca-ch,k} \cdot \Delta t}{\pi \cdot R_{ca,k}} \tag{16.3-23-1}$$

$$\Delta\rho'_{fi,k} = \rho'_{fi,k} \cdot \frac{u_{fu,ca-ch,k} \cdot \Delta t}{\pi \cdot R_{ca,k}} \tag{16.3-23-2}$$

$$\Delta\rho'_{fv,k} = \rho'_{fv,k} \cdot \frac{u_{fu,ca-ch,k} \cdot \Delta t}{\pi \cdot R_{ca,k}} \tag{16.3-23-3}$$

The pressure in the cavity is then calculated solving equation 16.3-8 for $P_{ca,k}$ and the pressure in the coolant channel is calculated using Eqs. 16.3-12 through 16.3-17. If

$$P_{ch,i}^{n+1} < P_{ca,k}^{n+1} \tag{16.3-23-4}$$

then no further iterations are necessary. If 16.3-23-4 is not satisfied then too much material was ejected from the cavity into the channel. The radial velocity is reduced:

$$u_{fu,ca-ch,k}^{n+1} = u_{fu,ca-ch,k}^{n+1} \cdot 0.5 \tag{16.3-23-5}$$

and the procedure for pressure calculation is repeated.

The key element in the calculation described above is the radial fuel velocity $u_{fu,ca-ch,k}$, which is calculated as described below.

The radial velocity calculation first updates all radial velocities considering only the radial acceleration $a_{fu,ca-ch,k}$, and ignoring temporarily the axial transport of radial momentum:

$$u_{fu,ca-ch,k}^{n+1} = u_{fu,ca-ch,k} + a_{fu,ca-ch,k} \cdot \Delta t \tag{16.3-23-6}$$

where $a_{fu,ca-ch,k}$ is the radial acceleration of the molten fuel in the cavity in the axial cell k. This acceleration is calculated using the simplified geometry illustrated in Fig. 16.3-1. The pressure difference between the pin cavity and the coolant channel is assumed to act on the fuel contained in the shaded volume. The rip size is considered to be of the same order of magnitude as the cavity radius. The acceleration is calculated as follows:

$$\begin{aligned} a_{fu,ca-ch,k} = \frac{\sum \text{Forces}}{\text{Mass}} = \frac{R_{ca,k} \cdot \Delta z_k}{0.9 \cdot R_{ca,k}^{z} \cdot \Delta z_k \cdot \rho_{fu,k}} \Big\{ & \Delta P_{ca-ch,k} - \\ & 0.5 \cdot \rho_{fu,k} \cdot u_{fu,ca-ch,k} \cdot \left| u_{fu,ca-ch,k} \right| \cdot C_{ORIFICE} - \\ & C_{SHEAR} \cdot \eta_{fu,k} \cdot \frac{u_{fu,ca-ch,k}}{R_{ca,k}} \Big\} \end{aligned} \tag{16.3-23-7}$$

where: $\Delta P_{ca-ch,k} = P_{ca,k} - P_{ch,i}$

C_{ORFICE} is an orifice coefficient used in the calculation of the flow pressure drop across the rip. This coefficient is currently zero in the code.

C_{SHEAR} is a coefficient associated with the shear forces exerted on the accelerating fuel. It can be determined from geometrical considerations. The current value is 6.88. $\eta_{fu,k}$ is the viscosity of the molten fuel in cell k

As the fuel from the radial control volume is ejected into the channel, it is replaced with new fuel from outside the control volume, assumed to carry no radial momentum. Thus, the radial velocity of the fuel has to be recalculated. into the channel, it is replaced with new fuel from outside the control volume, assumed to carry no radial momentum. Thus, the radial velocity of the fuel has to be recalculated.

$$u_{fu,ca-ch,k} = u_{fu,ca-ch,k} \cdot \frac{V_{control} - V_{ejected}}{V_{control}} = u_{fu,ca-ch,k} \cdot \frac{0.9\ R_{ca,k} - u_{fu,ca-ch,k} \cdot \Delta t}{0.9\ R_{ca,k}} \qquad (16.3\text{-}23\text{-}8)$$

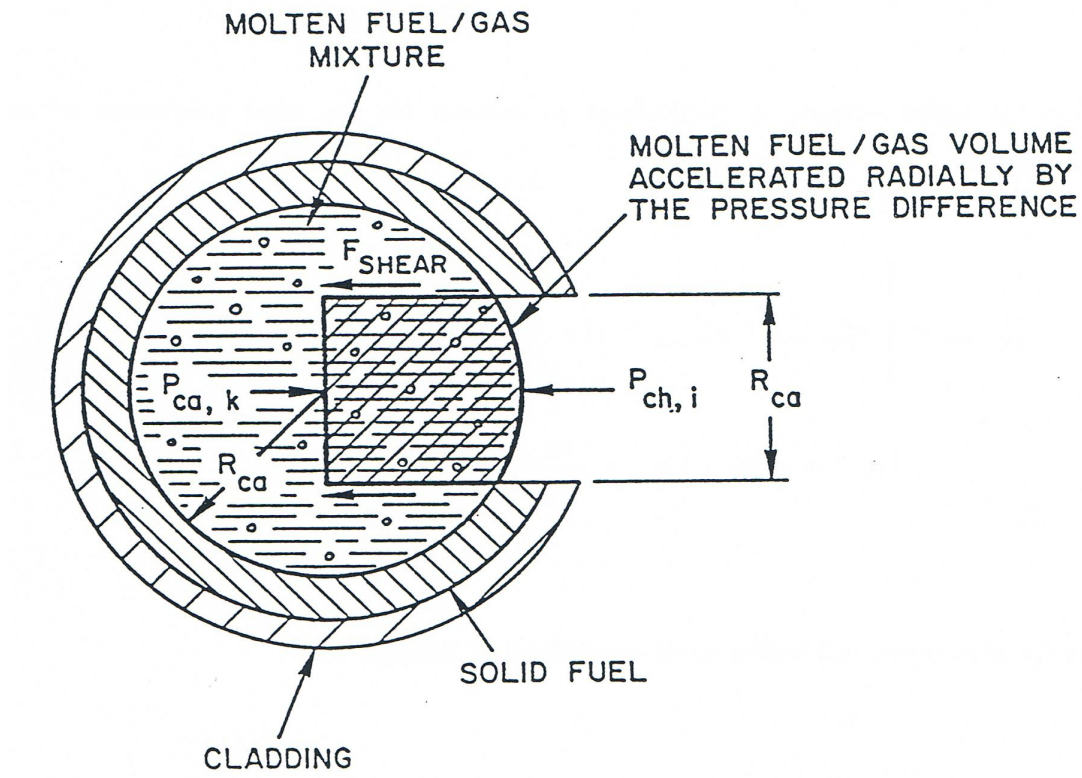

Fig. 16.3-1: Geometry for the Radial Acceleration Calcuation

Finally, the radial velocity is recalculated to account for the axial convection of radial momentum:

$$u^{n+1}_{fu,ca-ch,k} = \left\{ u^{n+1}_{fu,ca-ch,k} \cdot \rho'_{fu,ca,k} - \left(\left[\rho' \cdot u \cdot u_{ca-ch}\right]_{fu,k+1} - \left[\rho' \cdot u \cdot u_{ca-ch}\right]\right)_{fu,k} \cdot \frac{\Delta t}{\Delta z_k} \right\} \cdot \frac{1}{\rho'_{fu,ca,k}} \tag{16.3-23-9}$$

where the momentum convective terms are defined as follows:

$$\left[\rho' \cdot u \cdot u_{ca-ch}\right]_{fu,k} = \begin{cases} \rho'_{fu,ca,k-1} \cdot u_{fu,ca,k} \cdot u_{fu,ca-ch,k-1} & \text{if } u_{fu,ca,k} \geq 0 \\ \rho'_{fu,ca,k} \cdot u_{fu,ca,k} \cdot u_{fu,ca-ch,k} & \text{if } u_{fu,ca,k} < 0 \end{cases} \tag{16.3-23-10}$$

The mechanistic ejection model has been compared with the pressure equilibration ejection model (INEAEJ=0) in several calculations. It appears that the pressure equilibration ejection model provides generally a good approximation to the results calculated by the mechanistic model. The larger differences appear during high power excursions and during the time immediately following the pin failure, when the inertial forces accounted for in the mechanistic model delay the early fuel ejection into the channel. It is expected that after validation in several experiment analyses the mechanistic ejection model will become the standard model to be used in SAS4A calculations.

16.3.2 Fuel-pin Disruption

When certain conditions are satisfied, the fuel pins can be totally disrupted at certain axial locations. The decision process which triggers the pin disruption is performed in the LE1PIN routine and has been outlined in Section 16.2. The nodes to be disrupted are flagged in LE1PIN by setting IFLAG(I) = 9. The disruption process itself is performed in the LEDISR routine and is described below.

The LEDISR routine first checks whether a node that is to be disrupted is within the physical region for fuel, fission gas, steel and fuel chunks, since all these components are likely to be created via the disruption process. If the node to be disrupted lies outside the fuel physical region, for example, the fuel region will be extended so that the molten fuel generated via the disruption process will be modeled appropriately. Then, the generalized densities and the temperatures of the components present in the channel are reset to account for the addition of mass due to the pin disruption:

$$\Delta\rho'_{fu,i} = \rho'_{fu,ca,k} \tag{16.3-24}$$

$$\Delta\rho'_{fi,i} = \rho'_{fi,ca,k} \tag{16.3-25}$$

$$\Delta\rho'_{f\ell,i} = \rho'_{ffc,i} + \frac{M_{fu,i} \cdot N_{PIN}}{\Delta z_i \cdot AXMX} \tag{16.3-26}$$

$$\Delta\rho'_{s\ell,i} = \rho'_{sic,i} + \frac{M_{se,i} \cdot N_{PIN}}{\Delta z_i \cdot AXMX} \tag{16.3-27}$$

where $M_{fu,i}$ and $M_{se,i}$ represent the mass of solid stationary fuel and steel, respectively, present in the axial node i, per pin. The temperatures are reset using an energy balance. For example, the new fuel enthalpy is given by:

$$h_{fu,i} = \frac{h_{fu,i} \cdot \rho'_{fu,i} \; + \; h_{fu,ca,k} \cdot \Delta\rho'_{fu,i}}{\rho'_{fu,i} + \Delta\rho'_{fu,i}} \tag{16.3-28}$$

The new fuel temperature is obtained from $h_{fu,i}$, using the function $T_{fu}(h)$. The velocities are reset using a momentum conservation equation. For example, the new fuel velocity at boundary i, when node i is disrupted, is calculated as follows:

$$\begin{aligned} u''_{fu,i} = \Big[& u_{fu,i} \cdot \left(\rho'_{fu,i-1} + \rho'_{s\ell,i-1}\right) \cdot 0.5 \cdot \Delta z_{i-1} \\ & + u''_{fu,i} \cdot \left(\rho'_{fu,i-1} + \rho'_{s\ell,i-1}\right) \cdot 0.5 \cdot \Delta z_{i-1} \\ & + u_{fu,ca,k} \cdot 0.5 \cdot \Delta\rho'_{fu,i} \cdot \Delta z_i \Big] \\ & \div \Big[\left(\rho'_{fu,i-1} + \rho'_{s\ell,i-1}\right) \cdot 0.5 \cdot \Delta z_{i-1} \\ & + \left(\rho'_{fu,i} + \rho'_{s\ell,i}\right) \cdot 0.5 \cdot \Delta z_i \\ & + \Delta\rho'_{fu,i} \cdot 0.5 \cdot \Delta z_i \Big] \end{aligned} \tag{16.3-29}$$

Disruption of node i also affects the fuel velocity at the boundary i+1:

$$\begin{aligned} u''_{fu,i+1} = \Big[& u'_{fu,i+1} \cdot \left(\rho'_{fu,i} + \rho'_{s\ell,i}\right) \cdot 0.5 \cdot \Delta z_i \\ & + u''_{fu,i+1} \left(\rho'_{fu,i+1} + \rho'_{s\ell,i+1}\right) \cdot 0.5 \cdot \Delta z_{i+1} \\ & + u_{fu,ca,k} \cdot 0.5 \cdot \Delta\rho'_{fu,i} \cdot \Delta z_i \Big] \\ & \div \Big[\left(\rho'_{fu,i} + \rho'_{s\ell,i}\right) \cdot 0.5 \cdot \Delta z_i \\ & + \left(\rho'_{fu,i+1} + \rho'_{s\ell,i+1}\right) \cdot 0.5 \cdot \Delta z_{i+1} \\ & + \Delta\rho'_{fu,i} \cdot 0.5 \cdot \Delta z_i \Big] \end{aligned} \tag{16.3-30}$$

The velocities $u'_{fu,i}$ and $u''_{fu,i}$ represent the molten fuel velocities at the channel boundary i and are described in more detail in Section 16.4.2.1.

Finally, the densities are reset as follows:

$$\rho'_{fu,i} = \rho'_{fu,i} + \Delta\rho'_{fu,i} \tag{16.3-31}$$

$$\rho'_{fi,i} = \rho'_{fi,i} + \Delta\rho'_{fi,i} \tag{16.3-32}$$

$$\rho'_{f\ell,i} = \rho'_{f\ell,i} + \Delta\rho'_{f\ell,i} \tag{16.3-33}$$

$$\rho'_{s\ell,i} = \rho'_{s\ell,i} + \Delta\rho'_{s\ell,i} \tag{16.3-34}$$

The partial pressures are then reset to account for the new gas volume and gas densities in the disrupted node. A number of quantities related to the cladding are set to zero before the end of the routine. These quantities include the perimeter and thickness of cladding and the amount of fuel and steel in the cladding crust.

16.3.3 Fuel Ejection via the Open Pin Stubs

Once the fuel-pin disruption has occurred in a subassembly, the remaining pin stubs can eject fuel and fission gas axially into the disrupted region, in addition to the regular radial gas ejection. Fuel and fission gas can also reenter the fuel-pin stubs when the pressure in the disrupted region exceeds the pressure in the pin cavity. The ejection (or reentry) of the molten fuel via the open pin stubs is calculated by solving the momentum conservation equation for the cavity half-cells adjacent to the disrupted region. This equation is solved in the routine LE1PIN. It is derived in the same manner as described in the PLUTO2 chapter for all regular in-pin momentum cells, but using the cell geometry illustrated in Fig. 16.3-2. The momentum cell for the bottom pin stub extends from the center of the cell IDISBT-1 to the end of the stub. The pressure difference used in the momentum equation is $P_{IDISBT} - P_{ca,IDISBT-1}$, where P_{IDISBT} is the pressure in the disrupted region the convective flux coming from the disrupted region is defined using the generalized density $\rho'_{fu,IDISBT}$, i.e., the fuel generalized density in the disrupted region.

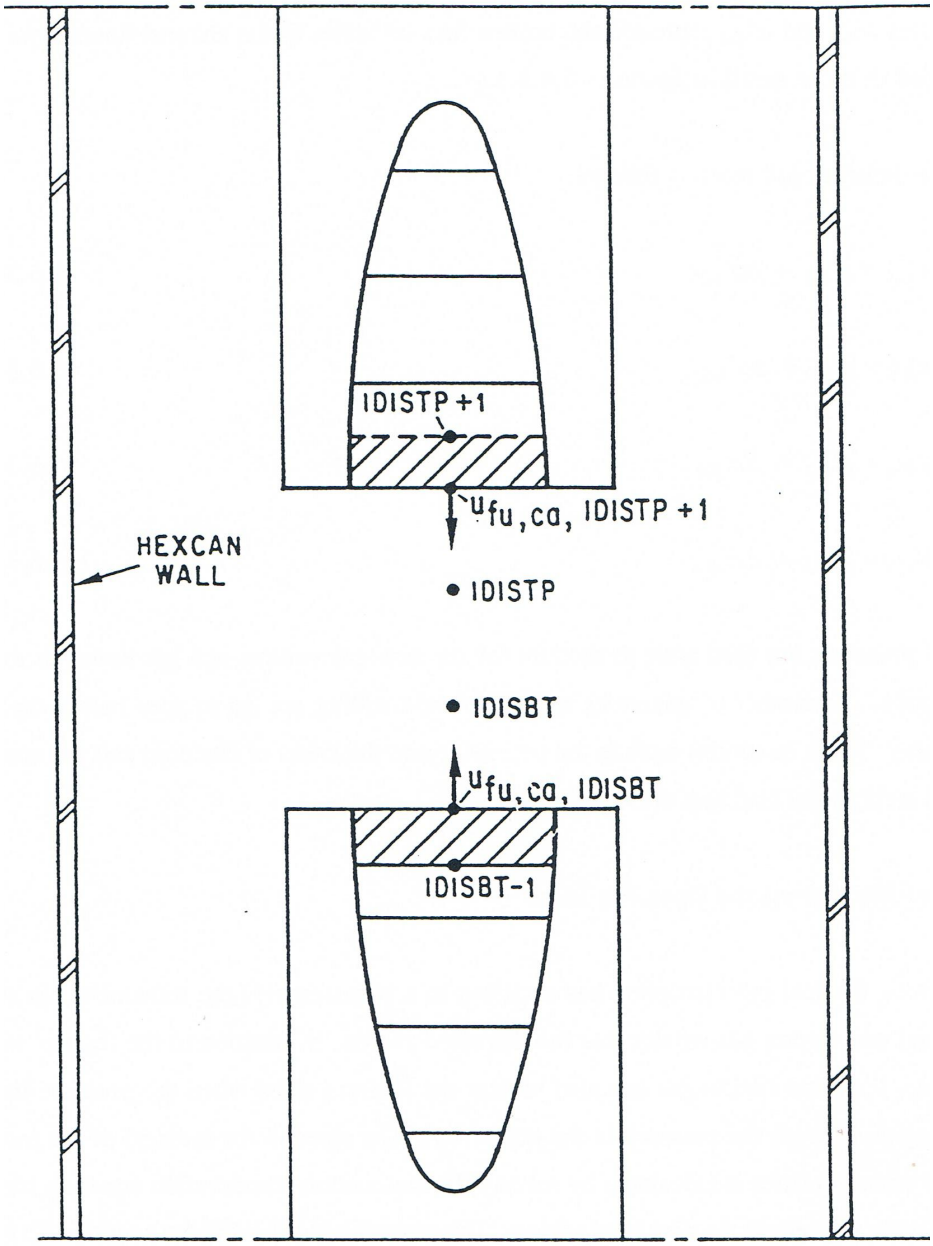

Fig. 16.3-2: Geometry Used in the Derivation of the Momentum Equations for Ejection via the Pin Stubs

16.4 Coolant Channel Hydrodynamic Model

16.4.1 Physical Models

16.4.1.1 Geometry

The coolant channel described by LEVITATE is delimited by the hexcan wall and the outer surface of the fuel pins. Axially, this channel is limited by the upper and lower sodium plena. Calculations are performed in a 1-D geometry, with the variables being functions of the axial height z. As illustrated in Fig. 16.1-1, the area of the coolant channel can vary widely due to the local disruption of the fuel pins, cladding and structure ablation, and fuel/steel blockage formation at various axial locations.

16.4.1.2 Hydrodynamic Models

The fluid dynamic models in LEVITATE calculate the motion of the materials in the channel. The materials that are tracked by LEVITATE are:

1. liquid fuel
2. liquid steel
3. sodium (liquid, two-phase mixture or superheated vapor)
4. fission gas
5. fuel vapor
6. steel vapor
7. solid fuel chunks
8. solid steel chunks

A separate mass and energy conservation equation is solved for each of these components. Momentum conservation equations are solved for three velocity fields, associated with the following component groups:

1. sodium, fission gas, fuel vapor, steel vapor
2. liquid fuel, liquid steel
3. solid fuel chunks, solid steel chunks

Phase transitions can occur, leading to mass, momentum and energy exchange among various moving components and/or among moving and stationary components. These exchanges are described in Section 16.4.1.5.

16.4.1.3 Structural Models

The structural models included in LEVITATE describe the thermodynamic behavior of the stationary components that act as boundaries for the coolant channel. The stationary components modeled in LEVITATE are:

1. steel cladding
2. steel hexcan wall

3. cladding frozen fuel crust (with possible steel inclusions)
4. hexcan wall frozen fuel crust (with possible steel inclusions)

One or more energy equations are solved for each of these components (e.g., two equations are needed for cladding, that has two radial nodes). Due to freezing/melting processes, mass and energy exchange can take place between these stationary components and the moving components in the channel, as explained in Section 16.4.1.5.

16.4.1.4 Fuel/Steel Flow Regimes

As indicated in Section 16.1, the interactions between the different components present in the channel, i.e., mass, energy and momentum transfer, are largely determined by the local configuration which, in turn, is determined by the flow regimes used. The fuel/steel flow regimes modeled in LEVITATE are presented conceptually in Fig. 16.4-1. They are a bubbly fuel flow regime, a partial annular fuel flow regime, an annular steel flow regime, and a bubbly steel flow regime. The bubbly fuel channel flow is characterized by the presence of large amounts of liquid fuel, with droplets of molten steel, solid fuel and steel chunks, and bubbles of fission gas and sodium vapor imbedded. There is no relative motion between the steel and fuel, and the relative velocity between the molten fuel and the vapor bubbles is quite low, due to the large drag and inertial forces acting on the bubbles.

As the volume fraction of fuel decreases, the bubbly flow regime is changed to the annular fuel flow regime, with the fuel blanketing the cladding partially or totally and the two-phase sodium/gas mixture flowing at the center of the channel. A stream of solid fuel chunks, interacting with both the two-phase sodium/gas mixture and the liquid fuel streams, can also be present. Molten steel droplets are imbedded in the fuel film. The relative velocities between the fuel and mixture are significantly higher than in the bubbly flow regime.

When molten steel is the dominant component at a certain axial location, the flow regime used can be either an annular or a bubbly steel regime. The bubbly steel flow regime is characterized by the presence of a large amount of molten steel, with droplets of molten fuel, solid fuel and steel chunks, and bubbles of fission gas and sodium vapor imbedded. As the volume fraction of molten steel decreases, the bubbly steel regime is changed to the annular steel flow regime. In this regime, the molten steel totally covers the cladding and the vapor mixture flows at the center of the channel. Molten fuel droplets can be imbedded in the molten steel, and solid fuel and steel chunks can interact with both the vapor mixture and the molten steel. In the Release 1.1 version, a partial annular steel flow regime has been introduced. The steel is assumed to cover the cladding only partially moving in the form of droplets and rivulets. This picture is supported by experimental evidence that indicates that the steel does not wet the cladding. As the local amount of molten steel increases, a full annular steel flow regime can develop. The partial annular steel flow regime is used only when the chunk model is active, i.e. ICHUNK=1. If the chunk model is not used, the full annular steel flow regime is still used. It is expected that, as the validation effort continues, the partial annular steel flow regime will be available, regardless of the chunk model option used.

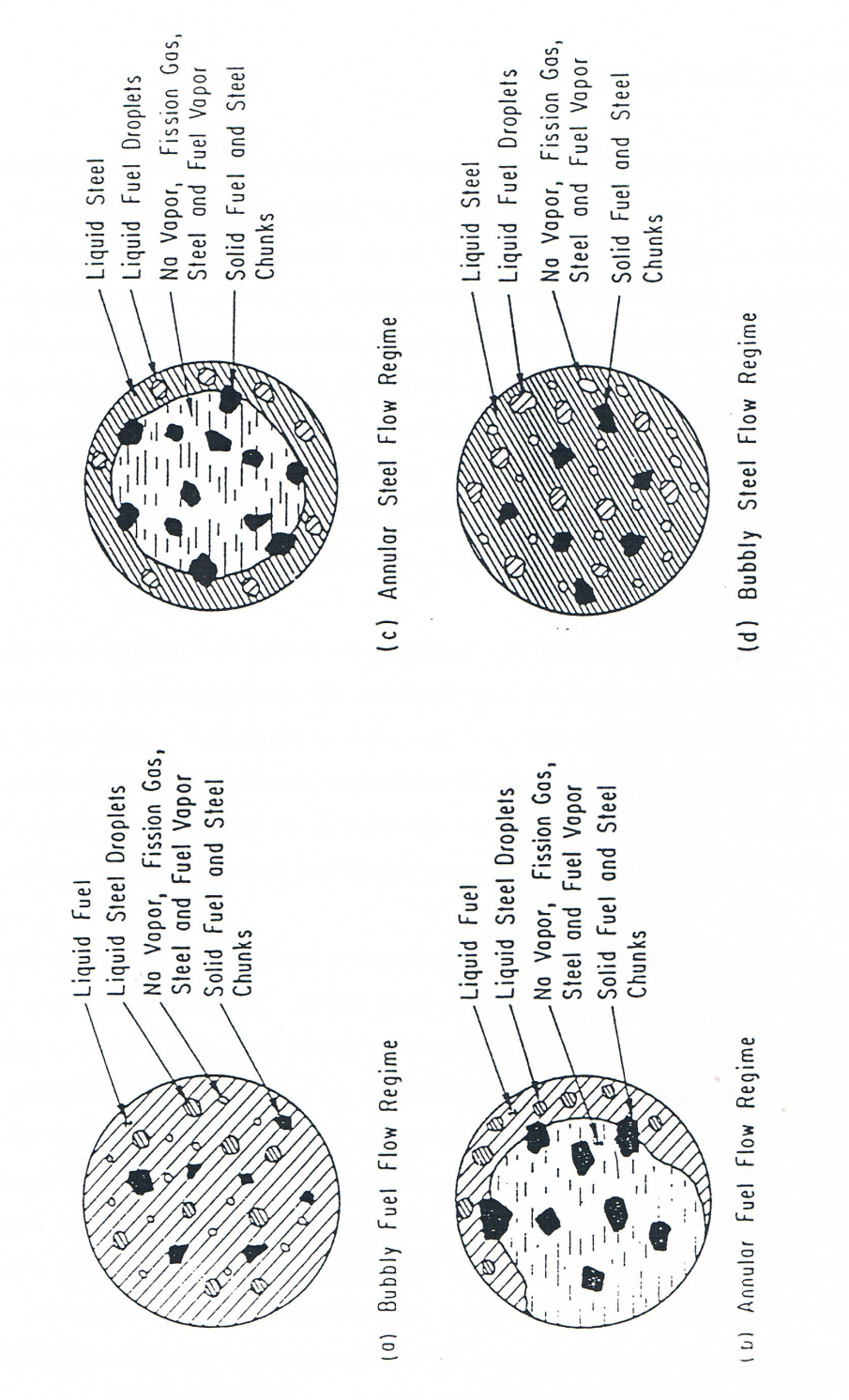

Fig. 16.4-1: Continuous Fuel/Steel Regimes Modeled in LEVITATE

Because only very limited information is currently available about the fuel-steel flow regime transitions in fuel pin bundles, these transitions are governed in LEVITATE by the fuel-steel volume fraction present at each axial location.

The continuous fuel flow regimes used in LEVITATE have been shown to slow down substantially the fuel dispersal, bringing the results of calculations in close agreement with the experimental data [16-1, 16-11].

16.4.1.5 Mass, Momentum and Energy Exchange (non-convective)

Mass, momentum and energy exchange can take place among various components at any given time and location. All these transfers are strongly dependent on the flow regime prevailing at the time and location considered. The mass transfers are due to phase changes (freezing, melting, vaporization, condensation) or to disruption events, such as the disruption of the solid fuel pins or fuel crust breakup. The mass transfer is largely independent of the local flow regime and the allowable transfers are summarized in Fig. 16.4-2.

The mass transfer in any given computational cell, together with the changes in the mass of each component due to convection, determine the mass of each component in the cell. These masses, together with the energy from the previous time step, determine the local flow regime and thus the local configuration. The local energy and momentum transfers are strongly dependent on the local flow regime. The allowable energy transfer paths among various LEVITATE components are illustrated in Figs. 16.4-3 to 16.4-6 for various flow regimes. Similarly, the allowable momentum paths are illustrated in Figs. 16.4-7 through 16.4-10.

COMPONENTS → / ↓		MOVING OR STATIONARY	VELOCITY	LF	LS	Na	FG	FV	SV	SFC	SSC	SC	SW	FFC	FFW	SIC	SIW	FP
LIQUID FUEL	LF	MOVING COMPONENTS	UFCH					Y		Y				Y	Y			
LIQUID STEEL	LS								Y		Y	Y	Y			Y	Y	
SODIUM	Na		UMCH															
FISSION GAS	FG																	
FUEL VAPOR	FV			Y														
STEEL VAPOR	SV				Y													
SOLID FUEL CHUNKS	SFC		ULCH	Y										Y	Y			Y
SOLID STEEL CHUNKS	SSC				Y							Y	Y					
STEEL CLADDING	SC	STATIONARY			Y						Y							
STEEL HEXCAN WALL	SW				Y						Y							
FROZEN FUEL ON CLADDING	FFC			Y						Y								
FROZEN FUEL ON HEXCAN WALL	FFW			Y						Y								
STEEL INCLUSIONS IN CLADDING CRUST	SIC				Y													
STEEL INCLUSIONS IN HEXCAN WALL CRUST	SIW				Y													
FUEL PIN	FP									Y								

Fig. 16.4-2: Mass exchange Possibilities among Various LEVITATE Components

COMPONENTS → / ↓		MOVING OR STATIONARY	VELOCITY	LF	LS	Na	FG	FV	SV	SFC	SSC	SC	SW	FFC	FFW	SIC	SIW	FP
LIQUID FUEL	LF	MOVING COMPONENTS	UFCH		Y	Y	Y	Y	Y	Y	Y	Y	Y	Y	Y	Y			Y
LIQUID STEEL	LS			Y															
SODIUM	Na		UMCH	Y			Y	Y	Y	Y	Y	Y	Y	Y	Y				Y
FISSION GAS	FG			Y		Y		Y	Y	Y	Y	Y	Y	Y	Y				Y
FUEL VAPOR	FV			Y		Y	Y		Y	Y	Y	Y	Y	Y	Y				Y
STEEL VAPOR	SV			Y		Y	Y	Y		Y	Y	Y	Y	Y	Y				Y
SOLID FUEL CHUNKS	SFC		ULCH	Y		Y	Y	Y	Y		Y	Y	Y	Y	Y				Y
SOLID STEEL CHUNKS	SSC			Y		Y	Y	Y	Y	Y		Y	Y	Y	Y				Y
STEEL CLADDING	SC	STATIONARY		Y		Y	Y	Y	Y	Y	Y			Y					Y
STEEL HEXCAN WALL	SW			Y		Y	Y	Y	Y	Y	Y				Y				
FROZEN FUEL ON CLADDING	FFC			Y		Y	Y	Y	Y	Y	Y	Y				Y			
FROZEN FUEL ON HEXCAN WALL	FFW			Y		Y	Y	Y	Y	Y	Y		Y				Y		
STEEL INCLUSIONS IN CLADDING CRUST	SIC													Y					
STEEL INCLUSIONS IN HEXCAN WALL CRUST	SIW														Y				
FUEL PIN	FP			Y		Y	Y	Y	Y	Y	Y	Y							

Fig. 16.4-3: Energy Exchange Possibilities among Various LEVITATE Components, for the Fuel Annular Flow Regime

COMPONENTS → / ↓		MOVING OR STATIONARY	VELOCITY	LF	LS	Na	FG	FV	SV	SFC	SSC	SC	SW	FFC	FFW	SIC	SIW	FP
LIQUID FUEL	LF	MOVING COMPONENTS	UFCH		Y													
LIQUID STEEL	LS			Y		Y	Y	Y	Y	Y	Y	Y	Y	Y	Y			Y
SODIUM	Na		UMCH		Y		Y	Y	Y									
FISSION GAS	FG				Y	Y		Y	Y									
FUEL VAPOR	FV				Y	Y	Y		Y									
STEEL VAPOR	SV				Y	Y	Y	Y										
SOLID FUEL CHUNKS	SFC		ULCH		Y						Y							
SOLID STEEL CHUNKS	SSC				Y					Y								
STEEL CLADDING	SC	STATIONARY			Y									Y				Y
STEEL HEXCAN WALL	SW				Y										Y			
FROZEN FUEL ON CLADDING	FFC				Y							Y				Y		
FROZEN FUEL ON HEXCAN WALL	FFW				Y								Y				Y	
STEEL INCLUSIONS IN CLADDING CRUST	SIC													Y				
STEEL INCLUSIONS IN HEXCAN WALL CRUST	SIW														Y			
FUEL PIN	FP				Y							Y						

Fig. 16.4-4: Energy Exchange Possibilities among Various LEVITATE Components, for the Fuel Bubbly Flow Regime

COMPONENTS →	MOVING OR STATIONARY	VELOCITY	LF	LS	Na	FG	FV	SV	SFC	SSC	SC	SW	FFC	FFW	SIC	SIW	FP
LIQUID FUEL LF	MOVING COMPONENTS	UFCH		Y													
LIQUID STEEL LS			Y		Y	Y	Y	Y	Y	Y	Y	Y	Y	Y			Y
SODIUM Na		UMCH		Y		Y	Y	Y	Y	Y							
FISSION GAS FG				Y	Y		Y	Y	Y	Y							
FUEL VAPOR FV				Y	Y	Y		Y	Y	Y							
STEEL VAPOR SV				Y	Y	Y	Y		Y	Y							
SOLID FUEL CHUNKS SFC		ULCH		Y	Y	Y	Y	Y		Y							
SOLID STEEL CHUNKS SSC				Y	Y	Y	Y	Y	Y								
STEEL CLADDING SC	STATIONARY			Y									Y				Y
STEEL HEXCAN WALL SW				Y										Y			
FROZEN FUEL ON CLADDING FFC				Y							Y				Y		
FROZEN FUEL ON HEXCAN WALL FFW				Y								Y				Y	
STEEL INCLUSIONS IN CLADDING CRUST SIC													Y				
STEEL INCLUSIONS IN HEXCAN WALL CRUST SIW														Y			
FUEL PIN FP				Y							Y						

Fig. 16.4-5: Energy Exchange Possibilities among Various LEVITATE Components, for the Steel Annular Flow Regime

COMPONENTS → / ↓	MOVING OR STATIONARY	VELOCITY	LF	LS	Na	FG	FV	SV	SFC	SSC	SC	SW	FFC	FFW	SIC	SIW	FP
LIQUID FUEL LF	MOVING COMPONENTS	UFCH		Y													
LIQUID STEEL LS			Y		Y	Y	Y	Y	Y	Y	Y	Y	Y	Y			Y
SODIUM Na		UMCH		Y		Y	Y	Y									
FISSION GAS FG				Y	Y		Y	Y									
FUEL VAPOR FV				Y	Y	Y		Y									
STEEL VAPOR SV				Y	Y	Y	Y										
SOLID FUEL CHUNKS SFC		ULCH		Y						Y							
SOLID STEEL CHUNKS SSC				Y					Y								
STEEL CLADDING SC	STATIONARY			Y									Y				Y
STEEL HEXCAN WALL SW				Y										Y			
FROZEN FUEL ON CLADDING FFC				Y							Y				Y		
FROZEN FUEL ON HEXCAN WALL FFW				Y								Y				Y	
STEEL INCLUSIONS IN CLADDING CRUST SIC													Y				
STEEL INCLUSIONS IN HEXCAN WALL CRUST SIW														Y			
FUEL PIN FP				Y							Y						

Fig. 16.4-6: Energy Exchange Possibilities among Various LEVITATE Components, for the Steel Bubbly Flow Regime

LEGEND

Y – ALLOWED MOMENTUM EXCHANGE

X – EQUAL VELOCITIES

COMPONENTS → / ↓		MOVING OR STATIONARY	VELOCITY	LF	LS	Na	FG	FV	SV	SFC	SSC	SC	SW	FFC	FFW	SIC	SIW	FP
LIQUID FUEL	LF	MOVING COMPONENTS	UFCH		X	Y	Y	Y	Y	Y	Y	Y	Y	Y	Y			Y
LIQUID STEEL	LS			X														
SODIUM	Na		UMCH	Y			X	X	X	Y	Y	Y	Y	Y	Y			Y
FISSION GAS	FG			Y		X		X	X	Y	Y	Y	Y	Y	Y			Y
FUEL VAPOR	FV			Y		X	X		X	Y	Y	Y	Y	Y	Y			Y
STEEL VAPOR	SV			Y		X	X	X		Y	Y	Y	Y	Y	Y			Y
SOLID FUEL CHUNKS	SFC		ULCH	Y		Y	Y	Y	Y		X	Y	Y	Y	Y			Y
SOLID STEEL CHUNKS	SSC			Y		Y	Y	Y	Y	X		Y	Y	Y	Y			Y
STEEL CLADDING	SC	STATIONARY																
STEEL HEXCAN WALL	SW																	
FROZEN FUEL ON CLADDING	FFC																	
FROZEN FUEL ON HEXCAN WALL	FFW																	
STEEL INCLUSIONS IN CLADDING CRUST	SIC																	
STEEL INCLUSIONS IN HEXCAN WALL CRUST	SIW																	
FUEL PIN	FP																	

Fig. 16.4-7: Momentum Exchange Possibilities among Various LEVITATE Components, for the Fuel Annular Flow Regime

LEGEND

Y – ALLOWED MOMENTUM EXCHANGE

X – EQUAL VELOCITIES

COMPONENTS → / ↓	MOVING OR STATIONARY	VELOCITY	LF	LS	Na	FG	FV	SV	SFC	SSC	SC	SW	FFC	FFW	SIC	SIW	FP
LIQUID FUEL LF	MOVING COMPONENTS	UFCH		X	Y	Y	Y	Y	Y	Y	Y	Y	Y	Y			Y
LIQUID STEEL LS			X														
SODIUM Na		UMCH	Y			X	X	X									
FISSION GAS FG			Y		X		X	X									
FUEL VAPOR FV			Y		X	X		X									
STEEL VAPOR SV			Y		X	X	X										
SOLID FUEL CHUNKS SFC		ULCH	Y							X							
SOLID STEEL CHUNKS SSC			Y						X								
STEEL CLADDING SC	STATIONARY																
STEEL HEXCAN WALL SW																	
FROZEN FUEL ON CLADDING FFC																	
FROZEN FUEL ON HEXCAN WALL FFW																	
STEEL INCLUSIONS IN CLADDING CRUST SIC																	
STEEL INCLUSIONS IN HEXCAN WALL CRUST SIW																	
FUEL PIN FP																	

Fig. 16.4-8: Momentum Exchange Possibilities among Various LEVITATE Components, for the fuel Bubbly Flow Regime

LEGEND

Y – ALLOWED MOMENTUM EXCHANGE
X – EQUAL VELOCITIES

COMPONENTS → ↓	MOVING OR STATIONARY	VELOCITY	LF	LS	Na	FG	FV	SV	SFC	SSC	SC	SW	FFC	FFW	SIC	SIW	FP
LIQUID FUEL LF	MOVING COMPONENTS	UFCH		X													
LIQUID STEEL LS			X		Y	Y	Y	Y	Y	Y	Y	Y	Y	Y			Y
SODIUM Na		UMCH		Y		X	X	X	Y	Y							
FISSION GAS FG				Y	X		X	X	Y	Y							
FUEL VAPOR FV				Y	X	X		X	Y	Y							
STEEL VAPOR SV				Y	X	X	X		Y	Y							
SOLID FUEL CHUNKS SFC		ULCH		Y	Y	Y	Y	Y		X							
SOLID STEEL CHUNKS SSC				Y	Y	Y	Y	Y	X								
STEEL CLADDING SC	STATIONARY																
STEEL HEXCAN WALL SW																	
FROZEN FUEL ON CLADDING FFC																	
FROZEN FUEL ON HEXCAN WALL FFW																	
STEEL INCLUSIONS IN CLADDING CRUST SIC																	
STEEL INCLUSIONS IN HEXCAN WALL CRUST SIW																	
FUEL PIN FP																	

Fig. 16.4-9: Momentum Exchange Possibilities among Various LEVITATE Components, for the Steel Annular Flow Regime

LEGEND

Y – ALLOWED MOMENTUM EXCHANGE

X – EQUAL VELOCITIES

COMPONENTS → / ↓		MOVING OR STATIONARY	VELOCITY	LF	LS	Na	FG	FV	SV	SFC	SSC	SC	SW	FFC	FFW	SIC	SIW	FP
LIQUID FUEL	LF	MOVING COMPONENTS	UFCH		X													
LIQUID STEEL	LS			X		Y	Y	Y	Y	Y	Y	Y	Y	Y	Y			Y
SODIUM	Na		UMCH		Y		X	X	X									
FISSION GAS	FG				Y	X		X	X									
FUEL VAPOR	FV				Y	X	X		X									
STEEL VAPOR	SV				Y	X	X	X										
SOLID FUEL CHUNKS	SFC		ULCH		Y						X							
SOLID STEEL CHUNKS	SSC				Y					X								
STEEL CLADDING	SC	STATIONARY																
STEEL HEXCAN WALL	SW																	
FROZEN FUEL ON CLADDING	FFC																	
FROZEN FUEL ON HEXCAN WALL	FFW																	
STEEL INCLUSIONS IN CLADDING CRUST	SIC																	
STEEL INCLUSIONS IN HEXCAN WALL CRUST	SIW																	
FUEL PIN	FP																	

Fig. 16.4-10: Momentum Exchange Possibilities among Various LEVITATE Components, for the Steel Bubbly Flow Regime

16.4.2 Method of Solution and general Numerical Considerations

16.4.2.1 Variables and Mesh Grid Used in Calculations

The independent variables used in LEVITATE are the axial coordinate, z, and the time, t. Only one spatial coordinate is necessary, as LEVITATE models the subassembly in a one-dimensional geometry. The dependent variables calculated by the hydrodynamic model for each component, are the generalized density ρ′, the enthalpy h (or temperature T), and the velocity u. The generalized densities have been introduced in Chapter 14 and, for component k, are defined as:

$$\rho'_{k,i} = \rho_{k,i} \cdot \frac{A_{k,i}}{AXMX} = \rho_{k,i} \cdot \theta_{k,i} \qquad (16.4\text{-}1)$$

where

$\rho_{k,i}$ = physical density of component k at location i

$A_{k,i}$ = cross sectional area occupied by component k at location i

AXMX = reference area

$\theta_{k,i}$ = generalized (area) fraction of component k at location i

The mass, energy and momentum partial differential conservation equations are solved using an Eulerian finite difference semi-explicit formulation, as explained below. The mesh grid used for the finite difference formulation is presented in Fig. 16.4-11. As indicated in this figure, the densities and enthalpies are defined at the center of each cell, while the velocities are defined at the boundaries. Because of the highly irregular geometry treated by LEVITATE, special attention was necessary for the treatment of abrupt area changes [16-12]. Fuel velocities are defined at each cell boundary, with u_i being the velocity just before boundary i, and $u"_i$ the velocity just after that boundary. The terms "before" and "after" are used in relation to the positive direction of the axial coordinate z.

In order to reduce the numerical diffusion, characteristic of Eulerian numerical schemes, the boundaries of each region containing a certain component are tracked separately as they move through the Eulerian cells.

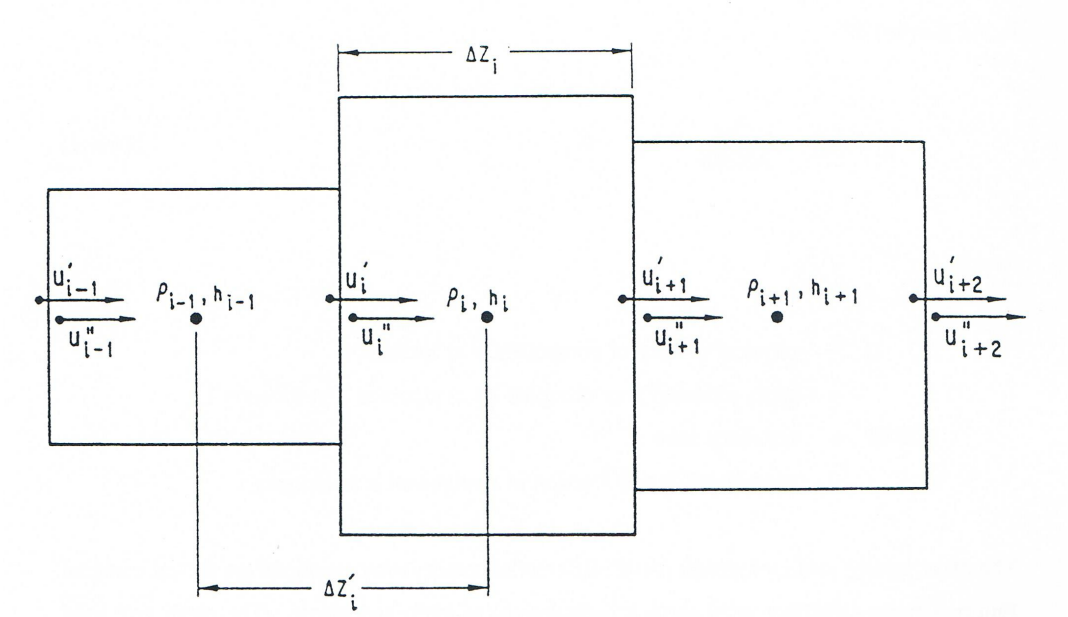

Fig. 16.4-11: Mesh Grid used in the Channel Hydrodynamic Model

16.4.2.2 Description of the Method of Solution and Logic Flow

A simplified modular chart of the LEVITATE model is presented in Fig. 16.1-5. The calculation begins by calculating the changes in the position of material boundaries during the current time step. The new interface positions, at the end of the time step, are calculated for all components, except sodium in the LEIF (LEVITATE INTERFACE) routine. The position of the sodium slugs, which determine the boundaries of the sodium region, is calculated in the LEREZO (LEVITATE REZONING) routine. This routine can add (or remove) nodes to the LEVITATE compressible region as the sodium slugs move out of (or into) the channel. The mass conservation equation is solved next, for all components and all axial locations. Each equation is solved explicitly, i.e., the convective fluxes are based on the generalized densities present in each cell at the beginning of the time step. These calculations are performed in the LEMACO (LEVITATE MASS CONSERVATION) routine. The new densities are then used in the LEVOFR (LEVITATE VOLUME FRACTION) routine to determine the volume fraction of each component at each axial location. Using these volume fractions, the LEVOFR routine also determines the flow regime in each axial cell. This flow regime will be assumed to exist in the cell for the duration of the time step. It is worth noting that this is an "implicit type" assumption as the flow regimes are based on the densities calculated at the end of the time step. The next routine called is LEGEOM (LEVITATE GEOMETRY) which determines the geometrical characteristics defining each local configuration. This routine will change the thickness of the fuel crust as necessary or determine the fraction of the cladding circumference covered by the liquid fuel in the partial annular flow regime. In general, LEGEOM calculates the area of contact between various components in various flow regimes. These areas will be used later in calculating the energy and momentum transfer between various components.

The next routine called is LETRAN (LEVITATE TRANSFER) which calculates the heat-transfer and friction coefficients for all axial locations and among all components that are in direct contact. Thus, the code will use the flow regimes present at a certain location to determine which heat transfer and friction coefficients have to be calculated. The allowable exchanges for each flow regime and each component have already been presented in Figs. 16.4-3 through 16.4-10. Once contact areas and the corresponding heat-transfer coefficients have been calculated, the energy conservation equation can be solved for all components. The LESOEN (LEVITATE SOLID, LIQUID AND STATIONARY ENERGY EQUATION) routine is called to solve the energy conservation equations for the fuel and steel channels, liquid fuel, liquid steel, stationary cladding, hexcan wall, frozen fuel on the cladding and frozen fuel on the hexcan wall. All equations are solved explicitly, i.e., the convective fluxes are based on beginning of time step densities, thus allowing the axial decoupling of the equations. The energy equation for sodium (two-phase or single-phase vapor) and fission gas is solved in LENAEN (LEVITATE SODIUM-NA ENERGY). The energy equations for fuel and steel vapor are solved in LEFUVA (LEVITATE FUEL VAPOR ENERGY) and LESEVA (LEVITATE STEEL VAPOR ENERGY), respectively. The new temperatures calculated in LENAEN, LEFUVA and LESEVA are used to determine the new pressure of each of the compressible components and thus the total new pressure. The hydrodynamic in-pin model is then used to advance the in-pin solution in the LElPIN and LE2PIN routines. These routines interact with the channel model via the fuel injection process, which is modeled in the LElPIN routine. Molten fuel and fission gas are ejected from the cavity into the channel, leading to changes in the local pressure. The momentum equation for each of the three velocity fields is then solved in the routine LEMOCO (LEVITATE MOMENTUM CONSERVATION). The method of solution is still explicit and the equations are uncoupled axially, but the equations for all three fields are solved simultaneously rather than independently, as was done in the mass and energy equations. Also it is important to note that the pressures used in the momentum equation are the pressures at the end of the time step. The routine called next, LELUME (LEVITATE CHUNK-LU MELTING), calculates the melting and the size changes of the solid fuel/steel chunks at all axial locations. The routine LEFREZ (LEVITATE FREEZING AND MELTING) then models a series of important processes, such as fuel/steel freezing and crust formation, fuel/steel chunk formation, fuel crust remelting and breakup. Next called is the routine LEABLA (LEVITATE ABLATION) which calculates the gradual melting and ablation of the cladding and hexcan wall. The routine LEDISR (LEVITATE DISRUPTION) performs the disruption of the fuel pin whenever a disrupted node is predicted. The disruption, which can occur in one or more nodes in any time step, leads to changes in geometry, mass, energy and pressure for various components present in the respective cell. Finally, the routine LESRME (LEVITATE STRUCTURE MELTING) calculates the rupture of the hexcan wall, due to melting and/or pressure burst effects.

16.4.3 Differential Equations and Finite Difference Equations

16.4.3.1 Mass Conservation Equations

This section describes the solution of the mass conservation equations for a generic component k, as performed in the routine LEMACO. The region where the k component

is present has been previously updated in the routines LEIF and LEREZO, and is defined by two integers $i_{k,BT}$ and $i_{k,TP}$, indicating the number of the bottom and top node of the region, respectively. A mass conservation equation is solved for each axial node i, with $i_{k,BT} \le i \le i_{k,TP}$. The original mass conservation is written as:

$$\frac{\partial}{\partial t}\left(\rho_{k,i} \cdot A_{k,i} \cdot \Delta z_i\right) + \left[(\rho A u)_{k,i+1/2} - (\rho A u)_{k,i-1/2}\right] = 0 \qquad (16.4\text{-}2)$$

No source terms are considered in LEMACO, as all phase changes and injections are treated in separate routines, which will be described later.

After dividing by AXMX $\cdot \Delta z_i$ and using the definition of generalized densities, we obtain:

$$\frac{\partial}{\partial t}\rho'_{k,i} = -\left[(\rho' u)_{k,i+1/2} - (\rho' u)_{k,i-1/2}\right] \cdot \frac{1}{\Delta z_i} \qquad (16.4\text{-}3)$$

Finally, after integrating over the length of the time step, Δt, we obtain:

$$\Delta\rho'_{k,i} = -\left[(\rho' u)_{k,i+1/2} - (\rho' u)_{k,i-1/2}\right] \cdot \frac{\Delta t}{\Delta z_i} \qquad (16.4\text{-}4)$$

or

$$\rho'^{n+1}_{k,i} = \rho'^{n}_{k,i} - \left[(\rho' u)_{k,i+1/2} - (\rho' u)_{k,i-1/2}\right] \cdot \frac{\Delta t}{\Delta z_i} \qquad (16.4\text{-}5)$$

In relation to the use of the superscripts, it is noted that whenever a time-dependent quantity such as (ρ′u) is written without a superscript, its value is evaluated at the beginning of the computational time step.

The quantity $(\rho' u)_{k,i-1/2}$ is the mass convective flux of component k at the boundary i-1/2 and is calculated using an upstream differencing approach:

If $u'_{k,i} \ge 0$,

$$(\rho' u)_{k,i-1/2} = \rho'_{k,i-1} \cdot u'_{k,i} \qquad (16.4\text{-}6a)$$

If $u'_{k,i} < 0$, then

$$(\rho' u)_{k,i-1/2} = \rho'_{k,i} \cdot u''_{k,i} \qquad (16.4\text{-}6b)$$

The velocities $u'_{k,i}$ and $u''_{k,i}$ are correlated by the mass continuity equation across boundary i-1/2:

$$u'_{k,i}\,\rho_{k,i-1}\,A_{k,i-1} = u''_{k,i}\cdot\rho_{k,i}\cdot A_{k,i} \tag{16.4-7}$$

The solution of the mass equation is illustrated below for the molten fuel component. The molten fuel region extends from $i_{fu,BT}$ = IFFUBT to $i_{fu,TP}$ = IFFUTP. The first step in the solution is to calculate the convective fuel fluxes at all internal cell boundaries. It is important to note that the convective fluxes defined at boundary i-1/2 have the subscript i, in the code, i.e., COFUCH(I). Similarly, those defined at the boundary i+1/2 have the subscript i+1.

Note that the velocity $u''_{k,i}$ is stored as UFCH(I), and the velocity $u'_{k,i}$ used in the previous equations is calculated as:

$$u'_{fu,i} = u''_{fu,i}\cdot CCFU(I) \tag{16.4-8}$$

where the coefficient CCFU(I) is defined by the Eq. 16.4-7 as:

$$CCFU(I) = \frac{u'_{fu,i}}{u''_{fu,i}} = \frac{\rho_{fu,i}\cdot A_{fu,i}}{\rho_{fu,i-1}\cdot A_{fu,i-1}} = \frac{\rho'_{fu,i}}{\rho'_{fu,i-1}} \tag{16.4-9}$$

The convective fluxes through the boundaries of the fuel region are set to zero, as no fuel is allowed to cross these boundaries in the LEMACO routine.

$$\left(\rho' u\right)_{fu,IFFUBT} = 0 \tag{16.4-10a}$$

$$\left(\rho' u\right)_{fu,IFFUTP+1} = 0 \tag{16.4-10b}$$

To preserve the accuracy of results in the boundary cells a correction is applied to the convective fluxes through all boundaries IFFUBT+1 and IFFUTP whenever the corresponding interface (bottom and top) crosses that boundary during the time step. This correction is explained below for the case when the top fuel boundary crosses the cell boundary. The location of the interface at the end of the time step has already been calculated in the routine LEIF and is shown in Fig. 16.4-12. The value of $(\rho' u)_{fu,IFFUTP}$ is calculated according to Eq. 16.4-7 and then used in Eq. 16.4-5. The implicit assumption in Eq. 16.4-5 is that the value of the convective fluxes is constant over the length of the time step. However, as shown in Fig. 16.4-12 the original location of the fuel interface was $FUIFTP^0(1)$, and, before the interface reaches the cell boundary ZC(IFFUTP), the flux across the boundary is zero. The fraction of Δt during which the convective flux is present is:

$$F_{correction} = \frac{FUIFTP(1) - ZC(IFFUTP)}{FUIFTP^0(1) - FUIFTP(1)} \tag{16.4-11}$$

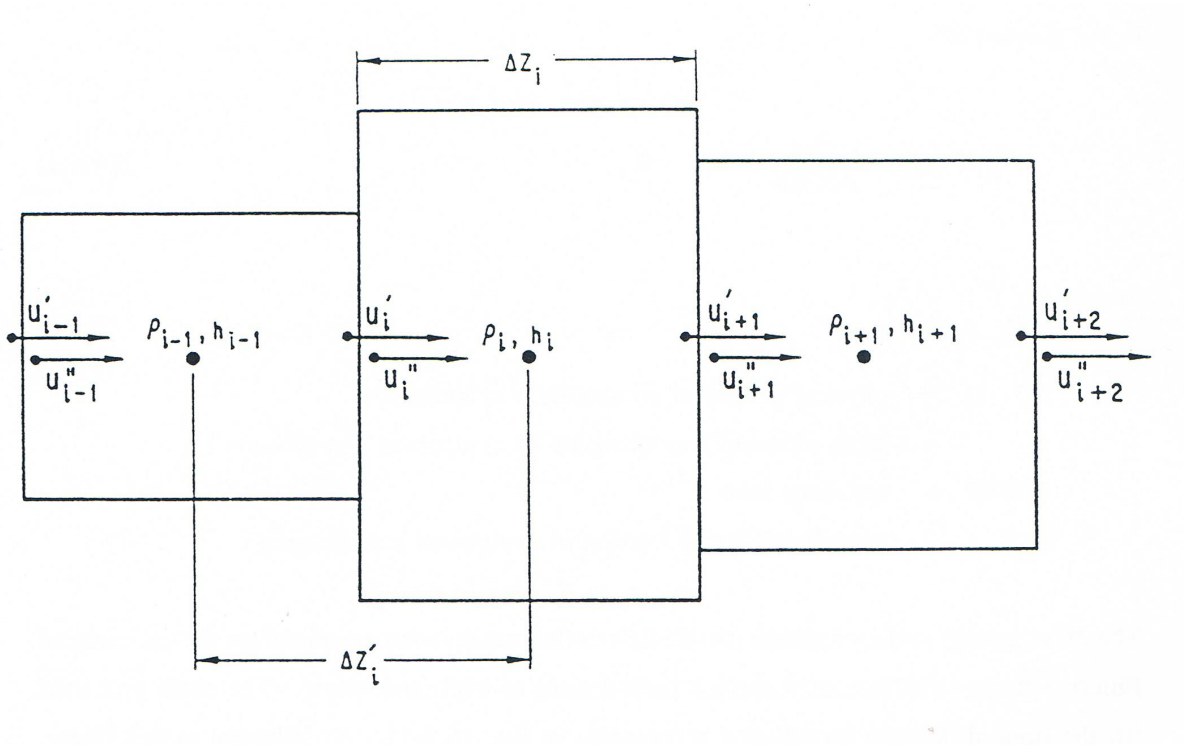

Fig. 16.4-12: Correction for Material Boundary Crossing a Cell Boundary

In order to maintain the form of Eq. 16.4-5, rather than changing the value of Δt associated with $(\rho' u)_{fu,IFFUTP}$ a corrected flux is defined, such that the product flux * time is correct:

$$(\rho' u)_{fu,IFFUTP} = (\rho' u)_{fu,IFFUTP} \cdot F_{correction} \tag{16.4-12}$$

A similar correction is applied for the bottom boundary.

Similar mass conservation equations are solved for all other LEVITATE components, i.e. molten steel, fuel and steel chunks, fission gas, sodium, steel vapor, fuel vapor, fission gas still present in the chunks and fission gas present in the molten fuel.

16.4.3.2 Liquid Fuel Energy Conservation Equations

The liquid fuel energy equation is solved in the routine LESOEN, for all cells in the molten fuel region, i.e., IFFUBT ≤I≤IFFUTP. We begin with the energy equation in conservation form:

$$\begin{aligned} &\frac{\partial}{\partial t}\left(\rho_{fu,i} \cdot h_{fu,i} \cdot A_{fu,i} \cdot \Delta z_i\right) + \left[(\rho A h u)_{i+1/2} - (\rho A h u)_{i-1/2}\right] \\ &\qquad = Q_{fu,i} \cdot \rho_{fu,i} \cdot A_{fu,i} \cdot \Delta z_i - \sum_j H_{fu,j,i} \cdot A_{fu,j,i} \cdot \Delta T_{fu,j,i} \end{aligned} \tag{16.4-13}$$

where:

$Q_{fu,i}$ = fission power source in cell i [J/(s · kg)]

$H_{fu,j,i}$ = heat-transfer coefficient between fuel and component *j* in cell *i* [J/(m² · s · K)]

$A_{fu,j,i}$ = heat-transfer area between fuel and component j in cell i [m²]

After dividing by AXMX · Δz_i and using the definition of generalized densities, we obtain:

$$\frac{\partial}{\partial t}\left(\rho'_{fu,i} \cdot h_{fu,i}\right) = -\left[\left(\rho' hu\right)_{i+1/2,fu} - \left(\rho' hu\right)_{i-1/2,fu}\right] \cdot \frac{1}{\Delta z_i} + Q_{fu,i} \cdot \rho'_{fu,i} - \sum_j H'_{fu,j,i} \cdot \Delta T_{fu,j,i} \tag{16.4-14}$$

where

$$H'_{fu,j,i} = H_{fu,j,i} \cdot \frac{A_{fu,j,i}}{AXMX \cdot \Delta z_i} \tag{16.4-15}$$

Integrating over Δt and using the identity:

$$\Delta\left(\rho' h\right) = \rho'^{n+1} \cdot \Delta h + h^n \cdot \Delta\rho' \tag{16.4-16}$$

we obtain:

$$\rho'^{n+1}_{fu,i} \Delta h_{fu,i} = -\left[\left(\rho' hu\right)_{i+1/2,fu} - \left(\rho' hu\right)_{i-1/2,fu}\right] \cdot \frac{\Delta t}{\Delta z_i} - h^n_{fu,i} \cdot \Delta\rho'_{fu,i} + Q'_{fu,i} \cdot \rho'_{fu,i} \cdot \Delta t - \sum_j H'_{fu,j,i} \cdot \Delta T_{fu,j,i} \cdot \Delta t \tag{16.4-17}$$

Finally, dividing Eq. 16.4-17 by $\rho'^{n+1}_{fu,i}$ and expressing $\Delta\rho'_{fu,i}$ as:

$$\Delta\rho'_{fu,i} = -\left[\left(\rho' u\right)_{fu,i+1/2} - \left(\rho' u\right)_{fu,i-1/2}\right] \cdot \frac{\Delta t}{\Delta z_i} \tag{16.4-18}$$

from the continuity Eq. 16.4-4, we obtain the change in the fuel enthalpy:

$$\Delta h_{fu,i} = \Big\{ -\left[(\rho' hu)_{fu,i+1/2} - (\rho' hu)_{fu,i-1/2}\right] \cdot \frac{1}{\Delta z_i} + h^n_{fu,i}\left[(\rho' u)_{fu,i+1/2} - (\rho' u)_{fu,i-1/2}\right] \cdot \frac{1}{\Delta z_i} + Q_{fu,i} \cdot \rho'_{fu,i} - \sum_j H'_{fu,j,i} \cdot \Delta T_{fu,j,i} \Big\} \cdot \frac{\Delta t}{\rho'^{n+1}_{fu,i}} \quad (16.4\text{-}19)$$

The new fuel enthalpy is obtained as:

$$h^{n+1}_{fu,i} = h^n_{fu,i} + \Delta h_{fu,i} \quad (16.4\text{-}20)$$

The energy convective terms in Eq. 16.4-19 are calculated using an upstream differencing approach, i.e.;

$$(\rho' hu)_{fu,i-1/2} = \begin{cases} \rho'_{fu,i-1} \cdot h_{fu,i-1} \cdot u'_{fu,i} & \text{if } u'_{fu,i} \geq 0 \\ \rho'_{fu,i} \cdot h_{fu,i} \cdot u''_{fu,i} & \text{if } u'_{fu,i} < 0 \end{cases} \quad (16.4\text{-}21)$$

These fluxes are based on the fuel densities, enthalpies and velocities at the of the time step. They are calculated in the routine LEMACO, before the calculation of the new densities, and stored in the array COFUOS(I). The sum of the heat-transfer contributions, $\sum_j H'_{fu,j,i} \cdot \Delta T_{fu,j,i}$ is presented in detail in Eq. 16.4-22.

In the code, Eq. 16.4-19 is written as:

$$\begin{aligned} DEGEOS = [&- COFUOA + COFUOB + HSFU(I) * DEFUCH(I) \\ &- HTFUNA(I) * (TEFUOS(I) - TENA(I)) \\ &- HTFUCL(I) * (TEFUOS(I) - TECLOS(I)) \\ &- HTFUFL(I) * (TEFUOS(I) - TELUCH(I)) \\ &- HTFUSL(I) * (TEFUOS(I) - TESELU(I)) \\ &- HTFUSR(I) * (TEFUOS(I) - TESROS(I)) \\ &- HTSEFU(I) * (TEFUOS(I) - TESECH(I))] \\ &* DTPLU / DEFUCH(I) \end{aligned} \quad (16.4\text{-}22)$$

where

$$COFUOA = \left[\left(\rho' hu\right)_{fu,i+1/2} - \left(\rho' hu\right)_{fu,i-1/2}\right] \cdot \frac{1}{\Delta z_i} \tag{16.4-23}$$

$$COFUOB = h^n_{fu,i} \cdot \left[\left(\rho' u\right)_{fu,i+1/2} - \left(\rho' u\right)_{fu,i-1/2}\right] \cdot \frac{1}{\Delta z_i} \tag{16.4-24}$$

HTFUNA(I) = $H'_{fu,mi,i}$ = generalized heat-transfer coefficient between fuel and gas mixture in cell *i*

HTFUCL(I) = $H'_{fu,cl,i}$ = generalized heat-transfer coefficient between fuel and cladding in cell *i*

HTFUFL(I) = $H'_{fu,fl,i}$ = generalized heat-transfer coefficient between fuel and fuel chunks in cell i

HTFUSL(I) = $H'_{fu,sl,i}$ = generalized heat-transfer coefficient between fuel and steel chunks in cell i

HTFUSR(I) = $H'_{fu,sr,i}$ = generalized heat-transfer coefficient between fuel and hexcan wall in cell i

HTSEFU(I) = $H'_{fu,se,i}$ = generalized heat-transfer coefficient between fuel and molten steel in cell i

The generalized transfer coefficients $H'_{fu,j,i}$ are related to the heat-transfer coefficients $H_{fu,j,i}$ and the transfer areas $A_{fu,j,i}$ by Eq. 16.4-15. These transfer coefficients are calculated prior to the energy equation solution in the routine LETRAN (LEVITATE TRANSFER). Depending on the flow regime, some of those coefficients can be zero, as illustrated in the decision arrays Figs. 16.4-3 through 16.4-6.

After the energy change is calculated, and the new energy is obtained according to Eq. 16.4-20, the temperature of the fuel is calculated by using an external function, TEFUEG, which uses the enthalpy as argument

$$T^{n+1}_{fu,i} = T\left(h^{n+1}_{fu,i}\right) \tag{16.4-25}$$

Several checks are performed on the final temperature in order to avoid numerical difficulties. Thus, if only small amounts of fuel are present (fuel volume less than .1% of the cell volume) the temperature of the fuel is set equal to the cladding temperature or, if the fuel is surrounded by molten steel, to the molten steel temperature.

The condensation/vaporization energy sources/sinks are not included here. They will be introduced later in this chapter, when presenting the energy conservation calculation for fuel vapor.

16.4.3.3 Liquid Steel Energy Conservation Equation

The liquid steel energy equation is solved in the routine LESOEN, for all cells in the molten steel region, i.e. IFSEBT ≤ I ≤ IFSETP. The energy conservation equation is similar to the molten fuel equation, but does not include a fission source term. Thus, the change in the steel enthalpy is:

$$\Delta h_{se,i} = \left\{ -\left[(\rho' hu)_{se,i+1/2} - (\rho' hu)_{se,i-1/2}\right] \cdot \frac{1}{\Delta z_i} + h^n_{se,i}\left[(\rho' u)_{se,i+1/2} - (\rho' u)_{se,i-1/2}\right] \cdot \frac{1}{\Delta z_i} - \sum_j H'_{se,j,i} \cdot \Delta T_{se,j,i} \right\} \cdot \frac{\Delta t}{\rho'^{n+1}_{se,i}} \tag{16.4-26}$$

The new steel enthalpy is obtained as:

$$h^{n+1}_{se,i} = h^n_{se,i} + \Delta h_{se,i} \tag{16.4-27}$$

The energy convective terms in Eq. 16.4-26 are calculated using an upstream differencing approach, similar to Eq. 16.4-19. They are calculated in routine LEMACO and stored under the name COSEOS(I). These fluxes are based on steel densities enthalpies and velocities at the beginning of the time step.

If $u'_{se,i} \geq 0$,

$$(\rho' hu)_{se,i-1/2} = \rho'_{se,i-1} \cdot h_{se,i-1} \cdot u'_{se,i} \tag{16.4-28a}$$

If $u'_{se,i} < 0$, then

$$(\rho' hu)_{se,i-1/2} = \rho'_{se,i} \cdot h_{se,i} \cdot u''_{se,i} \tag{16.4-28b}$$

As previously explained, the molten steel and molten fuel share the same velocity field. Thus $u'_{se,i}$ and $u'_{fu,i}$ have the same value, stored in the array UFCH(I).

In the code, Eq. 16.4-26 is written as:

$$
\begin{aligned}
DEEGSE = \big[& -COSEOA + COSEOB \\
& - HTSEFU(I) * (TESECH(I) - TEFUOL(I)) \\
& - HTSECL(I) * (TESECH(I) - TECLOS(I)) \\
& - HTSESR(I) * (TESECH(I) - TESROS(I)) \\
& - HTSEFL(I) * (TESECH(I) - TELUCH(I)) \\
& - HTSESL(I) * (TESECH(I) - TESELU(I)) \\
& - HTSENA(I) * (TESECH(I) - TENA(I))\big] \\
& * DTPLU / DESECH(I)
\end{aligned}
\tag{16.4-29}
$$

where

$$
COSEOA = \left[(\rho' hu)_{se,i+1/2} - (\rho' hu)_{se,i-1/2} \right] \cdot \frac{1}{\Delta z_i}
\tag{16.4-30}
$$

$$
COSEOB = h^n_{se,i} \cdot \left[(\rho' u)_{se,i+1/2} - (\rho' u)_{se,i-1/2} \right] \cdot \frac{1}{\Delta z_i}
\tag{16.4-31}
$$

HTSEFU(I) = $H'_{se,fu,i}$ = transfer coefficient between steel and fuel in cell *i*

HTSECL(I) = $H'_{se,cl,i}$ = transfer coefficient between steel and cladding in cell *i*

HTSESR(I) = $H'_{se,sr,i}$ = transfer coefficient between steel and hexcan wall in cell *i*

HTSEFL(I) = $H'_{se,fl,i}$ = transfer coefficient between steel and fuel chunks in cell *i*

HTSESL(I) = $H'_{se,sl,i}$ = transfer coefficient between steel and steel chunks in cell *i*

HTSENA(I) = $H'_{se,mi,i}$ = transfer coefficient between steel and gas mixture in cell *i*

The generalized heat-transfer coefficients are defined by:

$$
H'_{se,j,i} = H_{se,j,i} \cdot \frac{A_{se,j,i}}{AXMX \cdot \Delta z_i}
\tag{16.4-32}
$$

and are described in detail in Section 16.4.3.10.

After the energy change is calculated, the new energy of the steel is calculated according to Eq. 16.4-27, and the temperature of the steel is obtained by using an external function, TESEEG, which uses the enthalpy as argument:

$$T_{se,i} = T\left(h_{se,i}^{n+1}\right) \tag{16.4-33}$$

Several checks are performed during the steel temperature calculation in order to avoid numerical difficulties. Thus, if only small amounts of molten steel are present (steel volume less than .1% of the cell volume) the temperature of the steel is set equal to the cladding temperature or, if the steel is surrounded by molten fuel, to the molten fuel temperature.

The condensation/vaporization energy sources/sinks are not included here. They will be introduced later in this chapter, when the energy conservation calculation for steel vapor is presented.

16.4.3.4 Fuel and Steel Chunk Energy Conservation Equations

These equations are solved in the routine LESOEN. Separate equations are solved for the fuel and steel solid chunks, as described below.

16.4.3.4.1 The Energy Conservation Equation for the Fuel Chunks

The energy equation is written in conservative form as follows:

$$\begin{aligned}&\frac{\partial}{\partial t}\left(\rho_{f\ell,i} \cdot h_{f\ell,i}\ A_{f\ell,i} \cdot \Delta z\ \right) + \left[(\rho A h u)_{f\ell,i+1/2} - (\rho A h u)_{fl,i-1/2}\right] \\ &= Q_{f\ell,i} \cdot \rho_{f\ell,i} \cdot A_{f\ell,i} \cdot \Delta z_i - \sum_j H_{f\ell,j,i} \cdot A_{f\ell,j,i} \cdot \Delta T_{f\ell,j,i}\end{aligned} \tag{16.4-34}$$

where

$Q_{fl,i}$ = fission power source in the fuel in cell i [J/s·kg]

$A_{fl,i}$ = area covered by chunks in cell i, when imagined as a continuum with density ρ_{fl}.

Following the same steps as outlined in Eq. 16.4-14 through 16.4-19, we obtain:

$$\begin{aligned}\Delta h_{f\ell,i} = \Bigg\{ &-\left[(\rho' h u)_{f\ell,i+1/2} - (\rho' h u)_{f\ell,i-1/2}\right] \cdot \frac{1}{\Delta z_i} \\ &+ h_{f\ell,i}^{n} \cdot \left[(\rho' u)_{f\ell,i-1/2} - (\rho' u)_{f\ell,i-1/2}\right] \cdot \frac{1}{\Delta z_i} + Q_{f\ell,i} \cdot \rho'_{f\ell,i} \\ &- \sum_j H'_{f\ell,j,i} \cdot \Delta T_{f\ell,j,i} \Bigg\} \cdot \frac{\Delta t}{\rho'^{n+1}_{f\ell,i}}\end{aligned} \tag{16.4-35}$$

where

$$\sum_j H'_{f\ell,j,i} \cdot \Delta T_{f\ell,j,i} = H'_{fu,f\ell,i} \cdot \left(T_{f\ell,i} - T_{fu,i}\right) + H'_{se,f\ell,i} \cdot \left(T_{f\ell,i} - T_{se,i}\right) + H'_{Na,f\ell,i} \cdot \left(T_{f\ell,i} - T_{Na,i}\right) + H'_{cl,f\ell,i} \cdot \left(T_{f\ell,i} - T_{cl,i}\right) + H'_{sr,f\ell,i} \cdot \left(T_{f\ell,i} - T_{sr,i}\right) + H'_{ffc,f\ell,i} \cdot \left(T_{f\ell,i} - T_{ffc,i}\right) + H'_{ffs,f\ell,i} \cdot \left(T_{f\ell,i} - T_{ffs,i}\right) + H'_{f\ell,sl,i} \cdot \left(T_{f\ell,i} - T_{s\ell,i}\right) \quad (16.4\text{-}36)$$

The energy convective terms in Eq. 16.4-35 are calculated using an upstream differencing approach, similar to that used for Eq. 16.4-21. The convective fluxes are calculated in the routine LEMACO, before the calculation of the new fuel chunk densities, and stored in the array COLVOS(I). The new fuel chunk enthalpy and temperature are then calculated:

$$h_{f\ell,i}^{n+1} = h_{f\ell,i}^{n} + \Delta h_{f\ell,i}^{n} \quad (16.4\text{-}37)$$

$$T_{f\ell,i}^{n+1} = T\left(h_{f\ell,i}^{n+1}\right) \quad (16.4\text{-}38)$$

16.4.3.4.2 The Energy Conservation for the Steel Chunks

This equation is very similar to the equation used for the fuel chunks, but the fission energy source is not present anymore. Only the final form of the equation is presented here:

$$\Delta h_{s\ell,i} = \left\{ -\left[(\rho' hu)_{s\ell,i+1/2} - (\rho' hu)_{s\ell,i-1/2}\right] \cdot \frac{1}{\Delta z_i} + h_{s\ell,i}^{n} \cdot \left[(\rho' u)_{s\ell,i+1/2} - (\rho' u)_{s\ell,i-1/2}\right] \cdot \frac{1}{\Delta z_i} - \sum_j H'_{s\ell,j,i} \cdot \Delta T_{s\ell,j,i} \right\} \cdot \frac{\Delta t}{\rho'^{n+1}_{s\ell,i}} \quad (16.4\text{-}39)$$

where

$$\sum_j H'_{s\ell,j,i} \cdot \Delta T_{s\ell,j,i} = H'_{fu,s\ell,i} \cdot \left(T_{s\ell,i} - T_{fu,i}\right) + H'_{se,s\ell,i} \cdot \left(T_{s\ell,i} - T_{se,i}\right) + H'_{Na,s\ell,i} \cdot \left(T_{s\ell,i} - T_{Na,i}\right) + H'_{cl,s\ell,i} \cdot \left(T_{s\ell,i} - T_{cl,i}\right) + H'_{sr,s\ell,i} \cdot \left(T_{s\ell,i} - T_{sr,i}\right) + H'_{ffc,s\ell,i} \cdot \left(T_{s\ell,i} - T_{ffc,i}\right) + H'_{ffs,s\ell,i} \cdot \left(T_{s\ell,i} - T_{ffs,i}\right) + H'_{f\ell,s\ell,i} \cdot \left(T_{s\ell,i} - T_{f\ell,i}\right) \quad (16.4\text{-}40)$$

The new steel chunk enthalpy and temperature are then calculated as follows:

$$h_{s\ell,i}^{n+1} = h_{s\ell,i}^{n} + \Delta h_{s\ell,i}^{n} \tag{16.4-41}$$

$$T_{s\ell,i}^{n+1} = T\left(h_{s\ell,i}^{n+1}\right) \tag{16.4-42}$$

16.4.3.5 Sodium and Fission-gas Energy Conservation Equation

The sodium and the fission gas are assumed in LEVITATE to be in equilibrium at the same temperature $T_{Na,i}$. The sodium can exist in the form of superheated vapor or as a two-phase, vapor-liquid mixture. When required by the thermodynamic conditions the two-phase sodium component can become subcooled sodium. The two-phase sodium is assumed to be in thermodynamic equilibrium. The energy conservation equation is solved simultaneously for sodium and fission gas for all cells in the LEVITATE interaction region, i.e., IFMIBT ≤ I ≤ IFMITP. Because the fission-gas region extends only between IFFIBT ≤ I ≤ IFFITP, it is possible that some cells contain only sodium, without any fission gas. In these cells, the energy equation for the sodium-fission-gas mixture reduces to a sodium-only equation. Because significant differences exist between the behavior of superheated and two phase sodium, two separate equations are used.

16.4.3.5.1 The Energy Conservation Equation for Superheated Sodium and Fission Gas

The energy equation used for superheated sodium and fission gas is written in conservative form as:

$$\begin{aligned}
&\frac{\partial}{\partial t}\left(\rho_{Na,i}\, h_{Na,i} + \rho_{fi,i}\, h_{fi,i}\right)\cdot A_{Mi.i}\cdot \Delta z_i + \left[(\rho A h u)_{Na,i+1/2}\right. \\
&\quad \left. + (\rho A h u)_{fi,i+1/2} - (\rho A h u)_{Na,1-1/2} - (\rho A h u)_{fi.i-1/2}\right] \\
&\quad = A_{Mi,i}\left(\frac{\partial P_{Na,i}}{\partial t} + \frac{\partial P_{fi,i}}{\partial t}\right)\cdot \Delta z_i + A_{Mi.i}\cdot\left[u_{Mi,i}\cdot 0.5\cdot\left(P_{Na,i} + P_{fi,i}\right.\right. \\
&\quad \left.\left. - P_{Na,i-1} - P_{fi,i-1}\right) + U_{Mi,i+1}\cdot 0.5\cdot\left(P_{Na,i+1} + P_{fi,i+1} - P_{Na,i} - P_{fi,i}\right)\right] \\
&\quad + \sum_j H_{j,Mi,i}\cdot A_{j,Mi,i}\cdot \Delta T_{j,Mi,i}
\end{aligned} \tag{16.4-43}$$

where:

$H_{j,Mi,i}$ = heat-transfer coefficient between component j and sodium-fission gas mixture in cell i [J/m² - s- K]

$A_{j,Mi,i}$ = heat-transfer area between component j and the gas mixture in cell i [m²]

$\Delta T_{j,Mi,I}$ = temperature difference between component j and the gas mixture in cell i [K]

After dividing by AXMX · Δz_i and using the definition of generalized densities, we obtain:

$$\begin{aligned}\frac{\partial}{\partial t}\left(\rho'_{Na,i}\,h_{Na,i}+\rho'_{fi,i}\,h_{fi,i}\right)=&-\left[\left(\rho'hu\right)_{Na,i+1/2}+\left(\rho'hu\right)_{fi,i+1/2}\right.\\&\left.-\left(\rho'hu\right)_{Na,i-1/2}-\left(\rho'hu\right)_{fi,i-1/2}\right]\cdot\frac{1}{\Delta z_i}+\theta_{Mi,i}\cdot\left(\frac{\partial P_{Na,i}}{\partial t}+\frac{\partial P_{fi,i}}{\partial t}\right)\\&+\theta_{Mi,i}\cdot\frac{0.5}{\Delta z_i}\cdot\left[u_{Mi,i}\cdot\left(P_{Na,i}+P_{fi,i}-P_{Na,i-1}-P_{fi,i-1}\right)\right.\\&\left.+u_{Mi,i+1}\cdot\left(P_{Na,i+1}+P_{fi,i+1}-P_{Na,i}-P_{fi,i}\right)\right]+\sum_j H'_{j,Mi,i}\cdot\Delta T_{j,Mi,i}\end{aligned}\tag{16.4-44}$$

where the generalized heat-transfer coefficients are defined by:

$$H'_{j,Mi,i}=H_{j,Mi,i}\cdot\frac{A_{j,Mi,i}}{AXMX\cdot\Delta z_i}\tag{16.4-45}$$

and the sum of the heat-transfer terms $\sum_j H'_{j,Mi,i}\cdot\Delta T_{j,Mi,i}$ is presented in Eq. 16.4-54. Integrating over Δt and using the identity shown in Eq. 16.4-16 to express the quantity $\Delta(\rho' h)$, we obtain:

$$\begin{aligned}&\rho'^{n+1}_{Na,i}\cdot\Delta h_{Na,i}+\rho'^{n+1}_{fi,i}\cdot\Delta h_{fi,i}\\&\quad=-\left[\left(\rho'hu\right)_{Na,i+1/2}+\left(\rho'hu\right)_{fi,i+1/2}\right.\\&\qquad-h_{Na,i}\cdot\Delta\rho'_{Na,i}-h_{fi,i}\cdot\Delta\rho'_{fi,i}\\&\qquad\left.-\left(\rho'hu\right)_{Na,i-1/2}-\left(\rho'hu\right)_{fi,i-1/2}\right]\cdot\frac{\Delta t}{\Delta z_i}\\&\qquad+\theta_{Mi,i}\cdot\left(\Delta P_{Na,i}+\Delta P_{fi,i}\right)+\theta_{Mi,i}\cdot\frac{0.5\cdot\Delta t}{\Delta z_i}\cdot\left[u_{Mi,i}\cdot\left(P_{Na,i}+P_{fi,i}\right.\right.\\&\qquad\left.\left.-P_{Na,i-1}-P_{fi,i-1}\right)+u_{Mi,i+1}\cdot\left(P_{Na,i+1}+P_{fi,i+1}-P_{Na,i}-P_{fi,i}\right)\right]\\&\qquad+\sum_j H'_{j,Mi,i}\cdot\Delta T_{j,Mi,i}\cdot\Delta t\end{aligned}\tag{16.4-46}$$

Two sets of equation relating the thermodynamic characteristics of a gas are used to refine Eq. 16.4-46. These are:

$$h_{Na,i}=2.5\,R_{Na}\cdot\left(T_{Na}-T_{sat}\right)+h_{Na,vap}\tag{16.4-47a}$$

$$h_{fi,i} = 2.5\ R_{fi} \cdot T_{fi} \tag{16.4-47b}$$

and

$$P_{Na,i} = R_{Na} \cdot \rho'_{Na,i} \cdot T_{Na,i} \cdot \frac{1}{\theta_{Na,i}} \tag{16.4-48a}$$

$$P_{fi,i} = R_{fi} \cdot \rho'_{fi,i} \cdot T_{fi,i} \cdot \frac{1}{\theta_{fi,i}} \tag{16.4-48b}$$

where the constant R_j is defined as:

$$P_j = \frac{R}{M_j} \tag{16.4-49}$$

with

R = universal gas constant [J/mol - K]

M_j = molar mass of gas j [kg/mol]

T_{sat} = $T_{sat}(P_{Na,i})$; $h_{Na,vap} = h_{Na,vap}(P_{Na,i})$.

With $T_{Na,i} = T_{fi,i}$ and $\theta_{Na,i} = \theta_{fi,i} = \theta_{Mi,i}$, after expressing the quantity $\Delta T_{j,Mi,i}$ as:

$$\Delta T_{j,Mi,i} = T_{j,i} - T_{Mi,i}^{n+1} = T_{j,i} - T_{Mi,i} - \Delta T_{Mi,i} \quad , \tag{16.4-50}$$

and differencing Eqs. 16.4-47a and 16.4-47b to obtain $\Delta h_{Na,i}$ and $\Delta h_{fi,i}$, Eq. 16.4-46 becomes:

$$
\begin{aligned}
&\Delta T_{Mi,i}\left[2.5{\rho'}^{n+1}_{\mathrm{Na},i}R_{\mathrm{Na}}+2.5{\rho'}^{n+1}_{\mathrm{fi},i}R_{\mathrm{fi}}\right]\\
&\qquad+\sum_j H'_{j,Mi,i}\Delta T_{Mi,i}\Delta t\\
&\qquad=-\left[(\rho' hu)_{\mathrm{Na},i+1/2}+(\rho' hu)_{\mathrm{fi},i+1/2}-(\rho' hu)_{\mathrm{Na},i+1/2}\right.\\
&\qquad\left.-(\rho' hu)_{\mathrm{fi},i+1/2}\right]\frac{\Delta t}{\Delta z_i}-h_{\mathrm{Na},i}\Delta\rho'_{\mathrm{Na},i}-h_{\mathrm{fi},i}\Delta\rho'_{\mathrm{fi},i}\\
&\qquad+R_{\mathrm{Na}}\Delta\left(\rho'_{\mathrm{Na},i}T_{\mathrm{Na},i}\right)+R_{\mathrm{fi}}\Delta\left(\rho'_{\mathrm{fi},i}T_{\mathrm{fi},i}\right)\\
&\qquad+\theta_{Mi,i}\frac{0.5\Delta t}{\Delta z_i}\left[u_{Mi,i}\left(P_{\mathrm{Na},i}+P_{\mathrm{fi},i}-P_{\mathrm{Na},i-1}-P_{\mathrm{fi},i-1}\right)\right.\\
&\qquad\left.+u_{Mi,i+1}\left(P_{\mathrm{Na},i+1}+P_{\mathrm{fi},i+1}-P_{\mathrm{Na},i}-P_{\mathrm{fi},i}\right)\right]\\
&\qquad+\sum_j H'_{j,Mi,i}\left(T_{j,i}-T_{Mi,i}\right)\Delta t
\end{aligned}
\tag{16.4-51}
$$

After using the identity:

$$\Delta\left(\rho' T\right)=T^n\Delta\rho'+{\rho'}^{n+1}\cdot\Delta T \tag{16.4-51a}$$

and replacing $\Delta\rho'_{\mathrm{Na,i}}$ and $\Delta\rho'_{\mathrm{fi,i}}$ by using the continuity equation, Eq. 16.4-51 becomes:

$$\Delta T_{Mi,i}\cdot\Big[2.5\ \rho'^{n+1}_{Na,i}\,R_{Na}+2.5\ \rho'^{n+1}_{fi,i}\cdot R_{fi}+\sum_j H'_{j,Mi,i}\cdot\Delta t-R_{Na}\,\rho'^{n+1}_{Na,i}$$
$$-R_{fi}\cdot\rho'^{n+1}_{fi,i}\Big]=-\Big[(\rho' hu)_{Na,i+1/2}+(\rho' hu)_{fi,i+1/2}-(\rho' hu)_{Na,i-1/2}$$
$$-(\rho' hu)_{fi,i-1/2}\Big]\cdot\frac{\Delta t}{\Delta z_i}+\left(h_{Na,i}-T_{Na,i}\cdot R_{Na}\right)$$
$$\cdot\left[(\rho' u)_{Na,i+1/2}-(\rho' u)_{Na,i-1/2}\right]\frac{\Delta t}{\Delta z_i}+\left(h_{fi,i}-T_{fi,i}\,R_{fi}\right)$$
$$\cdot\left[(\rho' u)_{fi,i+1/2}-(\rho' u)_{fi,i-1/2}\right]\frac{\Delta t}{\Delta z_i}$$
$$+\theta_{Mi,i}\cdot\frac{0.5\cdot\Delta t}{\Delta z_i}\cdot\Big[u_{MI,i}\cdot\left(P_{Na,i}+P_{fi,i}-P_{Na,i-1}-P_{fi,i-1}\right)$$
$$+u_{Mi,i+1}\cdot\left(P_{Na,i+1}+P_{fi,i+1}-P_{Na,i}-P_{fi,i}\right)\Big]$$
$$+\sum_j H'_{j,Mi,i}\cdot\left(T_{j,i}-T_{Mi,i}\right)\cdot\Delta t \qquad (16.4\text{-}52)$$

The terms derived from the original $\frac{\partial P}{\partial t}$ and, $u\cdot\frac{\partial P}{\partial z}$ terms in Eq. 16.4-43 make a negligible contribution to the right hand side of Eq. 16.4-42. The terms are neglected in the initial release version, but have been added, for completeness, in the chunk development version. The left-hand-side coefficient is replaced by:

$$AUXLR=2.5\,\rho'^{n+1}_{Na,i}\,R_{Na}+2.5\,\rho'^{n+1}_{fi,i}\cdot R_{fi}\cdot\sum_j H'_{j,mi,i}\,\Delta t$$
$$-R_{Na}\,\rho'^{n+1}_{Na,i}-R_{fi}\,\rho'^{n+1}_{fi,i} \qquad (16.4\text{-}53)$$

After dividing Eq. 16.4-52 by AUXLR, the new mixture temperature is calculated as follows:

$$TENA(I)=TENA(I)+(-COENCH+COHELP+DTPLU)$$
$$*(HTNACL(I)*(TECLOL(I)-TENA(I))+HTSENA(I)*(TESEOL(I)-TENA(I)))$$
$$+HTNASR(I)*(TESROL(I)-TENA(I))+HTFUNA(I)*(TEFUOL(I)=TENA(I))$$
$$+HTNAFL(I)*(TEFLOL(I)-TENA(I))+HTNASL(I)*(TESLOL(I)=TENA(I))$$
$$+HTFCNA*(TEFFCO(I)-TENA(I))+HTFSNA*(TEFFSO(I)-TENA(I))/AUXLR \qquad (16.4\text{-}54)$$

where:

$$COENCH = \left[\left(\rho' hu\right)_{Na,i+1/2} + \left(\rho' hu\right)_{fi,i+1/2} - \left(\rho' hu\right)_{Na,i-1/2} - \left(\rho' hu\right)_{fi,i-1/2}\right] \cdot \frac{\Delta t}{\Delta z_i} \tag{16.4-55}$$

$$COHELP = h_{Na,i} \cdot \left[\left(\rho' u\right)_{Na,i+1/2} - \left(\rho' u\right)_{Na,i-1/2}\right] \cdot \frac{\Delta t}{\Delta z_i} + h_{fi,i} \cdot \left[\left(\rho' u\right)_{fi,i+1/2} - \left(\rho' u\right)_{fi,i-1/2}\right] \cdot \frac{\Delta t}{\Delta z_i} \tag{16.4-56}$$

HTNACL(I) = $H'_{cl,Na,i}$ = transfer coefficient between cladding and mixture in cell *i*

HTSENA(I) = $H'_{se,Na,i}$ = transfer coefficient between steel and gas mixture in cell *i*

HTNASR(I) = $H'_{sr,Na,i}$ = transfer coefficient between hexcan wall and gas mixture in cell *i*

HTFUNA(I) = $H'_{fu,Na,i}$ = transfer coefficient between molten fuel and gas mixture in cell *i*

HTNAFL(I) = $H'_{fl,Na,i}$ = transfer coefficient between steel chunks and mixture in cell *i*

HTFCNA = $H'_{ffc,Na,i}$ = transfer coefficient between frozen fuel on cladding and gas mixture in cell *i*

HTFSNA = $H'_{ffs,Na,i}$ = transfer coefficient between frozen fuel on can wall and gas mixture in cell *i*

The convective enthalpy fluxes used in Eq. 16.4-53 are calculated using an upstream differencing approach:

$$\text{If } u'_{Na,i} \geq 0, \quad \left(\rho' hu\right)_{Na,i-1/2} = \rho'_{Na,i-1} \cdot h_{Na,i-1} \cdot u'_{Na,i} \tag{16.4-57a}$$

$$\text{If } u'_{Na,i} < 0, \text{ then } \quad \left(\rho' hu\right)_{Na,i-1/2} = \rho'_{Na,i} \cdot h_{Na,i} \cdot u''_{Na,i} \tag{16.4-57b}$$

The enthalpy $h_{Na,i}$ is calculated as follows

If $X_{Na,i} \geq 1$ (single-phase sodium vapor),

$$h_{Na,i} = h_{Na,vap}\left(P_{Na,i}\right) + 2.5 \cdot R_{Na} \cdot \left(T_{Na,i} - T_{sat}\left(P_{Na,i}\right)\right) \quad (16.4\text{-}58a)$$

If $0 \leq X < 1$ (two-phase sodium), then

$$h_{Na,i} = h_{Na,liq}\left(T_{Na,i}\right) + h_{Na,fg}\left(T_{Na,i}\right) \cdot X_{Na,i} \quad (16.4\text{-}58b)$$

where

$h_{Na,fg}$ ($T_{Na,i}$) = the heat of vaporization of sodium at the temperature $T_{Na,i}$

$h_{Na,liq}$ ($T_{Na,i}$) = enthalpy of liquid sodium on the saturation curve at $T_{Na,i}$

$h_{Na,vap}$ ($P_{Na,i}$) = enthalpy of sodium vapor on the saturation curve at pressure $P_{Na,i}$

If injection of fission gas has taken place in the previous time step, a correction of the temperature is made to account for the enthalpy of the injected gas. When the injection is calculated, this gas is assumed to be at the same temperature as the sodium-fission gas mixture in the channel in order to avoid recalculating the mixture temperature.

$$T_{na,i} = T_{Na,i} + \left(T_{fi,ejected,i} - T_{Na,i}\right) \cdot \Delta\rho'_{fi,ejected,i} \cdot 2.5\ R_{fi} / AUXLR \quad (16.4\text{-}59)$$

The pressure of the mixture is then calculated as:

$$P_{ch,i} = P_{Na,i} + P_{fi,i} \quad (16.4\text{-}60)$$

where $P_{Na,i}$ and $P_{fi,i}$ are calculated using Eqs. 16.4-48a and 16.4-48b. In using this equation for sodium, it is recognized that in the neighborhood of the saturation curve the behavior of the sodium vapor will deviate from the perfect-gas behavior. Thus, the constant $R_{Na,i}$ is allowed to vary so that the pressure calculated by Eq. 16.4-48a will match the saturation pressure when the mixture is right on the saturation curve. The parameter used to decide if this procedure is necessary is the ratio:

$$r_i = \frac{\rho_{Na,i}}{\rho_{Na,vap}\left(T_{Na,i}\right)} \quad (16.4\text{-}61)$$

where

$\rho_{Na,i}$ = physical density of the sodium vapor

$\rho_{Na,vap}$ = physical density of the saturated sodium vapor

If $r_i < r_{min}$ the sodium vapor is far enough from saturation and the perfect-gas law is satisfactory. Otherwise, the constant $R'_{Na,i}$ is defined as:

$$R'_{Na,i} = \left[R_{Na,i} \cdot (1-r) + R_{Na,sat,i} \cdot (r - r_{\min})\right] / (1 - r_{\min}) \tag{16.4-62}$$

where

$$R_{Na,sat,i} = \frac{P_{Na,sat}(T_{Na,i}) \cdot \theta_{Na,i}}{\rho'_{Na,i} \cdot T_{Na,i}} \tag{16.4-63}$$

and r_{min} is the ratio obtained from the sodium thermodynamic properties tables for a wide range of interest; currently r_{min} = .067.

This derivation assumes that the sodium is in the superheated vapor region for the entire duration of the time step Δt. Occasionally, however, the sodium vapor might become saturated and this assumption would no longer hold. In the two-phase region the temperature changes are smaller than those in the single-phase region, since much of the energy lost will lead to condensation, rather than to a change in temperature. Thus, where necessary, a correction is performed which reduces the temperature drop in the two-phase region by bringing the final sodium temperature close to the saturation curve. The correction is considered necessary whenever the following condition is satisfied:

$$P_{Na,i} - P_{Na,sat,i} > \Delta P_{constant} \tag{16.4-64}$$

where $\Delta P_{constant}$ is a built-in constant, currently set to $0.05 \cdot 10^5$ Pa. This procedure is illustrated in Fig. 16.4-13. The corrected sodium temperature is calculated as follows:

$$T_{Na,i} = (T_1 \cdot \Delta P_o - T_o \cdot \Delta P_1) / (\Delta P_o - \Delta P_1) \tag{16.4-65}$$

where

T_o = sodium temperature at the beginning of the time step

T_1 = calculated new sodium temperature, from Eq. 16.4-59

ΔP_o, $\Delta P_1 = P_{Na,sat,i} - P_{Na,i}$ at the beginning and end of time step, respectively.

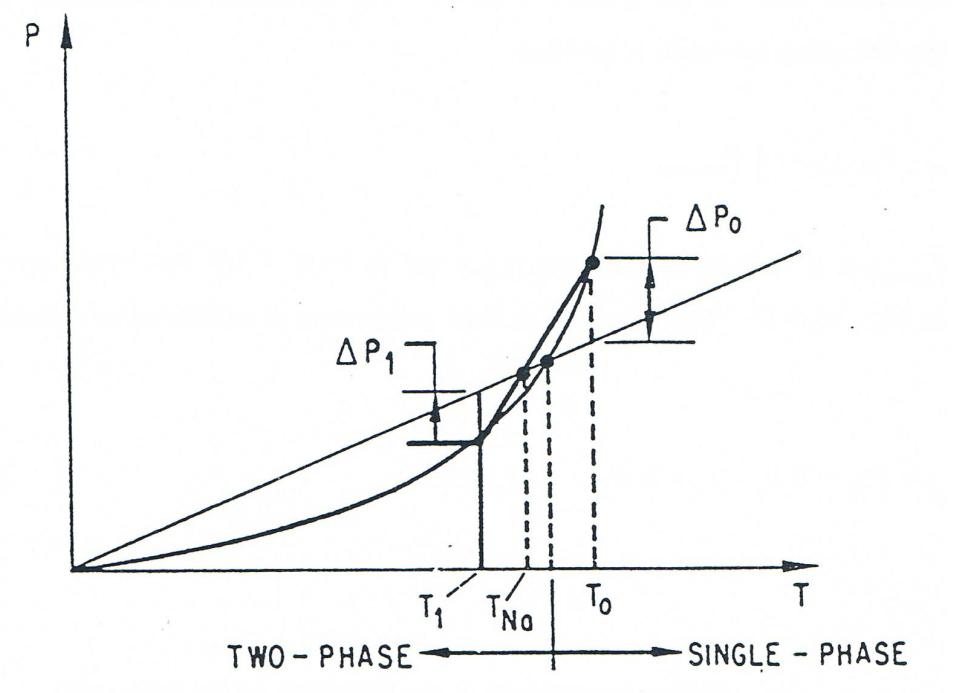

Fig. 16.4-13: Correction for Sodium Vapor Transition to a Two-phase Mixture

16.4.3.5.2 The Energy Equation for Two-phase Sodium and Fission Gas

The same considerations as before are made to arrive at the Eq. 16.4-46, but the compressible term, $\theta \frac{\partial P}{\partial t}$, is not included for the two-phase component. To express the quantity $\Delta h_{Na,i}$, we use the identity:

$$h_{Na,i} = h_{Na,liq,i} \cdot \left(1 - X_{Na,i}\right) + h_{Na,vap,i} \cdot X_{Na,i} \tag{16.4-66}$$

Thus:

$$\begin{aligned} \Delta h_{Na,i} = &\left(1 - X_{Na,i}\right) \cdot \frac{dh_{liq}}{dT} \cdot \Delta T_{Na,i} + X_{Na,i} \cdot \frac{dh_{vap}}{dT} \cdot \Delta T_{Na,i} \\ &+ \left(h_{vap,i} - h_{liq,i}\right) \cdot \Delta X_{Na,i} \end{aligned} \tag{16.4-67}$$

Using the definitions:

$$C_{liq} = \frac{dh_{liq}}{dT} \tag{16.4-68a}$$

$$C_{vap} = \frac{dh_{vap}}{dT} \tag{16.4-68b}$$

$$X = \frac{v - v_{liq}}{v_{vap} - v_{liq}} \tag{16.4-68c}$$

$$h_{lv,i} = h_{vap,i} - h_{liq,i} \tag{16.4-68d}$$

Eq. 16.4-66 becomes:

$$\begin{aligned} \Delta h_{Na,i} &= \left(1 - X_{Na,i}\right) C_{liq} \cdot \Delta T_{Na,i} + X_{Na,i} C_{vap} \cdot \Delta T_{Na,i} + h_{lv,i} \frac{\partial X}{\partial t} \cdot \Delta t \\ &= \left(1 - X_{Na,i}\right) \cdot C_{liq} \cdot \Delta T_{Na,i} + X_{Na,i} C_{vap} \cdot \Delta T_{Na,i} \\ &+ h_{lv,i} \cdot \frac{1}{v_{vap} - v_{liq}} \frac{\partial v}{\partial t} \cdot \Delta t - h_{lv,i} \frac{v - v_{liq}}{\left(v_{vap} - v_{liq}\right)^2} \cdot \frac{dv_v}{dT} \Delta T_{Na,i} \end{aligned} \tag{16.4-69}$$

By substituting:

$$v = \frac{1}{\rho} = \frac{1}{\left(\rho' / \theta\right)} \tag{16.4-70}$$

in Eq. 16.4-69, we obtain:

$$\begin{aligned} \Delta h_{Na,i} &= \left(1 - X_{Na,i}\right) \cdot C_{liq} \cdot \Delta T_{Na,i} + X_{Na,i} \cdot C_{vap} \cdot \Delta T_{Na,i} \\ &+ h_{lv,i} \cdot \frac{1}{v_{vap} - v_{liq}} \cdot \frac{\theta^2}{\rho'^2} \left[\frac{1}{\theta} \cdot \frac{\partial \rho'}{\partial t} \cdot \Delta t - \frac{\partial \theta}{\partial t} \cdot \Delta t \right] \\ &+ h_{lv,i} \cdot X_{Na,i} \cdot \frac{1}{v_{vap} - v_{liq}} \cdot \frac{\partial v_v}{\partial T} \cdot \Delta T \end{aligned} \tag{16.4-71}$$

Finally, substituting Eq. 16.4-71 into 16.4-46 and keeping the terms containing ΔT on the left-hand side, we have:

$$\Delta T_{Mi,i}\left\{\rho'^{n+1}_{Na,i}\cdot\left[\left(1-X_{Na,i}\right)\cdot C_{liq}+X_{Na,i}\cdot C_{vap}+h_{lv,i}\cdot\frac{1}{v_{vap}-v_{liq}}\right.\right.$$
$$\left.\cdot\frac{\partial v_v}{\partial T}\cdot X_{Na,i}\right]+2.5\ \rho'^{n+1}_{fi,i}\ R_{fi}\left.\right\}=-\left[\left(\rho' hu\right)_{Na,i+1/2}+\left(\rho' hu\right)_{fi,i+1/2}\right.$$
$$\left.-\left(\rho' hu\right)_{Na,i-1/2}-\left(\rho' hu\right)_{fi,i-1/2}\right]\cdot\frac{\Delta t}{\Delta z_i}+h_{lv,i}\cdot\frac{1}{v_{vap}-v_{liq}}\left[\frac{\theta^{n+1}_{Mi}}{\rho'^{n+1}_{Na,i}}\cdot\Delta\rho'_{Na,i}-\Delta\theta_{Mi}\right]$$
$$-h_{Na,i}\cdot\Delta\rho'_{Na,i}-h_{fi}\cdot\Delta\rho'_{fi,i}+\sum_j H'_{j,Mi,i}\cdot\Delta T_{j,Mi,i}\cdot\Delta t \qquad (16.4\text{-}72)$$

We now rewrite:

$$\Delta T_{j,Mi,i}=T_{j,i}-\left(T_{Mi,i}+\Delta T_{Mi,i}\right) \qquad (16.4\text{-}73)$$

$$\Delta\rho'_{Na}=-\left[\left(\rho u\right)_{Na,i+1/2}-\left(\rho u\right)_{Na,i-1/2}\right]\cdot\frac{\Delta t}{\Delta z_i} \qquad (16.4\text{-}74)$$

$$\Delta\rho'_{fi,i}=-\left[\left(\rho u\right)_{fi,i+1/2}-\left(\rho u\right)_{fi,i-1/2}\right]\cdot\frac{\Delta t}{\Delta z_i} \qquad (16.4\text{-}75)$$

and, after some regrouping following the same procedure as in the case in the single-phase sodium, we obtain:

$$T^{n+1}_{Mi,i}=T^n_{Mi,i}+\left\{-COENCH+h_{lv,i}\cdot\frac{1}{v_{vap}-v_{liq}}\cdot\frac{\theta^{n+1}_{Mi,i}}{\rho'^{n+1}_{Mi,i}}\cdot\Delta\rho'_{Na,i}-\Delta\theta_{Mi,i}\right.$$
$$+COHELP+\Delta T\cdot\left[H'_{cl,Mi,i}\cdot\left(T_{cl,os,i}-T_{Mi,i}\right)+\right.$$
$$+H'_{sr,Mi,i}\cdot\left(T_{sr,os,i}-T_{Mi,i}\right)+H'_{fu,Mi,i}\cdot\left(T_{fu,i}-T_{Mi,i}\right)$$
$$+H'_{se,Mi,i}\cdot\left(T_{se,,i}-T_{Mi,i}\right)+H'_{f\ell,Mi,i}\cdot\left(T_{f\ell,i}-T_{Mi,i}\right)$$
$$+H'_{s\ell,Mi,i}\cdot\left(T_{s\ell,i}-T_{Mi,i}\right)+H'_{ffc,Mi,i}\cdot\left(T_{fcc,i}-T_{Mi,i}\right)$$
$$\left.\left.+H'_{ffs,Mi,i}\cdot\left(T_{ffs}-T_{Mi,i}\right)\right\}\right/AUXLR \qquad (16.4\text{-}76)$$

where

$$COENCH = \left[\left(\rho' hu\right)_{Na,i+1/2} + \left(\rho' hu\right)_{fi,i+1/2} - \left(\rho' hu\right)_{Na,i-1/2} - \left(\rho' hu\right)_{fi,i-1/2}\right] \cdot \frac{\Delta t}{\Delta z_i} \tag{16.4-77}$$

$$COHELP = h_{Na,i} \cdot \left[\left(\rho' u\right)_{Na,i+1/2} - \left(\rho' u\right)_{Na,i-1/2}\right] \cdot \frac{\Delta t}{\Delta z_i} + h_{fi,i} \cdot \left[\left(\rho' u\right)_{fi,i+1/2} - \left(\rho' u\right)_{fi,i-1/2}\right] \cdot \frac{\Delta t}{\Delta z_i} \tag{16.4-78}$$

$$AUXLR = \rho'^{n+1}_{Na,i} \cdot \left[\left(1 - X_{Na,i}\right) \cdot C_{liq} + X_{Na,i} \cdot C_{vap} - h_{vi,i} \frac{1}{v_{vap} - v_{liq}} \cdot \frac{dv_v}{dT} \cdot X_{Na,i}\right] + 2.5\, \rho'^{n+1}_{fi,i}\, R_{fi} + \sum_j H'_{j,Mi,i} \cdot \Delta t \tag{16.4-79}$$

The heat-transfer coefficients are the same as those used in the single-phase energy equation. The pressure of the mixture is then calculated as follows:

$$P_{ch,i} = P_{Na,i} + P_{fi,i} \tag{16.4-80}$$

where

$$P_{Na,i} = P_{sat}\left(T_{Na,i}\right) \tag{16.4-81}$$

$$P_{fi,i} = R_{fi} \cdot \rho'_{fi,i} \cdot T_{fi,i} / \theta_{Mi,i} \tag{16.4-82}$$

However, if significant amounts of liquid sodium are present (more than 30% of the volume fraction), the compressibility of the liquid sodium is taken into account in calculating the partial fission-gas pressure. Eq. 16.4-82 is written in the form:

$$P_{fi,i} = \frac{R_{fi} \cdot \rho'_{fi,i} \cdot T_{fi,i}}{\theta_{Mi,i} + \Delta\theta_{Na,liq}} = \frac{R_{fi} \cdot \rho'_{fi,i} \cdot T_{fi,i}}{\theta_{Mi,i} + \theta_{Na,liq} \cdot P_{fi,i} \cdot C_{\Delta P,Na}} \tag{16.4-83}$$

where

$$C_{\Delta P,Na} = \frac{(\Delta V/V)_{Na,liq}}{\Delta P} \tag{16.4-84}$$

The value of $C_{\Delta P,Na}$ is given by the input constant CMNL. By solving Eq. 16.4-83 and retaining only the positive root, we obtain:

$$P_{fi,i} = \frac{-\theta_{Mi,i} + \sqrt{\theta_{Mi,i}^2 + 4\theta_{Na,liq} + C_{\Delta P,Na} \cdot R_{fi} \cdot \rho'_{fi,i} \cdot T_{fi,i}}}{2 \cdot \theta_{Na,liq} \cdot C_{\Delta P,Na}} \tag{16.4-85}$$

16.4.3.6 Fuel Vapor Energy Conservation Equation

The fuel vapor energy conservation equation is solved in the routine LEFUVA, which also models the fuel vaporization/condensation processes. These processes are not included in the formulation of the liquid fuel energy conservation equation, which is solved in the LESOEN routine. Thus, the mass and temperature of the liquid fuel is corrected in the routine LEFUVA, when necessary, to account for the mass and energy sources/sinks due to condensation and vaporization. Because the fuel vapor effects become dominant only during high-power transients that are associated with very short time periods, the fuel vapor is assumed not to be in equilibrium with the liquid fuel. The treatment of the vaporization and condensation processes will be described in detail later in this chapter.

16.4.3.6.1 Energy Conservation for Superheated Fuel Vapor

First, the energy equation is solved by assuming that all fuel vapor is initially superheated. This assumption is consistent with the method of solution, as all condensation and vaporization events are calculated in the routine LEFUVA, and the fuel vapor remaining in each cell at the end of this routine is always superheated, or, in the limit, saturated dry. Condensation or vaporization effects that might occur during the current time step are ignored during this first step. The energy equation is written in conservative form:

$$\begin{aligned}
&\frac{\partial}{\partial t}\left(\rho_{fv,i}\, h_{fv,i} \cdot A_{Mi,i} \cdot \Delta z_i\right) + \left[(\rho A h u)_{fv,i+1/2} - (\rho A h u)_{fv,i-1/2}\right] \\
&\quad = A_{Mi,i}\,\frac{\partial P_{fv,i}}{\partial t} \cdot \Delta z_i + A_{Mi,i} \cdot 0.5 \cdot \left[u_{Mi,i} \cdot \left(P_{fv,i} - P_{fv,i-1}\right)\right. \\
&\qquad \left. + u_{Mi,i+1} \cdot \left(P_{fv,i+1} - P_{fv,i}\right)\right] + \sum_j H_{j,fv,i}\, A_{j,fv,i} \cdot \Delta T_{j,fv,i} \\
&\qquad + Q_{fu,i} \cdot \rho_{fu,i} \cdot A_{Mi,i} \cdot \Delta z_i
\end{aligned} \tag{16.4-86}$$

After dividing by AXMX $\cdot \Delta z_i$ and using the definition of generalized densities, we obtain:

$$\frac{\partial}{\partial t}\left(\rho'_{fv,i}\, h_{fv,i}\right) = -\left[\left(\rho' hu\right)_{fv,i+1/2} - \left(\rho' hu\right)_{fv,i-1/2}\right] \cdot \frac{1}{\Delta z_i}$$
$$+ \theta_{Mi,i} \cdot \frac{\partial P_{fv,i}}{\partial t} + \sum_j H'_{j,fv,i} \cdot \Delta T_{j,fv,i} + Q_{fu,i} \cdot \rho'_{fv} \qquad (16.4\text{-}87)$$
$$+ \theta_{Mi,i} \cdot \frac{0.5}{\Delta z_i}\left[U_{Mi,i} \cdot \left(P_{fv,i} - P_{fv.i-1}\right) + U_{Mi,i+1} \cdot \left(P_{fv,i+1} - P_{fv.i}\right)\right]$$

Integrating over Δt and using the identity in Eq. 16.4-16 to express the quantity Δ(ρ′h), we obtain:

$$\rho'^{n+1}_{fv,i} \cdot \Delta h_{fv,i} = -\left[\left(\rho' hu\right)_{fv,i+1/2} - \left(\rho' hu\right)_{fv,i-1/2}\right] \cdot \frac{\Delta t}{\Delta z_i} - h_{fv,i} \cdot \Delta \rho'_{fv,i}$$
$$+ \theta_{Mi,i} \cdot \Delta P_{fv,i} + \sum_j H'_{j,fv,i} \cdot \Delta T_{j,fv,i} \cdot \Delta t + Q_{fu,i} \cdot \rho'_{fv} \cdot \Delta t$$
$$+ \theta_{Mi,i} \cdot \frac{0.5 \cdot \Delta t}{\Delta z_i} \cdot \left[u_{Mi,i} \cdot \left(P_{fv,i} - P_{fv,i-1}\right)\right. \qquad (16.4\text{-}88)$$
$$\left. + u_{Mi,i+1} \cdot \left(P_{fv,i+1} - P_{fv,i}\right)\right]$$

The fuel vapor is only present in calculations for short periods of time during high overpower transients. In addition, the gas-gas heat transfer is generally much more efficient than the gas-liquid or gas-surface heat transfer. For these reasons the only heat-transfer term maintained in Eq. 16.4-86 is the heat transfer between the fuel vapor and the sodium-fission gas mixture. Furthermore, because of the lack of experimental data on the gas-gas heat transfer, this term has been formulated such that it represents a sizable fraction of the transferable energy, i.e., the temperatures of the fuel vapor and gas mixture will equilibrate quite fast, within 10-50 time steps. The enthalpy of the fuel vapor at a certain temperature is:

$$h_{fv,i} = h_{fv,sat}\left(P_{fv,i}\right) + 2.5 \cdot R_{fv} \cdot \left[T_{fv,i} - T_{fv,sat,i}\left(P_{fv,i}\right)\right] \qquad (16.4\text{-}89)$$

A measure of the transferable enthalpy is obtained by assuming the lowest final temperature to be the temperature of the sodium-fission gas mixture. Thus:

$$\Delta h_{fv,i} = 2.5 \cdot R_{fv}\left[T_{fv,i} - T^{n+1}_{Na,i}\right] \qquad (16.4\text{-}90)$$

The total transferable enthalpy in cell i, during the time Δt is:

$$\Delta h_{fv,i} \cdot \rho_{fv,i} \cdot A_{Mi,i} \cdot \Delta z_i = 2.5 \cdot R_{fv} \cdot \left[T_{fv,i} - T_{Na,i}^{n+1}\right] \cdot \rho_{fv,i} \cdot A_{Mi,i} \cdot \Delta z_i \tag{16.4-91}$$

The fraction transferred is CFHTAX, which is defined as follows:

When $\Delta t \cdot 10^3 \le 0.1$

$$CFHTAX = \Delta t \cdot 10^3 \tag{16.4-92a}$$

When $\Delta t \cdot 10^3 > 0.1$

$$CFHTAX = 0.1 \tag{16.4-92b}$$

After multiplying by CFHTAX and dividing by AXMX $\cdot$ Δz_i, which was done for the original equation, the heat-transfer term in Eq. 16.4-88 is replaced by:

$$\sum_j H'_{j,f,i} \cdot \Delta T_{j,fv,i} \cdot \Delta t \rightarrow -2.5 \cdot R_{fv,i} \cdot CFHTAX \cdot \left[T_{fv,i} - T_{Na,i}^{n+1}\right] \cdot \rho'_{fv,i} \tag{16.4-93}$$

Substituting Eq. 16.4-93 in Eq. 16.4-88 and rewriting the $\theta_{Mi,i} \cdot \Delta P_{fv,i}$ and $\rho_{fv,i}^{n+1}$ terms in a manner similar to that used for the sodium-gas mixture, in Eqs. 16.4-47 through 16.4-51, we obtain:

$$\begin{aligned}
&\Delta T_{fv,i}\left[2.5(\rho')_{fv,i}^{n+1} R_{fv} - (\rho')_{fv,i}^{n+1} R_{fv}\right] \\
&\quad = -\left[(\rho' hu)_{fv,i+1/2} - (\rho' hu)_{fv,i-1/2}\right] \frac{\Delta t}{\Delta z_i} \\
&\quad + \left(h_{fv,i} - T_{fv,i} R_{fv}\right)\left[(\rho' u)_{fv,i+1/2} - (\rho' u)_{fv,i-1/2}\right] \frac{\Delta t}{\Delta z_i} \\
&\quad + \theta_{Mi,i} \frac{0.5\Delta t}{\Delta z_i}\left[u_{Mi,i}\left(P_{fv,i} - P_{fv,i-1}\right)\right. \\
&\quad \left. + u_{Mi,i+1}\left(P_{fv,i+1} - P_{fv,i}\right)\right] \\
&\quad - 2.5 R_{fv} \mathrm{CHFTAX}\left(T_{fv,i} - T_{\mathrm{Na},i}^{n+1}\right)\rho'_{fv,i} + Q_{fu}\rho'_{fv}\Delta t
\end{aligned} \tag{16.4-94}$$

The terms derived from the original $\partial P/\partial t$ and $\partial P/\partial z$ terms in Eq. 1.4-86 make a negligible contribution to the right hand side of Eq. 16.4-94. These terms were

neglected in the initial release version, but have been added for completeness, in the chunk development version. The left-hand-side coefficient is replaced by:

$$AUXLR = 2.5 \cdot \rho'^{n+1}_{fv,i} \cdot R_{fv} - \rho'^{n+1}_{fv,i} \cdot R_{fv} \tag{16.4-95}$$

The terms in Eq. 16.5-95 have not been combined because the term $\rho'^{n+1}_{fv,i} \cdot R_{fv}$ originates from the $\partial P/\partial t$ term and was dropped in the initial release version, together with the terms originating from the u $\frac{\partial P}{\partial u}$ term. The new fuel vapor temperature is calculated as follows:

$$TEFUVA(I) = TEFUVA(I) + (-COENCH + COHELP + HSFU(I) * DEFVCH(I) * DTPL - DEFVCH(I) * CFHTFN * (TEFUVA(I) - TENA(I)))/ AUXLR \tag{16.4-96}$$

where

$$COENCH = \left[(\rho' hu)_{fv,i+1/2} - (\rho' hu)_{fv,i-1/2}\right] \cdot \frac{\Delta t}{\Delta z_i} \tag{16.4-97}$$

$$COHELP = h_{fv,i} \cdot \left[(\rho' u)_{fv,i+1/2} - (\rho' u)_{fv,i-1/2}\right] \cdot \frac{\Delta t}{\Delta z_i} \tag{16.4-98}$$

and

$$DEFVCH(I) = \rho'_{fv,i} \tag{16.4-99}$$

$$CFHTFN = 2.5 \cdot R_{fv} \cdot CFHTAX \tag{16.4-100}$$

The new fuel vapor pressure is then calculated using the new temperatures:

$$P^{n+1}_{fv,i} = R_{fv} \cdot \rho'^{n+1}_{fv,i} \cdot T^{n+1}_{fv,i} / \theta^{n+1}_{Mi,i} \tag{16.4-101}$$

16.4.3.6.2 Condensation of the Fuel Vapor

Under certain circumstances the fuel vapor will enter the two-phase region and begin to condense. The decision that such a situation has occurred is made by comparing the pressure $P^{n+1}_{fv,i}$ with the saturation pressure in cell i. If:

$$P_{fv,i}^{n+1} < P_{fv,sat,i}\left(T_{fv,i}^{n+1}\right) \tag{16.4-102}$$

no condensation will occur during the current time step. Otherwise, some condensation will take place, and the calculation proceeds as outlined below.

First, we determine the temperature $T_{fv,sat,i}$ where the fuel vapor first reaches saturation. This temperature is obtained using the same method described in Section 16.4.3.5 to correct the sodium temperature where it crosses over from the single phase to the two-phase region. The formula used is similar to Eq. 16.4-65. The enthalpy change between the original temperature $T_{fv,i}^{n}$ and the saturation temperature is, by Eq. 16.4-94:

$$\Delta h'_{fv,i} = \left(T_{fv,sat,i} - T_{fv,i}^{n}\right) * AUXLR \tag{16.4-103}$$

The total enthalpy change originally calculated is:

$$\Delta h_{fv,i} = \left(T_{fv,i}^{n+1} - T_{fv,i}^{n}\right) * AUXLR \tag{16.4-104}$$

The enthalpy which still has to be removed via condensation once the vapor has reached the temperature $T_{fv,sat,i}$ is given by:

$$\Delta h_{fv,i}^{cond} = \Delta h_{fv,i} - \Delta h'_{fv,i} = \left(T_{fv,i}^{n+1} - T_{fv,sat}\right) * AUXLR \tag{16.4-105}$$

In order to find the temperature change leading to the enthalpy change $\Delta h_{fv,i}^{cond}$, we observe that at the final temperature we have to satisfy the condition for dry vapor:

$$P_{fv,sat}\left(T_{fv,i}\right) = R_{fv} \cdot \rho'_{fv} \cdot T_{fv,i} \cdot \frac{1}{\theta_{Mi,i}} \tag{16.4-106}$$

Also, with the assumption that the heat of vaporization for fuel $h_{fv,lg}$ is approximately constant for the range of temperatures of interest, the total enthalpy change due to condensation and temperature change can be written as:

$$\Delta h_{fv} = -\Delta\rho'_{fv,i}\ h_{fv,\mathrm{lg}} + 2.5\ \rho'_{fv,i}\ R_{fv} \cdot \Delta T_{fv} \tag{16.4-107}$$

where $\Delta\rho'_{fv,i}$ is the <u>decrease</u> in generalized density due to condensation. Because Eqs. 16.4-106 and (16.4-107) cannot be solved directly for the temperature, we use a trial and error approach to find the solution. First, assuming the final temperature if $T_{fv}^{1} = T_{fv,i}^{n+1}$, i.e., the temperature originally calculated, and the amount to condense $\Delta\rho'^{1}_{fv}$, Eq. 16.4-106 becomes:

$$P_{fv,sat}\left(T_{fv}^{1}\right)= R_{fv}\cdot\left(\rho'_{fv,i}-\Delta\rho'_{fv}\right)\cdot T_{fv}^{1}\cdot\frac{1}{\theta_{Mi}-\dfrac{\Delta\rho'_{fv}}{\rho_{fu,liq}}} \tag{16.4-108}$$

and, after solving for $\Delta\rho'_{fv}$:

$$\Delta\rho'^{1}_{fv}=\frac{\left(\rho'_{fv,i}\cdot R_{fv}\cdot T_{fv}^{1}-\theta_{Mi,i}\cdot P_{fv,sat}\left(T_{fv}^{1}\right)\right)}{R_{fv}\cdot T_{fv}^{1}-P_{fv,sat}\left(T_{fv}^{1}\right)/\rho_{fu,liq}} \tag{16.4-109}$$

The enthalpy change in Eq. 16.4-107 becomes:

$$\Delta h_{fv}^{1}=-\Delta\rho_{fv,i}^{1}\cdot h_{hv,\mathrm{lg}}+2.5\cdot\rho'_{fv,i}\cdot R_{fv}\cdot\left(T_{fv,i}^{n+1}-T_{fv,sat}\right) \tag{16.4-110a}$$

Then, we assume that the final temperature of the fuel vapor is $T_{fv}^{2}=T_{fv,sat}$, and obtain the new amount of condensate $\Delta\rho'^{2}_{fv}$ and the energy change:

$$\Delta h_{fv}^{2}=-\Delta\rho'^{2}_{fv}\cdot h_{fv,\mathrm{lg}} \tag{16.4-110b}$$

These two situations generally will bracket the actual final temperature of the fuel vapor, because the first assumption is practically equivalent to very little or no condensation, while the second assumes maximum condensation with no temperature change. The actual temperature is obtained by interpolating between T_{fv}^{1} and T_{fv}^{2}, with the condition that the final enthalpy change has to be $\Delta h_{fv,i}^{cond}$, calculated before from Eq. 16.4-105. Thus:

$$T_{fv,i}^{n+1}=T_{fv,i}^{1}+T_{fv,i}^{2}\cdot\frac{\Delta h_{fv,i}^{cond}-\Delta h_{fv}^{1}}{\Delta h_{fv}^{2}-\Delta h_{fv}^{1}} \tag{16.4-111}$$

Using this temperature, the actual condensation is calculated from Eq. 16.4-109 and the generalized density of the fuel vapor is updated:

$$\rho'_{fv,i}=\rho'_{fv,i}-\Delta\rho'^{cond}_{fu,i} \tag{16.4-112}$$

The temperature and generalized density of the liquid fuel is also modified to account for the addition of $\Delta\rho'^{cond}_{fv,i}$ at the temperature $T_{fv,i}^{n+1}$:

$$T_{fu,i}=\left[T_{fu,i}\,\rho'_{fu,i}+T_{fv,i}^{n+1}\cdot\Delta\rho_{fv,i}\right]/\left(\rho'_{fu,i}+\Delta\rho'^{cond}_{fv,i}\right) \tag{16.4-113}$$

$$\rho'_{fu,i} = \rho'_{fu,i} + \Delta\rho'^{cond}_{fv,i} \qquad (16.4\text{-}114)$$

16.4.3.6.3 Vaporization of Liquid Fuel

The vaporization model used is a quasi-equilibrium model [16-13] which allows the fuel and fuel vapor to have different temperatures at the same location. Bulk boiling of fuel is assumed to occur whenever the local total pressure is lower than the vapor pressure of the liquid fuel. This process is fast enough to allow a quasi-equilibrium to be established each time step, and is illustrated in Fig. 16.4-14 by the original sharp increase in pressure. Thus, the total pressure, including the partial pressure of the fuel vapor becomes equal to the fuel vapor pressure corresponding to the liquid-fuel temperature. When the total pressure exceeds the liquid-fuel vapor pressure, fuel vaporization can occur only by surface vaporization, which is generally a significantly slower process than bulk boiling. The efficiency of surface vaporization is a function of the local flow regime and time-step length. In the limit, if the surface vaporization is assumed to be very efficient, the partial pressure of the fuel vapor can become equal, in each time step, to the liquid-fuel pressure. In this case, the quasi-equilibrium model becomes equivalent to a thermal-equilibrium model.

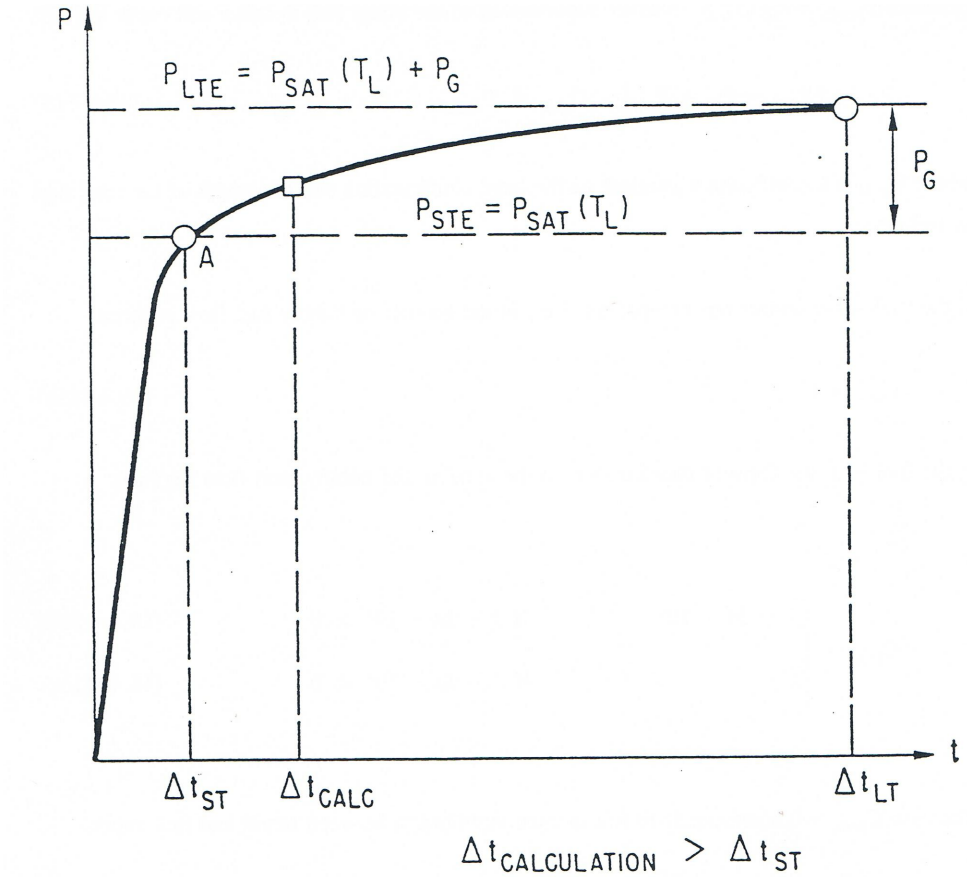

Fig. 16.4-14: Time Variation of Fuel Vapor Partial Pressure

This calculation is performed for all cells I, with IFFUBT<I<IFFUTP. First, we calculate $P_{fu,sat,i} = P_{sat}(T_{fu,i})$. Further vaporization of the liquid fuel in cell I will occur only if:

$$P_{fv,i} + \left(P_{Na,i} + P_{fi,i} + P_{sv,i}\right) \cdot C_{\mathrm{Pr},fu} < P_{fu,sat,i} \tag{16.4-115}$$

where $C_{Pr,fu}$ is a coefficient dependent on the local configuration and the length of the time step as follows:

If the fuel is the continuous component, i.e., in the annular or bubbly fuel flow regimes

$$C_{\mathrm{Pr},fu} = 1 \tag{16.4-116a}$$

If the fuel is in the form of droplets, i.e. in the annular and bubbly steel flow regimes,

$$C_{\mathrm{Pr},fu} = \begin{cases} 1 - \Delta t \cdot 10^4 & \text{if } 1 - \Delta t \cdot 10^4 > 0 \quad \text{(16.4-116b)} \\ 0 & \text{if } 1 - \Delta t \cdot 10^4 < 0 \quad \text{(16.4-116c)} \end{cases}$$

The case $C_{Pr,fu} = 0$ corresponds to full thermal equilibrium between liquid and fuel vapor.

The vaporization of liquid fuel will take place until the following condition is satisfied:

$$P_{fv,i} + \left(P_{Na,i} + P_{fi,i} + P_{sv,i}\right) \cdot C_{\mathrm{Pr},fu} = P_{fu,sat,i} \tag{16.4-117}$$

Note that all pressures change during vaporization, including $P_{fu,sat,i}$. Thus, Eq. 16.4-117 cannot be solved directly, and we need to use a trial-and-error approach. First, it is assumed that the final fuel temperature is:

$$T^1_{fu,i} = T_{fu,i} \tag{16.4-118}$$

and

$$P^1_{fu,sat,i} = P_{fu,sat}\left(T^1_{fu,j}\right) \tag{16.4-119}$$

We can now calculate the amount of new fuel vapor generated from Eq. 16.4-117:

$$\Delta\rho'_{fv,i} = \frac{\theta_{Mi,i}\left[P^1_{fu,sat,i} - P_{fv,i} - \left(P_{Na,i} + P_{fi,i} + P_{fv,i}\right) \cdot C_{p,vap,fu}\right]}{\left[R_{fv} \cdot T^1_{fv} - P^1_{fu,sat,i} \cdot \frac{1}{\rho_{fu,liq}}\right]} \tag{16.4-120}$$

The new fuel enthalpy is:

$$h'_{fu,i} = -\frac{\left(h_{fu,i} \cdot \rho'_{fu,i} - h_{fu,lq} \cdot \Delta\rho'_{fv,i}\right)}{\rho'_{fu,i} - \Delta\rho'_{fv,i}} \tag{16.4-121}$$

and the new fuel temperature and vapor pressure are:

$$T'_{fu,i} = T'_{fu}\left(h'_{fu,i}\right) \tag{16.4-122}$$

$$P'_{fu,sat,i} = P'_{fu,sat}\left(T_{fu,i}\right) \tag{16.4-123}$$

A new guess is now made about the final fuel temperature $T^2_{fu,i} = T'_{fu,i}$, and the above procedure is repeated, obtaining $P^2_{fu,sat,i}$, $\Delta\rho''_{fu,i}$, $T''_{fu,i}$ and $P''_{fu,sat,i}$. We can now obtain the real $P_{fu,sat,i}$, by imposing the condition that the final saturation pressure should be equal to the assumed saturation pressure:

$$P^{n+1}_{fu,sat,i} = P^{i}_{fu,sat,i} - \left(P^2_{fu,sat,i} - P^1_{fu,sat,i}\right) \cdot \frac{\Delta P^1}{\Delta P^2 - \Delta P^1} \tag{16.4-124}$$

where

$$\Delta P^1 = P'_{fu,sat,i} - P^1_{fu,sat,i} \tag{16.4-125a}$$

$$\Delta P^2 = P''_{fu,sat,i} - P^2_{fu,sat,i} \tag{16.4-125b}$$

Using $P^{n+1}_{fu,sat,i}$ in Eq. 16.4-120, we can calculate the new $\Delta\rho'_{fv,i}$. Then, the generalized densities and enthalpies of the fuel vapor and liquid fuel are updated:

$$T^{n+1}_{fv,i} = \left(\Delta\rho'_{fv,i} \cdot T_{fu,i} + \rho'_{fv,i} \cdot T_{fv,i}\right)/\left(\rho'_{fv,i} + \Delta\rho'_{fv,i}\right) \tag{16.4-126}$$

$$h^{n+1}_{fu,i} = \left(h_{fu,i} \cdot \rho'_{fu,i} - h_{lq} \cdot \Delta\rho'_{fv,i}\right)/\left(\rho'_{fu,i} - \Delta\rho'_{fv,i}\right) \tag{16.4-127}$$

$$\rho'^{n+1}_{fv,i} = \rho'_{fv,i} + \Delta\rho'_{fv,i} \tag{16.4-128}$$

$$\rho'_{fu,i} = \rho'_{fu,i} - \Delta\rho'_{fv,i} \tag{16.4-129}$$

Finally, the new pressure due to fuel vapor is calculated:

$$P_{fv,i}^{n+1} = R_{fv} \cdot \rho_{fv,i}'^{n+1} \cdot T_{fv,i}^{n+1} \cdot \frac{1}{\theta_{Mi,i}^{n+1}} \tag{16.4-130}$$

and is added to the total channel pressure:

$$P_{ch,i}^{n+1} = P_{ch,i}^{n+1} + P_{fv,i}^{n+1} \tag{16.4-131}$$

16.4.3.7 Steel Vapor Energy Conservation Equation

The steel vapor energy conservation equation is solved in the routine LESEVA. This routine is practically identical to the LEFUVA routine, which solves the fuel vapor energy equation and was described in detail in Section 16.4.3.6. At the end of the LESEVA routine, the new pressure due to steel vapor is calculated

$$P_{sv,i}^{n+1} = R_{sv} \cdot \rho_{sv,i}'^{n+1} \cdot T_{sv,i}^{n+1} \cdot \frac{1}{\theta_{Mi,i}^{n+1}} \tag{16.4-132}$$

and is added to the total channel pressure:

$$P_{ch,i}^{n+1} = P_{ch,i}^{n+1} + P_{sv,i}^{n+1} \tag{16.4-133}$$

16.4.3.8 Momentum Conservation Equation

The momentum conservation equations are solved in the routine LEMOCO. As indicated previously, the channel hydrodynamic model in LEVITATE calculates three velocity fields, each of them describing the motion of a group of material components, as follows:

$u'_{Mi,i}$, $u''_{Mi,i}$	the velocity of the gas mixture; described the motion of the two-phase (or superheated) sodium, fission gas, fuel vapor and steel vapor. The code symbol is UMCH.
$u'_{fu,i}$, $u''_{fu,i}$	the velocity of the liquid fuel and/or liquid steel components. The code symbol is UFCH.
$u_{lu,i}$	the velocity of the solid fuel and/or steel chunks. The code symbol is ULCH.

One is reminded that LEVITATE uses dual velocities to model the motion of the gas mixture and liquid components. Thus, $u'_{Mi,i}$ represents the velocity of the gas mixture before the i - 1/2 boundary and $u''_{Mi,i}$ represents the velocity of the mixture after the same boundary. (Before and after velocities are ordered here by the positive sense of the axial coordinate). As already shown in Section 16.4.3.1, the dual velocities at the boundary i - 1/2 are related by:

$$C_{Mo,fu,i} = \frac{u'_{fu,i}}{u''_{fu,i}} = \frac{\rho'_{fu,i}}{\rho'_{fu,i-1}} \,. \tag{16.4-134}$$

In the code, only the velocity $u''_{fu,i}$ is stored in the array UFCH(I). The velocity $u'_{fu,i}$ is always obtained from Eq. 16.4-134, using the coefficient $C_{Mo,fu,i}$, which is stored in the array CCFU(I). A similar approach is used for the gas mixture dual velocities, which are related at the boundary i - 1/2 by the coefficients $C_{Mo,Mi,i}$, stored in the array CCMI(I).

The three momentum equations are solved simultaneously to avoid numerical instabilities due to the generally low inertia of the gas mixture. In cells where only two velocity fields are necessary (e.g., no fuel/steel chunks are present) a system of only two momentum equations is solved. Finally, in cells where the gas mixture only is present, the corresponding momentum equation is solved, while the other two velocity fields remain zero. We first present the derivation of the momentum equations.

16.4.3.8.1 The Momentum Conservation Equation for the Gas Mixture

We begin with the equation written in conservative form for the control volume illustrated in Fig. 16.4-15:

$$\begin{aligned}
&\frac{\partial}{\partial t}\left[\rho_{Mi,i-1}\cdot\frac{\Delta z_{i-1}}{2}\cdot A_{Mi,i-1}\cdot u'_{Mi,i}+\rho_{Mi,i}\cdot\frac{\Delta z_i}{2}\cdot A_{Mi,i}\cdot u''_{Mi,i}\right] \\
&\quad+\left[\left(\rho A u^2\right)_{Mi,i}-\left(\rho A u^2\right)_{Mi,i-1}\right]=-A_{Mi,i-1/2}\cdot\left(P_i-P_{i-1}\right) \\
&\quad+\sum_{\ell}\left(\Gamma^{\ell}_{Mo,i-1}\cdot\frac{\Delta z_{i-1}}{2}+\Gamma^{l}{}_{Mo,i}\cdot\frac{\Delta z_1}{2}\right)-\rho_{Mi,i-1}\cdot\frac{\Delta z_{i-1}}{2}\,A_{Mi,i-1}\cdot g \\
&\quad-\rho'_{Mi,i}\cdot\frac{\Delta z_1}{2}\cdot A_{Mi,i}\cdot g
\end{aligned} \tag{16.4-135}$$

where $\sum \Gamma'_{Mo,i-1}$ represents the momentum sources and sinks for the mixture and will be presented in detail later in this chapter. We now divide Eq. 16.4-135 by AXMX and using the definition of the generalized density, the notation:

$$\frac{\Delta z_i}{2} = \Delta z_2 \;;\; \frac{\Delta z_{i-1}}{2} = \Delta z_1 \tag{16.4-136}$$

and the correlation of $u'_{Mi,i}$ and $u''_{Mi,i}$, obtain

$$\begin{aligned}
&\frac{\partial}{\partial t}\left[\rho'_{Mi,i-1}\cdot\Delta z_i\cdot u_{Mi,i}\cdot C_{Mo,Mi,i}+\rho'_{Mi,i}\cdot\Delta z_2\cdot u_{Mi,i}\right] \\
&\quad=-\left[\left(\rho' u^2\right)_{Mi,i}-\left(\rho' u^2\right)_{Mi,i-1}\right]-\theta_{Mi,i-1/2}\cdot\left(P_i-P_{i-1}\right) \\
&\quad+\sum\left(\Gamma'^{\ell}_{Mo,i-1}\cdot\Delta z_i+\Gamma'^{l}{}_{Mo,i}\cdot\Delta z_2\right)-\rho'_{Mi,i-1}\cdot\Delta z_1\cdot g-\rho'_{Mi,i}\cdot\Delta z_2\cdot g
\end{aligned} \tag{16.4-137}$$

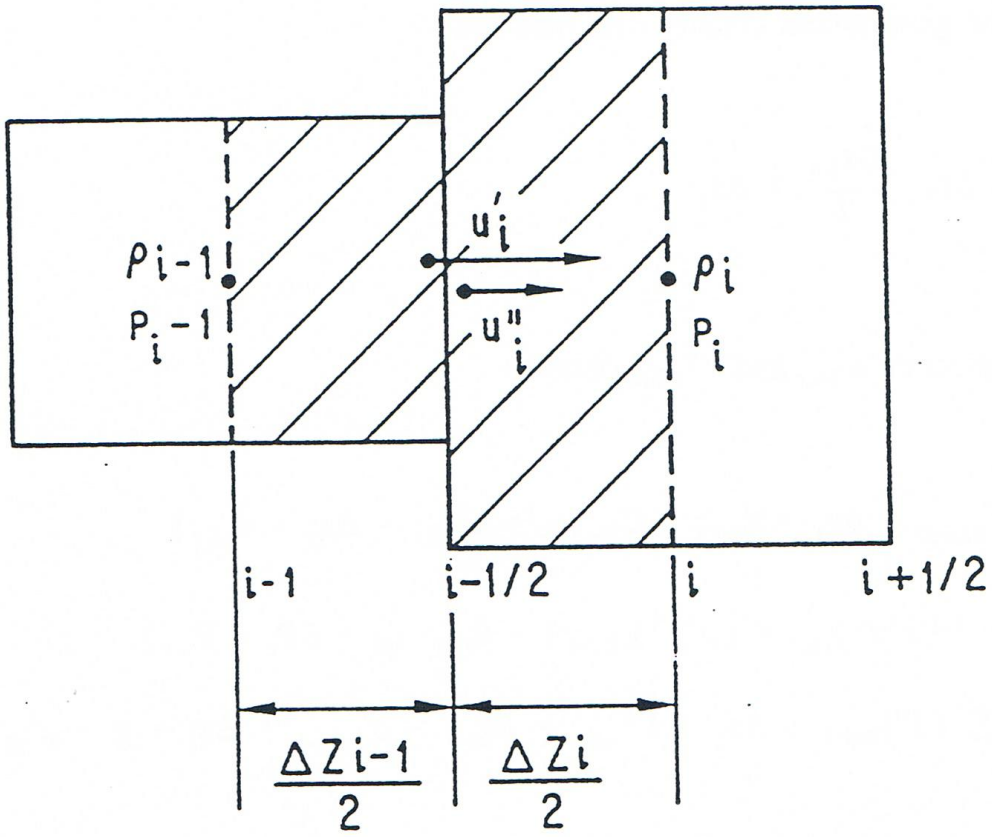

Fig. 16.4-15: Control Volume Used for the Solution of the Momentum Equation

where we used

$$u_{mi,i} = u''_{Mi,i} \tag{16.4-138}$$

in order to simplify the notation and:

$$\Gamma'^{\ell}_{Mo,i} = \Gamma^{\ell}_{Mo,i} / AXMX. \tag{16.4-139}$$

The convective fluxes in Eq. 16.4-137 are defined as follows:

$$\left(\rho' u^2\right)_{Mi,i} = \rho'_{Mi,i} \cdot \frac{\left(u''_{Mi,i} + u'_{Mi,i+1}\right)^2}{4} \tag{16.4-140}$$

An optional formulation of the convective fluxes can be obtained by setting the input parameter IMOMEN = 1, in which case:

$$\left(\rho' u^2\right)_{Mi,i} = \rho'_{Mi,i} \cdot u^2_{Mo,Mi,i} \tag{16.4-141}$$

where

$$u_{Mo,Mi,i} = \begin{cases} u''_{Mi,i} & \text{if } u''_{Mi,i} \geq 0 \text{ and } u'_{Mi,i+1} \geq 0 \quad \text{(16.4-142a)} \\ \sqrt{u''^2_{Mi,i} + u'^2_{Mi,i+1}} & \text{if } u''_{Mi,i} \geq 0 \text{ and } u'_{Mi,i+1} \leq 0 \quad \text{(16.4-142b)} \\ 0 & \text{if } u''_{Mi,i} < 0 \text{ and } u'_{Mi,i+1} \geq 0 \quad \text{(16.4-142c)} \\ u'_{Mi,i+1} & \text{if } u''_{Mi,i} < 0 \text{ and } u'_{Mi,i+1} < 0 \quad \text{(16.4-142d)} \end{cases}$$

This option has been added only recently and has not been tested extensively. It is expected that in future release versions this formulation will become the basic option. The quantity $\theta_{Mi,i-1/2}$ is defined differently for expansions and contractions [16-5]. For an expansion:

$$\theta_{Mi,i-1/2} = \begin{cases} \theta_{Mi,i} & \text{if } u'_{mi,i} \geq 0 \quad \text{(16.4-143a)} \\ \theta_{Mi,i-1} & \text{if } u''_{Mi,i} < 0 \quad \text{(16.4-143b)} \end{cases}$$

and for contraction:

$$\theta_{Mi,i-1/2} = C_{\Delta p} \cdot \frac{\theta_{Mi,i-1} \cdot \theta_{Mi,i}}{\theta_{Mi,i-1} + \theta_{Mi,i}} \quad \text{(16.4-144)}$$

with $C_{\Delta p}$ currently having the value of 1.67. Equation 16.4-137 is integrated over the time interval and then divided by Δt. Using the identities:

$$\Delta(\rho' u) = \rho'^{n+1} \cdot \Delta u + u^n \cdot \Delta\rho' \quad \text{(16.4-145a)}$$

$$\Delta(\rho' u\, C_{Mo}) = \rho'^{n+1} C^{n+1}_{Mo}\, \Delta u + \rho'^{n+1} \cdot u^n \cdot \Delta C_{Mo} + u^n C^n \cdot \Delta\rho' \quad \text{(16.4-145b)}$$

we obtain:

$$\begin{aligned} &\Delta u_{Mi,i} \cdot \left(\rho'^{n+1}_{Mi,i-1} \cdot C^{n+1}_{Mo,Mi,i} \cdot \Delta z_i + \rho'^{n+1}_{Mi,i} \cdot \Delta z_2\right) \cdot \frac{1}{\Delta t} \\ &\quad = -\left[\left(\rho' u^2\right)_{Mi,i} - \left(\rho' u^2\right)_{Mi,i-1}\right] - \theta_{Mi,i-1/2} \cdot \left(P_i - P_{i-1}\right) \\ &\qquad - u_{Mi,i} \cdot C_{Mo,Mi,i} \cdot \Delta z_i \cdot \frac{\Delta\rho'_{Mi,i}}{\Delta t} - u_{Mi,i} \cdot \Delta z_2 \cdot \frac{\Delta\rho'_{Mi,i}}{\Delta t} \\ &\qquad - \rho'^{n+1}_{Mi,i-1} \cdot u_{Mi,i} \cdot \Delta z_i \cdot \frac{\Delta C_{Mo,Mi,i}}{\Delta t} + \sum_{\ell} \left(\Gamma'^{\ell}_{Mo,Mi,i-1} \cdot \Delta z_1 + \Gamma'^{\ell}_{Mo,Mi,i} \cdot \Delta z_2\right) \\ &\qquad - \rho'_{Mi,i-1} \cdot \Delta z_i \cdot g - \rho'_{Mi,i} \cdot \Delta z_2 \cdot g \end{aligned}$$

(16.4-146)

We will now present the term $\sum_{\ell} \Gamma'^{\ell}_{Mo,i}$ in more detail:

$$\sum_{\ell} \Gamma'^{\ell}_{Mo,Mi,i} = \Gamma'^{cond}_{Mo,Mi,i} + \Gamma'^{vap}_{Mo,Mi,i} + \Gamma'^{friction\ wall}_{Mo,Mi,i} + \Gamma'^{drag\ fuel}_{Mo,Mi,i} + \Gamma'^{drag\ chunks}_{Mo,Mi,i} + \Gamma'^{inertial}_{Mo,Mi,i} \tag{16.4-147}$$

The momentum sink $\Gamma'^{cond}_{Mo,Mi,i}$ is due to possible condensation of steel and/or fuel vapor:

$$\Gamma'^{cond}_{Mo,Mi,i} = -\frac{\Delta\rho'^{cond}_{sv,i}}{\Delta t} u_{Mi,i} - \frac{\Delta\rho'^{cond}_{fv,i}}{\Delta t} \cdot u_{Mi,i} \tag{16.4-148}$$

Similarly, the vaporization source is defined as:

$$\Gamma'^{vap}_{Mo,Mi,i} = \frac{\Delta\rho'^{vap}_{sv,i}}{\Delta t} \cdot u_{fu,i} + \frac{\Delta\rho'^{vap}_{fv,i}}{\Delta t} \cdot u_{fu,i} \tag{16.4-149}$$

The quantities $\Delta\rho'^{cond}_{fv}$ and $\Delta\rho'^{vap}_{fv}$ are calculated in the routine LEFUVA. These calculations are presented in Section 16.4.3.6. The quantities $\Delta\rho'^{cond}_{sv}$ and $\Delta\rho'^{vap}_{sv}$ are obtained in the LESEVA routine in the same manner.

The momentum sink due to the wall friction has the form:

$$\begin{aligned}\Gamma'^{\text{friction wall}}_{Mo,Mi,i} &= -f_{Mi,i} \cdot \frac{\rho'_{Mi,i}}{2D_{H,Mi,i}} \cdot u^{n+1}_{Mi,i} \cdot \left| u^{n}_{Mi,i} \right| \\ &= -f_{Mi,i} \cdot \frac{\rho'_{Mi,i}}{2D_{H,Mi,i}} \cdot \left(u^{n}_{Mi,i} + \Delta u_{Mi,i} \right) \cdot \left| u^{n}_{Mi,i} \right|\end{aligned} \tag{16.4-150}$$

The wall friction factor $f_{Mi,i}$ will be described in Section 16.4.3.10. The hydraulic diameter of the gas mixture $D_{H,Mi,i}$ will be described in Section 16.4.3.9. The fuel/steel-gas mixture drag source has the form

$$\begin{aligned}\Gamma'^{drag\ fuel}_{Mo,Mi,i} &= C'_{D,Mi,fu,i} \left(u^{n+1}_{fu,i} - u^{n+1}_{Mi,i} \right) \cdot \left| u_{fi,i} - u_{Mi,i} \right| \\ &= C'_{D,Mi,fu,i} \cdot \left(u_{fu,i} + \Delta u_{fu,i} - u_{Mi,i} - \Delta u_{Mi,i} \right) \cdot \left| u_{fu,i} - u_{Mi,i} \right|\end{aligned} \tag{16.4-151}$$

The drag coefficient between fuel and mixture has different forms, depending on the local flow regime, as shown below:

For the annular fuel and steel flow regimes:

$$C'_{D,Mi,fu,i} = f_{Mi,fu,i} \cdot \frac{\rho'_{Mi,i}}{2 \cdot D_{H,Mi,i}} \tag{16.4-152a}$$

$$C'_{D,Mi,se,i} = f_{Mi,se,i} \cdot \frac{\rho'_{Mi,i}}{2 \cdot D_{H,Mi,i}} \tag{16.4-152b}$$

For the bubbly fuel flow regime:

$$C'_{D,Mi,fu,i} = \theta_{Mi,i} \cdot \rho_{fu,i} \cdot CIA6 \cdot \sqrt{\frac{g}{\sigma_{fu}} \cdot \left(\frac{\rho'_{fu,i} + \rho'_{se,i}}{\theta_{fu,i} + \theta_{se,i}} - \frac{\rho'_{Mi,i}}{\theta_{Mi,i}} \right)} \cdot \left(\frac{\theta_{fu,i} + \theta_{se,i}}{\theta_{ch,op,i}} \right)^2 \tag{16.4-153a}$$

where CIA6 is an input constant, currently equal to 0.107. This form of $C'_{D,Mi,fu,i}$ is explained in more detail in Ch. 14.0, Section 14.4.6.1, which describes the PLUTO2 model.

For the bubbly steel flow regime:

$$C'_{D,Mi,se,i} = \theta_{Mi,i} \cdot \rho_{se,i} \cdot CIA6 \cdot \sqrt{\frac{g}{\sigma_{se}} \cdot \left(\frac{\rho'_{fu,i} + \rho'_{se,i}}{\theta_{fu,i} + \theta_{se,i}} - \frac{\rho'_{Mi,i}}{\theta_{Mi,i}} \right)} \cdot \left(\frac{\theta_{fu} + \theta_{se}}{\theta_{ch,op,i}} \right)^2 \tag{16.4-153b}$$

The factor $f_{Mi,fu,i}$ which appears in Eq. 16.4-152a will be described in Section 16.4.3.10.

The chunk-mixture drag source has the form:

$$\begin{aligned} \Gamma'^{drag\ chunk}_{Mo,Mi,i} &= C'_{D,Mi,\ell u,i} \cdot \left(u^{n+1}_{\ell u,i} - u^{n+1}_{Mi,i} \right) \cdot \left| u_{\ell u,i} - u_{Mi,i} \right| \\ &= C'_{D,Mi,lu,i} \cdot \left(u_{\ell u,i} + \Delta u_{\ell u,i} - u_{Mi,i} - \Delta u_{Mi,i} \right) \cdot \left| u_{\ell u,i} - u_{Mi,i} \right| \end{aligned} \tag{16.4-154}$$

The drag coefficient $C'_{D,Mi,lu,i}$ is defined as follows:

For the annular steel or fuel flow regime:

$$C'_{D,Mi,\ell u,i} = \theta_{\ell u,i} \cdot \rho_{Mi,i} \cdot \frac{1}{R_{\ell u,i}} \cdot \left(\frac{\theta_{Mi,i}}{\theta_{ch,i}} \right)^{CIA5} \cdot C_{DRAG} \cdot C_{AREA,Mi,\ell u,i} \tag{16.4-155}$$

Where CIA4 and CIA5 are input constants, with the values 0.375 and -2.7, respectively. The coefficient C_{DRAG} is defined as follows:

If $\mathrm{Re}_{lu,i} > 500$,

$$C_{DRAG} = 0.44 \tag{16.4-156a}$$

If $\mathrm{Re}_{lu,i} \le 500$, then

$$C_{DRAG} = 18.5 \cdot \left(\mathrm{Re}_{\ell u,i}\right)^{-6} \tag{16.4-156b}$$

The chunk Reynolds number $\mathrm{Re}_{lu,i}$ used in Eq. 16.4-156 is defined as follows:

$$\mathrm{Re}_{\ell u,i} = 2 \cdot R_{\ell u,i} \cdot \left| u_{Mi,i} - u_{\ell u,i} \right| \cdot \rho_{Mi,i} \cdot \frac{1}{\mu_{Mi,i}} \tag{16.4-157}$$

The coefficient $C_{AREA,Mi,\ell\ u,i}$ is used to take into account the fact that the chunks are in contact not only with the gas mixture, but with other components too, such as molten fuel or steel and cladding. This coefficient will be described in Section 16.4.3.10.

For the bubbly steel and fuel flow regimes:

$$C'_{D,Mi,\ell u,i} = 0 \tag{16.4-158}$$

Finally, the inertial (or apparent mass) momentum source term has the form:

$$\Gamma'^{inertial}_{Mo,Mi,i} = C'_{IN,Mi,fu,i} \cdot \left[\frac{\Delta\left(u_{fu,i} - u_{Mi,i}\right)}{\Delta t} + u_{Mi,i} \frac{\Delta\left(u_{fu} - u_{Mi}\right)}{\Delta t} \right] \tag{16.4-159}$$

where

$$\frac{\Delta\left(u_{fu} - u_{Mi}\right)}{\Delta z} = \begin{cases} \dfrac{\left(u'_{fu,i} - u'_{Mi,i}\right) - \left(u''_{fu,i-1} - u''_{Mi,i-1}\right)}{2\Delta z_1} & \text{if } u_{Mi,i} > 0 \\ \dfrac{\left(u'_{fu,i+1} - u'_{Mi,i+1}\right) - \left(u''_{fu,i} - u''_{Mi,i}\right)}{2\Delta z_2} & \text{if } u_{Mi,i} < 0 \end{cases} \tag{16.4-160}$$

and the generalized inertial coefficient is defined as follows:

For annular steel or fuel flow, no inertial effects are present:

$$C'_{IN,Mi,fu,i} = 0. \tag{16.4-161}$$

For bubbly steel flow:

$$C'_{IN,Mi,fu,i} = 0.5 \cdot \rho_{se,i} \cdot \theta_{Mi,i}. \tag{16.4-162}$$

For bubbly fuel flow:

$$C'_{IN,Mi,fu,i} = 0.5 \cdot \rho_{fu,i} \cdot \theta_{Mi,i}. \tag{16.4-163}$$

The source terms $\sum \Gamma'^{\ell}_{Mo,i-1}$ in Eq. 16.4-147 are similar to the $\sum \Gamma'^{\ell}_{Mo,i}$ terms that have been presented in detail, but they cannot be obtained from $\Gamma'^{\ell}_{Mo,i}$ by simply replacing the subscript i by i-1. The velocity $u_{Mi,i}$ in these terms has to be replaced by $u'_{Mi,i}$, i.e., $C_{Mo,Mi,i} \cdot u_{Mi,i}$. The components of $\sum \Gamma'^{\ell}_{Mo,i-1}$ are presented below:

$$\Gamma'^{cond}_{Mo,Mi,i} = -\frac{\Delta\rho'^{cond}_{sv,i-1}}{\Delta t} \cdot C^{n+1}_{Mo,Mi,i} \cdot u_{Mi,i} - \frac{\Delta\rho'^{cond}_{fv,i-1}}{\Delta t} \cdot C^{n+1}_{Mo,Mi,i} \cdot u_{Mi,i} \tag{16.4-164}$$

$$\Gamma'^{vap}_{Mo,Mi,i-1} = \frac{\Delta\rho^{vap}_{sv,i-1}}{\Delta t} C^{n+1}_{Mo,fu,i}\ u_{fu,i} + \frac{\Delta\rho^{vap}_{fv,i-1}}{\Delta t}\ C^{n+1}_{Mo,fu,i} \cdot u_{fu,i} \tag{16.4-165}$$

$$\begin{aligned}\Gamma'^{friction\ wall}_{Mo,Mi,i-1} = &-f_{Mi,i-1} \cdot \frac{\rho'_{Mi,i-1}}{2 \cdot D_{H,Mi,i-1}} \cdot \left(u_{Mi,i} + \Delta u_{Mi,i}\right) \\ &\cdot \left|u_{MI,i}\right| \cdot \left(C^{n+1}_{Mo,Mi,i}\right)^2\end{aligned} \tag{16.4-166}$$

$$\begin{aligned}\Gamma'^{drag\ fuel}_{Mo,Mi,i-1} = C'_{D,Mi,fu,i-1}\Big[&\left(u_{fu,i} + \Delta u_{fu,i}\right) \cdot C^{n+1}_{Mo,fu,i} - \left(u_{Mi,i} + \Delta u_{Mi,i}\right) \\ &\cdot C^{n+1}_{Mo,Mi,i}\Big] \cdot \left|u_{fu,i} \cdot C_{Mo,fu,i} - u_{Mi,i} \cdot C_{Mo,Mi,i}\right|\end{aligned} \tag{16.4-167}$$

$$\begin{aligned}\Gamma'^{drag\ chunk}_{Mo,Mi,i-1} = C'_{D,Mi,\ell u,i-1} \cdot \Big[&\left(u_{\ell u,i} + \Delta u_{\ell u,i}\right) - \left(u_{Mi,i} + \Delta u_{Mi,i}\right) \\ &\cdot C^{n+1}_{Mo,Mi,i}\Big] \cdot \left|u_{\ell u,i} - u_{Mi,i} \cdot C_{Mo,Mi,i}\right|\end{aligned} \tag{16.4-168}$$

$$\begin{aligned}\Gamma'^{inertial}_{Mo,Mi,i-1} = C'_{IN,Mi,fu,i} \cdot &\frac{\Delta\left[\left(u_{fu,i} \cdot C_{Mo,fu,i}\right) - \left(u_{Mi,i} \cdot C_{Mo,Mi,i}\right)\right]}{\Delta t} \\ &+ u_{Mi,i} \cdot C^{n+1}_{Mo,Mi,i} \cdot \frac{\Delta\left(u_{fu} - u_{Mi}\right)}{\Delta z}\end{aligned} \tag{16.4-169}$$

where the definition of $\frac{\Delta\left(u_{fu}-u_{Mi}\right)}{\Delta z}$ is the same as Eq. 16.4-160. It should be noted that, in the definition of the source terms, we used the assumption that changes in the coefficients $C_{Mo,fu,i}$ can be neglected during one time step, and thus only the new coefficients at time n+1 have been used.

We can now replace the expression $\sum_{\ell}\left(\Gamma'^{\ell}_{Mo,i-1}\cdot\Delta z_i+\Gamma'^{\ell}_{Mo,i}\cdot\Delta z_2\right)$ in Eq. 16.4-147 using Eqs. 16.4-148 through 16.4-167. We then rearrange Eq. 16.4-147 in the form:

$$DMX\cdot\Delta u_{Mi,i}=AMX+BMX\cdot\Delta u_{fu,i}+CMX\cdot\Delta u_{\ell u,i} \tag{16.4-170}$$

All terms containing the time change of the gas mixture velocity $\Delta u_{Mi,i}$ were moved to the left-hand side of the Eq. 16.4-170, and after factoring $\Delta u_{Mi,i}$, put in the form DMX · $\Delta u_{Mi,i}$. Similarly, all terms containing $\Delta u_{fu,i}$ and $\Delta u_{\ell u,i}$ were grouped together on the right-hand side. All other terms were grouped under the coefficient AMX. It should be observed that the term $\frac{\Delta\left(u_{fu}-u_{Mi}\right)}{\Delta z}$ which appears in Eqs. 16.4-159 and 16.4-169 does not contain time changes and thus will be included in the AMX coefficient.

16.4.3.8.2 The Momentum Conservation Equation for the Molten Fuel/Steel Component

Using an integration procedure similar to that used for the gas-mixture equation, we obtain the following equation:

$$\begin{aligned}
&\Delta u_{fu,i}\left[\left(\rho'^{n+1}_{fu,i-1}+\rho'^{n+1}_{se,i-1}\right)\cdot C^{n+1}_{Mo,fu,i}\cdot\Delta z_1+\left(\rho'^{n+1}_{fu,i}+\rho'^{n+1}_{se,}\right)\cdot\Delta z_2\right]\cdot\frac{1}{\Delta t}\\
&\quad=-\left[\left(\rho' u^2\right)_{fu,i}-\left(\rho' u^2\right)_{fu,i}\right]-\theta_{fu,i-1/2}\cdot\left(P_I-P_{i-1}\right)\\
&\qquad-u_{fu,i}\cdot C_{Mo,fu,i}\cdot\Delta z_i\cdot\left(\frac{\Delta\rho'_{fu,i-1}}{\Delta t}+\frac{\Delta\rho'_{se,i-1}}{\Delta t}\right)\\
&\qquad-u_{fu,i}\cdot\Delta z_2\cdot\left(\frac{\Delta\rho'_{fu,i}}{\Delta t}+\frac{\Delta\rho'_{se,i}}{\Delta t}\right)-\left(\rho'^{n+1}_{fu,i-1}+\rho'^{n+1}_{se,i-1}\right)\cdot u_{fu,i}\cdot\Delta z_i\cdot\frac{\Delta C_{Mo,fu,i}}{\Delta t}\\
&\qquad+\sum_{m}\left(\Gamma'^{m}_{Mo,fu,i-1}\cdot\Delta z_1+\Gamma'_{Mo,fu,i}\cdot\Delta z_2\right)-\left(\rho'_{fu,i-1}+\rho'_{se,i-1}\right)\cdot\Delta z_1\cdot g\\
&\qquad-\left(\rho'_{fu,i}+\rho'_{se,i}\right)\cdot\Delta z_2\cdot g
\end{aligned} \tag{16.4-171}$$

where

$$\left(\rho' u^2\right)_{fu,i}=\left(\rho'_{fu,i}+\rho'_{se,i}\right)\cdot\left(u''_{fu,i}+u'_{fu,i+1}\right)^2\cdot.25 \tag{16.4-172}$$

The optional formulation, which can be obtained using IMOMEN=1 is:

$$\left(\rho' u^2\right)_{fu,i} = \left(\rho'_{fu,i} + \rho'_{se,i}\right) \cdot u^2_{Mo,fu,i} \tag{16.4-173}$$

where

$$u_{Mo,Mi,i} = \begin{cases} u''_{fu,i} & \text{if } u''_{fu,i} \geq 0 \text{ and } u'_{fu,i+1} \geq 0 \quad (16.4\text{-}174a) \\ \sqrt{u''^2_{fu,i} + u'^2_{fu,i+1}} & \text{if } u''_{fu,i} \geq 0 \text{ and } u'_{fu,i+1} \leq 0 \quad (16.4\text{-}174b) \\ 0 & \text{if } u''_{fu,i} < 0 \text{ and } u'_{fu,i+1} \geq 0 \quad (16.4\text{-}174c) \\ u'_{fu,i+1} & \text{if } u'_{fu,i} < 0 \text{ and } u'_{fu,i+1} < 0 \quad (16.4\text{-}174d) \end{cases}$$

The quantity $\theta_{fu,i-1/2}$ is defined by Eqs. 16.4-142 and 16.4-143, where the $\theta_{Mi,i}$ is replaced by $(\theta_{fu,i} + \theta_{se,i})$. The source/sink terms in $\sum_m \Gamma'^m_{Mo,fu,i}$ are defined in detail below:

The condensation term:

$$\Gamma'^{cond}_{Mo,fu,i} = \frac{\Delta \rho'^{cond}_{fv,i}}{\Delta t} \cdot u_{Mi,i} \tag{16.4-175}$$

The vaporization term:

$$\Gamma'^{vap}_{Mo,fu,i} = -\frac{\Delta \rho'_{fv,i}}{\Delta t} \cdot u_{fu,i} \tag{16.4-176}$$

The wall friction term is dependent on the flow regime:

For the annular or bubbly fuel flow regimes:

$$\begin{aligned} \Gamma'^{friction\ wall}_{Mo,fu,i} = & -f_{se,i} \cdot \frac{\rho_{se,i} \cdot \left(\theta_{fu,i} + \theta_{se,i}\right)}{2 \cdot D_{H,se,i}} \cdot C_{AREA,se,i} \cdot u^{n+1}_{fu,i} \cdot \left| u^n_{fu,i} \right| \\ & - f_{se,i} \frac{\rho_{se,i} \left(\theta_{fu,i} + \theta_{se,i}\right)}{2\, D_{H,se,i}} \cdot C_{AREA,se,i} \cdot \left(u_{fu,i} + \Delta u_{fu,i}\right) \cdot \left| u_{fu,i} \right| \end{aligned} \tag{16.4-177}$$

For the annular or bubbly fuel flow regimes:

$$\Gamma'^{friction\ wall}_{Mo,fu,i} = -f_{fu,i} \cdot \frac{\rho_{fu,i} \left(\theta_{fu,i} + \theta_{se,i}\right)}{2\, D_{H,fu,i}} \cdot C_{AREA,fu,i} \cdot \left(u_{fu,i} + \Delta u_{fu,i}\right) \cdot \left| u_{fu,i} \right| \tag{16.4-178}$$

where

the $D_{H,se,i}$ and $D_{H,fu,i}$ are the hydraulic diameters for steel and fuel, respectively, and are described in Section 16.4.3.9.

the contact coefficients $C_{AREA,se,i}$ and $C_{AREA,fu,i}$ account for the fact that only a fraction of the steel or fuel perimeter is in contact with the stationary walls; they are described in Section 16.4.3.10; and the friction coefficients $f_{se,i}$ and $f_{fu,i}$ are defined below:

$$f_{se,i} = \begin{cases} CIFRFU & \text{if } \mathrm{Re}_{se,i} \geq CIREFU \quad (16.4\text{-}179a) \\ \dfrac{80}{\mathrm{Re}_{se,i}} & \text{if } \mathrm{Re}_{se,i} < CIREFU \quad (16.4\text{-}179b) \end{cases}$$

$$f_{fu,i} = \begin{cases} CIFRFU & \text{if } \mathrm{Re}_{fu,i} \geq CIREFU \quad (16.4\text{-}179c) \\ \dfrac{80}{\mathrm{Re}_{fu,i}} & \text{if } \mathrm{Re}_{fu,i} < CIREFU \quad (16.4\text{-}179a) \end{cases}$$

where CIFRFU and CIREFU are input constants. Currently, CIFRFU = .03 and CIREFU = 2100.

The fuel/steel-gas mixture drag source is similar, but of opposite sign, to the term already presented for the gas mixture.

$$\Gamma'^{drag\ mixture}_{Mo,fu,i} = -C'_{D,Mi,fu,i} \cdot \left(u_{fu,i} + \Delta u_{fu,i} - u_{Mi,i} - \Delta u_{Mi,i}\right) \cdot \left|u_{fu,i} - u_{Mi,i}\right| \quad (16.4\text{-}180)$$

The drag coefficient $C'_{D,Mi,fu,i}$ is defined by Eqs. 16.4-152 and 16.4-153.

The fuel/steel - chunk drag source is defined as follows:

$$\begin{aligned} \Gamma'^{drag\ chunk}_{Mo,fu,i} &= C'_{D,fu,\ell u,i} \cdot \left(u^{n+1}_{\ell u,i} - u^{n+1}_{fu,i}\right) \cdot \left|u^{n}_{\ell u,i} - u^{n}_{fu,i}\right| \\ &= C'_{D,fu,\ell u,i} \cdot \left(u_{\ell u,i} + \Delta u_{\ell u,i} - u_{fu,i} - \Delta u_{fu,i}\right) \cdot \left|u_{\ell u,i} - u_{fu.i}\right| \end{aligned} \quad (16.4\text{-}181)$$

The generalized drag coefficient $C'_{D,fu,\ell u,i}$ is flow regime dependent and is defined below:

For the steel annular and bubbly flow regimes:

$$C'_{D,fu,\ell u,i} = \theta_{\ell u,i} \cdot \rho_{se,i} \cdot CIA4 \cdot \frac{1}{R_{\ell u,i}} \cdot \left[\frac{\theta_{Mi,i}}{\theta_{Mi,i} + \theta_{\ell u,i}}\right]^{CIA5} \cdot C_{DRAG} \cdot C_{AREA,se,\ell u,i} \quad (16.4\text{-}182)$$

For the fuel annular and bubbly flow regimes:

$$C'_{D,fu,\ell u,i} = \theta_{\ell u,i} \cdot \rho_{fu,i} \cdot CIA4 \cdot \frac{1}{R_{\ell u,i}} \cdot \left[\frac{\theta_{Mi,i}}{\theta_{Mi,i} + \theta_{\ell u,i}} \right]^{CIA5} \cdot C_{DRAG} \cdot C_{AREA,fu,\ell u,i} \qquad (16.4\text{-}183)$$

In the above equations, the drag coefficient C_{DRAG} is defined by 16.4-156. The area coefficients, which account for the fact that only a fraction of the chunk lateral area is in contact with the molten fuel or steel, are defined below:

$$C_{AREA,se,\ell u,i} = \begin{cases} \left(1 - C_{AREA,Mi,\ell u,i}\right) \cdot C_{AREA,se,c\ell,i} & \text{for annular steel flow} \\ 1 & \text{for } \textit{bubbly} \text{ steel flow} \end{cases} \qquad (16.4\text{-}184)$$

where $C_{AREA,Mi,\ell u,i}$ indicates the fraction of the lateral chunk area in contact with the gas mixture. The quantity 1 - $C_{AREA,Mi,\ell u,i}$ thus represents the fraction of the chunk area in contact with the molten fuel/steel and cladding/hexcan wall. The coefficient $C_{AREA,se,cl}$ represents the fraction of the cladding/hexcan wall area covered by molten steel/fuel. Both these area coefficients will be explained in more detail in Section 16.4.3.9.

The momentum source due to fuel injection from the pin

$$\Gamma'^{injection}_{Mo,fu,i} = \frac{\Delta\rho'_{fu,injection,i}}{\Delta t} \cdot u_{fu,ca,i} \cdot C_{Mo,injection,i} \qquad (16.4\text{-}185)$$

The quantity $\Delta\rho'_{fu,injection,i}$ represents the change in the fuel generalized density due to injection via the pin rip or via the end of the pin stubs, as explained in Section 16.3. The velocity of the injected material is $u_{fu,ca,i}$, which is also explained in Section 16.3. The coefficient $C_{Mo,injection,i}$ accounts for the axial momentum loss due to lateral acceleration and mixing during the injection process, and is defined as follows:

$$C_{Mo,injection,i} = \begin{cases} 1, & \text{if injection is taking place via the pin stubs} \quad (16.4\text{-}186a) \\ \text{CIFUMO}, & \text{if injection is taking place via the pin up} \quad (16.4\text{-}186b) \end{cases}$$

where CIFUMO is an input constant, with values between 0 and 1.

To summarize, the term $\sum_m \Gamma'^m_{Mo,fu,i}$, which appears in Eq. 16.4-171, has the form,

$$\sum_m \Gamma'^m_{Mo,fu,i} = \Gamma'^{cond}_{Mo,fu,i} + \Gamma'^{vap}_{Mo,fu,i} + \Gamma'^{friction\ wall}_{Mo,fu,i} + \Gamma'^{drag\ mixture}_{Mo,fu,i} + \Gamma'^{drag\ chunk}_{Mo,fu,i} + \Gamma'^{injection}_{Mo,fu,i} \qquad (16.4\text{-}187)$$

The term $\sum_m \Gamma'^m_{Mo,fu,i-1}$ has a similar composition, and its terms are presented below:

$$\Gamma'^{cond}_{Mo,fu,i-1} = \frac{\Delta\rho'^{cond}_{fv,i-1}}{\Delta t}\ u_{Mi,i} \cdot C_{Mo,Mi,i} \tag{16.4-188}$$

$$\Gamma'^{vap}_{Mo,fu,i-1} = -\frac{\Delta\rho'_{fv,i-1}}{\Delta t} \cdot u_{fu,i} \cdot C_{Mo,fu,i} \tag{16.4-189}$$

For the steel flow regimes,

$$\Gamma'^{friction\,l}_{Mo,fu,i-1} = -f_{se,i-1} \cdot \frac{\rho_{se,i-1} \cdot \left(\theta_{fu,i-1} + \theta_{se,i-1}\right)}{2\ D_{H,se,i-1}} \cdot C_{AREA,se,i-1} \cdot C^2_{Mo,fu,i} \cdot \left(u_{fu,i} + \Delta u_{fu,i}\right) \left|u_{fu,i}\right| \tag{16.4-190a}$$

For the fuel flow regimes:

$$\Gamma'^{friction}_{Mo,fu,i-1} = -f_{fu,i-1} \cdot \frac{\rho_{fu,i-1} \cdot \left(\theta_{fu,i-1} + \theta_{se,i-1}\right)}{2\ D_{H,fu,i-1}} \cdot C_{AREA,fu,i-1} \cdot C^2_{Mo,fu,i} \cdot \left(u_{fu,i} + \Delta u_{fu,i}\right) \left|u_{fu,i}\right| \tag{16.4-190b}$$

$$\Gamma'^{drag\ mixture}_{Mo,fu,i-1} = -C'_{D,Mi,fu,i-1} \cdot \left[\left(u_{fu,i} + \Delta u_{fu,i}\right) \cdot C^{n+1}_{Mo,fu,i} - \left(u_{Mi,i} + \Delta u_{Mi,i}\right) \cdot C^{n+1}_{Mo,Mi,i}\right] \cdot \left|u_{fu,i} \cdot C_{Mo,fu,i} - u_{Mi,i}\ C_{Mo,Mi,i}\right| \tag{16.4-191}$$

$$\Gamma'^{drag\ chunk}_{Mo,fu,i-1} = C'_{D,fu,\ell u,i-1} \left[\left(u_{\ell u,i} + \Delta u_{\ell u,i}\right) - \left(u_{fu,i} + \Delta u_{fu,i}\right) \cdot C^{n+1}_{Mo,fu,i}\right] \cdot \left|u_{\ell u,i} - u_{fu,i} \cdot\ C_{Mo,fu,i}\right| \tag{16.4-192}$$

$$\Gamma'^{injection}_{Mo,fu,i-1} = \frac{\Delta\rho'_{fu,injection,\,i-1}}{\Delta t} \cdot u_{fu,ca,i-1} \cdot\ C_{Mo,injection,\,i-1} \tag{16.4-193}$$

The source terms, as given by Eqs. 16.4-175 through 16.4-193 are substituted in Eq. 16.4-171, and, after rearranging, the fuel momentum equation is written in the form

$$DFX \cdot \Delta u_{fu} = AFX + BFX \cdot \Delta u_{Mi} + CFX \cdot \Delta u_{fu} \tag{16.4-194}$$

16.4.3.8.3 The Momentum Conservation Equation for the Fuel/Steel Chunks

Using an integration procedure similar to that used for the gas mixture, we obtain the following equation in finite difference form:

$$\begin{aligned}
&\Delta u_{\ell u,i}\left[\left(\rho'^{n+1}_{f\ell,i-1}+\rho'^{n+1}_{s\ell,i-1}\right)\cdot\Delta z_i+\left(\rho'^{n+1}_{f\ell,i-1}+\rho'^{n+1}_{s\ell,i-1}\right)\cdot\Delta z_2\right]\cdot\frac{1}{\Delta t}\\
&=-\left[\left(\rho' u^2\right)_{\ell u,i}-\left(\rho' u^2\right)_{\ell u,i-1}\right]-\theta_{\ell u,i-1/2}\cdot\left(P_i-P_{i-1}\right)\\
&-u_{\ell u,i}\cdot\Delta z_1\cdot\left(\frac{\Delta\rho'_{f\ell,i-1}}{\Delta t}+\frac{\Delta\rho'_{s\ell,i-1}}{\Delta t}\right)-u_{\ell u,i}\cdot\Delta z_2\cdot\left(\frac{\Delta\rho'_{f\ell,i}}{\Delta t}+\frac{\Delta\rho'_{s\ell,i}}{\Delta t}\right)\\
&+\sum_n\left(\Gamma'^n_{Mo,\ell u,i}\cdot\Delta z_i+\Gamma'^n_{Mo,\ell u,i}\cdot\Delta z_2\right)-\left(\rho'_{f\ell,i-1}+\rho'_{s\ell,i-1}\right)\cdot\Delta z_1\cdot g\\
&-\left(\rho'_{f\ell,i}+\rho'_{s\ell,i}\right)\cdot\Delta z_2\cdot g
\end{aligned}\qquad(16.4\text{-}195)$$

where

$$\left(\rho' u^2\right)_{\ell u,i}=\left(\rho'_{f\ell,i}+\rho'_{s\ell,i}\right)\cdot\left(u_{\ell u,i}+u_{\ell u,i+1}\right)^2\cdot 0.25\qquad(16.4\text{-}196)$$

The optimal formulation of the convective terms can be obtained by using the input variable IMOMEN = 1 and is similar to Eq. 16.4-174, where $u''_{fu,i}$ and $u'_{fu,i}$ are replaced by $u_{\ell u,i}$ and $u_{\ell u,i}$ and $u_{\ell u,i+1}$, respectively. The quantity $\theta_{\ell u,i-1/2}$ is defined by Eqs. 16.4-143 and 16.4-144, where $\theta_{Mi,i}$ is replaced by $\theta_{\ell u,i}$. The source terms are defined below:

$$\sum_n\Gamma'^n_{Mo,\ell u,i}=\Gamma'^{\text{drag mixture}}_{Mo,\ell u,i}+\Gamma'^{\text{drag fuel}}_{Mo,\ell u,i}+\Gamma'^{\text{friction wall}}_{Mo,lu,i}+\Gamma'^{\text{contraction}}_{Mo,\ell u,i}\qquad(16.4\text{-}197)$$

No momentum sources due to chunk formation or remelting are present in Eq. 16.4-197, because the routines modeling these processes are called after the LEMOCO routine, and thus these effects will be considered later. The individual sources are presented below:

The term due to the gas mixture/chunk drag:

$$\begin{aligned}
\Gamma'^{drag\ mixture}_{Mo,\ell u,i}&=-C'_{D,Mi,lu,i}\cdot\left(u_{\ell u,i}+\Delta u_{\ell u,i}-u_{Mi,i}-\Delta u_{Mi,i}\right)\\
&\cdot\left|u_{\ell u,i}+u_{Mi,i}\right|
\end{aligned}\qquad(16.4\text{-}198)$$

The generalized drag coefficient $C'_{D,Mi,\ell u,i}$ has been presented in Eq. 16.4-181.

The term due to the molten fuel/steel-chunk drag is as follows:

$$\begin{aligned}
\Gamma'^{drag\ fuel}_{Mo,\ell u,i}&=-C'_{D,fu,\ell u,i}\cdot\left(u_{\ell u,i}+\Delta u_{\ell u,i}-u_{fu,i}-\Delta u_{fu,i}\right)\\
&\cdot\left|u_{\ell u,i}+u_{fu,i}\right|
\end{aligned}\qquad(16.4\text{-}199)$$

The generalized drag coefficient $C'_{D,fu,\ell u,i}$ has been presented in Eq. 16.4-181.

The momentum sink due to wall friction is:

$$\Gamma'^{\,friction\ wall}_{Mo,\ell u,i} = -0.5 \cdot 10^{-3} \cdot P_i \cdot A'_{\ell u,cl,i} \cdot SIGN\left(u_{\ell u,i}\right)$$

where the generalized area of contact between chunks and clad/hexcan wall, $A'_{\ell u,cl,i}$ is defined as:

$$A'_{\ell u,cl,i} = \frac{A_{\ell u,cl,i}}{\Delta z_i \cdot AXMX} \tag{16.4-200}$$

and is presented in section 16.4.3.9. Equation 16.4-199 was obtained assuming that the frictional force between chunks and wall is due to the normal force generated by the pressure P_i and that the friction coefficient between the two solid surfaces is $0.5 \cdot 10^{-3}$.

The momentum sink due to jumbling at the contraction at the boundary i is due to chunks arriving at an abrupt contraction, where they lose momentum upon hitting the wall normal to the flow path:

If $u_{\ell u,i} < 0$ and $A_i > A_{i-1}$,

$$\Gamma'^{\,jumbling}_{Mo,\ell u,i} = \left(\rho'_{f\ell,i} + \rho'_{s\ell,i}\right) \cdot \; u^2_{\ell u,i} \cdot \frac{A_i - A_{i-1}}{A_i} \tag{16.4-201a}$$

Otherwise,

$$\Gamma'^{\,jumbling}_{Mo,\ell u,i} = 0 \tag{16.4-201b}$$

The sources $\sum_n \Gamma'^{n}_{Mo,\ell u,i-1}$ are defined in a similar way, as shown below:

$$\begin{aligned}\Gamma'^{\,drag\ mixture}_{Mo,\ell u,i-1} = -C'_{D,Mi,\ell u,i-1} \cdot \Big[&\left(u_{\ell u,i} + \Delta u_{\ell u,i}\right) - \left(u_{Mi,i} + \Delta u_{Mi,i}\right) \\ &\cdot C^{n+1}_{Mo,Mi,i}\Big] \cdot \left| u_{\ell u,i} - u_{Mi,i} \cdot C_{Mo,Mi,i} \right|\end{aligned} \tag{16.4-202}$$

$$\begin{aligned}\Gamma'^{\,drag\ fuel}_{Mo,\ell u,i-1} = -C'_{D,fu,\ell u,i-1} \cdot \Big[&\left(u_{\ell u,i} + \Delta u_{\ell u,i}\right) - \left(u_{fu,i} + \Delta u_{fu,i}\right) \\ &\cdot C^{n+1}_{Mo,fu,i}\Big] \cdot \left| u_{\ell u,i} - u_{fu,i} \cdot C_{Mo,fu,i} \right|\end{aligned} \tag{16.4-203}$$

$$\Gamma'^{\,friction\ wall}_{Mo,\ell u,i-1} = -0.5 \cdot 10^{-3} \cdot P_{i-1} \cdot A'_{\ell u,cl,i-1} \cdot SIGN\left(u_{\ell u,i}\right) \tag{16.4-204}$$

If $u_{\ell u,i} \geq 0$ and $A_{i-1} > A_i$,

$$\Gamma'^{\,contraction}_{Mo,\ell u,i-1} = \left(\rho'_{f\ell,i-1} + \rho'_{s\ell,i-1}\right) \cdot u^2_{\ell u,i} \cdot \frac{A_{i-1} - A_i}{A_{i-1}} \tag{16.4-205a}$$

Otherwise,

$$\Gamma'^{\,contraction}_{Mo,\ell u,i-1} = 0 \tag{16.4-205b}$$

The source terms given by Eqs. 16.4-198 through 16.4-205 are substituted in Eq. 16.4-195 and after rearranging, we obtain the chunk momentum equation

$$DLX \cdot \Delta u_{\ell u,i} = ALX + BLX \cdot \Delta u_{fu,i} + CLX \cdot \Delta u_{Mi,i} \tag{16.4-206}$$

16.4.3.8.4 The Simultaneous Solution of the Momentum Conservation Equations

The calculation of the new velocities in momentum cell i begins by calculating the coefficients AMX and DMX for the gas-mixture Eq. 16.4-170. The terms due to the mixture interaction with the molten fuel/steel and chunks are not included in AMX and DMX at this time. A check is then performed to verify if the momentum cell I contains only the gas mixture. If this is the case, the only equations solved is

$$DMX \cdot \Delta u_{Mi,i} = AMX \tag{16.4-207}$$

and only the gas-mixture velocity is updated:

$$u^{n+1}_{Mi,i} = u^n_{Mi,i} + \Delta u_{Mi,i} \tag{16.4-208}$$

If either half of the momentum cell i contains molten fuel and/or steel, the coefficients are calculated for the momentum equations:

$$DMX \cdot \Delta u_{Mi,i} = AMX + BMX \cdot \Delta u_{fu,i} \tag{16.4-209a}$$

$$DFX \cdot \Delta u_{fu,i} = AFX + BFX \cdot \Delta u_{Mi,i} \tag{16.4-209b}$$

If the momentum cell does not contain fuel/steel chunks, these equations are solved simultaneously for $\Delta u_{Mi,i}$ and $\Delta u_{fu,i}$ and the new velocities are calculated:

$$u_{Mi,i}^{n+1} = u_{Mi,i}^{n} + \Delta u_{Mi,i} \tag{16.4-210a}$$

$$u_{fu,i}^{n+1} = u_{fu,i}^{n} + \Delta u_{fu,i} \tag{16.4-210b}$$

It is noted that the coefficients AMX and DMX in Eqs. 16.4-209 are obtained by adding to the values calculated for Eq. 16.4-207 the additional terms due to the gas mixture-fuel interaction. If either half of the momentum cell contains fuel/steel chunks, the coefficients are calculated for the momentum equations in the form below:

$$DMX \cdot \Delta u_{Mi,i} = AMX + BMX \cdot \Delta u_{fu,i} + CMX \cdot \Delta u_{\ell u,i} \tag{16.4-211a}$$

$$DFX \cdot \Delta u_{fu,i} = AFX + BFX \cdot \Delta u_{Mi,i} + CFX \cdot \Delta u_{\ell u,i} \tag{16.4-211b}$$

$$DLX \cdot \Delta u_{\ell u,i} = ALX + BLX \cdot \Delta u_{fu,i} + CLX \cdot \Delta u_{Mi,i} \tag{16.4-211c}$$

The coefficients that have been calculated using for Eqs. 16.4-210 are updated by adding the terms due to the presence of chunks. Equations 16.4-211 are solved simultaneously for $\Delta u_{Mi,i}$, $\Delta_{fu,i}$, $\Delta u_{\ell u,i}$, by using a substitution method and the new velocities are calculated:

$$u_{Mi,i}^{n+1} = u_{Mi,i}^{n} + \Delta u_{Mi,i} \tag{16.4-212a}$$

$$u_{fu,i}^{n+1} = u_{fu,i}^{n} + \Delta u_{fu,i} \tag{16.4-212b}$$

$$u_{\ell u,i}^{n+1} = u_{\ell u,i}^{n} + \Delta u_{\ell u,i} \tag{16.4-212c}$$

16.4.3.9 Description of the Local Geometry

In order to fully define the energy and momentum source terms used in the conservation equations, we must supply the areas of contact between various components. These areas are obtained in LEVITATE by defining the local geometry in the routine LEGEOM. The definition of the geometry is based on the local flow regime and the configuration of the stationary elements, i.e., presence of fuel pins, presence of cladding, presence of frozen fuel crusts, etc.

16.4.3.9.1 Local Flow Regime Definition

Because the flow regimes are important in defining the local geometry, the decision about the local flow regime is made before the geometry definition in the LEVOFR routine. The physical models for the flow regimes are described in Section 16.4.1.4, and

this section will describe only the decision process used to select the appropriate flow regime. The total flow regime is dependent on the local volumetric fraction of various components in the cell and on the previously established flow regime. The volumetric fraction for component i, α_i, is defined as follows:

$$\alpha_i = \frac{A_i \cdot \Delta z_i}{A_{ch,op,i} \cdot \Delta z_i} = \frac{\theta_i}{\theta_{ch,op}} \qquad (16.4\text{-}213)$$

Where $A_{ch,op}$ is the local cross sectional area of the open flow channel. The flow regime in each cell is determined in the following manner:

(I) If the previously established flow regime is bubbly fuel flow and

(a) – if $\frac{\theta_{fu,i} + \theta_{se,i}}{\theta_{ch,op,i} - \theta_{\ell u,i}}$ > CIBBLY * 0.7 and

1. - if $\theta_{fu,i} \geq \theta_{se,,i} \cdot 0.9 \rightarrow$ bubbly fuel flow regime
2. - if $\theta_{fu,i} < \theta_{se,i} \cdot 0.9 \rightarrow$ bubbly steel flow regime

(b) – if $\frac{\theta_{fu,i} + \theta_{se,i}}{\theta_{ch,op,i} - \theta_{\ell u,i}} \leq$ CIBBLY $\cdot$ 0.7 and

1. - if $\theta_{fu,i} \geq \theta_{se,i} \rightarrow$ annular fuel flow regime
2. - if $\theta_{fu,i} < \theta_{se,i} \rightarrow$ annular steel flow regime

(II) If the previously established flow regime is bubbly steel flow and

(a) – if $\frac{\theta_{fu,i} + \theta_{se,i}}{\theta_{ch,op,i} - \theta_{\ell u,i}}$ > CIBBLY $\cdot$ 0.7 and

1. - if $\theta_{se,i} > \theta_{fu,i} \cdot 0.9 \rightarrow$ bubbly steel flow regime
2. - if $\theta_{se,i} \leq \theta_{fu,i} \cdot 0.9 \rightarrow$ bubbly fuel flow regime

(b) – if $\frac{\theta_{fu,i} + \theta_{se,i}}{\theta_{ch,op,i} - \theta_{\ell u,i}} \leq$ CIBBLY $\cdot$ 0.7 and

1. - if $\theta_{se,i} \geq \theta_{fu,i} \rightarrow$ annular steel flow regime
2. - if $\theta_{se,i} < \theta_{fu,i} \rightarrow$ annular fuel flow regime

(III) If the previously established flow regime is annular fuel or steel flow and

(a) – if $\frac{\theta_{fu,i} + \theta_{se,i}}{\theta_{ch,op,i} - \theta_{\ell u,i}} <$ CIBBLY and

1. - if $\theta_{fu,i} \geq \theta_{se,i} \rightarrow$ annular fuel flow regime
2. - if $\theta_{fu,i} < \theta_{se,i} \rightarrow$ annular steel flow regime

(b) – if $\frac{\theta_{fu,i} + \theta_{se,i}}{\theta_{ch,op,i} - \theta_{\ell u,i}} \geq$ CIBBLY and

1. - if $\theta_{fu,i} \geq \theta_{se,i} \rightarrow$ bubbly fuel flow regime

2. - if $\theta_{fu,i} < \theta_{se,i} \rightarrow$ bubbly steel fuel flow regime

The input constant CIBBLY defines the threshold for the transition from the annular to the bubbly flow regime. In the axial cells where the pins have not yet been disrupted the value of CIBBLY is given by the input constant CIBBIN. In disrupted nodes the value of CIBBLY is given the input constant CIBBDI. The recommended value for CIBBIN is 0.7, and for CIBBDI the recommended value is 0.2. Once a bubbly flow regime has been established, a hysteresis effect is assumed to exist and the transition threshold back to annular flow is CIBBLY · 0.7. Similar hysteresis effects are used for the transitions from steel to fuel and vice versa within the bubbly flow regime. Finally, it is noted that the volume fractions used in the flow regime decision are based on the newly calculated densities and thus are consistent with the conditions at the end of the current time step.

16.4.3.9.2 Description of the Local Geometry of the Stationary and Moving Components

The definition of the local geometry of both stationary and moving components is performed by the LEGEOM routine. The physical boundaries of the rod bundle channel modeled in LEVITATE are the pin cladding and the hexcan wall. Because of the different behavior of these boundaries, the channel is visualized as being divided into two separate channels, one associated with the fuel pins and another associated with the hexcan wall, as shown in Fig. 16.4-16. The flow area is partitioned between these two channels in proportion to the wetted perimeter of the boundaries:

$$A_{ch,cl,i} = \frac{A_{ch,i}}{L_{cl,i} + L_{sr,i}} \cdot L_{cl,i} \tag{16.4-214}$$

$$A_{ch,sr,i} = \frac{A_{ch,i}}{L_{cl,i} + L_{sr,i}} \cdot L_{sr,i} \tag{16.4-215}$$

where $L_{cl,i}$ and $L_{sr,i}$ represent the perimeter of the pins and hexcan wall in cell i, respectively. It is emphasized that LEVITATE models the whole subassembly, and not one pin representing the subassembly. Thus, $L_{cl,i}$ represents the perimeter of all the pins in the bundle. In the special situation when no pins are present at a certain axial location due to pin disruption, the perimeter $L_{cl,i} = 0$, and the area of the channel associated with the cladding, $A_{ch,cl,i}$ becomes zero. Each of the two channel is treated, for the purpose of defining the geometry, as a rectangular channel, with one dimension being the perimeter L and the other a characteristic length, l. This characteristic length is defined as follows:

$$l_{cl,i} = A_{ch,cl,i}/L_{cl,i} \text{ and}$$
$$l_{sr,i} = A_{ch,sr,i}/L_{sr,i} \tag{16.4-216}$$

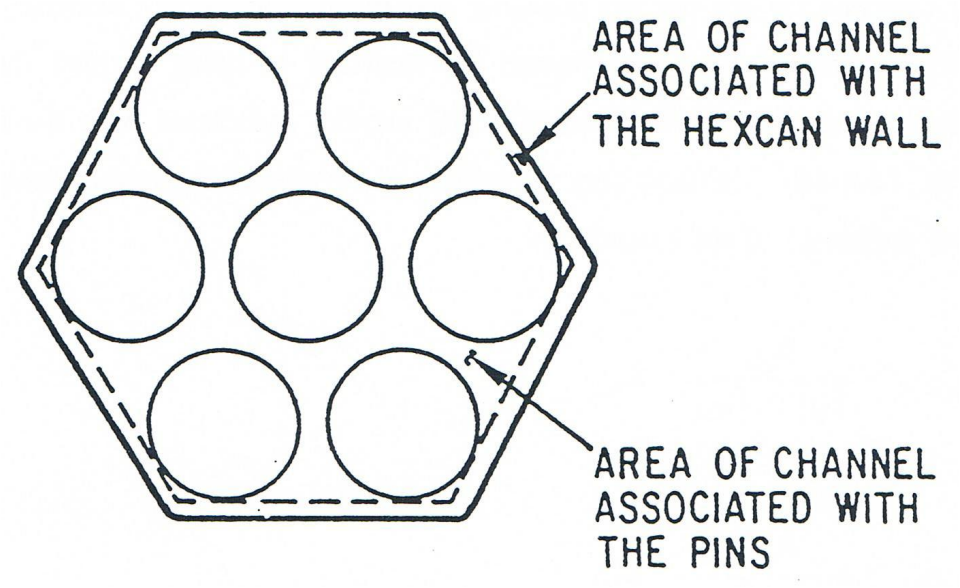

Fig. 16.4-16: Partition of Subassembly Flow Area into Two Distinct Channels

The characteristics length l characterizes the width of the channel and serves as an indicator for the maximum thickness of the fuel crusts that can form on the pins and/or the hexcan wall. The conceptual representation of these channels is presented in Fig. 16.4-17. The fuel crust, when present, is characterized by length $L_{ff,cl,i}$ (and $L_{ff,sv,i}$) and thickness $l_{ff,cl,i}$ (and $l_{ff,sv,i}$). However, instead of storing the crust L_{ff}, two area coefficient are used:

$$C_{ff,cl,i} = \frac{L_{ff,cl,i}}{L_{cl,i}} \tag{16.4-217}$$

and

$$C_{ff,sr,i} = \frac{L_{ff,sr,i}}{L_{sr,i}} \tag{16.4-218}$$

As explained in Section 16.5, the fuel crust can occasionally contain molten or frozen steel, which is taken into account when the crust size is calculated. The crust growth is dependent on the initial conditions, the amount of new frozen fuel, and the local flow regime. This process will be presented later in this chapter.

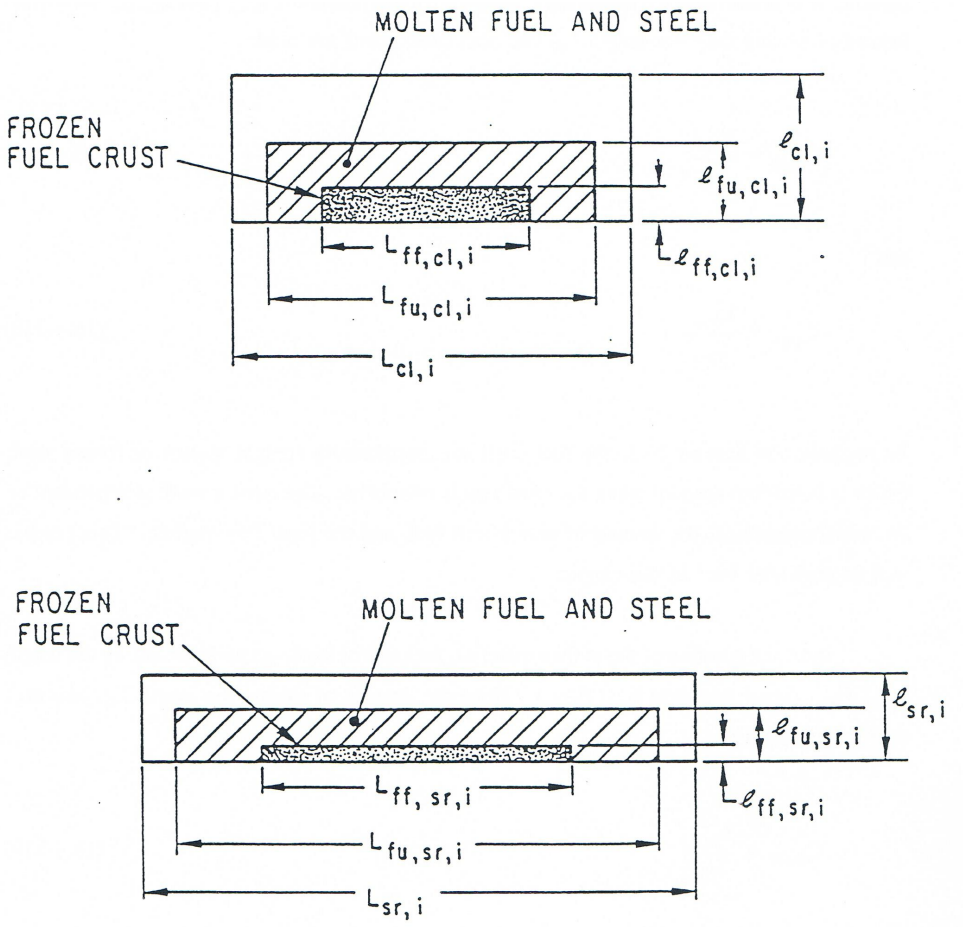

Fig. 16.4-17: Conceptual Representation of the Pin and Hexcan Wall Channels

The configuration of the molten material, fuel and/or steel, is characterized by the length $L_{fu,cl,i}$ ($L_{fu,sr,i}$) and thickness $l_{fu,cl,i}$ ($l_{fu,sr,i}$). However, instead of storing the length L_{fu}, two are coefficients are used:

$$C_{fu,cl,i} = \frac{L_{fu,cl,i}}{L_{cl,i}} \tag{16.4-219}$$

$$C_{ff,sr,i} = \frac{L_{ff,sr,i}}{L_{sr,i}} \tag{16.4-220}$$

Note that the coefficient $C_{fu,cl,i}$ represents the fraction of clading area covered by molten fuel and fuel crust. The same applies to $C_{fu,sr,i}$. All the contact areas required for the energy and momentum equations are defined by using the lateral area of the clad $A^L_{cl,i}$

and hexcan wall $A^{L}_{sr,i}$ and the appropriate area coefficients. Other area conditions used are:

$C_{fu,ff,cl,i}$ - fraction of cladding crust area covered by molten fuel in cell i

$C_{fu,ff,sr,i}$ - fraction of structure crust area covered by molten fuel in cell i

$C_{se,cl,i}$ - fraction of cladding area covered by molten steel and fuel crust in cell i

$C_{se,sr,,i}$ - fraction of hexcan wall area covered by molten steel and fuel crust in cell i

$C_{se,ff,cl,i}$ - fraction of cladding crust area covered by molten steel in cell i

$C_{se,ff,sr,i}$ - fraction of hexcan wall crust area covered by molten steel in cell i

To each of these coefficients is attributed a specific value in the routine LEGEOM, depending on the flow regime and the initial conditions. Most of these values are self-explanatory and can be understood by looking a Fig. 16.4-1, which illustrates the material configuration in each LEVITATE flow regime. Some additional comments are required for the partial annual fuel flow regime. To fully describe this flow regime, the following assumptions were made:

1. The molten fuel film maintains a constant ratio $l_{fu,i}/L_{fu,i}$ both for the clad and the hexcan wall. This ratio is defined by:

$$1_{fu,i} / L_{fu,i} = \frac{A_{ch,op,i} \cdot CIANLR}{\left(L_{cl,i} + L_{sr,i}\right)^2} \qquad (16.4\text{-}221)$$

   when no fuel crusts are present. It is built into the Eq. 16.4-223 and the user can affect it value only by changing the input constant CIANLR. This assumption leads to a gradual increase of the film-covered perimeter, together with a film thickness increase, whenever the amount of molten fuel increases.

2. The partial annual flow becomes fully annular when the volume fraction of the molten fuel/steel reaches a certain input value, i.e., when

$$\frac{\theta_{fu,i} + \theta_{sc,i}}{\theta_{ch,op,i}} = CIANLR \qquad (16.4\text{-}222)$$

3. The existing fuel crust should be taken into account when calculating the coefficients $C_{fu,cl,i}$ and $C_{fu,sr,i}$.

These assumptions lead to the following definition for the area coefficient $C_{fu,cl,i}$ in the annular fuel flow regime

$$C_{fu,cl,i} = \begin{cases} \dfrac{\theta_{fu,i} + \theta_{sc,i}}{\theta_{ch,op}} + \dfrac{A_{ff,cl,i}}{A_{ch,cl,i}} / CIANLR & \text{(16.4-223a)} \\ 1, \text{if the above expression} > 1 & \text{(16.4-223b)} \end{cases}$$

For nodes where the fuel pins are undisrupted, CIANLR is set equal to the input value CIANIN, currently 0.5. For disrupted nodes, CIANLR is equal CIANDI. A similar formula applies to $C_{fu,sr,i}$.

Another aspect treated in LEGEOM, which will be discussed in this section, is the change in the fuel crust geometry due to additional fuel freezing. It is noted that other aspects such as steel freezing, crust breakup and remelting are treated in the routine LEFREZ and will be discussed in Section 16.5. Also, other aspects related to the chunk geometry are treated in the LETRAN routine and will be introduced in Section 16.4.3.10.

The amounts of fuel/steel which have to be added to the fuel crusts due to freezing are calculated in the LEFREZ routine in the previous time step. In the routine LEGEOM, these amounts are converted to corresponding are changes $\Delta A_{ff,cl,i}$ and $\Delta A_{ff,se,i}$. The decision on how to modify the crust parameters $L_{ff,cli,i}$, $l_{ff,cl,i}$, $L_{ff,sr,i}$ and $l_{ff,sr,i}$ is made in the following way (we will refer to the crust on the cladding only):

> If no previous fuel crest is present and if the local fuel flow regime is partially annular flow, the original crust has the same thickness as the molten fuel film; however, if the local fuel flow regime is bubbly, the original crust is rather thin and the area coefficient $C_{ff,cl,i}$ is obtained as follows:

$$C_{ff,cl,i} = \begin{cases} \sqrt{\dfrac{A_{ff,cl,i}}{A_{ch,cl,i}} / CIBBFZ} & \text{(16.4-224)} \\ 1, \text{ if above expression} > 1 \end{cases}$$

> where CIBBFZ is a constant, which is currently set equal to the input constant CIBBDI. If a previously formed crust is present the thickness of the crust is first increased until it reaches the thickness of he fuel film or the channel characteristic size $l_{cl,i}$, which ever comes first. Then the length of the crust $L_{ff,cl,i}$ is increased until $C_{ff,cl,i} = 1$.

16.4.3.9.3 Description of the Fuel/Steel Chunk Geometry

The chunks modeled in LEVITATE have a cylindrical geometry, as shown in Fig. 16.4-18. They are characterized by the radius R, which is different in each axial cell. The length is related to the radius by the input constant ASRALU, which defines the ratio L/2R and has currently the recommended value 1. Each chunk can contain either fuel, or steel or both. The density of the steel chunks is constant and determined by the input variable RHSESO. The fuel chunks, however, have a variable density, which accounts for the possible porosity of the frozen fuel.

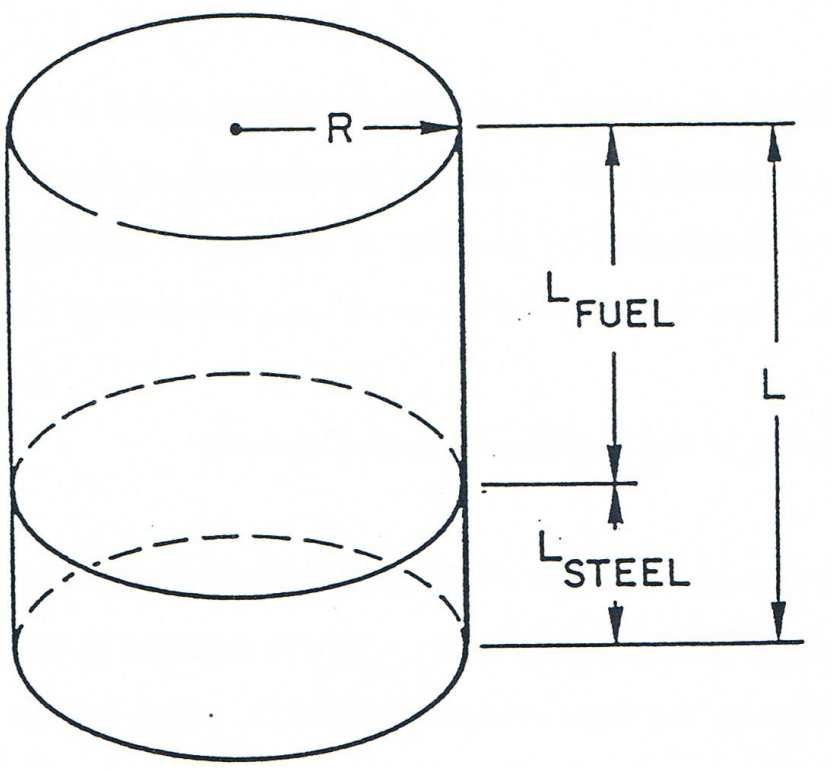

Fig. 16.4-18: Fuel/Steel Chunk Geometry

The original geometry of the chunks depends on their origin. Several mechanisms have been identified which lead to the formation of solid fuel/steel chunks:

A. Disruption of the original fuel pins, which can occur when the cladding is locally molten, leading to the formation of relatively large fuel chunks. In this case the characteristic radius of the chunks is determined from:

$$R_{fu,i}^{NEW} = \sqrt{\Delta R_{pin,i} \cdot \Delta L_{perimeter,\,pin,i}} \qquad (16.4\text{-}224\text{-}1)$$

where

$\Delta R_{pin,i}$ - is the thickness of the solid fuel pin wall which separate the pin cavity from the coolant channel

$\Delta L_{perimeter,pin,i}$ - is the characteristic size of the chunks which is obtained by dividing the pin perimeter by the number of radial cracks present at any axial location. The number of radial crack currently used is 8.

If the input variable RALUDI is zero, the code will use the above formula to determine the radius of the new chunks. However, this calculation can be

overridden by setting RALUDI to a non-zero value. The radius of the newly formed chunks will be set equal to RALUDI.

B. Breakup of the frozen fuel crust that was formed previously on the cladding and hexcan wall. The characteristic radius of these chunks is determined from:

$$R_{\ell u,i}^{NEW} = \sqrt{\Delta A_{ffc,i}} \tag{16.4-224-2}$$

or

$$R_{\ell u,i}^{NEW} = \sqrt{\Delta A_{ffs,i}} \tag{16.4-224-3}$$

where

$\Delta A_{ffc,i}$ - is the cross sectional area of the frozen fuel crust which breaks up during the current time step, in the axial cell i

$\Delta A_{ffs,I}$ - is similar to $\Delta A_{ffc,i}$, but applies to the fuel crust associated with the hexcan wall.

C. Local bulk freezing of the fuel when no solid support for crust formation is present. The characteristic radius of the chunks is obtained from:

$$R_{fu,i}^{NEW} = \sqrt{\Delta A_{fu,i}} \tag{16.4-224-4}$$

where

$\Delta A_{fu,I}$ - is the change in the cross sectional area of the molten fuel component due to removal of frozen fuel.

The volume of all the newly formed chunks in the axial cell *i* is calculated as follows:

$$\Delta V_{\ell u,i} = \left(\frac{\Delta \rho'_{f\ell,i}}{\rho_{fl,i}} + \frac{\Delta \rho'_{s\ell,i}}{\rho_{s\ell,i}} \right) \cdot \Delta z_i \cdot AXMX \tag{16.4-224-5}$$

where

$\Delta \rho'_{fl,i}$ - is the generalized density of the fuel component in the newly formed chunks

$\Delta \rho'_{sl,i}$ - is the generalized density of the fuel component in the newly formed chunks

The number of new chunks is obtained by dividing the total volume $\Delta V_{\ell u,i}$ by the volume of a single chunk:

$$\Delta N_{fu,i} = \frac{\Delta V_{fu,i} \cdot ASRALU}{2 \cdot \pi \cdot \left(R_{lu,i}^{NEW}\right)^3} \qquad (16.4\text{-}224\text{-}6)$$

The new chunks will generally have different characteristics from the chunks already present in a cell. Because only one type of chunks can exist in one cell, the two categories are merged in one chunk population with properties reflecting the characteristics of both original components. This process is outlined below. Note that the same problem can arise in any cell even without the formation of new chunks due to the flux of chunk from neighboring cells. The first step in the merging of the two chunk categories is to define the radius of the resulting chunks.

$$R_{\ell u,i}^{n+1} = \frac{R_{\ell u,i} \cdot \left[N_{\ell u,i} \cdot R_{lu,i}^{ILUMER}\right] + R_{\ell u,i}^{NEW} \cdot \left[\Delta N_{\ell u,i} \cdot \left(R_{\ell u,i}^{NEW}\right)^{ILUMBER}\right]}{N_{\ell u,i} \cdot R_{\ell u,i}^{ILUMER} + \Delta N_{\ell u,i} \cdot \left(R_{\ell u,i}^{NEW}\right)^{ILUMBER}} \qquad (16.4\text{-}224\text{-}7)$$

The new chunk radius is a weighted average of the radii of the two chunk categories. The weights can be selected b the user, by changing the input integer ILUMER, which can have the values 0, 1, 2, or 3. For ILUMER=0, the weights are equal to the number of chunks in the two populations. The recommended value is 3, for which the weights are proportional to the total volume. The number of resulting chunks is given by:

$$N_{\ell u,i} = \frac{V_{\ell u,i} + \Delta V_{\ell u,i}}{2\,\pi\left(R_{\ell u,i}^{n+1}\right)^3}\, ASRALU \qquad (16.4\text{-}224\text{-}8)$$

where the radius $R_{\ell,u,i}^{n+1}$ is defined by 16.4-224-7. Finally the fraction of steel in the chunks is given by:

$$FR_{s\ell,\ell u,i}^{n+1} = \frac{L_{STEEL,\ell u,i}}{L_{STEEL,\ell u,i} + L_{FUEL,\ell u,i}} = \frac{\left(\rho'_{s\ell,i} + \Delta\rho'_{s\ell,i}\right) AXMX\ \Delta z_i}{2\,\pi\ ASRALU\ N_{\ell u,i}\ R_{\ell u,i}^{n+1}\ \rho_{s\ell}} \qquad (16.4\text{-}224\text{-}9)$$

The quantities L_{FUEL} and L_{STEEL} are introduced in Fig. 16.4-18.

If the input variable RALUFZ is zero, then the code will use the above formulas to determine the radius of the new chunks formed by crust break-up and/or bulk freezing. However, if RALUFZ is not zero, the radius of the newly formed chunks will be set equal to RALUFZ.

16.4.3.10 Source Terms in the Energy and Momentum Equations

This section completes the description of the channel hydrodynamic model. It presents in detail the formulation of the source terms used in the energy equations, as introduced previously. It also presents some components of the source terms used in the momentum equations. The description of these source terms has been delayed until now for two reasons: first, the geometry elements introduced in section 16.4.3.9 are needed for the definition of the source terms; second, all the elements described below are calculated in the routine LETRAN, and thus it was deemed preferable to describe them separately from the energy and momentum equations which are solved elsewhere.'

16.4.3.10.1 Source Terms in the Energy Equations

In the energy conservation equations, we introduced the source terms in the following form:

(1) For the fuel energy Eq. 16.4-14:

$$\begin{aligned}\sum_k H'_{fu,k,i}\cdot\Delta T_{fu,k,i} = {} & H'_{fu,Na,i}\cdot\Delta T_{fu,Na,i} + H'_{fu,cl,i}\cdot\Delta T_{fu,cl,i} \\ & + H'_{fu,f\ell,i}\cdot\Delta T_{fu,f\ell,i} + H'_{fu,s\ell,i}\cdot\Delta T_{fu,s\ell,i} \\ & + H'_{fu,sr,i}\cdot\Delta T_{fu,sr,i} + H'_{se,fu,i}\cdot\Delta T_{fu,se,i} \\ & + H'_{fu,ffc,i}\cdot\Delta T_{fu,ffc,i} + H'_{fu,ffs,i}\cdot\Delta T_{fu,ffs,i}\end{aligned} \tag{16.4-225}$$

(2) For the steel energy eq. 16.4-26:

$$\begin{aligned}\sum_k H'_{se,k,i}\cdot\Delta T_{se,k,i} = {} & H'_{se,fu,i}\cdot\Delta T_{fu,se,i} + H'_{se,cl,i}\cdot\Delta T_{se,cl,i} \\ & + H'_{se,sr,i}\cdot\Delta T_{se,sr,i} + H'_{se,f\ell,i}\cdot\Delta T_{se,f\ell,i} \\ & + H'_{se,s\ell,i}\cdot\Delta T_{se,s\ell,i} + H'_{se,Na,i}\cdot\Delta T_{se,Na,i} \\ & + H'_{se,ffc,i}\cdot\Delta T_{se,ffc,i} + H'_{se,ffs,i}\cdot\Delta T_{se,ffs,i}\end{aligned} \tag{16.4-226}$$

(3) For the fuel chunk energy

$$\begin{aligned}\sum_k H'_{f\ell,k,i}\cdot\Delta T_{f\ell,k,i} = {} & H'_{fu,f\ell,i}\cdot\Delta T_{f\ell,fu,i} + H'_{se,f\ell,i}\cdot\Delta T_{f\ell,se,i} \\ & + H'_{Na,f\ell,i}\cdot\Delta T_{f\ell,Na,i} + H'_{c\ell,f\ell,i}\cdot\Delta T_{f\ell,cl,i} \\ & + H'_{sr,f\ell,i}\cdot\Delta T_{f\ell,sr,i} + H'_{ffc,f\ell,i}\cdot\Delta T_{f\ell,ffc,i} \\ & + H'_{ffs,f\ell,i}\cdot\Delta T_{f\ell,ffs,i} + H'_{f\ell,s\ell,i}\cdot\Delta T_{f\ell,s\ell,i}\end{aligned} \tag{16.4-227}$$

(4) For the steel chunk energy equation:

$$\sum_k H'_{s\ell,k,i} \cdot \Delta T_{s\ell,k,i} = H'_{fu,s\ell,i} \cdot \Delta T_{s\ell,fu,i} + H'_{se,s\ell,i} \cdot \Delta T_{s\ell,se,i} + H'_{Na,s\ell,i} \cdot \Delta T_{s\ell,Na,i} + H'_{cl,s\ell,i} \cdot \Delta T_{s\ell,cl,i} + H'_{sr,s\ell,i} \cdot \Delta T_{s\ell,sr,i} + H'_{ffc,s\ell,i} \cdot \Delta T_{s\ell,ffc,i} + H'_{ffs,s\ell,i} \cdot \Delta T_{s\ell,ffs,i} + H'_{f\ell,s\ell,i} \cdot \Delta T_{s\ell,f\ell,i} \quad (16.4\text{-}228)$$

(5) For the gas-mixture equation

$$\sum_k H'_{k,Mi,i} \cdot \Delta T_{k,Mi,i} = H'_{Na,c\ell,i} \cdot \Delta T_{cl,Na,i} + H'_{se,Na,i} \cdot \Delta T_{se,Na,i} + H'_{Na,sr,i} \cdot \Delta T_{sr,Na,i} + H'_{fu,Na,i} \cdot \Delta T_{fu,Na,i} + H'_{Na,f\ell,i} \cdot \Delta T_{f\ell,Na,i} + H'_{Na,s\ell,i} \cdot \Delta T_{s\ell,Na,i} + H'_{ffc,Na,i} \cdot \Delta T_{ffc,Na,i} + H'_{ffs,Na,i} \cdot \Delta T_{ffs,Na,i} \quad (16.4\text{-}229)$$

where

$$H'_{j,k,i} = H_{j,k,i} \cdot \frac{A^L_{j,k,i}}{\Delta z_i \cdot AXMX} \quad (16.4\text{-}230)$$

We will now proceed to define all generalized heat-transfer coefficients that appear in Eqs. 16.4-225 through 16.4-230. As shown in Eq. 16.4-230 both $H_{j,k,i}$ and $A_{j,k,i}$ will have to be defined. Special reference will be made to each flow regime, and a short description of the physical model will be included.

16.4.3.10.1.1 Heat-transfer Coefficient between Fuel and Sodium $H'_{fu,Na,i}$

For the annular and bubbly steel flow regimes, there is no contact between the fuel and sodium:

$$H'_{fu,Na,i} = 0 \quad (16.4\text{-}231)$$

For the annular fuel flow regime, the heat-transfer coefficient is defined as follows:

$$H_{fu,Na,i} = \frac{1}{\frac{1}{H_{fu,i}} + \frac{1}{H_{Na,i}}} \quad (16.4\text{-}232)$$

where $H_{fu,i}$ is a convection-type transfer coefficient on the fuel side:

$$H_{fu,i} = \frac{1}{D_{H,fu,i}} \cdot CIA3 \cdot \mu_{fu} \cdot c_{p,fu} \cdot \mathrm{Re}_{fu,i}^{0.8} \tag{16.4-233}$$

and the sodium heat-transfer coefficient in the two-phase region is defined as:

$$H_{Na,i} = \begin{cases} 10^5, & \text{if } \alpha_{Na,i} < 0.5 \\ \left[10^5 \cdot \left(1-\alpha_{na,i}\right) + H_{Na,i}^{Single\ Phase} \cdot \left(\alpha_{Na,i} - 0.5\right)\right] \cdot 2, & \text{if } 0.5 \le \alpha_{Na,i} < 1 \end{cases} \tag{16.4-234}$$

where $H_{Na,i}^{Single,Phase}$ is defined in Eq. 16.4-235.

The convective sodium heat-transfer coefficient in the single-phase region is defined below:

$$H_{Na,i}^{Single,Phase} = \left\{ C1 \cdot \left[D_{H,Mi,i} \cdot \rho_{Mi,i} \cdot \left| u_{Mi,i} - u_{fu,i} \right| \cdot C_{p,Mi,i} \cdot \frac{1}{k_{Mi,i}} \right]^{C2} + C3 \right\} \cdot \frac{k_{Mi,i}}{D_{H,Mi,i}} \quad for\ \alpha_{Na,i} > 1 \tag{16.4-235}$$

The area of contact between sodium and molten fuel is defined as follows:

$$A_{fu,Na,i}^{L} = A_{cl,i}^{L} \cdot \left[\left(C_{fu,cl,i} - C_{ff,cli,i} \right) + C_{ff,cl,i} \cdot C_{fu,ff,cl,i} \right] + A_{sr,i}^{L} \cdot \left[\left(C_{fu,sr,i} - C_{ff,sr,i} \right) + C_{ff,sr,i} \cdot C_{fu,ff,sr,i} \right] \tag{16.4-236}$$

For the bubbly fuel flow regime, the heat-transfer between sodium and fuel is described as taking place between a continuous fuel component and spherical sodium bubbles. The number of sodium bubbles (and thus their radius) varies from one bubble at the transition boundary between annular and bubbly flow to a maximum number determined by a maximum number determined by a minimum radius of the bubble:

$$R_{\min,bubble,i} = 0.05\ R_{\max,bubble,i} \tag{16.4-237}$$

$$R_{\max,bubble,i} = \begin{cases} R_1 = \left(\frac{3 \cdot V_{Na,i}}{4 \cdot \pi} \right)^{1/3} & \text{if } R_1 < D_{H,Mi,i} \cdot 0.5 \\ D_{H,Mi,i} \cdot 0.5 & \text{if } R_1 \ge D_{H,Mi,i} \cdot 0.5 \end{cases} \tag{16.4-238}$$

The actual radius of the bubbles is obtained by assuming an exponential variation between R_{max} and R_{min}, dependent on how far from the flow regime transition we are in the cell i:

$$R_{bubble,i} = R_{\min,bubble,i} + \left(R_{\max,bubble,i} - R_{\min,bubble,i}\right) \cdot \exp\left[\frac{-\left(\theta_{Mi,bubbly} - \theta_{Mi,i}\right)}{\theta_{Mi,i}}\right] \quad (16.4\text{-}239)$$

where $\theta_{Mi,bubbly}$ is the mixture volume fraction required for the transition from the annular to bubbly flow.

The number of bubbles is defined by:

$$N_{bubble,i} = \frac{3 \cdot V_{Na,i}}{4 \cdot \pi \cdot R^3_{bubbles,i}} \quad (16.4\text{-}240)$$

and the heat-transfer area becomes:

$$A^L_{fu,Na,i} = N_{bubble,i} \cdot 4\pi \cdot R^2_{bubble,i} \quad (16.4\text{-}241)$$

The heat-transfer coefficient is determined by the heat-transfer resistance on the fuel side and the resistance of the bubble:

$$H_{fu,Na,i} = \frac{1}{\frac{1}{H_{fu,i}} + \frac{1}{H_{Na,i}}} \quad (16.4\text{-}242)$$

where $H_{fu,i} = 3 \cdot 10^4$ J/m2 · s · K and wad determined by analyzing the transient solution describing the propagation of a step change in temperature in a semi-infinite medium. For a typical LEVITATE time step Δt and a temperature change ΔT, $H_{fu,i}$ was determined from:

$$H_{fu,i} = \frac{1}{\Delta T \cdot \Delta t} \int_0^{\Delta t} Q(x=0)\, dt \quad (16.4\text{-}243)$$

Where Q(x=0) is the heat flux at the boundary of the semi-infinite medium, in J/m^2 · s.

The heat-transfer coefficient in the bubble, $H_{Na,i}$ is defined by Eq. 16.4-234 for the two-phase sodium region. For single-phase sodium:

$$H_{Na,i} = \frac{k_{Mi,i}}{R_{bubble,i}} \quad \text{if } \alpha_{Na,i} = 1 \quad (16.4\text{-}244)$$

16.4.3.10.1.2 Heat-transfer Coefficient between Fuel and Cladding or Structure $H'_{fu,cl,i}$ and $H'_{fu,sr,i}$

For the annular and bubbly steel flow regimes the fuel is in contact with neither the cladding nor the structure.

$$H'_{fu,cl,i} = H'_{fu,sr,i} = 0 \tag{16.4-245}$$

For the annular fuel flow regime, the heat-transfer coefficient from fuel to cladding and structure is defined as:

$$H_{fu,cl,i} = H_{fu,sr,i} = \frac{1}{D_{H,fu,i}} \cdot CIA3 \cdot \mu_{fu,i} \cdot C_{p,fu} \cdot \mathrm{Re}_{fu,i}^{0.8} \tag{16.4-246}$$

and the respective heat-transfer areas are:

$$\begin{aligned} A^L_{fu,cl,i} &= A^L_{cl,i} \cdot \left(C_{fu,cl,i} - C_{ff,cl,i}\right) \\ A^L_{fu,sr,i} &= A^L_{sr,i} \cdot \left(C_{fu,sr,i} - C_{ff,sr,i}\right) \end{aligned} \tag{16.4-247}$$

For the bubbly fuel flow regime, the heat-transfer coefficients are defined as follows:

$$H_{fu,cl,i} = H_{fu,sr,i} = \frac{1}{D_{H,fu,i}} \cdot CIA3 \cdot \mu_{fu} \cdot C_{p,fu} \cdot \mathrm{Re}_{fu,i}^{0.8} + \frac{4 \cdot k_{fu}}{D_{H,fu,i}} \tag{16.4-248}$$

and the respective heat-transfer areas are:

$$A^L_{fu,cl,i} = A^L_{cl,i} \; ; A^L_{fu,sr,i} = A^L_{sr,i} \tag{16.4-249}$$

16.4.3.10.1.3 Heat Transfer between Fuel and Frozen Fuel Crusts on Cladding and Structure $H'_{fu,ffc,i}$ and $H'_{fu,ffs,i}$

These coefficients are zero in the annular and bubbly steel flow regimes.

$$H'_{fu,ffc,i} = H'_{fu,ffs,i} = 0 \tag{16.4-250}$$

For the annual fuel flow regime, the heat-transfer coefficients are defined as:

$$H_{fu,ffc,i} = \frac{1}{\frac{1}{H_{fu,i}} + \frac{0.5 \cdot 1_{ff,cl,i}}{k_{fu}}} \tag{16.4-251}$$

$$H_{fu,ffs,i} = \frac{1}{\frac{1}{H_{fu,i}} + \frac{0.5 \cdot 1_{ff,sr,i}}{k_{fu}}} \tag{16.4-252}$$

where $H_{fu,i}$ is given by Eq. 16.4-246 and $l_{ff,cl,i}$ and $l_{ff,sr,i}$ have been defined in Section 16.4.3.9, which describes the local geometry. The respective heat-transfer areas are:

$$A_{fu,ffc,i} = A^L_{cl,i} \cdot C_{ff,cl,i} \cdot C_{fu,ff,cl,i} \tag{16.4-253}$$

and

$$A_{fu,ffs,i} = A^L_{sr,i} \cdot C_{ff,sr,i} \cdot C_{fu,ff,sr,i} \tag{16.4-254}$$

For the bubbly fuel flow regime, the heat-transfer coefficients are given by Eqs. 16.4-251 and 16.4-252, but $H_{fu,i}$ in these is given by Eq. 16.4-248 rather than Eq. 16.4-246. The heat-transfer areas are given by:

$$A_{fu,ffc,i} = A^L_{cl,i} \cdot C_{ff,cl,i} \tag{16.4-255}$$

$$A_{fu,ffs,i} = A^L_{sr,i} \cdot C_{ff,sr,i} \tag{16.4-256}$$

16.4.3.10.1.4 Heat-transfer Coefficient between Fuel and Steel $H'_{se,fu,i}$

In the annular and bubbly steel flow regimes, the fuel exists in the form of droplets imbedded in the continuous molten steel. The radius of the fuel droplets varies between $R_{fu,droplet,min,i} = 1 \cdot 10^{-4}$ m and $R_{fu,droplet,max,i} = 1_{fu,cl,i}$. The actual radius is calculated as follows:

If $1 \geq \theta_{fu,i}/\theta_{se,i} \geq 0.5$

$$R_{fu,droplet,i} = \left[R_{fu,droplet,min,i} \cdot \left(1 - \frac{\theta_{fu,i}}{\theta_{se,i}} \right) + R_{fu,droplet,max,i} \cdot \left(\frac{\theta_{fu,i}}{\theta_{se,i}} - 0.5 \right) \right] \cdot 2 \tag{16.4-257a}$$

If $\theta_{fu,i}/\theta_{se,i} < 0.5$, then

$$R_{fu,droplet,i} = R_{fu,droplet,\min,i} \tag{16.4-257b}$$

The number of fuel droplets and heat-transfer area are calculated from:

$$N_{fu,droplets,i} = \frac{3\,V_{fu,i}}{4\,\pi \cdot R^3_{fu,droplet,i}} \tag{16.4-258}$$

and

$$A^L_{se,fu,i} = N_{fu,droplets,i} \cdot 4\,\pi \cdot R^3_{fu,droplet,i} \tag{16.4-259}$$

The heat-transfer coefficient is obtained as follows:

$$H_{se,fu,i} = \frac{1}{\frac{R_{fu,droplet,i}}{k_{fu}} + \frac{1}{H_{se,i}}} \tag{16.4-260}$$

where $H_{se,i} = 4 \cdot 10^4$ and is obtained in a manner similar to Eq. 16.4-243.

For the annual and bubbly fuel flow regimes, the situation is reversed, and the steel exists in the form of droplets imbedded in the continuous molten fuel. The radius of the steel droplet is defined as follows:

For $\theta_{se,i}/\theta_{fu,i} > 0.5$

$$R_{se,droplet,i} = \left[R_{se,droplet,\min,i} \cdot \left(1 - \frac{\theta_{se,i}}{\theta_{fu,i}} \right) + R_{se,droplet,\max,i} \cdot \left(\frac{\theta_{se,i}}{\theta_{fu,i}} - 0.5 \right) \right] \cdot 2 \tag{16.4-261a}$$

For $\theta_{se,i}/\theta_{fu,i} \leq 0.5$

$$R_{se,droplet,i} = R_{se,droplet,min,i} \tag{16.4-261b}$$

Note that the definitions 16.4-257 and 16.4-261 lead to a continuous change in $R_{droplet,i}$ across the transition from a fuel to a steel flow regime. The number of steel droplets and the heat-transfer area are obtained from formulas similar to 16.4-258 and 16.4-259. The heat-transfer coefficient is defined by:

$$H_{se,fu,i} = \frac{1}{\frac{R_{se,droplet,i}}{k_{se}} + \frac{1}{H_{fu,i}}} \tag{16.4-262}$$

where $H_{fu,i} = 3 \cdot 10^4$ and has already been explained in Eq. 16.4-243.

16.4.3.10.1.5 Heat-transfer Coefficients between Fuel and Fuel and Steel Chunks $H'_{fu,fl,i}$ and $H'_{fu,sl,i}$

As explained in 16.4.3.9.2, the fuel and steel chunks have a cylindrical geometry and the aspect ratio R/L can be varied via the input. Thus, it is necessary to distinguish between the heat transfer across the surface normal to the flow $A^N_{f\ell,i}$ and that across the surface parallel to the flow direction, $A^L_{f\ell,i}$. Note that the chunks are always assumed to be parallel to the flow direction, and that the total surface of the fuel chunks is given by $A^L_{f\ell,i} + A^N_{f\ell,i}$. Thus, the generalized heat-transfer coefficient between the fuel and the fuel and steel chunks can be written as:

$$H'_{fu,f\ell,i} = H^L_{fu,f\ell,i} \cdot \frac{A^L_{fu,f\ell,i}}{AXMX \cdot \Delta z_i} + H^N_{fu,f\ell,i} \cdot \frac{A^N_{fu,f\ell,i}}{AXMX \cdot \Delta z_i} \tag{16.4-263}$$

$$H'_{fu,s\ell,i} = H^L_{fu,s\ell,i} \cdot \frac{A^L_{fu,s\ell,i}}{AXMX \cdot \Delta z_i} + H^N_{fu,s\ell,i} \cdot \frac{A^N_{fu,s\ell,i}}{AXMX \cdot \Delta z_i} \tag{16.4-264}$$

For the steel flow regimes, both bubbly and annular, no contact is present between the molten fuel and chunks:

$$H'_{fu,f\ell,i} = H'_{fu,s\ell,i} = 0 \tag{16.4-265}$$

For the bubbly fuel flow regime, the heat-transfer coefficients are defined as follows:

$$H^L_{fu,f\ell,i} = \frac{1}{\frac{1}{H_{fu,i}} + \frac{R_{f\ell,i}}{k_{fu}}}; \quad H^N_{fu,f\ell,i} = \frac{1}{\frac{1}{H_{fu,i}} + \frac{L_{f\ell,i}}{2k_{fu}}} \tag{16.4-266}$$

and

$$H^L_{fu,s\ell,i} = \frac{1}{\frac{1}{H_{fu,i}} + \frac{R_{s\ell,i}}{k_{se}}}; \quad H^N_{fu,s\ell,i} = \frac{1}{\frac{1}{H_{fu,i}} + \frac{L_{s\ell,i}}{2k_{se}}} \tag{16.4-267}$$

where $H_{fu,i}$ has been defined in Eq. 16.4-243. The corresponding heat-transfer areas are:

$$A^L_{fu,f\ell,i} = A^L_{f\ell,i}; \; A^N_{fu,f\ell,i} = 0.5 \; A^N_{f\ell,i} \; . \tag{16.4-268}$$

$$A^L_{fu,s\ell,i} = A^L_{s\ell,i}\ ;\ A^N_{fu,s\ell,i} = 0.5\ A^N_{s\ell,i}\ . \tag{16.4-269}$$

For the annular fuel flow regime, the chunks can have velocities quite different from those of the molten fuel, and convective effects must be taken into account. The heat-transfer coefficients are still defined by Eqs. 16.4-266 and 16.4-267, but $H_{fu,i}$ is replaced by $H_{fu,i} + H_{fu,convective,i}$, where $H_{fu,convective,i}$ is defined as:

$$H_{fu,convective,i} = \frac{1}{D_{H,fu,i}} \cdot\ CIA3 \cdot \mu_{fu} \cdot C_{p,fu} \cdot \mathrm{Re}^{0.8}_{fu,i} \tag{16.4-270}$$

where

$$\mathrm{Re}_{\ell u,i} = \rho_{fu} \cdot \left| u_{fu,i} - u_{\ell u,i} \right| \cdot \frac{2R_{\ell u,i}}{\mu_{fu}} \tag{16.4-270-1}$$

The heat-transfer areas for the annular flow are significantly different from those used for the bubbly fuel flow. The normal surface is not in contact with the molten fuel, thus:

$$A^N_{fu,f\ell,i} = A^L_{fu,s\ell,i} = 0 \tag{16.4-271}$$

The lateral heat transfer areas are defined as follows:

$$A^L_{fu,f\ell,i} = A^L_{f\ell,i} \cdot F_{area.bd,\ell u,i} \cdot C_{fu,cl,i} \cdot \frac{A^L_{cl,i}}{A^L_{cl,i} + A^L_{sr,i}} + C_{fu,sr,i} \cdot \frac{A^L_{sr,i}}{A^L_{cl,i} + A^L_{sr,i}} \tag{16.4-272}$$

where $F_{area,bd,\ell u,i}$ is the fraction of the area of the chunks in contact with the channel boundaries. It is obtained by assuming that chunks are uniformly distributed across the channel area and defining the contact area for the chunks near the boundary (currently the contact area is equal to $0.5 \cdot\ A^L_{fl,i}$). $A^L_{fu,s\ell,i}$ is defined similarly to Eq. 16.4-272, but $A^L_{f\ell,i}$ is replaced by $A^L_{s\ell,i}$.

16.4.3.10.1.6 Heat-transfer Coefficients between the Molten Steel and Fuel and Steel Chunks $H'_{se,fl,i}$ and $H'_{se,sl,i}$

For the annular and bubbly fuel flow regimes, these coefficients are zero because the steel and the chunks are not in contact.

For the annular and bubbly steel flow regimes, the considerations made in Section 16.4.3.10.1.5 still apply and the Eqs. 16.4-263 through 16.4-272 can be used, but $H_{fu,i}$ is

replaced by $H_{se,i}$, defined similarly for steel, and $H_{fu,convective,i}$ is replaced by $H_{se,convective,i}$ defined below:

$$H_{se,convective,i} = \frac{1}{D_{H,se,i}} \cdot CIA3 \cdot \mu_{se} \cdot C_{p,se} \cdot \mathrm{Re}_{\ell u,i}^{0.8} \tag{16.4-273}$$

16.4.3.10.1.7 Heat-transfer Coefficients between Molten Steel and Cladding and Structure $H'_{se,cl,i}$ and $H'_{se,sr,i}$

The coefficients are zero for the fuel flow regimes, both annular and bubbly:

$$H'_{se,cl,i} = H'_{se,sr,i} = 0 \tag{16.4-274}$$

For the annular steel flow regime, heat-transfer coefficients are defined as follows:

$$H_{se,cl,i} = H_{se,sr,i} = \frac{1}{D_{H,se,i}} \cdot CIA3 \cdot \mu_{se} \cdot C_{p,se} \cdot \mathrm{Re}_{se,i}^{0.8} \tag{16.4-275}$$

and the respective areas, $A_{se,c\ell,i}$ and $A_{se,sr,i}$ are identical to Eqs. 16.4-247.

For the bubbly steel regime, the heat-transfer is given by:

$$H_{se,cl,i} = H_{se,sr,i} = \frac{1}{D_{H,se,i}} \cdot CIA3 \cdot \mu_{se} \cdot C_{p,se} \cdot \mathrm{Re}_{se,i}^{0.8} + \frac{4k_{se}}{D_{H,se,i}} \tag{16.4-276}$$

and the heat-transfer areas $A^{L}_{se,cl,i}$ and $A^{L}_{se,sr,i}$ are defined by Eq. 16.4-249.

16.4.3.10.1.8 Heat-transfer Coefficients between Steel and the Frozen Fuel on Cladding Structure $H'_{se,ffc,i}$ and $H'_{se,ffs,i}$

These coefficients are zero for the fuel annular and bubbly flow regimes:

$$H'_{se,ffc,i} = H'_{se,ffs,i} = 0 \tag{16.4-277}$$

For the steel regimes, the considerations made in Section 16.4.3.10.1.3 for the fuel regimes apply. Thus, Eqs. 16.4-250 through 16.4-256 can be used to define the corresponding heat-transfer coefficients and transfer areas if one replaces $H_{fu,i}$ by $H_{se,i}$, defined as follows:

$$H_{se,i} = \frac{1}{D_{H,se,i}} \cdot CIA3 \cdot \mu_{se} \cdot C_{p,se} \cdot \mathrm{Re}_{se,i}^{0.8} \tag{16.4-278}$$

16.4.3.10.1.9 Heat Transfer between Steel and Sodium/Fission Gas $H'_{se,\mathrm{Na},i}$

The coefficient is zero for the fuel flow regimes:

$$H'_{se,Na,i} = 0 \tag{16.4-279}$$

All considerations made for the fuel flow regimes in Section 16.4.3.10.1.1 apply here and Eqs. 16.4-232 through 16.4-244 should be used, if $h_{fu,i}$ is replaced by $H_{se,i}$, as appropriate. Thus, the heat-transfer coefficient for the annual steel regime becomes from Eq. 16.4-232:

$$H_{se,Na,i} = \frac{1}{\frac{1}{H_{se,i}} + \frac{1}{H_{Na,i}}} \tag{16.4-280}$$

where $H_{se,i}$ is defined by Eq. 16.4-278. The same formula applies for the bubbly steel regime from Eq. 16.4-242, but $H_{se,i}$ is defined in a manner similar to Eq. 16.4-243.

16.4.3.10.1.10 Heat-transfer Coefficients between Fuel Steel Chunks and Cladding and Structure $H'_{cl,f\ell,i}$, $H'_{cl,s\ell,i}$, $H'_{sr,f\ell,i}$, $H'_{sr,s\ell,i}$

The chunks can be in contact with the cladding and structure only in the partial annular fuel flow regime (this is also the default when neither fuel not steel is present in the channel). For all other regimes, the above coefficients are equal to zero.

For the partial annular fuel flow regime, the heat-transfer coefficients are defined below:

$$H_{cl,f\ell,i} = H_{sr,f\ell,i} = \frac{k_{fu}}{R_{\ell u,i}} \tag{16.4-281}$$

$$H_{cl,s\ell,i} = H_{sr,s\ell,i} = \frac{k_{se}}{R_{\ell u,i}} \tag{16.4-282}$$

The definition of the heat-transfer areas accounts for the fact that only the chunks close to the boundaries not covered by molten fuel exchange energy directly with the cladding and structure.

$$A_{cl,f\ell,i} = A^L_{f\ell,i} \cdot F_{area,bd,\ell u,i} \cdot \frac{A^L_{c\ell,i}}{A^L_{cl,i} + A^L_{sr,i}} \cdot \left(1 - C_{fu,cl,i}\right) \tag{16.4-283}$$

$$A_{sr,f\ell,i} = A^L_{f\ell,i} \cdot F_{area,bd,\ell u,i} \cdot \frac{A^L_{sr,i}}{A^L_{cl,i} + A^L_{sr,i}} \cdot \left(1 - C_{fu,sr,i}\right) \tag{16.4-284}$$

$$A_{cl,s\ell,i} = A^L_{s\ell,i} \cdot F_{area,bd,\ell u,i} \cdot \frac{A^L_{c\ell,i}}{A^L_{cl,i} + A^L_{sr,i}} \cdot \left(1 - C_{fu,cl,i}\right) \tag{16.4-285}$$

$$A_{sr,s\ell,i} = A^L_{s\ell,i} \cdot F_{area,bd,\ell u,i} \cdot \frac{A_{sr,i}}{A^L_{cl,i} + A^L_{sr,i}} \cdot \left(1 - C_{fu,sr,i}\right) \tag{16.4-286}$$

16.4.3.10.1.11 Heat-transfer between Sodium/Fission Gas Mixture and the Fuel/Steel Chunks $H'_{Na,f\ell,i}$ $H'_{Na,s\ell,i}$

These coefficients are zero in the bubbly flow regimes when there is no contact between sodium and chunks.

$$H'_{Na,f\ell,i} = H'_{Na,s\ell,i} = 0 \tag{16.4-287}$$

For the annular fuel and steel regimes the generalized coefficients are defined as follows:

$$H'_{Na,f\ell,i} = H^L_{Na,f\ell,i} \cdot \frac{A^L_{Na,f\ell,i}}{\Delta z_i \cdot AXMX} + H^N_{Na,f\ell,i} \cdot \frac{A^N_{Na,f\ell,i}}{\Delta z_i \cdot AXMX} \tag{16.4-288}$$

$$H'_{Na,s\ell,i} = H^L_{Na,s\ell,i} \cdot \frac{A^L_{Na,s\ell,i}}{\Delta z_i \cdot AXMX} + H^N_{Na,s\ell,i} \cdot \frac{A^N_{Na,s\ell,i}}{\Delta z_i \cdot AXMX} \tag{16.4-289}$$

The heat-transfer coefficients in Eqs. 16.4-288 and 16.4-289 are defined below:

$$H^L_{Na,f\ell,i} = \frac{1}{\frac{1}{H_{Na,i}} + \frac{R_{\ell u,i}}{k_{fu}}}; \quad H^N_{Na,f\ell,i} = \frac{1}{\frac{1}{H_{Na,i}} + \frac{L_{f\ell,i}}{2k_{fu}}}; \tag{16.4-290}$$

$$H^L_{Na,s\ell,i} = \frac{1}{\frac{1}{H_{Na,i}} + \frac{R_{\ell u,i}}{k_{se}}}; \quad H^N_{Na,s\ell,i} = \frac{1}{\frac{1}{H_{Na,i}} + \frac{L_{s\ell,i}}{2k_{se}}}; \tag{16.4-291}$$

The respective heat-transfer areas are defined as follow:

$$A^L_{Na,f\ell,i} = A^L_{f\ell,i} \cdot \left(1 - F_{area,bd,\ell u,i}\right); \; A^N_{Na,f\ell,i} = 0.5 \cdot A^N_{f\ell,i} \tag{16.4-292}$$

$$A^L_{Na,s\ell,i} = A^L_{s\ell,i} \cdot \left(1 - F_{area,bd,\ell u,i}\right);\ A^N_{Na,s\ell,i} = 0.5 \cdot A^N_{s\ell,i} \tag{16.4-293}$$

16.4.3.10.1.12 Heat-transfer between the Fuel and Steel Solid Chunks $H'_{fl,sl,i}$

This coefficient is different from zero only when both fuel and steel chunks are present in a cell. Given the geometry of the chunks presented in Section 16.4.3.9, the heat-transfer coefficient is defined by:

$$H_{f\ell,s\ell,i} = \frac{1}{\frac{L_{f\ell,i}}{2k_{fu}} + \frac{L_{s\ell,i}}{2k_{se}}} \tag{16.4-294}$$

and the heat-transfer area by:

$$A_{f\ell,s\ell,i} = 0.5 \cdot A^N_{f\ell,i} \tag{16.4-295}$$

16.4.3.10.1.13 Heat Transfer between Fuel/Steel Chunks and the Frozen Fuel on Cladding and Structure, $H'_{f\ell,ffc,i}\ H'_{f\ell,ffs,i}$, $H'_{s\ell,ffc,i}\ H'_{s\ell,ffs,i}$

These coefficients are non-zero only if there is little molten fuel and/or steel present, i.e.:

$$\frac{\theta_{fu,i} + \theta_{se,i}}{\theta_{ch,op,i} - \theta_{\ell u,i}} \le 0.1 \tag{16.4-296}$$

and the frozen fuel crust covers a significant fraction of the channel perimeter, i.e.:

$$C_{ff,cl,i} \ge 0.1 \text{ or } C_{ff,sr,i} \ge 0.1 \tag{16.4-297}$$

If the above conditions are satisfied, the heat-transfer coefficients are defined as follows:

$$H_{f\ell,ffc,i} = \frac{1}{\frac{l_{ff,cl,i}}{2k_{fu}} + \frac{R_{\ell u,i}}{k_{fu}}};\ H_{s\ell,ffc,i} = \frac{1}{\frac{l_{ff,cl,i}}{2k_{fu}} + \frac{R_{\ell u,i}}{k_{se}}} \tag{16.4-298}$$

$$H_{f\ell,ffs,i} = \frac{1}{\frac{l_{ff,sr,i}}{2k_{fu}} + \frac{R_{\ell u,i}}{k_{fu}}};\ H_{s\ell,ffs,i} = \frac{1}{\frac{l_{ff,sr,i}}{2k_{fu}} + \frac{R_{\ell u,i}}{k_{se}}} \tag{16.4-299}$$

The respective heat-transfer areas are defined below:

$$A_{f\ell,ffc,i} = A^L_{f\ell,i} \cdot F_{area,bd,\ell u,i} \cdot \frac{A^L_{cl,i}}{A^L_{cl,i} + A^L_{sr,i}} \cdot C_{ff,cl,i} \tag{16.4-300}$$

$$A_{f\ell,ffs,i} = A^L_{f\ell,i} \cdot F_{area,bd,\ell u,i} \cdot \frac{A^L_{sr,i}}{A^L_{cl,i} + A^L_{sr,i}} \cdot C_{ff,sr,i} \tag{16.4-301}$$

The areas for the steel chunks, $A_{s\ell,ffc,i}$ and $A_{s\ell,ffs,i}$ can be obtained from the above definitions by replacing $A^L_{f\ell,i}$ with $A^L_{s\ell,i}$.

16.4.3.10.1.14 Heat-transfer Coefficients between Sodium/Fission Gas and Cladding or Structure $H'_{Na,cl,i}$ and $H'_{Na,sr,i}$

These coefficients are non-zero only for the partial annular fuel flow regime. In all other regimes, the sodium/fission gas mixture is not in direct contact with the cladding and structure. The heat-transfer coefficient is calculated as follows:

If $\alpha_{Na,i} \le 0.15$,

$$H_{Na,cl,i} = H_{Na,sr,i} = \left[C1 \cdot \left(D_{H,Mi,i} \cdot \rho_{N1} \cdot \left| u_{Mi,i} + u_{Mi,i+1} \cdot C_{Mo,Mi,i+1} \right| \cdot 0.5 \cdot \frac{C_{p,N1}}{k_{N1}} \right)^{C2} + C3 \right] \cdot \frac{k_{N1}}{D_{H,Mi,i}} \tag{16.4-302}$$

The value of k_{N1} is given by the input constant CDNL. The constants C1, C2 and C3 are the source input constants used in the preboiling model.

If $\alpha_{Na,i} > 0.15$ and

a) $T_{Na,i} \le T_{cl,i}$ (boiling situation)

$$H_{Na,cl,i} = \begin{cases} H_{Na,boiling} = CFNAEV & \text{for } .15 < \alpha < 0.5 \\ \left[H_{Na,boiling} \cdot \left(1-\alpha_{Na,i}\right) + H_{Nv,i} \right. & \\ \qquad \left. \cdot \left(\alpha_{Na,i} - 0.5\right)\right] \cdot 2 & \text{for } 0.5 \le \alpha < 1 \\ H_{NV,i} = \left[C_1 \cdot \left(D_{H,Mi,i} \cdot \rho_{Mi,i} \right.\right. & \\ \cdot \left| u_{Mi,i} \right| \cdot \dfrac{C_{p,Mi}}{k_{Mi}} \Big)^{C2} & \\ \left. + C3 \right] \cdot \dfrac{k_{Mi}}{D_{H,Mi,i}} & \text{for } \alpha = 1 \end{cases} \tag{16.4-303}$$

(a-c)

The value of k_{Mi} is given by the input constant CDVG.

b) $T_{Na,i} > T_{cl,i}$ (condensation situation)

$$H_{Na,cl,i} = \begin{cases} H_{Nv,i} \text{ as defined in Eq. 16.4 - 303c} & \text{for } \alpha_{Na,i} = 1 \\ & \text{and } T_{cl,i} < T_{sat,Na}\left(P_{Na,i}\right) \\ CFNACN \cdot \dfrac{\rho'_{Na}}{\rho'_{Na} + \rho'_{fi}} + H_{Nv} & \text{for } \alpha_{Na,i} = 1 \\ \qquad \cdot \dfrac{\rho'_{fi}}{\rho'_{Na} + \rho'_{fi}} & \text{and } T_{cl,i} \ge T_{sat,Na}\left(P_{Na,i}\right) \\ H_{Na,cond} = CFNACN & \text{for } 0.5 \le \alpha_{Na,i} < 1 \\ \left[H_{Na,cond} \cdot \alpha_{Na,i} + H_{Na,cond} \cdot 10^{-2} \right. & \\ \qquad \left. \cdot \left(0.5 - \alpha_{Na,i}\right)\right] \cdot 2 & \text{for } 0.15 < \alpha < 0.5 \end{cases} \tag{16.4-304}$$

(a-d)

It is noted that the branch 16.4-304b has not been implemented in the initial release version but exists in the chunk version.

For $\alpha_{Na,i} > .15$, the heat-transfer coefficient between sodium and structure is obtained from Eq. 16.4-303 for $T_{Na,i} \le T_{sr,i}$ and from Eq. 16.4-304 for $T_{Na,i} > T_{sr,i}$.

The respective heat-transfer areas are defined as follows:

$$A^L_{Na,cl,i} = A^L_{cl,i} \cdot \left(1 - C_{fu,cl,i}\right) \cdot \left(1 - C_{\ell u,cl,i}\right) \tag{16.4-305}$$

and

$$A^L_{Na,sr,i} = A^L_{sr,i} \cdot \left(1 - C_{fu,sr,i}\right) \cdot \left(1 - C_{\ell u,sr,i}\right) \tag{16.4-306}$$

16.4.3.10.1.15 Heat-transfer coefficients between sodium and Frozen Fuel on Cladding and Structure $H'_{ffc,\mathrm{Na},i}$ and $H'_{ffs,\mathrm{Na},i}$

These coefficients are non-zero only in the partial annual flow regime. For this regime, the heat transfer, coefficients are defined below:

$$H_{ffc,Na,i} = \frac{1}{\frac{1}{H_{Na,i}} + \frac{0.5 \cdot 1_{ff,cl,i}}{k_{fu}}} \tag{16.4-307}$$

$$H_{ffs,Na,i} = \frac{1}{\frac{1}{H_{Na,i}} + \frac{0.5 \cdot 1_{ff,sr,i}}{k_{fu}}} \tag{16.4-308}$$

where $H_{Na,i}$ is defined by Eq. 16.4-234.

The respective heat-transfer areas are defined as follows:

$$A^L_{ffc,Na,i} = A^L_{cl,i} \cdot C_{ff,cl,i} \cdot \left(1 - C_{fu,ff,cl,i}\right) \tag{16.4-309}$$

$$A^L_{ffs,Na,i} = A^L_{sr,i} \cdot C_{ff,sr,i} \cdot \left(1 - C_{fu,ff,sr,i}\right) \tag{16.4-310}$$

16.4.3.10.2 Friction Coefficients Used in the Momentum Equations

In Section 16.4.3.8, which describes the momentum equations, several friction coefficients used in the momentum source terms were left undefined. These coefficients are calculated in the routine LETRAN and are presented in this section.

16.4.3.10.2.1 Friction Factor Between Mixture and Cladding/Structure $f_{Mi,i}$

This factor was referenced in Eq. 16.4-150. It is zero for all flow regimes except the partial annual fuel flow regime. For this flow regime, it is defined as follows:

$$f_{Mi,i} = AFRV \cdot \mathrm{Re}^{BFRV}_{Mi,i} \cdot C_{Mi,bd,i} \tag{16.4-311}$$

where AFRV, BFRV are input constants and $C_{Mi,bd,i}$ is the fraction of the channel boundary (cladding + structure + crust) which is in direct contact with the gas mixture in cell i. It is defined as:

$$C_{Mi,bd,i} = \left[A^L_{cl,i} \cdot \left(1 - C_{mfu,cl,i} - Cf_{ff,cl,i} \cdot C_{fu,ff,cl,i}\right) + A^L_{sr,i} \cdot \left(1 - C_{mfu,sr,i} - C_{ff,sr,i} \cdot C_{fu,ff,sr,i}\right)\right] / \left(A^L_{cl,i} + A^L_{sr,i}\right) \quad (16.4\text{-}312)$$

where

$$C_{mfu,cl,i} = C_{fu,cl,i} - C_{ff,cl,i} \quad (16.4\text{-}313)$$

and

$$C_{mfu,sr,i} = C_{fu,sr,i} - C_{ff,sr,i} \quad (16.4\text{-}314)$$

16.4.3.10.2.2 Friction Factor Between Mixture and Fuel $f_{Mi,fu,i}$ and $f_{Mi,se,i}$

These factors were referenced in Eq. 16.4-152. The factor $f_{Mi,fu,i}$ is used only in the partial annular fuel flow regime and is defined below:

$$f_{Mi,fu,i} = AFRV \cdot \mathrm{Re}^{BFRV}_{Mi,fu,i} \cdot C_{Mi,fu,i} \quad (16.4\text{-}315)$$

$\mathrm{Re}_{Mi,fu,i}$ is defined as:

$$\mathrm{Re}_{Mi,fu,i} = D_{H,Mi,i} \cdot \left|u_{MI,i} - u_{fu,i}\right| \cdot \rho_{Mi,i} \cdot \frac{1}{\mu_{Mi,i}} \quad (16.4\text{-}316)$$

and $C_{Mi,fu,i}$, the fraction of the mixture perimeter in contact with the molten fuel is given by:

$$C_{Mi,fu,i} = \left[A^L_{cl} \cdot \left(C_{mfu,cl,i} + C_{ff,cl,i} \cdot C_{fu,ff,cl,i}\right) + A^L_{sr} \cdot \left(C_{mfu,sr,i} + C_{ff,sr,i} \cdot C_{fu,ff,sr,i}\right)\right] / \left(A^L_{cl,i} + A^L_{sr,i}\right) \quad (16.4\text{-}317)$$

The factor $f_{Mi,se,i}$ is used in the annular steel flow regime and takes into account the possibility of flooding. It is defined as follows:

$$f_{Mi,se,i} = AFRV \cdot \mathrm{Re}^{BRFV}_{Mi,fu,i} \cdot C_{FLOOD,i} \quad (16.4\text{-}318)$$

Where the flooding coefficient depends on the velocity ratio V_{RATIO}:

$$V_{RATIO,i} = \frac{\left(U_{Mi,i} + u_{Mi,i+1} \cdot C_{Mo,Mi,i+1}\right) \cdot 0.5}{u_{FLOOD,i}} \tag{16.4-319}$$

$$u_{FLOOD,i} - 2.3\sqrt{\frac{\rho_{se,i}}{\rho_{Mi,i}} \cdot \frac{2g \cdot 1_{se,ch,i}}{AFRV \cdot \mathrm{Re}_{Mi,fu,i}^{BFRV} \cdot F_{FLOOD}\left(\alpha_{Na,i}\right)}} \tag{16.4-320}$$

$$F_{FLOOD}\left(\alpha_{Na,i}\right) = \begin{cases} 1 + 75 \cdot \left(1 - \alpha_{Na,i}\right) & 0.5 < \alpha \le 1 \\ 38.5 & \alpha \le 0.5 \end{cases} \tag{16.4-321}$$

The value of $C_{FLOOD,i}$ is also dependent on the previous flooding history as shown below:

If $C_{FLODD,i}^{n} \le 1$:

$$C_{FLODD,i}^{n} = \begin{cases} F_{FLOOD}\left(\alpha_{Na,i}\right) & \text{if } V_{RATIO,i} \ge 1.1 \\ C_{FLODD,i}^{n} & \text{otherwise} \end{cases} \tag{16.4-322}$$

If $C_{FLODD,i}^{n} > 1$

$$C_{FLODD,i}^{n+1} = \begin{cases} 1 & \text{if } V_{RATIO} < 0.9 \\ C_{FLODD,i}^{n} & \text{otherwise} \end{cases} \tag{16.4-323}$$

16.4.3.10.2.3 Several Area Coefficients Used in the Momentum Source Terms

The area coefficient $C_{AREA,Mi,fu,i}$ has been introduced in Eq. 16.4-155. It defines the fraction of the lateral area of chunks in contract with the mixture and is zero for the fuel and steel bubbly flow regimes. For the annular flow regimes, it is calculated as follows:

$$C_{AREA,Mi,fu,i} = \left(1 - F_{area,bd,fu,i}\right) \tag{16.4-324}$$

The area coefficients $C_{AREA,se,i}$ and $C_{AREA,fu,i}$ have been introduced in Eqs. 16.4-177 and 16.4-178. They account for the fact that only a fraction of the fuel steel perimeter is in contact with the stationary walls. They are defined below:

For the fuel bubbly flow regime:

$$C_{AREA,fu,i} = 1;\ C_{AREA,se,i} = 0 \tag{16.4-325}$$

For the steel bubbly flow regime:

$$C_{AREA,fu,i} = 0;\ C_{AREA,se,i} = 1 \tag{16.4-326}$$

For the annular steel flow regime:

$$C_{AREA,fu,i} = 0;\ C_{AREA,se,i} = 1 \tag{16.4-327}$$

For the partial annular fuel flow regime:

$$\begin{aligned} C_{AREA,fu,i} = \Big[& A^L_{cl,i} \cdot \left(C_{mfu,cl,i} + C_{ff.cl,i} \cdot C_{fu,ff,cl,i} \right) \\ & + A^L_{sr,i} \cdot \left(C_{mfu,sr,i} + C_{ff.sr,i} \cdot C_{fu,ff,sr,i} \right) \Big] / \left(A^L_{cl,i} + A^L_{sr,i} \right) \end{aligned} \tag{16.4-328}$$

$$C_{AREA,se,i} = 0$$

16.4.3.11 Time Step Determination for the Channel Hydrodynamic Model

This section describes the calculation of the maximum time step for the coolant channel hydrodynamic model. This time step will be used in the determination of the LEVITATE time step as outlined in Section 16.7.3. The maximum channel time step is calculated using the sonic Courant condition for the multicomponent channel flow. Only a fraction of the Courant calculated time is used, to account for inaccuracies in the sonic velocity calculation. Thus:

$$\Delta t_{LE,ch} = 0.4 \cdot \min \left[\Delta z_i / \left(u_{sonic,i} + \left| u_{Mi,i} \right| \right) \right]_{i=IFMIBT,IFMITP} \tag{16.4-329}$$

The minimum in Eq. 16.4-329 is evaluated over all axial cells of the interaction region. The sonic velocity in each cell is calculated using an expression [16-14] for an adiabatic homogeneous two-phase mixture of liquid sodium and fission gas/sodium vapor. The compressibility of liquid fuel is much smaller than that of liquid sodium and thus the fuel is assumed to be incompressible in the calculation of the sonic velocity in the channel. The effect of fuel and steel vapor is not included.

$$\begin{aligned} u^2_{sonic,i} = \gamma_{vg} \cdot \left(P_{fi,i} + P_{Na,i} \right) / \Big\{ & \alpha^2_{vg,i} \left(\rho_{fi} + \rho_{Nv} \right) + \alpha_{vg,i} \cdot \left(1 - \alpha_{vg,i} \right) \\ & \cdot \rho_{N1} + \left[\alpha_{vg,i} \cdot \left(1 - \alpha_{vg,i} \right) \cdot \left(\rho_{fi} + \rho_{Nv} \right) + \left(1 - \alpha_{vg,i} \right)^2 \right. \\ & \left. \cdot \rho_{N1} \right] \cdot \gamma_{vg} \cdot \left(P_{fi} + P_{Na} \right) \cdot CMNL \Big\} \end{aligned} \tag{16.4-330}$$

where:

$$\alpha_{vg,i} = \frac{\theta_{vg,i}}{\theta_{ch,op,i} - \theta_{fu,i} - \theta_{se,i} - \theta_{\ell u,i}} \qquad (16.4\text{-}331)$$

γ_{vg} = ratio of specific heat at constant pressure to that at constant volume for the fission gas/sodium vapor mixture. A value of 1.4 is used in the LEVITATE code

CMNL = compressibility of liquid sodium, an input constant

The fission-gas pressure P_{fi} and the sodium pressure P_{Na} are obtained as explained in Section 16.4.3.5.

16.5 Freezing, Melting and Heat-transfer Processes Related to Stationary Pin Stubs and Hexcan Wall

16.5.1 Physical Models

The models presented in this section describe a series of physical processes related to the stationary pin stubs and the hexcan wall. Except for the heat transfer in the cladding and in the hexcan wall, the processes described lead to geometry changes that affect directly the hydrodynamic model of the coolant channel.

One of the most important phenomena during a LOF accident is the freezing of the initially molten fuel and the formation of the fuel crusts. The molten fuel ejected from the pin cavity is accelerated in the coolant channel by the local pressure gradients and begins to move toward the extremities of the channel. In the process, however, it exchanges heat with the sodium, cladding and structure, all of which have a temperature well below the fuel freezing temperature. Eventually the fuel will begin to freeze, forming stationary fuel crusts on the cladding and/or structure or leading to the formation of solid fuel chunks which continue to move in the channel. Steel freezing can also occur occasionally, particularly at locations where the molten steel is the dominant component and is in contact with cold cladding or structure. The freezing of steel leads, in LEVITATE, to a local increase in the thickness of the cladding and/or structure, rather than to the formation of a distinct steel crust.

The fuel crusts formed at various axial locations can begin to melt if the power level increases, thus releasing the fuel again and allowing it to move in the coolant channel. Another mechanism which could also release the fuel crust is the crust breakup, which can occur when the underlying steel support melts and the crust becomes unstable. The continuous heating of the cladding and hexcan wall leads eventually to steel melting. The molten steel is ablated, becoming part of the moving components in the channel, and the thickness of the cladding and/or structure is reduced, increasing the flow area of the coolant channel.

In a similar manner, the solid fuel and steel chunks generated via the fuel-pin disruption can begin to melt due to the direct heating and heat exchange with other

components. This will result in a transfer of fuel from the chunk field to the molten fuel field in the coolant channel. This transfer of mass is accompanied by a transfer of energy and momentum as well as a change in the geometry of the solid chunks.

16.5.2 Description of the Method of Solution and Logic Flow

The heat-transfer equations in the cladding and structure, which are not directly related to a geometry change, are solved in the LESOEN routine, i.e., while advancing the solution for the hydrodynamic model in the channel. All other processes related to the stationary pin stubs and to the hexcan wall involve a change in the local geometry and the routines describing them are called after completing the solution for both the in-pin and coolant channel hydrodynamic models. All melting/freezing processes modeled here affect the hydrodynamic parameters of the coolant channel. Changes in the local temperatures, velocities, or pressures are performed in each of the routines described below, whenever necessary. The routine LELUME (LEVITATE CHUNK-LU MELTING) calculates the melting and the size changes of the solid fuel/steel chunks at all axial locations. The routine LEFREZ (LEVITATE FREEZING AND MELTING) then models a series of important processes, such as fuel/steel freezing and crust formation, fuel/steel chunk formation, fuel crust remelting and breakup. Next called is the routine LEABLA (LEVITATE ABLATION) which calculates the gradual melting and ablation of the cladding and hexcan wall. The routine LEDISR (LEVITATE DISRUPTION) performs the disruption of the fuel pin, whenever a disrupt node is predicted. The disruption, which can occur in one or more nodes in any time step, leads to changes in geometry, mass, energy and pressure for various components present in the respective cell. Finally, the routine LESRME (LEVITATE STRUCTURE MELTING) calculates the rupture of the hexcan wall due to melting and/or pressure burst effects.

16.5.3 Fuel/steel Freezing and Crust Formation

The calculation of fuel/steel freezing is performed in the routine LEFREZ. The fuel flow regimes lead to a situation very different from the steel flow regimes in terms of freezing and are treated separately.

16.5.3.1 The Freezing Process when a Fuel Flow Regime is Present

In this case, the molten steel component exists in the form of droplets imbedded in the molten fuel and has a temperature well above freezing. Thus, only the freezing of the molten fuel must be considered. The freezing calculation decides what amount of fuel, if any, will freeze in each node during the current time step. It also has to decide where the frozen fuel will go, when leaving the moving molten-fuel field. Three possibilities exist:

1. The freezing fuel will form (or add to) a crust on the cladding; (when the cladding has been completely ablated, the fuel can freeze on the bare fuel pins).
2. The freezing fuel will form (or add to) a crust on the hexcan wall (Fig. 16.5-1a).

3. The freezing fuel will generate solid fuel chunks, which will be added to the chunk field

The freezing calculation begins by examining the enthalpy of the molten fuel:

1. If $h_{fu,i} > h_{fu,freeze}$, no fuel freezing occurs. The enthalpy $h_{fu,freeze}$ is an input parameter, i.e., $h_{fu,freeze}$ = EGBBLY. It has to satisfy the conditions:
$$h_{fu,so} < h_{fu,freeze} < h_{fu,liq} \tag{16.5-1}$$
2. If $h_{fu,i} < h_{fu,so}$, rapid fuel freezing occurs, leading to the formation of solid fuel chunks only. In order to avoid numerical problems, only one tenth of the fuel mass ($0.1 \cdot \rho_{fu,i} \cdot A_{fu,i} \cdot \Delta z_i$) in the cell is allowed to freeze in each time step under these circumstances.
3. If $h_{fu,so} < h_{fu,i} < h_{fu,freeze}$, only partial fuel freezing is allowed to occur. The amount of freezing fuel is determined as follows:
$$\Delta\rho'_{fu,i} = \rho'_{fu,i} \cdot \frac{h_{fu,\text{freeze}} - h_{fu,i}}{h_{fu,\text{freeze}} - h_{fu,so}} \tag{16.5-2}$$

The area occupied by this newly frozen fuel is:

$$\Delta A_{fu,i} = \frac{\Delta\rho'_{fu,i}}{\rho_{fu,so}} \cdot AXMX \tag{16.5-3}$$

The assumption is made that the fuel looses most of he energy at the channel boundaries, i.e., by exchanging heat with the cladding and hexcan wall. Thus, the frozen fuel is first used to form a fuel crust on the solid boundaries. The distribution of $\Delta\rho'_{fu,i}$ between the clad and hexcan wall is made as follow:

$$\Delta\rho'_{fu,cl,i} = \Delta\rho'_{fu,i} \cdot \frac{WTCL}{WTCL + WTSR} \tag{16.5-4}$$

$$\Delta\rho'_{fu,sr,i} = \Delta\rho'_{fu,i} \cdot \frac{WTSR}{WTCL + WTSR} \tag{16.5-5}$$

where the weights WTCL and WTSR are:

$$WTCL = A^L_{cl,i} \cdot \left[\left(T_{fu,i} - T_{cl,i}\right) \cdot C_{mfu,cl,i} + \left(T_{fu,i} - T_{ffc,i}\right) \cdot C_{ff,cl,i} \right] \tag{16.5-6}$$

$$WTSR = A^L_{sr,i} \cdot \left[\left(T_{fu,i} - T_{sr,i}\right) \cdot C_{mfu,sr,i} + \left(T_{fu,i} - T_{ffs,i}\right) \cdot C_{ff,sr,i} \right] \tag{16.5-7}$$

Occasionally, one or both of these weights can be set to zero. This happens for WTCL when the cladding surface is molten and thus no solid support for freezing exists or when the pins are totally disrupted in the cell considered. In these cases, WTCL = 0.

Similarly, WTSR = 0 whenever the hexcan wall surface is molten and no crust formation can occur. In this case, we will still use Eqs. 16.5-4 and 16.5-5 to calculate the distribution of the frozen fuel between cladding and hexcan wall. The situation can arise, however, where the amount of frozen fuel is too large for the available freezing area. For example, let us assume that the cladding surface is molten and WTCL = 0. In this case, we can have:

$$\Delta A_{fu,i} > A_{ch,op,sr} \tag{16.5-8}$$

where

$$A_{ch,op,sr} = A_{ch,sr} - A_{ff,sr} \tag{16.5-9}$$

$$A_{ff,sr} = L_{ff,sr} \cdot l_{ff,sr} \tag{16.5-10}$$

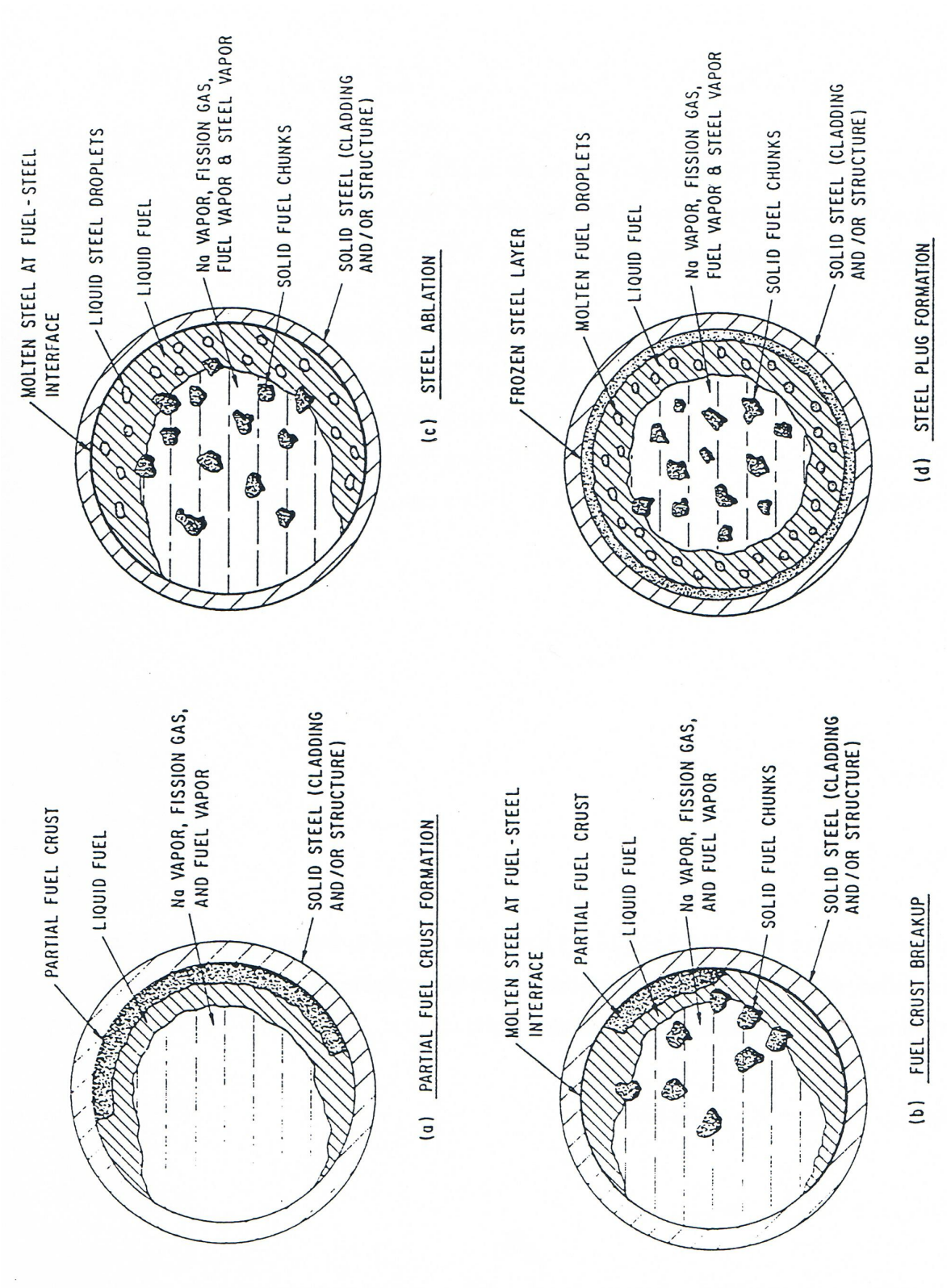

Fig. 16.5-1: Freezing, Melting and Crust Breakup Processes

and the elements used in Eqs. 16.5-7 and 16.5-8 have been defined in Section 16.4.3.9. If Eq. 16.5-6 is satisfied, only an amount of fuel consistent with the available area is allowed to freeze on the structure, while the remaining fuel generates solid chunks:

$$\Delta\rho'_{fu,sr,i} = \rho_{fu,so} \cdot A_{ch,op,sr} / AXMX \tag{16.5-11}$$

$$\Delta\rho'_{fu,lu,i} = \Delta\rho'_{fu,i} - \Delta\rho'_{fu,sr,i} \tag{16.5-12}$$

When both WTCL = 0 and WSTR = 0 all the freezing fuel is used to generate solid fuel chunks:

$$\Delta\rho'_{fu,\ell u,i} = \Delta\rho'_{fu,i} \tag{16.5-13}$$

Another decision that has to be made in connection with the fuel freezing is the steel entrapment in the frozen fuel. Based on experimental evidence obtained in the posttest examination of several fuel motion tests, it appears that only small steel droplets are trapped in the frozen fuel. LEVITATE assumes that small droplets exist only when small amounts of steel are locally present. Otherwise, the steel exists in large droplets that will tend to separate from the freezing fuel. Thus, if:

$$\frac{\theta_{se,i}}{\theta_{fu,i}} > 0.1 \tag{16.5-14}$$

no steel entrapment occurs. Otherwise, the amount of steel trapped in the frozen fuel is calculated from:

$$\Delta\rho'_{se,i} = \rho'_{se,i} \cdot \frac{\Delta\rho'_{fu,i}}{\rho'_{fu,i}} \tag{16.5-15}$$

The actual geometry of the fuel crust (i.e. thickness and area coefficient) is not changed in LEFREZ when fuel freezing occurs. The geometry is changed in LEGEOM at the beginning of the next time step. The geometry of the chunks is changed in LEFREZ due to the condition of the new chunks. The radius of the resulting chunks is a mass-weighted average of the chunks being combined. A more detailed discussion about the chunk geometry can be found in Section 16.4.3.9.

16.5.3.2 The Freezing Process when a Steel Flow Regime is Present

In a steel flow regime, both steel freezing and fuel freezing can occur. The molten fuel is in the form of droplets imbedded in the molten steel and can freeze as it approaches the steel temperature. The amount of fuel freezing in cell i, $\Delta\rho'_{fu,i}$ is calculated using the same procedure outline in Section 16.5.1.1. However, because no direct contact between the freezing fuel and the channel boundaries exists, crust formation cannot occur. All freezing fuel is used to generate solid fuel chunks:

$$\Delta\rho'_{fu,\ell u,i} = \Delta\rho'_{fu,i} \tag{16.5-16}$$

The steel-freezing calculation follows the same lines as the fuel calculation, but is keyed to the steel temperature rather than enthalpy:

1. If $T_{se,i} > T_{se,freeze}$, no steel freezing occurs. The temperature $T_{se,freeze}$ is determined using the input parameter FRMRSE:
$$T_{se,freeze} = T_{se,so} + \left(T_{se,\ell q} - T_{se,so}\right) \cdot FRMRSE \tag{16.5-17}$$
2. If $T_{se,i} < T_{se,so}$, rapid steel freezing occurs, leading to the formation of steel chunks only.
3. If $T_{se,so} < T_{se,i} < T_{se,freeze}$, only partial steel freezing is allowed to occur. The amount of freezing steel is calculated from:
$$\Delta\rho'_{se,i} = \rho'_{se,i} \cdot \frac{T_{se,freeze} - T_{se,i}}{T_{se,freeze} - T_{se,so}} \tag{16.5-18}$$

The steel can freeze on the cladding and/or on the hexcan wall, leading to an increase in the thickness of these structures. This increase is uniformly distributed along the perimeter, as opposed to the partial crust formed initially in the fuel flow regimes (Fig. 16.5-1d). The distribution of $\Delta\rho'_{sei}$, follows the same procedure presented in Section 16.5.3 for fuel. If not all the freezing steel can be distributed between cladding and structure (e.g., in a cell where the pins have been disrupted and/or the hexcan wall surface is molten), part or all of the freezing steel is used to generate solid steel chunks, as appropriate.

16.5.4 Fuel Crust Breakup and Remelting

The fuel crust formation on the cladding and the fuel crust formed on the hexcan wall are completely independent. Either one can be present in any axial cell, having its own temperature and geometry. The formation of the crusts was explained in Section 16.5.3. Once present, the fuel crust can disappear in two ways: via breakup and via remelting. These processes can occur in any flow regime modeled by LEVITATE.

16.5.4.1 Fuel Crust Breakup

It is assumed that the frozen fuel crust is unstable and is allowed to break up whenever there is no underlying solid support. In general, this means that the underlying steel is molten. However, when fuel crusts are present on bare fuel pins, the underlying support is also fuel. Thus, the breakup of the crust on the clad will occur when:

$$T_{cl,os} > T_{se,\ell q} \tag{16.5-19}$$

In this case, a gradual but fairly rapid breakup occurs. The crust is reduced each time step by:

$$\Delta\rho'_{ffc} = \rho'_{ffc} \cdot CIBREK \tag{16.5-20}$$

where CIBREK = 0.01 is a built-in constant, defined in the routine LEFREZ. Both the thickness $1_{ff,cl,i}$ and the length (i.e., the area coefficient $C_{ff,c\ell,i}$) are reduced proportionately:

$$1_{ff,cl,i} = 1_{ff,cl,i} \cdot \sqrt{1 - CIBREK} \tag{16.5-21}$$

$$C_{ff,cl,i} = C_{ff,cl,i} \cdot \sqrt{1 - CIBREK} \tag{16.5-22}$$

The fuel breaking loose from the crust generates chunks, which are then merged if necessary with the chunks already present in the cell. If steel inclusions are present in the crust, they are also reduced proportionately and added to the steel chunk field. A similar procedure is used for the structure crust breakup. The process is illustrated in Fig. 16.5-1b.

16.5.4.2 Remelting of the Fuel Crust

If the fuel crusts are present in a cell and breakup does not occur, the crust can still disappear via remelting. Melting of the cladding crust occurs if:

$$T_{ffc,i} > T_{fu,\text{melt}} \tag{16.5-23}$$

where

$$T_{fu,\text{melt}} = \left(T_{fu,so} + T_{fu,\ell q}\right) \cdot 0.5 \tag{16.5-24}$$

The amount of fuel crust melting in one time step is given by:

$$\Delta\rho'_{ffc,i} = \rho'_{ffc,i} \cdot \frac{T_{ffc,i} - T_{fu,melt}}{T_{fu,\ell q} - T_{fu,melt}} \tag{16.5-25}$$

If steel inclusions are present, they are reduced in the same proportion. The resulting molten fuel and steel are added to the molten fuel and steel fields in the channel, respectively.

A similar procedure is used for the remelting of the fuel crust on the hexcan wall.

16.5.5 Cladding and Hexcan Ablation

When the coolant channel contains molten fuel, which is in an annular or bubbly flow regime, the temperature at the cladding surface rises rapidly, leading to steel melting and ablation. These processes are modeled in the routine LEABLA. The melting occurs only at the surface, while the bulk of the cladding can remain below the melting

point. To model this situation, the cladding is divided into two radial cells, with a thick inner cell and a thin cell at the outer surface (Fig. 16.5-2). The thin cladding cell at the outer surface has a small thermal capacity and is thus quite sensitive to variations in the magnitude of the boundary heat fluxes. This cell is of key importance in the melting and ablation process. Ablation of the cladding can occur only if no fuel crust is present on cladding and:

$$T_{cl,os,i} > T_{se,\text{ablation}} \tag{16.5-26}$$

where

$$T_{se,\text{ablation}} = \left(T_{se,so} + T_{se,\ell q}\right) \cdot 0.5 \tag{16.5-27}$$

The fraction of the outer cell mass which is ablated is given by:

$$F_{\text{ablation},i} = \frac{T_{cl,os,i} - T_{se,\text{ablation}}}{T_{se,\ell q} - T_{se,\text{ablation}}} \tag{16.5-28}$$

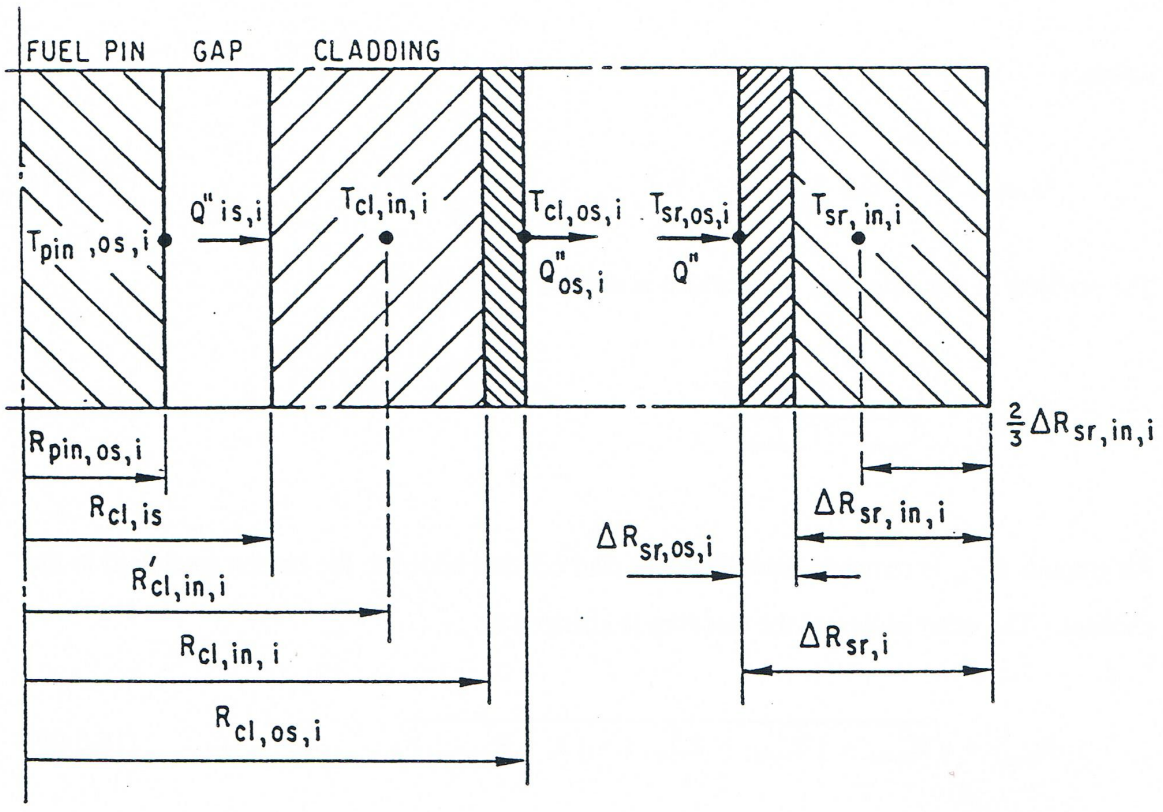

Fig. 16.5-2: Temperature Grid in the Cladding and Structure

An amount $\Delta\rho'_{se}$ is removed from the outer clad cell and added to the molten steel field in the channel. The outer radius of the cladding is changed to:

$$R_{cl,os,i} = \sqrt{R^2_{cl,in,i} - \left(R^2_{cl,os,i} - R^2_{cl,in,i}\right) \cdot \left(1 - F_{\text{ablation},i}\right)} \tag{16.5-29}$$

Due to the explicit solution technique used in the cladding temperature calculation, a very thin outer cladding cell can lead to numerical instabilities in the temperature calculation or alternatively might require very small time steps. To avoid this difficulty while still maintaining an explicit method of solution in the temperature calculation, a lower limit ΔR_{min} is imposed on the thickness of the outer cladding cell. Whenever:

$$R_{cl,in,i} = R_{cl,os,i} - R_{cl,in,i} \le \Delta R_{\min} \tag{16.5-30}$$

The temperature calculation grid is restructured. The internal radius $R_{cl,in,i}$ is set to:

$$R_{cl,in,i} = R_{cl,os,i} - 2 \cdot \Delta R_{\min} \tag{16.5-31}$$

and the temperature of the cladding cells is adjusted appropriately. This process continues until $R_{cl,in,i} = R_{cl,is,i}$, at which time the internal cladding cell disappears completely. The ablation process can still continue until the outer (and only) cladding cell reaches the thickness ΔR_{min}. Afterwards, no ablation is allowed until the remaining cladding reaches the melting point, when the cladding is completely removed and the fuel pin begins to transfer energy directly to the flowing components in the channel.

A similar procedure is used for the ablation of the hexcan wall. The ablation process is illustrated in Fig. 16.5-1c.

16.5.6 Fuel/Steel Chunk Melting

The moving solid chunks in the channel, both fuel and steel, can begin to melt due to heat transfer from the surrounding components and, in the case of the fuel chunks, due to internal heat generation. This process is modeled in the routine LELUME. The remelting of the fuel chunks occurs when:

$$h_{f\ell,i} > h_{f\ell,\text{melt}} \tag{16.5-32}$$

where

$$h_{f\ell,\text{melt}} = \left(h_{fu,so} + h_{fu,\ell q}\right) \cdot 0.5 \tag{16.5-33}$$

The amount of molten fuel is obtained from:

$$\Delta\rho'_{f\ell,i} = \rho'_{f\ell,i} \cdot \frac{h_{f\ell,i} - h_{f\ell,\text{meltlimit}}}{h_{fu,\ell q} - h_{f\ell,\text{meltlimit}}} \tag{16.5-34}$$

where

$$h_{f\ell,\text{melt limit}} = \left(h_{f\ell,\text{melt}} - 0.1\, h_{fu,\ell q}\right)/0.9 \tag{16.5-35}$$

The quantity $h_{\ell\ell,\text{melt limit}}$ is defined by Eq. 16.5-35 to be slightly below $h_{\ell\ell,\text{melt}}$. When melting occurs, as defined by eq. 16.5-34, the enthalpy of the molten material is $h_{fu,\ell q}$, and the enthalpy of he remaining chunks is $h_{\ell\ell,\text{melt limit}}$. Because $h_{\ell\ell,\text{melt limit}}$ is lower than $h_{\ell\ell,\text{melt}}$, which is used in Eq. 16.5-32 to trigger the melting process, the continuous melting of very small amounts of fuel is avoided. Melting of the fuel chunks in cell i will occur only when their enthalpy again reaches $h_{\ell\ell,\text{melt limit}}$. The size of the chunks is decreased appropriately, but their number remains unchanged. The molten fuel is added to the molten fuel in the channel:

$$\rho'_{fu,i} = \rho'_{fu,i} + \Delta\rho'_{fu,i} \tag{16.5-36}$$

and the energy and velocity of the molten fuel field are adjusted to reflect the addition of the molten fuel resulting from the remelting of the chunks.

A similar procedure is used for melting the steel chunks, which occurs when:

$$h_{s\ell,i} > h_{s\ell,\text{melt}} \tag{16.5-37}$$

where

$$h_{s\ell,melt} = \left(h_{se,so} + h_{se,\ell q}\right) \cdot 0.5 \tag{16.5-38}$$

The amount of molten steel is obtained from

$$\Delta\rho'_{s\ell,i} = \rho'_{s\ell,i} \cdot \frac{h_{s\ell,i} - h_{s\ell,\text{meltlimit}}}{h_{se,lq} - h_{s\ell,\text{meltlimit}}} \tag{16.5-39}$$

16.5.7 Heat-transfer Calculation for the Steel Cladding and the Hexcan Wall

These calculations are performed in the routine LESOEN.

16.5.7.1 Heat-transfer Calculation for the Steel Cladding

The heat-transfer calculation for the steel cladding is performed using the two-node mesh illustrated in Fig. 16.5-2. Two energy equations, one for each node, are solved

explicitly. Due to ablation the geometry of the two cladding nodes can change in any time step.

The energy conservation equation for the outer cladding node in the axial cell i is:

$$\begin{aligned}\rho_{se} \cdot \frac{\partial h_{cl,os,i}}{\partial t} \cdot \left(R_{cl,os,i}^2 - R_{cl,in,i}^2\right) \cdot \pi \cdot \Delta z_i \\ = k_{se} \cdot \frac{T_{cl,in,i} - T_{cl,os,i}}{R_{cl,os,i} - R'_{cl,in,i}} \cdot 2\,\pi\, R_{cl,in,i} \cdot \Delta z_i - \sum_j H_{cl,j,i} \\ \cdot \left(T_{cl,os,i} - T_{j,i}\right) \cdot \frac{A_{cl,j,i}^L}{N_{pins}} + Q_{cl,j} \cdot \frac{R_{cl,os,i} - R_{cl,in,i}}{\Delta R_{cl}^0}\end{aligned} \tag{16.5-40}$$

where the $\sum_j$ is performed over all the components in the channel that are in contact with the cladding and $Q_{cl,i}$ is the energy source in the cladding in cell i. The subscript se refers here to the solid steel, as opposed to the previous occurrences where it was followed by i (e.g. $\rho_{se,i}$), when it was referring to the molten steel in the channel. After integration over Δt, division by Δz_i and rearrangement, e.g., Eq. 16.5-40 becomes:

$$\begin{aligned}h_{cl,os,i}^{n+1} = h_{cl,os,i} + \frac{\Delta t}{\rho_{se} \cdot \pi \left(R_{cl,os,i}^2 - R_{cl,in,i}^2\right)} \left\{ \frac{k_{se} \cdot 2\pi R_{cl,in,i}}{R_{cl,os,i} - R'_{cl,in,i}} \right. \\ \times \left(T_{cl,in,i} - T_{cl,os,i}\right) - \frac{AXMX}{N_{pins}} \left[H'_{Na,cl,i} \left(T_{cl,os,i} - T_{Na,i}\right) \right. \\ + H'_{fu,cl,i} \left(T_{cl,os,i} - T_{fu,i}\right) + H'_{se,cl,i} \left(T_{cl,os,i} - T_{se,i}\right) \\ + H'_{cl,fi,i} \left(T_{cl,os,i} - T_{fl,i}\right) + H'_{cl,sl,i} \left(T_{cl,os,i} - T_{sl,i}\right) \\ \left. \left. + H'_{cl,ffc,i} \left(T_{cl,os,i} - T_{ffc,i}\right) \right] + Q_{cl,i} \cdot \frac{R_{cl,os,i} - R_{cl,in,i}}{\Delta z_i \cdot \Delta R_{cl}^o} \right\}\end{aligned} \tag{16.5-41}$$

where $H'_{j,cl,i}$ are the generalized heat-transfer coefficients which have been defined previously.

The energy conservation equation for the inner cladding node in the axial cell is shown below:

$$\begin{aligned}
&\rho_{se}\,\frac{\partial h_{cl,in,i}}{\partial t}\cdot\left(R_{cl,in,i}^2-R_{cl,is,i}^2\right)\cdot\pi\cdot\Delta z_i \\
&\quad=-k_{se}\,\frac{T_{cl,in,i}-T_{cl,os,i}}{R_{cl,os,i}-R_{cl,in,i}}\cdot 2\,\pi\,R_{cl,in,i}\cdot\Delta z_i \\
&\qquad+H_{cl,in,pin,i}\cdot 2\pi\cdot R_{cl,is,i}\cdot\Delta z_i\cdot\left(T_{pin,os,i}-T_{cl,in,i}\right) \\
&\qquad+Q_{cl,i}\cdot\frac{R_{cl,in,i}-R_{cl,is,i}}{\Delta R_{cl}^{o}}\,,
\end{aligned} \tag{16.5-42}$$

where $H_{cl,in,pin,i}$ is the heat-transfer coefficient between the inner cladding node and the outer fuel node. It takes into account the gap heat conductance and is defined as follows:

$$H_{cl,in,pin,i}=\frac{1}{\dfrac{1}{H_{gap}}+\dfrac{R'_{cl,in,i}-R_{cl,is,i}}{k_{se}}} \tag{16.5-43}$$

After integration over Δt and rearrangement, Eq. 16.5-42 becomes:

$$\begin{aligned}
h_{cl,in,i}^{n+1}=h_{cl,in,i}-\frac{\Delta t}{\rho_{se}\cdot\pi\cdot\left(R_{cl,in,i}^2-R_{cl,is,i}^2\right)}\cdot\Bigg[&\frac{k_{se}\cdot 2\pi R_{cl,in,i}}{R_{cl,os,i}-R_{cl,in,i}} \\
&\cdot\left(T_{cl,in,i}-T_{cl,os,i}\right)-H_{cl,in,pin,i}\cdot 2\pi R_{cl,is,i} \\
&\cdot\left(T_{pin,os,i}-T_{cl,in,i}\right)-Q_{cl,i}\cdot\frac{R_{cl,in,i}-R_{cl,is,i}}{\Delta R_{cl}^{o}\cdot\Delta z_i}\Bigg]
\end{aligned} \tag{16.5-44}$$

A special situation occurs whenever the inner cladding node disappears as a consequence of the ablation process, which has been described previously. This situation is indicated by setting the temperature $T_{cl,in,i}$, which is not longer used, to a negative arbitrary value, i.e., $T_{cl,in,i}$ = -100. In this case, the outer cladding node exchanges heat directly with the fuel pin and the energy Eq. 16.5-41 is changed to:

$$\begin{aligned}
h_{cl,os,i}^{n+1}=h'_{cl,os,i}+&\frac{\Delta t}{\rho_{se}\cdot\pi\cdot\left(R_{cl,os,i}^2-R_{cl,in,i}^2\right)} \\
&\cdot\Bigg[-\frac{AXMX}{N_{pins}}\cdot\sum_j H'_{cl,j,i}\left(T_{cl,os,i}-T_{j,1}\right)+H_{cl,os,pin,i}\cdot 2\pi R_{cl,in,i} \\
&\cdot\left(T_{pin,os,i}-T_{cl,os,i}\right)+Q_{cl,i}\;\frac{R_{cl,os,i}-R_{cl,in,i}}{\Delta z_i\cdot\Delta R_{cl}^{o}}\Bigg]
\end{aligned} \tag{16.5-45}$$

where $H_{cl,os,pin,i}$ is the heat-transfer coefficient between the outer cladding node and the outer pin node (when the inner node was vanished):

$$H_{cl,os,pin,i} = \frac{1}{\frac{1}{H_{gap}} + \frac{R_{cl,os,i} - R_{cl,os,i}}{k_{se}}} \tag{16.5-46}$$

The energy transferred between the cladding and the pin in each LEVITATE time step is integrated over the heat-transfer time step and stored under the name HFPICL(I). This quantity is then used in the pin heat-transfer calculation, in the routine PLHTR, as the pin boundary condition at $R = R_{pin,os,i}$.

Another special situation is the case when the cladding has been totally ablated, and the moving components in the channel are in direct contact with the fuel pin. For this case, the cladding temperature $T_{cl,os,i}$ is set equal to $T_{pin,os,i}$:

$$T_{cl,os,i} = T_{pin,os,i} \tag{16.5-47}$$

This allows all heat transfer to the channel components, as well as the freezing/melting processes, to be calculated correctly. Freezing of fuel on the bare fuel pin can still occur, if predicted by the freezing model. This situation can be identified in the output by the presence of undisrupted pin nodes, i.e., IDISR(I) ≠ 1 with no cladding on them, i.e., WICLAD(I) = 0. In these cells, the output will indicate that no inner cladding node is present, i.e., $T_{cl,in,i}$ = -100, and the temperature printed under $T_{cl,os,i}$ will represent the outer temperature of the fuel pin, according to Eq. 16.5-47.

The procedure outlined above is used in the fuel and blanket region of the fuel pin. A similar but simplified procedure is used for the remainder of the pin, where no fuel is present. A zero heat-flux boundary condition is used in these nodes.

The new cladding temperatures are finally obtained from the new enthalpies:

$$T^{n+1}_{cl,os,i} = T\left(h^{n+1}_{cl,os,i}\right) \;;\; T_{cl,in,i} = T\left(h^{n+1}_{cl,in,i}\right) \tag{16.5-48}$$

16.5.7.2 Heat-transfer Calculation for the Hexcan Wall

The heat-transfer calculation for the hexcan wall (the hexcan wall is alternatively referred to as structure) is performed using the two-cell mesh illustrated in Fig. 16.5-2. The outer structure cell is the cell facing the coolant channel. This cell is fairly thin, and responds rapidly to changes in the heat-transfer from the coolant channel. This is necessary for the correct modeling of the structure ablation process, which has been described previously. It is assumed that no heat transfer occurs at the outer boundary of the hexcan wall, i.e., at the boundary facing the neighboring subassemblies. Because of this condition, and in order to improve the accuracy of the two-node calculation for the fairly thick structure, the temperature in the structure is assumed to have a parabolic variation:

$$T(\Delta R) = a \cdot \Delta R^2 + b \cdot \Delta R + c \tag{16.5-49}$$

where ΔR is the radial coordinate measured from the hexcan boundary facing the channel towards the pin. The coefficients a, b, and c are defined each time step by the conditions:

$$\frac{dT}{d(AR)}\Big|_{\Delta R} = -\Delta R_{sr,i} = 0 \tag{16.5-50}$$

$$T(0) = T_{sr,os,i} \tag{16.5-51}$$

$$T\left(-\Delta R_{sr,os,i} - \frac{1}{3}\Delta R_{sr,in,i}\right) = T_{sr,in,i} \tag{16.5-52}$$

Using Eqs. 16.5-50 through 16.5-52, it is found that the temperature gradient at the boundary between the outer and the inner structure nodes is given by:

$$\frac{dT}{d(\Delta R)}\Big|_{\Delta R=-\Delta R_{sr,os,i}} = \left(T_{sr,os,i} - T_{sr,in,i}\right) \cdot \frac{18 \cdot \Delta R_{sr,in,i}}{5\Delta R_{sr,i}^2 + 8\Delta R_{sr,i} \cdot \Delta R_{sr,os,i} - 4\Delta R_{sr,os,i}^2} \tag{16.5-53}$$

This temperature gradient expression will be used in the energy-conservation equations for the structure. The equation for the outer structure cell is written:

$$\begin{aligned} &\rho_{se} \cdot \frac{\partial h_{sr,os,i}}{\partial t} \cdot \Delta R_{sr,os,i} \cdot \Delta z_i \cdot L_{sr,i} \\ &= -k_{se} \cdot \frac{\partial T}{\partial(\Delta R)}\Big|_{\Delta R=-\Delta R_{sr,os,i}} \cdot \Delta z_i \cdot L_{sr,i} \\ &\quad + \sum_j H_{sr,j,i} \cdot \left(T_{j,i} - T_{sr,os,i}\right) \cdot A^L_{sr,j,i} \end{aligned} \tag{16.5-54}$$

where $\sum_j$ is performed over all the components in the channel that are in contact with the structure. Although ΔR is used as the "radial" coordinate, the hexcan wall is in fact assumed to be flat, with thickness ΔR_i and perimeter $L_{sr,i}$.

After integration over Δt, rearrangement and use of Eq. 16.5-53, the above equation becomes:

$$h_{sr,os,i}^{n+1} = h_{sr,os,i} + \frac{\Delta t}{\rho_{se} \cdot \Delta R_{sr,os,i} \cdot L'_{sr,i}} \cdot \left[- \frac{k_{se} L'_{sr,i} \cdot 18 \Delta R_{sr,in,i}}{5\Delta R_{sr,i}^2 + 8\Delta R_{sr,i} \cdot \Delta R_{sr,os,i} - 4\Delta R_{sr,os,i}^2} \cdot \left(T_{sr,os,i} - T_{sr,in,i}\right) + H'_{Na,sr,i} \cdot \left(T_{Na,i} - T_{sr,os,i}\right) + H'_{fu,sr,i} \cdot \left(T_{fu,i} - T_{sr,os,i}\right) + H'_{se,sr,i} \cdot \left(T_{se,i} - T_{sr,os,i}\right) + H'_{fl,sr,i} \cdot \left(T_{fl,i} - T_{sr,os,i}\right) + H'_{s\ell,sr,i} \cdot \left(T_{s\ell,i} - T_{sr,os,i}\right) + H'_{ffs,sr,i} \cdot \left(T_{ffs,i} - T_{sr,os,i}\right) \right] \quad (16.5\text{-}55)$$

where

$$L'_{sr,i} = \frac{L_{sr,i}}{AXMX} \quad (16.5\text{-}56)$$

and $H'_{j,sr,i}$ are the generalized heat-transfer coefficients which were defined previously as follows:

$$H'_{j,sr,i} = H_{j,sr,i} \cdot \frac{A_{j,sr,i}}{AXMX \cdot \Delta z_i} \quad (16.5\text{-}57)$$

The new temperature of the structure outer node is then obtained from its enthalpy:

$$T_{sr,os,i}^{n+1} = T\left(h_{sr,os,i}^{n+1}\right) \quad (16.5\text{-}58)$$

The energy equation for the inner structure cell (i.e., the cell which is not in contact with the coolant channel) is written as follows:

$$\rho_{se} \cdot \frac{\partial h_{sr,in,i}}{\partial t} \cdot \Delta R_{sr,in,i} \cdot \Delta z_i \cdot L_{sr,i} = k_{se} \left. \frac{\partial T}{\partial(\Delta R)} \right|_{\Delta R = -\Delta R_{sr,os,i}} \cdot \Delta z_i \cdot L_{sr,i} \quad (16.5\text{-}59)$$

After integration over Δt and rearrangement, the above equation becomes:

$$h_{sr,in,i}^{n+1} = h_{sr,in,i} + \frac{\Delta t \cdot k_{se} \cdot 18 \Delta R_{sr,in,i} \cdot \left(T_{sr,in,i}\right)}{\rho_{se} \cdot \Delta R_{sr,in,i} \cdot \left(5\Delta R_{sr,i}^2 + 8 \cdot \Delta R_{sr,i} \cdot \Delta R_{sr,os,i} - 4\Delta R_{sr,os,i}^2\right)} \quad (16.5\text{-}60)$$

The new temperature of the structure node is then obtained from its enthalpy:

$$T_{sr,in,i}^{n+1} = T\left(h_{sr,in,i}^{n+1}\right) \tag{16.5-61}$$

A special situation occurs when the "inner" structure cell has disappeared completely as a result of the ablation process. This situation is indicated by setting $T_{sr,in,i}$ to an arbitrary negative value, i.e., $T_{sr,in,i} = -100$. In this case, only the Eq. 16.5-54 for the outer structure cell is solved in a simplified form. The term $k_{se}\frac{\partial T}{\partial(\Delta R)}|_{\Delta R=-\Delta R_{sr,os,i}}$ is set to zero, and the final equation is shown below:

$$h_{sr,os,i}^{n+1} = h_{sr,os,i} + \frac{\Delta t}{\rho_{se}\cdot\Delta R_{sr,os,i}\cdot L'_{sr,i}}\cdot\sum_j H'_{j,sr,i}\cdot\left(T_{j,i} - T_{sr,os,i}\right) \tag{16.5-62}$$

When the "inner" structure cell has been removed and the outer cell has reached both a minimum thickness and the melting point, the hexcan wall is assumed to be breached. Intersubassembly fuel motion is likely to begin. Theoretically, this should be the end of the LEVITATE calculation and the beginning of a transition-phase calculation. However, the code will only print a warning message and the calculation will continue assuming that the hexcan wall will maintain the minimum thickness, although its temperature has risen above the melting range.

16.6 LEVITATE Interaction with Other Modules

16.6.1 Interaction with the Point Kinetics Module

The LEVITATE interface with the point kinetics model has been described briefly in Section 16.1.3.3.3.

The axial mass and temperature distributions needed to calculate the reactivity feedbacks in the point kinetics module are calculated in the LEVITATE driver routine, LEVDRV, at the end of each PRIMAR time step. The changes in reactivity are due to changes in the distribution of sodium, fuel and steel in the active core region, and changes in the fuel temperature. The formulation for these feedbacks is given in Chapter 4, Section 4.5.

16.6.2 Coupling with the Primary Loop Module

As explained briefly in Section 16.1.3.3.1, LEVITATE can be coupled with either PRIMAR-1 or the more advanced PRIMAR-4 module. The PRIMAR-1 model is used whenever the input variable IPRION has a value less than 4. In this case, LEVITATE uses the constant outlet plenum pressure PX which is input and an inlet plenum pressure which is determined by PRIMAR-1. This is the only information needed in LEVITATE to calculate the motion of the liquid sodium slugs. A temperature calculation within the sodium slugs is not currently performed in LEVITATE and thus no plenum

temperature information is expected. If the PRIMAR-1 option has been chosen, LEVITATE will not return any information to the primary loop module.

When the PRIMAR-4 option is selected (IPRION=4), LEVITATE will use the time-dependent inlet and outlet pressures which are calculated by PRIMAR-4 to determine the dynamics of the liquid sodium slugs. The inlet pressure used in each LEVITATE time step is calculated as follows:

$$P_{inlet}(t) = P_{inlet}(t_{PR1}) + (t - t_{PR1}) \cdot \frac{\partial P_{inlet}}{\partial t} \tag{16.6-1}$$

where

P_{inlet} (t_{PR1}) - is the inlet pressure calculated by PRIMAR-4 at the beginning of the current primary loop time step.

$\frac{\partial P_{inlet}}{\partial t}$ - is the rate of change of the inlet pressure during the previous primary loop time step, calculated by PRIMAR-4

t_{PR1} - is the time at the beginning of the current primary loop time step.

The outlet pressure is calculated in the same manner:

$$P_{outlet}(t) = P_{outlet}(t_{PR1}) + (t - t_{PR1}) \cdot \frac{\partial P_{outlet}}{\partial t} \tag{16.6-2}$$

When the PRIMAR-4 option is used, LEVITATE provides PRIMAR-4 with the total sodium masses ejected into or received from the plena during a primary loop time step:

$$\Delta M_{Na,ic,inlet} = N_{subas,ic} \cdot \int_{t_{PR1}}^{t_{PR2}} W_{Na,inlet} \cdot dt \tag{16.6-3}$$

and

$$\Delta M_{Na,ic,outlet} = N_{subas,ic} \cdot \int_{t_{PR1}}^{t_{PR2}} W_{Na,outlet} \cdot dt \tag{16.6-4}$$

where

t_{PR1} - is the time at the beginning of the PRIMAR-4 time step

t_{PR2} - is the time at the end of the PRIMAR-4 time step

W_{Na} - is the sodium mass flow rate in kg/s

LEVITATE also provides PRIMAR-4 with the channel mass flow rates at the end of the primary loop time step. As long as single phase liquid sodium is ejected into the upper or lower plena, temporal integrals of the product (sodium flow rate · temperature) are also provided by LEVITATE. However, when the upper liquid sodium slug has been ejected out of the subassembly, LEVITATE calculates the total enthalpy of the two-phase mixture ejected during a primary loop time step:

$$\Delta h_{ic} = \left[\left(1 - X_{Na,IITP-1}\right) \cdot h_{N\ell} + X_{Na,IITP-1} \cdot h_{Nv}\right] \cdot W_{Na} \cdot N_{subs,ic} \cdot \left(t_{PR2} - t_{PR1}\right) \tag{16.6-5}$$

where

$X_{Na,\ IITP-1}$ - is the sodium quality in the axial node IITP-1, the highest full node in the subassembly.

$h_{N1,}$ h_{Nv} - are the enthalpies of the liquid sodium and sodium vapor, respectively, in the axial node IITP-1.

16.7 Detailed Logic Flow Description

This section describes in detail the logical sequence of the solution method used in LEVITATE. The structure of the LEVITATE driver as well as initiation and interfacing considerations have been presented in Section 16.1.3. Some information about the interaction between LEVITATE models was presented in Section 16.1.2.4 and the method of solution for the coolant channel model was described in Section 16.4.2. This section will use, and occasionally repeat some of this information in order to present a comprehensive picture of the general solution method. Some considerations about the data management and time-step selection are also presented.

16.7.1 Data Management Considerations

Every time LEVITATE begins calculations in a channel, the permanently stored information is retrieved from the data container and loaded in the common blocks. This operation is performed in the TSTHRM module. A number of arrays and other data, however, which can be calculated from the permanently stored variables, are not stored in the permanent storage. These data are recalculated in the routine LESET2 every time LEVITATE receives control in a certain channel, i.e., at the beginning of a primary time step. These variables are stored in temporary common blocks, and kept only as long as LEVITATE retains control in the channel. At the end of the primary time step, when LEVITATE returns control to TSTHRM, these variables are lost. Only the permanent common blocks are saved in the data container. This procedure is used in order to reduce the amount of storage required for SAS4A.

16.7.2 Logic Flow for Solution Advancement

As explained in Section 16.1.2, the LEVITATE model can be viewed as being made up of three large models, i.e, the coolant channel hydrodynamic model, the in-pin fuel

motion model and the freezing/melting model describing the fuel pins and the hexcan wall. During each time step, LEVITATE advances the solution for these models by calculating the value of all variables at the end of the time step. The time-step selection is described in Section 14.7.3. The simplified modular chart of the LEVITATE model is shown again in Fig. 16.7-1.

The LEVITATE calculation begins by advancing the solution for the channel hydrodynamic model. The changes in the position of material boundaries are calculated first. The new interface positions, at the end of the time step, are calculated for all components, except sodium in the LEIF (LEVITATE INTERFACE) routine. The position of the sodium slugs, which determine the boundaries of the sodium region, is calculated in the LEREZO LEVITATE REZONING) routine. This routine can add (or remove) nodes to the LEVITATE compressible region as the sodium slugs move out of (or remove) nodes to the LEVITATE compressible region as the sodium slugs move out of (or into) the channel.

The mass conservation equation is solved next for all components and all axial locations. Each equation is solved explicitly, i.e., the convective fluxes are based on the generalized densities present in each cell at the beginning of the time step. These calculations are performed in the LEMACO (LEVITATE MASS CONSERVATION) routine.

The LEVOFR (LEVITATE VOLUME FRACTION) routine uses the new densities to determine the volume fraction of each component at each axial location. Using these volume fractions, the LEVOFR routine also determines the flow regime in each axial cell. This flow regime will be assumed to exist in the cell of the duration of the time step. It is worth noting that this is an “implicit type” assumption as the flow regimes are based on the densities calculated at the end of the time step.

The next routine called is LEGEOM (LEVITATE GEOMETRY) which determines the geometrical characteristics defining each local configuration. This routine will change the thickness of the fuel crust as necessary or determine

the fraction of the cladding circumference covered by the liquid fuel in the partial annular flow regime. In general, LEGEOM calculates the area of contact between various components in various flow regimes. These areas will be used later in calculating the energy and momentum transfer between various components.

The next routine called is LETRAN (LEVITATE TRANSFER) which calculates the heat-transfer and friction coefficients for all axial locations and among all components that are in direct contact. Thus, the code will use the flow regimes present at a certain location to determine which heat-transfer and friction coefficients have to be calculated. The allowable exchanges for each flow regime and each component have already been presented in Figs. 16.4-3 through 16.4-10. Once contact areas and the corresponding heat-transfer coefficients have been calculated, the energy conservation equation can be solved for all components.

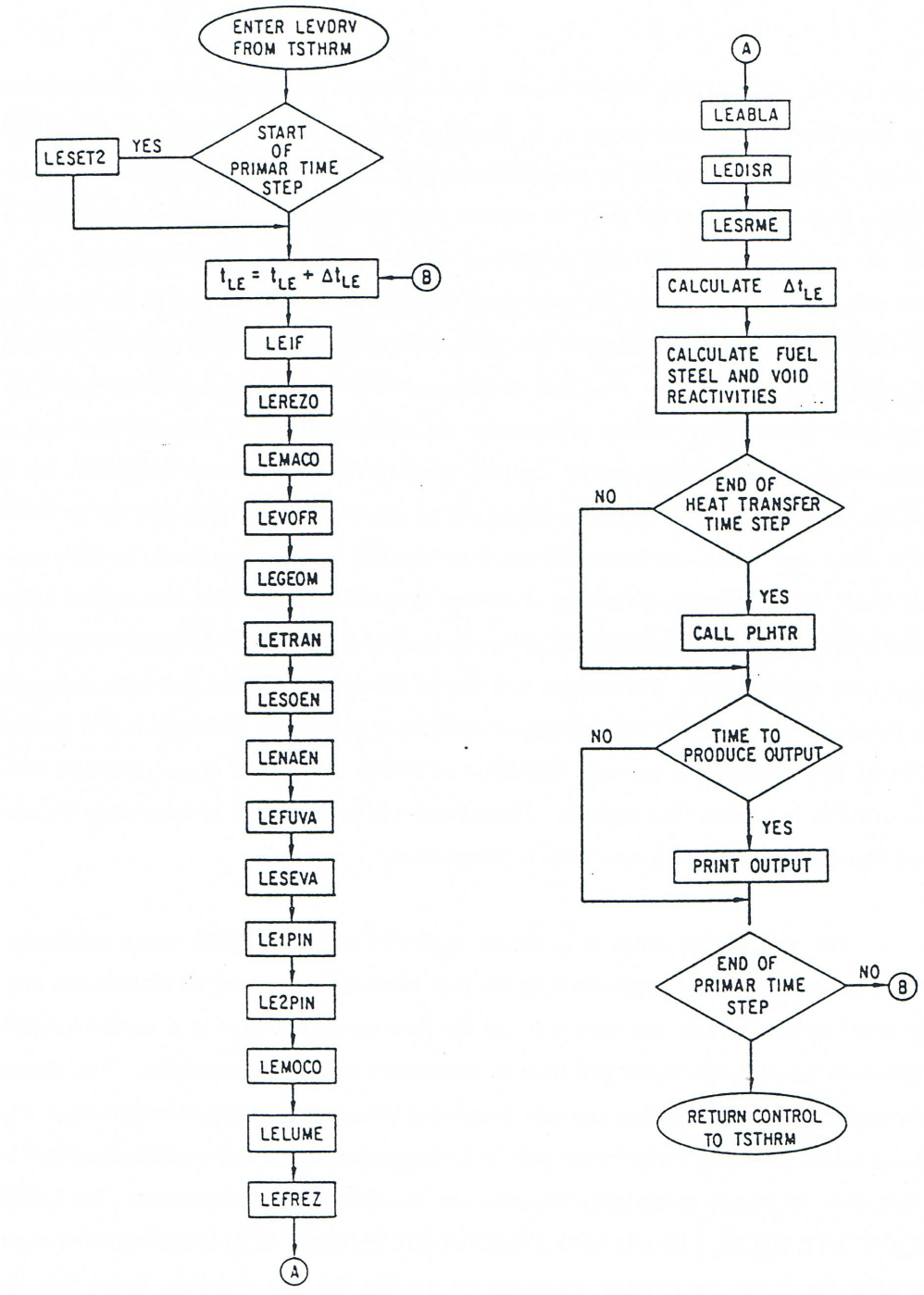

Fig. 16.7-1: Simplified Modular Chart of the LEVITATE Module

The LESOEN (LEVITATE SOLID, LIQUID AND STATIONARY ENERGY EQUATION) routine is called to solve the energy conservation equations for the fuel and steel channels, liquid fuel, liquid steel, stationary cladding, hexcan wall, frozen fuel on the cladding and frozen fuel on the hexcan wall. All equations are solved explicitly, i.e., the convective fluxes are based on beginning of time-step densities, thus allowing the axial decoupling of the equations. The energy equation for sodium (two-phase or single-phase vapor) and fission gas is solved in LENAEN (LEVITATE SODIUM-NA ENERGY). The energy equations for fuel and steel vapor are solved LEFUVA (LEVITATE FUEL VAPOR ENERGY) and LESEVA (LEVITATE FUEL VAPOR ENERGY) and LESEVA (LEVITATE STEEL VAPOR ENERGY), respectively. The new temperatures calculated in LENAEN, LEFUVA and LESEVA are used to determine the new pressure of each of the compressible components and thus the total new pressure.

At this point, the only variables that remain to be calculated in order to complete the solution for the coolant channel hydrodynamic model are the velocities of various components. However, before calculating the new velocities, the hydrodynamic in-pin model is used to advance the in-pin solution in the LE1PIN and LE2PIN routines. Due to the strategy, the changes n the channel hydrodynamics due to the interaction with the in-pin motion will be taken into account in the velocity calculation. The routine LE1PIN solves the mass and energy conservation equations for the in-pin hydrodynamic model. It also calculates the enlargement of the pin cavity and the amount of molten fuel added to the cavity, as well as the amount of fuel ejected from the cavity via the cladding rip and/or the ends of the fuel-pin stubs. The LE2PIN routine completes the solution of the in-pin hydrodynamic model by solving the momentum conservation equations for all the cells in the cavity and determining the new in-pin velocities at the end of the time step. This routine determines the next maximum time step acceptable for the in-pin hydrodynamic model, DTPIN which will then be used in the LEVIATE driver as explained in Section 16.7.3. The in-pin model interacts directly with the channel model via the fuel injection process, which, as mentioned above, is described in the LE1PIN routine. Molten fuel and fission gas are ejected from cavity into the channel, leading to changes in the local pressure.

The solution of the channel hydrodynamic model is then completed by solving the momentum equation for each of the three velocity fields (fuel/steel, gas mixture and solid chunks) in the routine LEMOCO (LEVITATE MOMENTUM CONSERVATION). The method of solution is still explicit and the equations are uncoupled axially, but the equations for all three fields are solved simultaneously rather than independently, as was done in the mass and energy equations. Also it is important to note that the pressures used in the momentum equation are the pressures at then end of the time step. The LEMOCO routine also calculates the new velocities of the lower and upper liquid sodium slugs, which will be used in the next time step in the LEREZO routine. It also calculates the quantities which are fed back to the primary loop model as explained in Sections 16.1.3.3.1 and 16.6.1.2. The sodium slugs provide the axial boundaries for the interactive region modeled by LEVITATE and their molten can affect significantly the fuel motion in the coolant channel.

All the routine called after LEMOCO describe melting or freezing processes related to the solid chunks, cladding or the hexcan wall. The routine LELUME (LEVITATE CHUNK-LU MELTING) calculates the melting and the size changes of the solid fuel/steel chunks at all axial locations. The routine LEFREZ (LEVITATE FREEZING AND MELTING) then models a series of important processes, such as fuel/steel freezing and crust formation, fuel/steel chunk formation, fuel crust remelting and breakup. Next called is the routine LEABLA (LEVITATE ABLATION) which calculates the gradual melting and ablation of the cladding and hexcan wall. The routine LEDISR (LEVITATE DISTRUPTION) performs the disruption of the fuel pin, whenever a node disruption is predicted. The disruption, which can occur in one or more nodes in any time step, leads to changes in geometry, mass, energy and pressure various components present in the respective cell. Finally, the routine LESRME (LEVITATE STRUCTURE MELTING) calculates the rupture of the hexcan wall, due to melting and/or pressure burst effects.

Using the material distributions at the end of the time step, LEVITATE then calculates the fuel, steel and sodium mass distributions, which, at the end of the primary time step, are fed back to the point kinetics module, as explained in Sections 16.1.3.3.3 and 16.6.1. Finally, if the end of a heat-transfer time step is reached, LEVITATE class the routine PLHTR, which calculates the new temperatures in the solid fuel pin at all axial locations. These temperatures will be used in the next time step in the LE1PIN routine to calculate the new cavity diameter and the heat flux between the outer fuel pin surface and the cladding.

16.7.3 Time-step Considerations

The LEVITATE driver routine, LEVDRV can be called by the SAS4A transient driver TSTHRM at any time during a primary loop time step. The primary time step is common for all SAS4A calculational channels and is always smaller than or equal to the main time step used in the point kinetics calculation.

When the fuel-pin failure is detected in a given channel, the LEVITTE and PLUTO2 time, TIMEPL, is set to zero in the FAILUR routine. Then LEVITATE is entered directly after pin failure, TIMEPL is initially advanced by adding the LEVITATE minimum time step DTPLIN to the time TIMEPL. However, if LEVITATE is entered after PLUTO2 has been active in a given channel, the TIMEPL will be incremented by the last time step calculated by PLUTO2, as explained in Section 14.7.2. Subsequently, the time TIMEPL will be advanced by the time step calculated by LEVITATE< as described below.

A maximum time step DTPIN, is calculated first for the in-pin hydrodynamic model, as outlined in Section 14.2.8. Then, once all LEVITATE calculations for the current time step are completed, a new time step for the channel hydrodynamic model is calculated in the LEVDRV routine. The details of this calculation are presented in Section 16.4.3.11. This time step is then compared with the in-pin time step and with the present maximum value $2 \cdot 10^{-4}$s. The smallest value is retained as the LEVITATE time step. This value is further compared with the input minimum time step, DTPLIN and the larger value is retained. Finally, the LEVITATE time step can be cut back if the newly determined time:

$$t_{LE}^{n+1} = t_{LE}^{n} + \Delta t \qquad (16.7\text{-}1)$$

extends beyond the end of a heat-transfer time step. In this case, the new LEVITATE time step will be reduced so that the new LEVITATE time t_{LE}^{n+1} will coincide with the end of the heat-transfer time step.

As shown in the flow diagram 16.7-1, LEVITATE retains control and advances the solution a given channel until the end of a primary loop time step is reached.

16.7.4 List of LEVITATE Subroutines

This section contains a list of all the subroutines that are part of the LEVITATE model. These routines are listed in the order they are called:

LEVDRV	**LEVITATE driver routine.**
LEIF	Calculates the new boundary region locations for all the material components, except sodium.
LEREZO	Calculates the new boundary locations for the sodium region, as determined by the dynamics of the liquid sodium slugs.
LEMACO	Solves the conservation equations for all the components present in the coolant channel.
LEVOFR	Calculates the volume fraction occupied by each channel component at all axial locations. It also determines the flow regime present in the channel at all axial locations.
LEGEOM	Determines the local geometry, taking into account the previous configuration and the current flow regime.
LETRAN	Calculates the heat and momentum transfer coefficients between various components.
LESOEN	Solves the coolant channel energy conservation equations for liquid fuel and steel, chunks, fuel crusts, cladding and hexcan wall.
LENAEN	Solves the coolant channel energy conservation equation for the sodium and fission-gas mixture in the coolant channel.
LEFUVA	Solves the energy conservation equation for the fuel vapor in the channel.
LESEVA	Solves the energy conservation equation for the steel vapor in the channel.
LE1PIN	Solves the mass and energy conservation equation for the in-pin hydrodynamic model. It also calculates the

LEVDRV	LEVITATE driver routine.
	ejection of molten fuel from the cavity into the coolant channel.
LE2PIN	Solves the momentum conservation equations for the in-pin hydrodynamic model. Determines the next maximum time step for the in-pin model.
LEMOCO	Solves the momentum conservation equations for the channel hydrodynamic model. Also solves the momentum equations for the liquid sodium slugs.
LELUME	Examines the melting of the fuel and steel chunks. When melting occurs, performs al the required operations.
LEFREZ	Models the freezing of fuel and steel in the channel, crust formation, crust remelting, and heat-up. This routine is used when the chunk model is not active (ICHUCK=O).
LEFRLU	Models the freezing of fuel and steel in the channel, crust and chunk formation, crust remelting and breakup. This routine is used instead of LEFREZ when the chunk model is used (ICHUNK=1).
LEABLA	Models the ablation of cladding and/or hexcan wall, whenever necessary.
LEDISR	Models the disruption of the fuel pins at any axial location.

Other routines called in LEVITATE, which are shared with other modules, are:

PLHTR	Calculates the transient heat transfer in the solid fuel pin. It is called from the LEVITATE driver. This routine can also be called from eh PLUTO2 driver routine.
HHGAP	Determines the heat-transfer coefficient between the fuel pin and cladding. This routine is called from LESOEN. It can also be called from PLUTO2 or DEFORM.
UTS	Determines the ultimate tensile strength of the cladding. It is called from LEIF in order to determine the cladding rip propagation.
EGFUTE	Provides the fuel enthalpy as a function of temperature. It is used frequently in LEVITATE and PLUTO2.
TEFUEG	Provides the fuel temperature as a function of enthalpy.
EGSETE	Provides the steel enthalpy as a function of temperature.
TESEEG	Provides the steel temperature as a function of enthalpy.

16.8 Input Parameters Relevant to LEVITATE

The input parameters relevant to LEVITATE are summarized in Table 16.8-1. A description of these parameters can be found in the SAS4A input listing attached to this document. Table 16.8-1 lists the recommended values for these parameters and the sections and equations were those parameters are mentioned in the text. This list of equations is not necessarily exhaustive, and some input parameters might appear in other equations, in addition to those listed in the table (e.g., AXMX appears in many places and it was not possible to list all occurrences). Comments have been also added occasionally to complement the description given in the SAS4A input listing.

Table 16.8-1: Input Description

Input Location	FORTRAN Variable	Symbol	Section Reference	Equation Reference	Suggested Value (MKS)	Comments
Block 1, INPCOM						
37	KFAILP		14.3.3		0	Controls the axial pin failure propagation calculation.
38	NCPLEV		14.3.4 14.4.3.2 16.1.3.1		3	Switch from PLUTO2 to LEVITATE when NCPLEV axial clad nodes have exceeded the cladding liquidus temperature.
39	NFUELD		16.1.3.4		-5	Number of dollars of fuel reactivity which has to be reached to terminate the calculation.
42	NSLEEX		16.1.3.4		10	Number of fully molten hexcan cells in a subassembly which has to be reached to terminate the calculation.
44	INRAEJ		16.3.1		1	If INRAEJ=1 the ejection of in-pin fuel is calculated using a mechanistic model. If 0 the parametric fuel ejection calculation is used (see CIPINJ, Block 13 loc 1276).
47	ICHUNK				0	If ICHUNK=1 the chunk model is operational. Although the physical picture is more complete when ICHUNK-1, the chunk model has not yet been thoroughly validated. When ICHUNK=0 the chunk model is disabled.

Input Location	FORTRAN Variable	Symbol	Section Reference	Equation Reference	Suggested Value (MKS)	Comments
48	ILUBLK				0	This variable is relevant only when the chunk model is active i.e. ICHUNK=1. If ILUBLK=1 the bulk fuel freezing leads to chunk formation when no solid support for crust formation is available. If ILUBLK=0 no chunk formation occurs under the circumstances mentioned above.
Block 13, PMATCM						
1126	CIBBIN		16.4.3.9.1		0.7	
1127	CIREFN		16.4.3.8.2	16.4-179	2100	
1128	CIFRFU		16.4.3.8.2	16.4-179	0.03	
1129	CIFUMO		16.4.3.8.2	16.4-186	1	Some of the in-pin axial momentum might be lost during the ejection process, due to interactions with the stationary components.
1133	CIA3		16.4.3.10.1.5 16.4.3.10.1.6 16.4.3.10.1.7	16.4-270 16.4-273 16.4-278		
1135	CIA5		16.4.3.8.1	16.4-155	-2.7	
1136	CIA6		16.4.3.8.1	16.4-153 16.4-154	0.1068	
1139	CPFU	$c_{p,fu}$	16.4.3.10.1.2	16.4-246 16.4-248	500.0	

Input Location	FORTRAN Variable	Symbol	Section Reference	Equation Reference	Suggested Value (MKS)	Comments
1140	CDFL	k_{fu}	16.4.3.10.1.2 16.4.3.10.1.5	16.4-251 16.4-252 16.4-266	3.0	
1141	CMNL	$C_{\Delta P,Na}$	16.4.3.5	16.4-83 16.4-84 16.4-85	$4.6 \cdot 10^{-10}$	
1142	CDNL	$k_{n\ell}$	16.4.3.10.1.14	16.4.302	50	
1144	CDVG	k_{Mi}	16.4.3.10.14	16.4-303	0.067	
1146	CFNACN		16.4.3.10.1.14	16.4-304	$6.0 \cdot 10^{4}$	
1147	CFNAEV		16.4.3.10.1.14	16.4-303	$6.0 \cdot 10^{5}$	
1148	FIFNGB			14.2-16	0.1	
1150	VIVG	μ_{vg}	16.4.3.8.1	14.2-16	0.1	
1151	EGFUSO	$H_{fu,so}$	16.5.3.1	16.5-2	$1.0 \cdot 10^{6}$	
1155	C1VIPR				$3.0 \cdot 10^{-3}$	
1157	SUFU	σ_{fu}	16.4.3.8.1	16.4-153	0.45	
1161	EGBBLY	$H_{fu,freeze}$	16.5.3.1	16.5-1		Fuel freezing is initiated when the fuel enthalpy drops below EGBBLY should be between EGFUSO and EGFULQ.
1162	VIFULQ	μ_{fu}	16.4.3.10.1.2	16.4-246		
1164	DTPLIN		16.7.3		$2.5 \cdot 10^{-5}$	
1165	AXMX		16.4.2	16.4-1 etc.		Cross sectional area of subassembly, limited by the outside perimeter
1166	EPCH		14.3.2	14.2-1	1	
1168	DTPLP		16.7			The frequency of the LEVITATE output should be selected by the user.

Input Location	FORTRAN Variable	Symbol	Section Reference	Equation Reference	Suggested Value (MKS)	Comments
1169	FNMELT		14.2.2 14.2.3		0.9	
1170	CIRTFS			14.2-18	16.67	
1174	CIANIN		16.4.3.9.2		0.5	
1175	TEFAIL			14.3-11	TESOL(1)	
1176	FNARME			14.3-10	FSPEC Blk 65, Loc 1	FNARME should be consistent with FSPEC when the input controlled failure propagation is used. However, a compromise might be necessary because FSPEC is channel dependent while FNARME is not.
1177	PRFAIL		14.3-13		0	
1188	CMFU		14.2-33		$6.0 \cdot 10^{-11}$	
1195	CDCL	k_{se}		16.5-41 16.5-42	32.0	
1198	RHSLBT	$\rho_{N\ell,\ell s}$	14.4.6.3		728	This is the liquid sodium density at about 1200 K.
1199	RHSLTP	$\rho_{N\ell,us}$	14.4.6.3		0.975 * RHSLBT	
1206	RHSSLQ				6.10^3	This is the density of the steel entrapped in the frozen fuel crust. It is used in LEFREZ to determine the volume of the newly formed crust.
1207	CIBBDI		16.4.3.9.1		0.2	
1208	CIANDI		16.4.3.9.2		0.1	

Input Location	FORTRAN Variable	Symbol	Section Reference	Equation Reference	Suggested Value (MKS)	Comments
1210	EGSESO				$8.834 \cdot 10^{6}$	Used in the functions T(h) and $H_{se}(t)$. Should correspond to the steel solidus temperature TME.
1211	EGSELQ				EGSESO + UEMELT(1)	Used in the functions $T_{se}(h)$ and $H_{se}(T)$. Should correspond to the steel liquidus temperature TME + DETEMS.
1212	CPSE	$c_{p,se}$	16.4.3.10.1.8	16.4-278	774.0	
1213	FRMRSE		16.5.32	16.5-17	0.5	
1215	RHSSSO				$6.95 \cdot 10^{-3}$	
1216	RGFV	R_{fv}	16.4.3.6	16.4-90 16.4-106	31	
1217	RGSV	R_{sv}	16.4.3.7		148	
1229	FNDISR		16.2.3	16.2.1	0.9	
1231	SRFMLE				1.0	This input value maintains the sodium in the structure film when initiating LEVITATE. If SRFMLE = 0 the film on the structure is ignored.
1280	ASRALU		16.4.3.9.3		1	The aspect ratio of solid chunks, defined as L/2R.
1284	RALUDI		16.4.3.9.3		0.0	This is the radius of the chunks generated by disruption of the fuel pin. If 0.0, the code will determine the appropriate radius using the local geometry.

Input Location	FORTRAN Variable	Symbol	Section Reference	Equation Reference	Suggested Value (MKS)	Comments
1285	RALUFZ		16.4.3.9.3		0.0	This is the radius of the chunks generated by the frozen crust break-up and bulk fuel freezing. If 0.0, the code will determine the appropriate radius using the local geometry.
Block 51, INPCHN						
71	NRPI1				NPIN	All pins are assumed to fail coherently.
72	NRPI2				0	This input constant should be zero whenever NRP11 = NPIN is desired.
182	IMOMEN	16.4.3.8.1 16.4.3.8.2	16.4-142 16.4-174		0	
Block 65, FUELIN						
2	FMELTM	14.1.2			0.2	
19	FCFAIL				0.0	The molten fuel cavity pressure calculated by DEFORM will be used.

16.9 Output Description

16.9.1 Regular Output

The LEVITATE output has been designed to provide the essential information about the subassembly at a given point in time. The output is printed from LEVDRV and can be obtained at equal time intervals, by specifying the input quantity DTPLP. Additional output can be obtained by specifying the input integers IPGO, IPSTOP and IPNEW. The LEVITATE output will then be printed between cycles IPGO and IPSTOP every IPNEW cycles. It is emphasized that this section describes the output produced by the chunk version. The output produced by the initial release version is very similar, but a number of chunk-related variables are not shown. Some chunk-related variables are shown in the output, but their values remain zero at all times.

The regular output is divided into two large sections, one containing information about the fuel-pin cavity and the other one – significantly more extensive – containing information about all the components present in the coolant channel.

The first line in the pin-related output Fig. 16.9-1 contains the computational cycle number and the current time, TIMEPL. This time is measured from the initiation of the out-of-pin fuel motion due to pin failure in the given channel.

The second lien contains some summary information about the fuel-pin cavity, as described below. All these quantities refer to the whole subassembly:

SMFUCA	Total mass of molten fuel in the pin cavity, kg.
SMFICA	Total mass of free fission gas in the pin cavity, kg.
SMFSCA	Total mass of dissolved fission gas in the pin cavity, kg.
SMFUME	Total mass of pin fuel that has molten since LEVIATE initiation, kg.
SMFIME	Total mass of free fission gas released to the cavity due to fuel melting, kg.
SMFSRT	Total mass of fission gas that was originally dissolved in the molten fuel but was released in the meantime, kg.
SMFUEJ	Total amount of molten fuel ejected from the cavity into the coolant channel, kg.
SMFIEJ	Total amount of free fission gas ejected from the cavity into the coolant channel, kg.

Two groups of columns follow, providing more detailed information for all axial cells in the cavity. These columns are described below. Whenever masses are involved, they refer to the whole subassembly, rather than to a single pin.

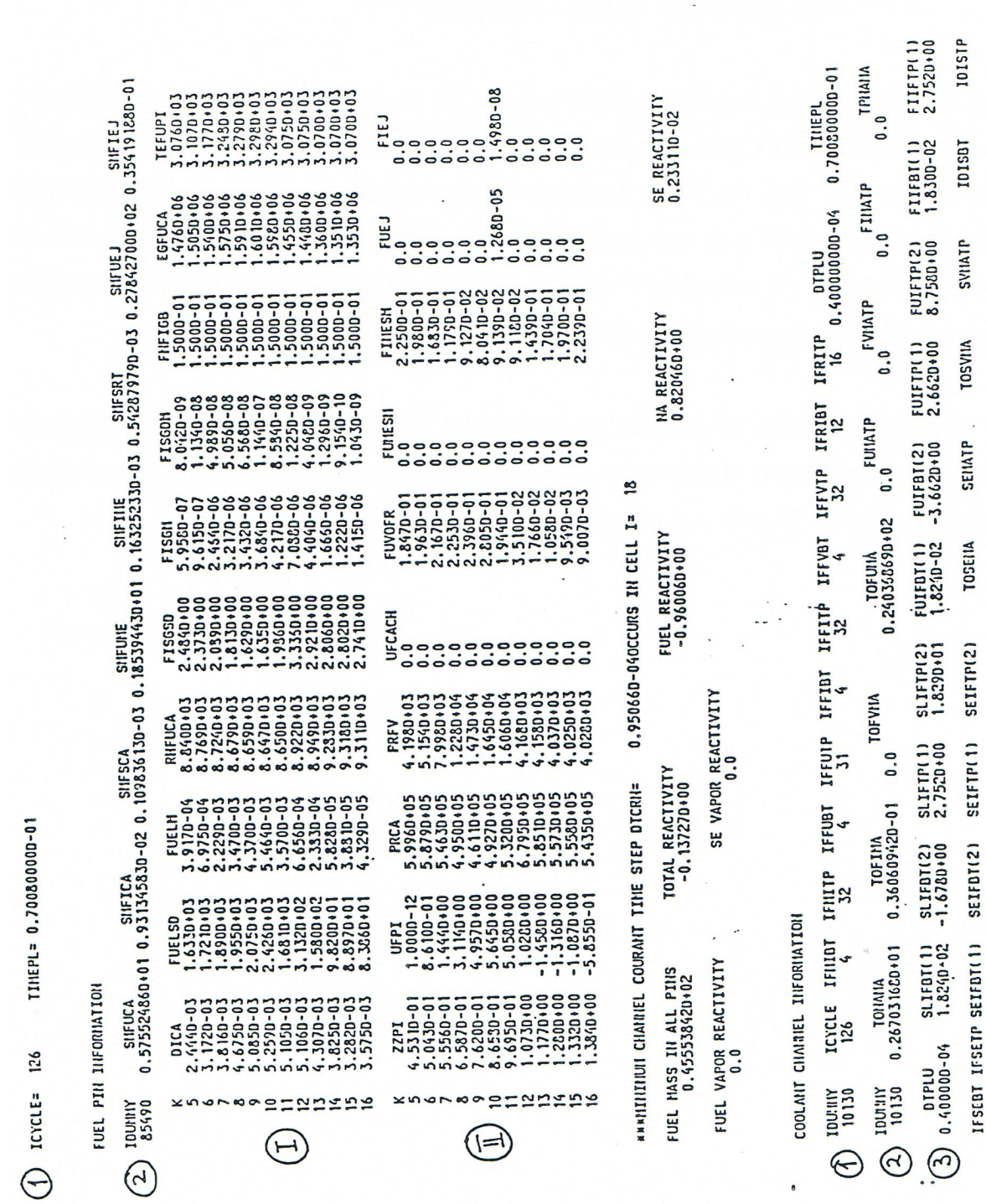

Fig. 16.9-1: Output Description

First group of columns:

k	The number of the axial cell in the cavity. This number refers to the cavity grid, which differs form the channel grid by the integer IDIFF, i.e., k = I – IDIFF.
DICA	Diameter of the cavity, m.
FUELSD	Molten fuel density smeared over the cavity area, kg/m^3.
FUELM	Molten fuel mass, kg.
RHFUCA	Physical density of the molten fuel, kg/m^3.
FISGSD	Free fission-gas density, smeared over the cavity area, kg/m^3.
FISGM	Free fission-gas mass, kg.
FISGDM	Dissolved fission-gas mass, kg.
FNFIGB	Fraction of the fission gas which is released instantaneously upon fuel melting. This fraction is currently an input constant, independent of the axial location.
EGFUCA	Enthalpy of the molten fuel in the cavity, J/kg.
TEFUPI	Temperature of the molten fuel, K

The second group of columns:

k	The number of the axial cell in the cavity.
ZZPI	Axial location of the lower boundary of cell k, measured from the bottom of the pin, m.
UFPI	Velocity of the molten fuel/fission gas mixture in the cavity, at the axial location ZZPI, m/s.
PRCA	Total pressure in the cavity, Pa.
PRFV	Fuel vapor pressure in the cavity, Pa.
UFCACH	Radial velocity of fuel/gas mixture being ejected from the pin cavity into the channel, m/s. This velocity is only calculated when the mechanistic ejection model is used, i.e., INRAEJ=1.
FUVOFR	Volume fraction of molten fuel in the pin cavity.
FUMESM	Mass of fuel molten during the current time step, kg.
FIMESM	Mass of free fission gas added to cell K of cavity during the current time step, kg.
FUEJ	Mass of fuel ejected from cavity during the current time step, kg.
FIEJ	Mass of free fission gas ejected from cavity during the current time step, kg.

An important characteristic LEVITATE is that the fuel pins can be disrupted at certain axial locations. The disrupted nodes can be identified by zeros in the columns headed: FUELSD, FUELM, FISGSD, FISGM, FISGDM, FUMESM, FIMESM, FUEJ and FIEJ. The other columns are not zeroed out, but the numbers appearing in the locations corresponding to disrupted nodes should be disregarded. One exception is the column PRCA (cavity pressure). In this column the nodes adjacent to the still intact pin stubs always contain a pressure. This is the pressure in the channel and was used in the in-pin momentum calculation as a boundary condition. The column headed PRVI (viscous pressure) should be totally disregarded, as the viscous pressure is not used in LEVITATE. Finally, the columns FUEJ and FIEJ (fuel and fission gas ejected during the last cycle) can occasionally contain negative quantities in the LEVITATE output. This is indicative of fuel and fission gas reentry in the pin cavity, via the open ends of the still intact pin stubs. The quantities SMFUEJ and SMEIEJ (total amount of fuel and fission gas ejected from the pin) have not yet been modified to account for the axial ejection via the pin stubs. Thus, after pin disruption, the amount of fuel ejected SMFUEJ might be different from the total amount of fuel in the channel, TOFUMA (to be described below).

The printout about the fuel pins is followed by two lines of summary information, listing the fuel mass in all the pins in the subassembly and the various reactivity components for the channel being printed, in dollars.

The section on the coolant channel follows. The first 6 lines contain information about the boundaries of various component regions and several integral quantities (Figs. 16.9-1 and 16.9-2). This summary information is followed by detailed information about each cell in the LEVITATE region. This information is printed in columns which are described below.

Summary information (left to right and top to bottom):

ICYCLE	The cycle number. Note that it starts from 0, because the increment is performed after the main printout.
IFMIBT, IFMITP	Bottom and top cells of the interaction region where LEVITATE performs calculations. This region is bounded by the liquid sodium slugs.
IFFUBT, IFFUTP	Bottom and top cell of the molten fuel region.
IFFIBT, IFFITP	Bottom and top cell of the fission gas region.
IFFVBT, IFFVTP	Bottom and top cell of the fission fuel vapor region.
IFRIBT, IFRITP	Bottom and top cell of the fuel-pin rip.
DTPLU	Time step used in this cycle.
TIMEPL	Current LEVITAT time, measured since the fuel motion initiation in this channel.
TONAMA	Total sodium mass in the channel.
TOFIMA	Total fission-gas mass in the channel.
TOFVMA	Total fuel vapor mass in the channel.
TOFUMA	Total molten fuel mass in the channel.
FUMATP	Molten fuel mass in the upper plenum.
FVMATP	Fuel vapor mass in the upper plenum.
FIMATP	Fission-gas mass in the upper plenum.
TPNAMA	Sodium mass in the upper plenum.
SLIFBT (1), SLIFBT (2)	Location and velocity of the upper boundary of the lower sodium slug.
SLIFTP (1), SLIFTP (2)	Location and velocity of the lower boundary of the upper sodium slug.
FUIFBT (1), FUIFTP (2)	Location and velocity of the lower boundary of the molten fuel region.
FUIFBT (1), FUIFTP (2)	Same as above, for the upper boundary.
FIFFBT (1), FIIFTP (2)	Location of the lower and upper interface of the fission-gas region.
IFSEBT, IFSETP	Bottom and top cell of the molten steel region.
SEIFBT (1), SEIFBT (2)	Location and velocity of the lower boundary of the molten steel region.
SEIFTP (1), SEIFTP (2)	Same as above, for the upper boundary.
TOSEMA	Total mass of molten steel in the channel.

SEMATP	Molten steel mass in the upper plenum.
TOSVMA	Total mass of steel vapor in the channel.
SVMATP	Steel vapor mass in the upper plenum.
IDISBT, IDISTP	Bottom and top cell of the disrupted pin region.
IFLUBT, IFLUTP	Bottom and top cell of the chunk region.
FLFBT (1), FLFBT (2)	Location and velocity of the lower boundary of the solid chunk region.
FLIFTP (1), FLIFTP (2)	Same as above for the upper boundary.
TOLUMA	Total mass of fuel chunks in the channel.
FLMATP	Fuel chunk mass in the upper plenum.
PRIN	Inlet pressure (at the bottom of the lower slug).
PREX	Outlet pressure (at the top of the upper slug).
IFSVBT, IFSVTP	Bottom and top cell of the steel vapor region.
SVIFBT (1), SVIFTP (2)	Location and velocity of the lower boundary of the steel vapor region.
SVIFTP (1), SVIFTP (2)	Same as above, for the upper boundary.
FVIFBT (1), FVIFTP (1)	Location of the lower and upper boundaries of the fuel vapor region.
TOSLMA	Total mass of steel chunks in the channel.
SLMATP	Steel chunk mass in the upper plenum.

The first group of columns (Fig. 16.9-2):

I	The current cell number.
ZC	Axial location of the lower boundary of cell i, measured from the bottom of the pin.
UMCH	Velocity of the gas mixture at boundary I, in cell I. Note that because of the use of dual velocities at the cell boundaries, it is necessary to specify whether the velocity printed for boundary I is in cell I or in cell I-1.
UFCH	Velocity of the molten fuel and molten steel at boundary I, in cell I.
PRCH	Total pressure in cell I.
SDNA	Density of sodium smeared over the open channel.
FISD	Density of fission gas smeared over the open channel.
THSECH	Volume fraction occupied by molten steel in cell I. This fraction always refers to the reference channel, with area AXMX.
THCHOP	Volume fraction occupied by the open channel. It is suggested that AXMX be selected such that the original THCHOP (I) = 1.

THFUCH	Volume fraction occupied by the molten fuel in cell i.
THNAFM	Volume fraction of the sodium film. Not used in LEVITATE currently; should always be zero.
THNL	Volume fraction of liquid sodium.

The second group of columns (Figs. 16.9-2 and 16.9-3).

I	The current cell number.
IFLAG	Flow regime indicator. Has the following significance: 2 – annular steel regime; 3 – annular fuel regime; 4 – bubbly fuel region; 5 – bubbly steel regime.
ZC	Same as previously described.
TEFUOS	Temperature of the molten fuel in cell I.
TENA	Temperature of the sodium vapor and fission gas.
TECLOS	Temperature of the outer cladding node, K.
TECLIN	Temperature of inner cladding node. If this quantity is –100, it indicates that the inner node has been removed due to ablation, K.
TESROS	Temperature of the "outer" structure node, i.e., the node facing the channel, K.
TESRIN	Temperature of the "inner" structure node, K.
PRNV	Saturation pressure of sodium at TENA. It is meaningful only for the nodes where two-phase sodium is present, i.e., THNL(I) ≠ O.
FUCH	Fuel mass in cell I, in kg.
CFFFCL	Fraction of cladding perimeter (or area) covered by the frozen fuel crust, in cell i.

The third group of columns (Fig. 16.9-3):

I	The current cell number.
IFLAG	Described above.
ZC	Described above.
DESECH	Generalized steel density: $\rho'_{se,i} = \rho_{se}\, A_{se,i}/\mathrm{AXMX}$.
TESECH	Temperature of the molten steel, K.
DEFUCL	Generalized density of frozen fuel on the clad.
DEFUSR	Generalized density of frozen fuel on the hexcan wall.
DESECL	Generalized density of steel entrapped in the fuel crust on the clad.
DESESR	Generalized density of steel entrapped in the fuel crust on the structure.
CFFFSR	Fraction of structure perimeter (or area) covered by frozen fuel.
TEFFCL	Temperature of the frozen fuel crust on the cladding.
TEFFSR	Temperature of the frozen fuel crust on the structure.

The fourth group of columns (Fig. 16.9-3 and 16.9-4):

I	The current cell number.
IDISR	Pin disruption indicator. Has the following significance: 0 – no disruption and no pin rip present; 1 – total disruption of the pins has occurred at this location; 2 – pin undisrupted but ripped. No injection taking place; 3 – pin undisrupted but ripped. Injection of molten fuel in the channel has occurred during this cycle.
ZC	Described above.
WICLAD	Thickness of the cladding in cell I. If zero, the pin has been disrupted (IDISR = 1) or the cladding was totally ablated (IDISR ≠ 1, TECLIN = -100).
WISTRC	Thickness of the structure in cell I.
TEFFSS	Surface temperature of the frozen fuel crust on the structure.
DELUCH	Generalized density of fuel chunks, kg/m^3.
TELUCH	Temperature of fuel chunks, K.
ULCH	Velocity of fuel chunks at boundary I (no dual velocities are used for the chunks).
THLUCH	Volume fraction occupied by the fuel and steel chunks.
RALUCH	Radius of chunks in cell I, m.
XNLUCH	Number of chunks in cell I.

The fifth group of columns (Figs. 16.9-4 and 16.9-5):

I	The current cell number.
IDISR	Described above.
ZC	Described above.
DEFVCH	Generalized density of the fuel vapor, kg/m^3.
DESVCH	Generalized density of the steel vapor, kg/m^3.
TEFUVA	Temperature of fuel vapor, K.
PRFV	Partial pressure of fuel vapor, Pa.
PRSV	Partial pressure of steel vapor, Pa.
TESEVA	Temperature of steel vapor, K.
PRFI	Partial pressure of fission gas, Pa.
PRNA	Partial pressure of the sodium vapor, Pa.
RHFULU	Density of fuel chunks. It can be different from the theoretical fuel density due to porosity.

The sixth group of columns: (This group refers entirely to the fuel/steel chunks and was not present in the initial release version).

I	The current cell number.
IDISR	Described above.
ZC	Described above.
DESELU	Generalized density of steel chunks, kg/m^3.

TESELU	Temperature of steel chunks, K.
FRSELU	Volume fraction of steel in the fuel/steel chunks. Can vary from 0 to 1.
DEFILU	Generalized density of fission gas associated with the fuel chunks.

The seventh group of columns has the title "Temperature Map of Region Outside the Interaction Zone." This output provides information about temperatures in the liquid sodium slug regions. It was not available in the Release 1.0 version of LEVITATE. It should be noted that these values are calculated at the end of the last heat-transfer time which can be fractions of a millisecond before the time of the current printout.

I	Axial channel index.
ZCOOL	Location of the lower boundary of mesh cell I.
TREFL2(2)	Inner reflector node temperature. Reflectors can be located only below or above the pin zone K2PIN.
TREFL2(1)	Temperature of the outer reflector node which is facing the coolant.
T1(NEPP)	Inner cladding surface temperature (i.e., next to the fuel).
T1(NE)	Cladding temperature of the middle cladding node.
T1(NEP)	Outer cladding surface temperature (i.e., next to the coolant).
TENA	Sodium temperature.
TSAT	Sodium saturation temperature. This is calculated only for the pin zone to detect sodium-boiling initiation.
TSTR2(1)	Temperature of the structure node facing the coolant channel.
TSTR2(2)	Temperature of the structure node facing the neighboring hexcan wall.
PRCH	Pressure in the coolant channel. This is calculated outside the fuel-pin zone only if the interaction region extends beyond it.

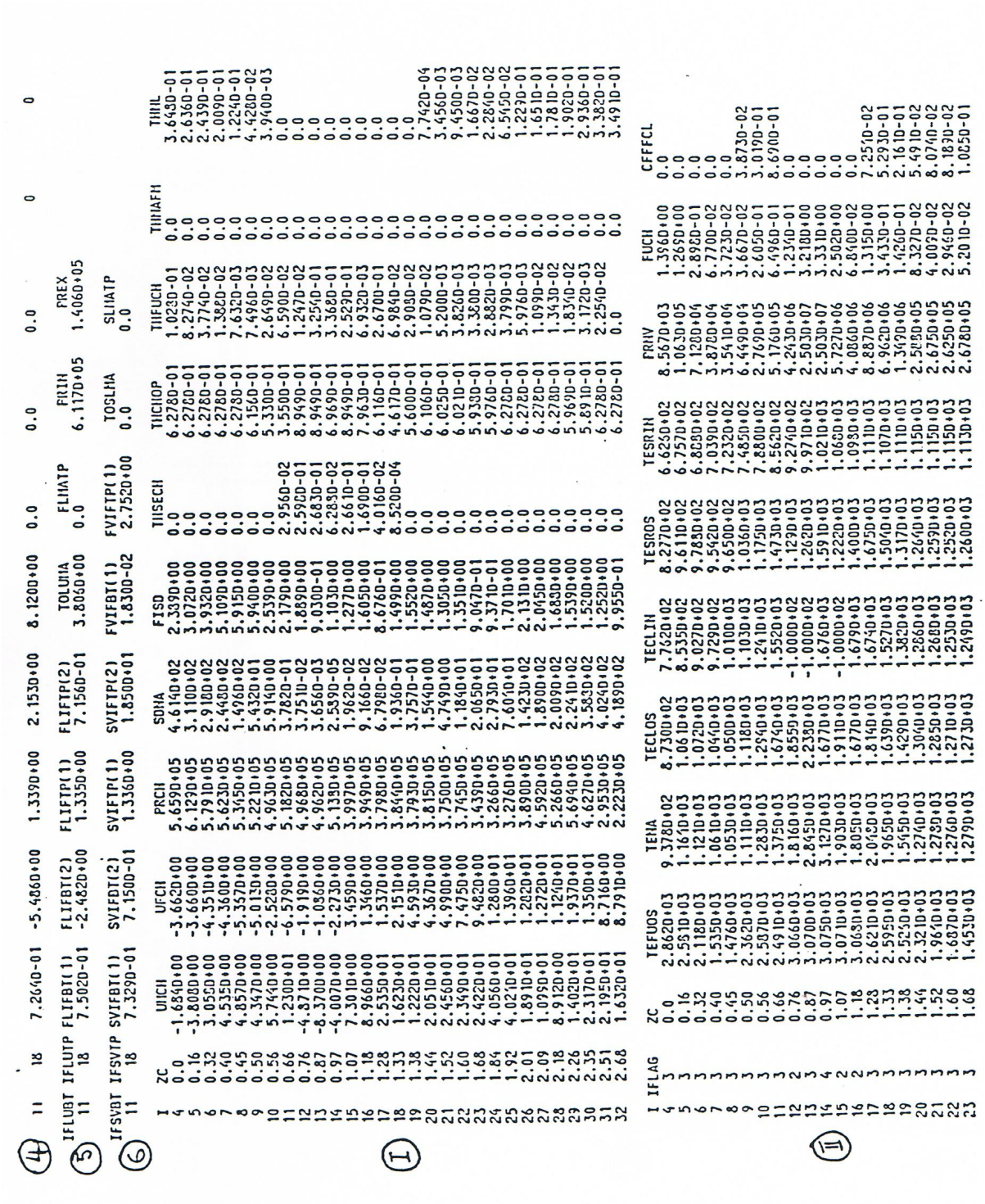

Fig. 16.9-2: Output Description (First Continuation)

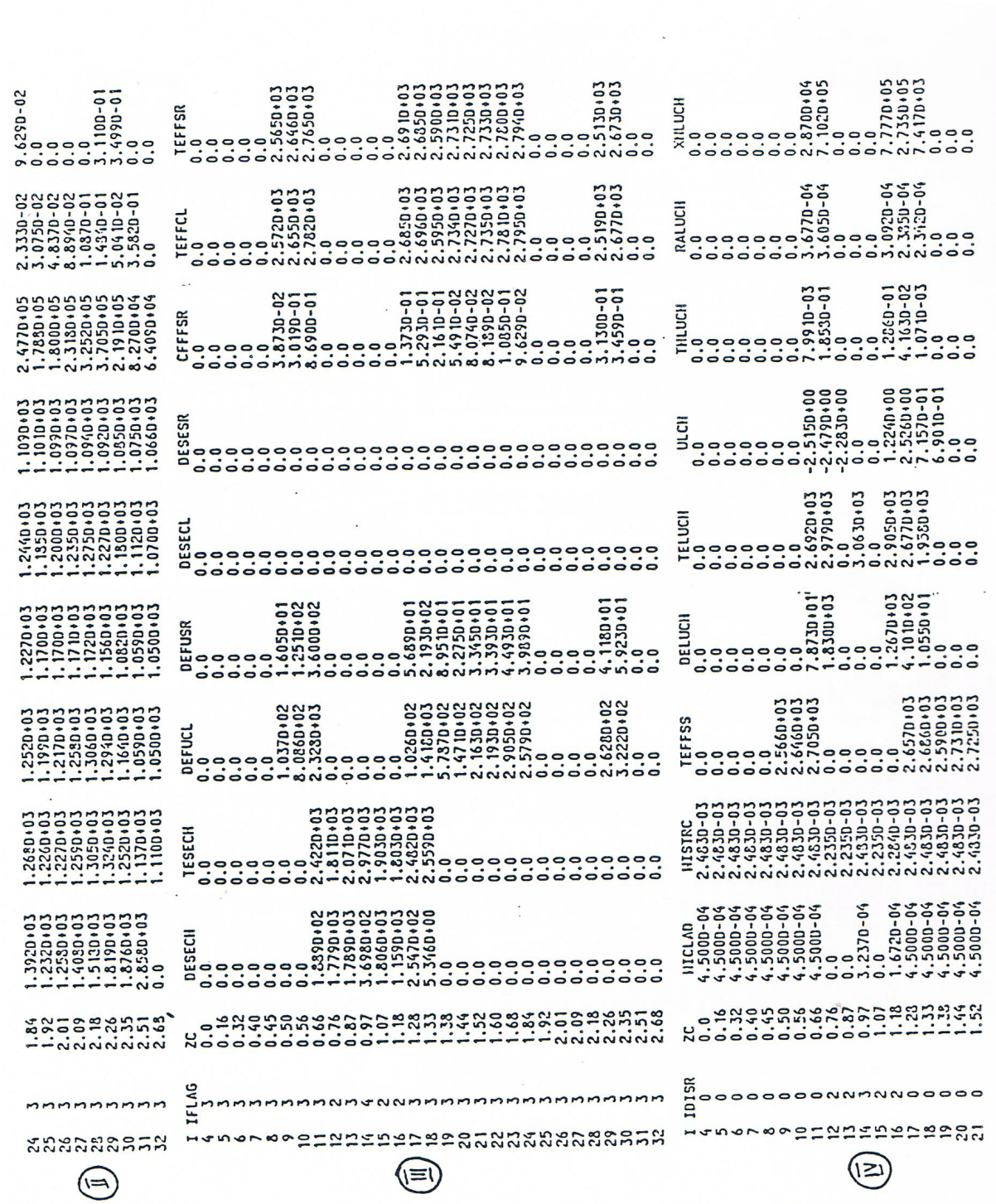

Fig. 16.9-3: Output Description (Second Continuation)

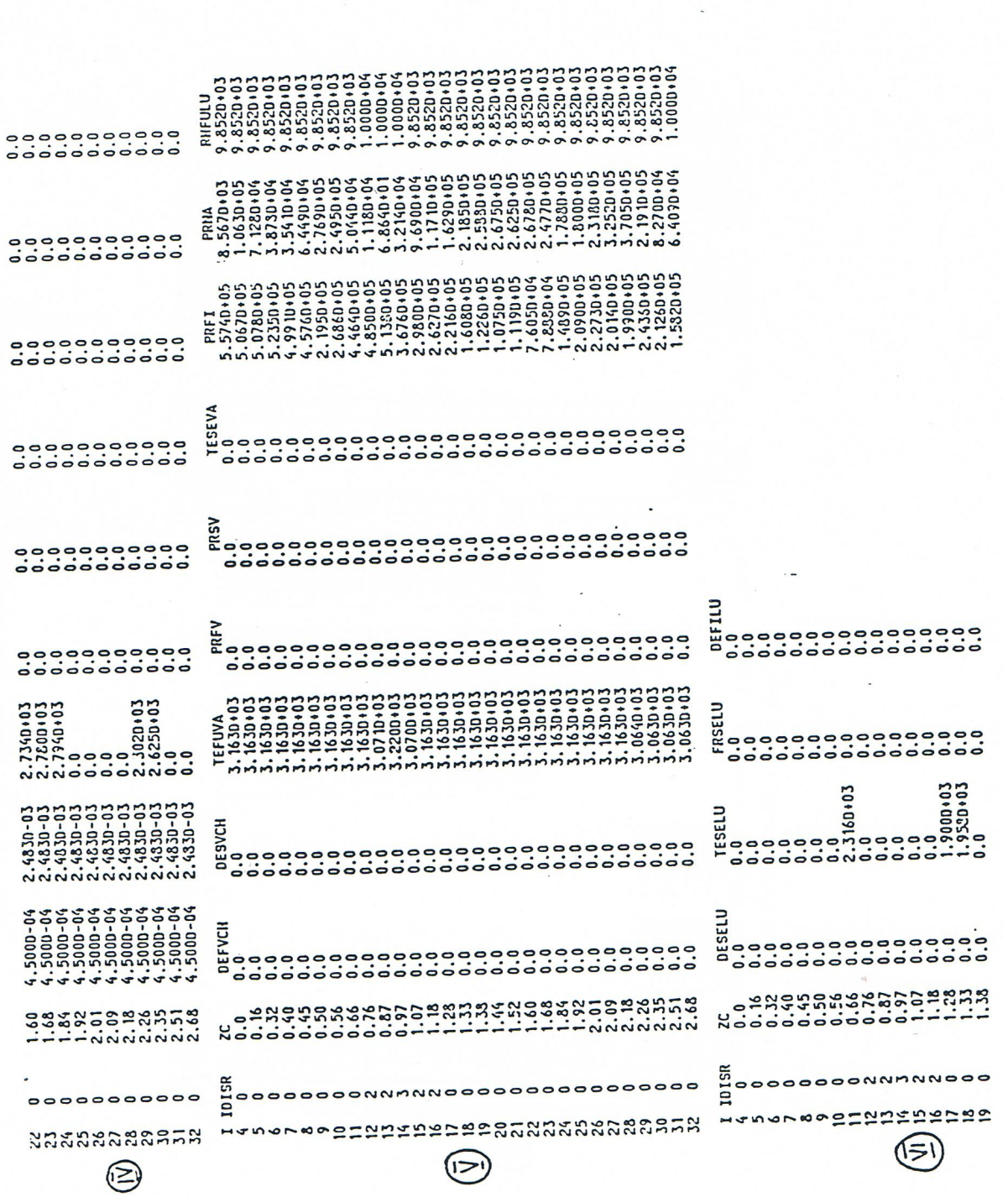

Fig. 16.9-4: Output Description (Third Continuation)

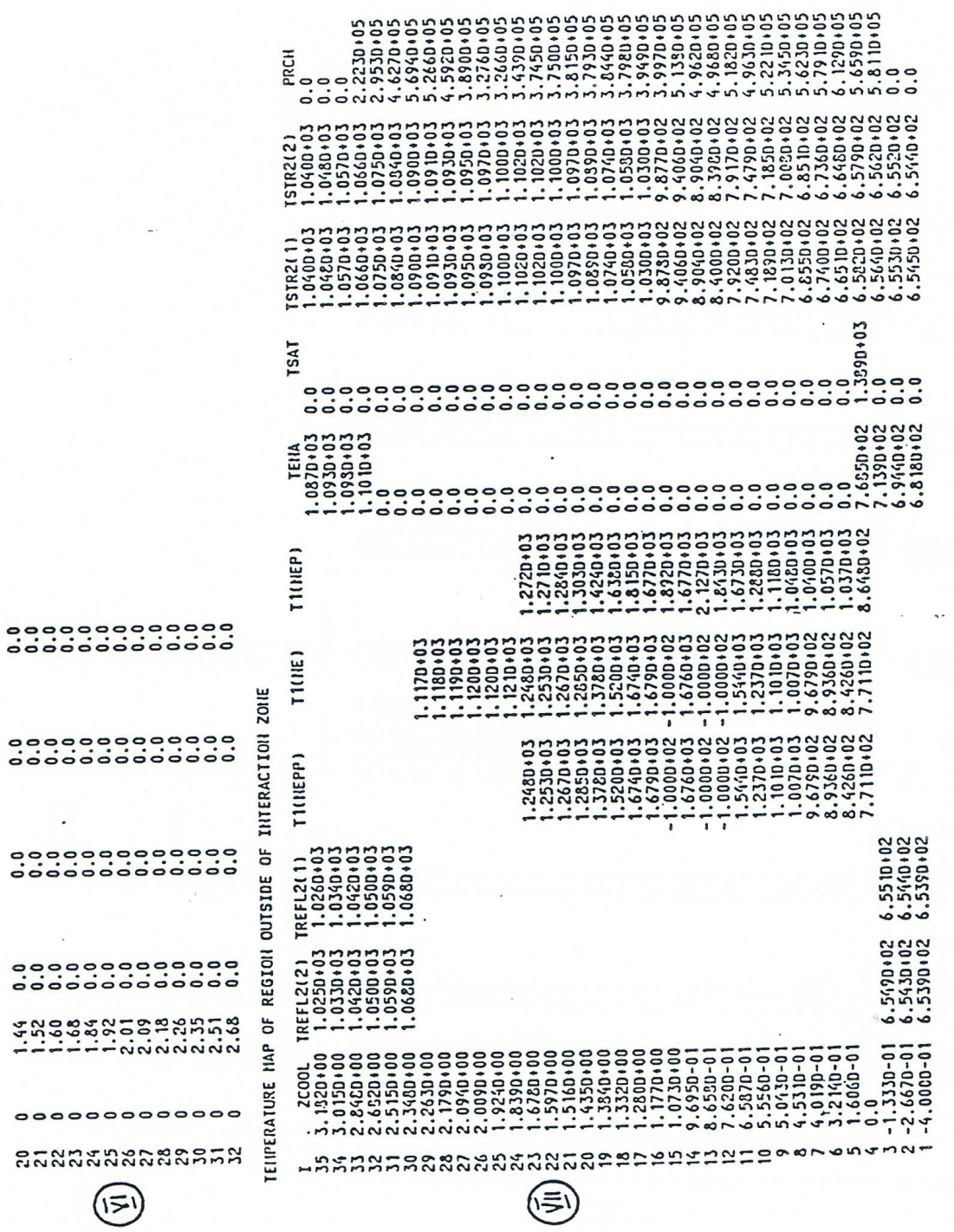

Fig. 16.9-5: Output Description (Fourth Continuation)

16.9.2 Auxiliary and Debug Output

Several auxiliary WRITE statement are incorporated in LEVITATE. These statements are activated only when some special situation occurs. The definition of the term "special situation" is somewhat loose, and it is possible that the situation indicated by the WRITE statement printout is legitimate for the given run. The user should attempt to familiarize himself with the meaning of these messages. Their general form is:

*** Brief explanatory message. XXXX-999***

where XXXX are the first four letters in the name of the routine printing the message and 999 is the label of the FORMAT statement printing the message. Several integers and floating point numbers may follow. They depend on the list of variables associated with the particular WRITE statement. An example of such messages which are used for information only, rather than to indicate a problem, are the messages

*** LEVITATE STARTS ***

and

*** LEVITATE ENDS ***

printed from the driver routine LEVDRV (Fig. 16.9-5).

Debug printout can be obtained between cycles IBGO and IBSTOP by specifying the input variables in block 51. The amount of debug printout can be increased by increasing the input variable IBNEW from 0 to 4 (acceptable values are 0,1,2,3,4).

REFERENCES

16-1. A. M. Tentner and H. U. Wider, "LEVITATE – A Mechanistic Model for the Analysis of Fuel and Cladding Dynamics under LOF Conditions," *Intl. Mtg. on Fast Reactor Safety Technology*, Seattle, WA, August 1979.

16-2. W.R. Bohl and T.J. Heames, Unpublished information, Argonne National Laboratory, 1974.

16-3. W.R. Bohl and M.G. Stevenson, "A Fuel Motion Model for LMFBR Unprotected Loss-of-Flow Accident Analysis," CONF-730414-P2, Ann Arbor, MI, April 1973.

16-4. M.G. Stevenson, et al., "Current Status and Experimental Basis of the SAS LMFBR Accident Analysis Code System," *Proc. of the Fast Reactor Safety Meeting, Beverly Hills*, CA, April 1974.

16-5. H.U. Wider, "PLUTO2: A Computer Code for the Analysis of Overpower Accident in LMFBRs," *Trans. Am. Nucl. Soc.*, vol. 27, p. 533, 1977.

16-6. A.M. Tentner, H.U. Wider and C.H. Bowers, "A Mechanistic Model for Fuel Flow Regimes and Fuel Plateout," *Trans. Am. Nucl. Soc.*, vol. 30, p. 448, 1978.

16-7. M. Epstein and G.M. Hauser, "The Melting of Finite Steel Slabs in Flowing Nuclear Reactor Fuel," *Nucl. Eng. Des.*, vol. 52, 1979.

16-8. B. Spencer, et al., "Results of Fuel Freezing Tests with Simulated CRBR-Type Fuel Pins," *Trans. Am. Nucl. Soc.*, vol. 30, 1978.

16-9. S.J. Hakim, "Analysis of a Prototypic and a Simulant Experiment Related to Freezing in Flow Channels," Specialists' Workshop on Predictive Analysis of Material Dynamics in LMFBR Safety Experiments, Los Alamos Scientific Laboratory, NM, March 1979.

16-10. C.H. Bowers, et al., Unpublished information, Los Alamos Scientific Laboratory, 1979.

16-11. A.M. Tentner and H.U. Wider, "New Aspects in the Analysis of Fuel, Dynamics during Loss-of-Flow Transients," *Trans. Am. Nucl. Soc.*, vol. 38, 1982.

16-12. A.M. Tentner and H.U. Wider, "Pressure Drop Modeling in Variable Area, Multiphase, Transient Flow," in *Multiphase Transport: Fundamentals, Reactor Safety Applications*, N. Veziroglu, Ed., Hemisphere Publishing Co. N.Y., May 1980.

16-13. A.M. Tentner and H.U. Wider, "The Influence of Steel Vapor Pressure on Fuel Motion in Voided LMFBR Channels," *Trans. Am. Nucl. Soc.*, vol. 34, 1980.

16-14. R.E. Henry et al. "Pressure Pulse Propagation in Two-Phase One- and Two-component Mixtures," ANL-7792, Argonne, IL, March 1971.